DATE ISSUED FEB 17 1988

ORNL
MASTER COPY

ORNL/Sub/81-07685/02&77

TRANSFORMATION, METALLURGICAL RESPONSE AND BEHAVIOR OF THE WELD FUSION ZONE AND HEAT AFFECTED ZONE IN Cr-Mo STEELS FOR FOSSIL ENERGY APPLICATION

Final Technical Report for Period January 1985 to September 1987

Research sponsored by the U.S. Department of Energy
Advanced Research and Technology Development
Fossil Energy Materials Program

Report Prepared by

C.D. Lundin
J.A. Henning
R. Menon
K.K. Khan

Welding Research and Engineering
Materials Science and Engineering
The University of Tennessee
Knoxville, TN 37996-2200

September 30, 1987

Under Subcontract 7685X77

for

Oak Ridge National Laboratory
Oak Ridge, Tennessee, 37831

operated by

MARTIN MARIETTA ENERGY SYSTEMS, INC.

for the
U.S. DEPARTMENT OF ENERGY
Under contract No. DE-AC05-840R21400

Printed in the United States of America. Available from
National Technical Information Service
U.S. Department of Commerce
5285 Port Royal Road, Springfield, Virginia 22161
NTIS price codes—Printed Copy: Microfiche A01

This report was prepared as an account of work sponsored by an agency of the United States Government. Neither the United States Government nor any agency thereof, nor any of their employees, makes any warranty, express or implied, or assumes any legal liability or responsibility for the accuracy, completeness, or usefulness of any information, apparatus, product, or process disclosed, or represents that its use would not infringe privately owned rights. Reference herein to any specific commercial product, process, or service by trade name, trademark, manufacturer, or otherwise, does not necessarily constitute or imply its endorsement, recommendation, or favoring by the United States Government or any agency thereof. The views and opinions of authors expressed herein do not necessarily state or reflect those of the United States Government or any agency thereof.

PRICING SCHEDULE FOR DOE REPORTS*

Page Range	Domestic Price	NTIS Price Code	Page Range	Domestic Price	NTIS Price Code
001—025	$ 5.00	A02	326—350	$24.50	A15
026—050	6.50	A03	351—375	26.00	A16
051—075	8.00	A04	376—400	27.50	A17
076—100	9.50	A05	401—425	29.00	A18
101—125	11.00	A06	426—450	30.50	A19
126—150	12.50	A07	451—475	32.00	A20
151—175	14.00	A08	476—500	33.50	A21
176—200	15.50	A09	501—525	35.00	A22
201—225	17.00	A10	526—550	36.50	A23
226—250	18.50	A11	551—575	38.00	A24
251—275	20.00	A12	576—600	39.50	A25
276—300	21.50	A13	601—up	†	A99
301—325	23.00	A14			

*All microfiche are priced A01.

†Add $1.50 for each additional 25-page increment or portion thereof for 601 pages and more.

ORNL/Sub/81-07685/02&77

TRANSFORMATION, METALLURGICAL RESPONSE AND BEHAVIOR OF THE WELD FUSION ZONE AND HEAT AFFECTED ZONE IN Cr-Mo STEELS FOR FOSSIL ENERGY APPLICATION

Final Technical Report for Period January 1985 to September 1987

Research sponsored by the U.S. Department of Energy
Advanced Research and Technology Development
Fossil Energy Materials Program
Report Prepared by

C.D. Lundin
J.A. Henning
R. Menon
K.K. Khan

Welding Research and Engineering
Materials Science and Engineering
The University of Tennessee
Knoxville, TN 37996-2200

September 30, 1987

Under Subcontract 7685X77

for

Oak Ridge National Laboratory
Oak Ridge, Tennessee, 37831

operated by

MARTIN MARIETTA ENERGY SYSTEMS, INC.

for the
U.S. DEPARTMENT OF ENERGY
Under contract No. DE-AC05-84OR21400

ACKNOWLEDGEMENT

The financial support provided through research contracts from the Advanced Research and Technology Development Fossil Energy Materials Program, Oak Ridge National Laboratory is gratefully acknowledged. Special thanks are extended to Mr. R.A. Bradley, Mr. R.W. Swindeman and Dr. V.K. Sikka at Oak Ridge National Laboratory for their help and assistance.

The authors would also like to thank Dr. D.A. Canonico and the staff at the Metallurgical Laboratory of Combustion Engineering, Chattanooga, Tennessee, for their assistance in preparing the literature review and help in providing chemical analysis.

SUMMARY

This research program was undertaken to provide fundamental and basic metallurgical information on the behavior of the heat affected zone (HAZ) in Cr-Mo steel welds as well as practical information on their relative weldability. The principal work was the evaluation of the post weld heat treatment (PWHT) cracking of Cr-Mo steels ranging in Cr content from 2 1/4% to 9%. Differences in observed cracking behavior were contrasted with composition, on cooling transformation behavior and HAZ microstructure. Hydrogen assisted cracking (HAC) studies using a large scale cracking test were conducted on 2 1/4 Cr and 3Cr steels. Soft zone studies were conducted on 9Cr NKK steel to determine the reason for the development of a low hardness region ("Soft Zone") at the outer boundary of the HAZ.

The literature review provides a concise historical review and the basis of theories for PWHT cracking and HAC in Cr-Mo steels which were employed to explain the weld cracking susceptibility of various Cr-Mo alloys.

PWHT cracking susceptibility was investigated using Gleeble simulated heat affected zone (HAZ) specimens. A new test was developed at the University of Tennessee, the C-ring test, to evaluate the PWHT cracking behavior. The C-ring test was found to be an extremely useful test for PWHT cracking susceptibility and for verifying the results obtained from Gleeble testing. An excellent correlation was obtained for the two tests.

The standard Y-groove test was selected for HAC susceptibility testing. This test is very suitable for evaluating the HAC of the base metal and is defined in Japanese Industrial Standard JIS Z 3158.

The samples generated during testing provided test data as well as metallographic specimens for examination by optical, scanning electron (SEM) and transmission electron (TEM) microscopy techniques. Evaluation of the metallographic specimen defined the effect of microstructure on the weld cracking susceptibility. The soft zone studies conducted on the 9Cr NKK steel used weldment and synthetically cycled samples to provide the metallographic specimen examined by using optical, SEM and STEM techniques.

The Gleeble apparatus was employed to determine the continuous cooling transformation (CCT) behavior of the coarse grained heat affected zone in the 2 1/4Cr, 3Cr and 9Cr steels of standard and modified composition. The result of CCT determination in 9Cr-1Mo commercial heats shows that the primary microstructural constituents are martensite and autotempered martensite. Also, presence of delta ferrite was observed in the HAZ microstructure. Results of the CCT behavior determination for the coarse grained HAZ of 3Cr-1.5Mo and 2 1/4Cr-1Mo show that the on-cooling microstructure is dependent on the cooling rate. Over the range of cooling rate associated with commonly employed energy inputs the following type of HAZ microstructures may be observed: (1) for a fast cooling rate the microstructure is acicular martensite and lenticular martensite; (2) the microstructure at a slower cooling rate consists of lenticular martensite and bainite; (3) a further reduction in the cooling rate produces a microstructure which contains bainite or bainite plus ferrite. Although significant amounts of retained austenite have been reported as a result of very slow cooling rates, in the present study with the cooling rates and materials employed, no retained austenite was observed. (Very slow cooling of 3Cr-1.5Mo-Ni can result in upto 17% retained austenite.)

The PWHT cracking susceptibility of the Cr-Mo steels employed in this investigation is related to the extent of grain matrix strengthening which occurs during PWHT. An increase in the grain matrix strength increases the susceptibility to PWHT cracking. During PWHT the matrix of 2 1/4Cr-1Mo and 3Cr-1.5Mo is strengthened more than 9Cr-1Mo and as a result 2 1/4Cr and 3Cr materials are more susceptible to PWHT cracking. PWHT at a lower temperature (1150°F) results in increased strengthening over PWHT at a higher temperature (1250°F), so the susceptibility to PWHT cracking is higher at lower PWHT temperature.

The Climax composition 3Cr-1.5Mo had the highest susceptibility to PWHT cracking. However, an experimental heat and a 50 ton commercial heat made to the same chemistry showed significantly better response, primarily due to a reduced P content. Matrix strengthening due to high C, Si content and grain boundary embrittlement due to the higher P content of the 3Cr-1.5Mo and 2 1/4Cr-1Mo material appear to act synergistically resulting in greater susceptibility. An increase in the C or Si content in the nominal 2 1/4Cr-1Mo increases the likelihood of strengthening the matrix, thus increasing the PWHT cracking susceptibility.

Five state-of-the-art commercial heats of modified 2 1/4Cr-1Mo (Ti-V-B) were also evaluated for PWHT potential using the Gleeble and C-ring tests. These heats had a superior PWHT cracking resistance as compared to the JSW and Lukens 2 1/4Cr-1Mo materials. One heat displayed outstanding PWHT cracking resistance, and this behavior is attributed to the addition of Ca during melting practice, which modifies the sulphide inclusion morphology and distribution. This indicates that sulphide inclusion

distribution and morphology may have a more pronounced effect than previously considered.

Carbide morphology changes during weld HAZ thermal exposure and PWHT were determined utilizing STEM and TEM methods employing convergent beam and EDAX analysis techniques. The original carbides were completely dissolved in the coarse grained HAZ of the unmodified Berkeley alloy but were not completely dissolved in the V modified alloys during this thermal exposure. The precipitation of fine M_2C type carbides took place rapidly upon PWHT for all materials after HAZ thermal cycle exposure. However, in the V modified material the M_2C type carbide persisted for longer periods than for the Berkeley modified material. This gives rise to the matrix strengthening in the unmodified alloys and contributes to their higher PWHT cracking susceptibility. In general, the relative PWHT cracking susceptibility of Cr-Mo steels depends on the alloying elements, residual elements and the inclusion morphology and distribution.

The limited Y-groove testing at different preheat temperatures and at various levels of diffusible hydrogen on 2 1/4Cr-1Mo and 3Cr materials indicate that there is no decipherable difference in behavior between the modified and unmodified steels.

The soft zone studies on 9Cr NKK steel showed that the soft zone was located in the region heated to just below the Ac_1 during the weld thermal cycle. SEM and STEM studies revealed that the softening is related to the coarsening of carbides in this region (an overtempering effect).

The basic metallurgical information derived from this investigation clarified the reasons for the relative cracking behavior of the different Cr-Mo materials. The practical data from this investigation provide a

basis for the determination of suitable welding conditions as well as a guide for the selection of materials from the standpoint of fabricability.

TABLE OF CONTENTS

PAGE

INTRODUCTION 1

LITERATURE REVIEW 4

Phase Transformation 4

Weldability 17

Hydrogen Assisted Cracking 19

Theory of Hydrogen Assisted Cracking 24

Prevention of Hydrogen Assisted Cracking 27

Compositional and Microstructural Effects on Hydrogen Assisted Cracking 30

Weldability Testing of Chromium-Molybdenum Steels 32

Post Weld Heat Treatment Cracking 37

Origin of Residual Stresses Responsible for Post Weld Heat Treatment Cracking 41

Microstructural Effects on Post Weld Heat Treatment Cracking 43

Effects of Composition on Post Weld Heat Treatment Cracking 43

Testing Techniques for Post Weld Heat Treatment Cracking 65

Prevention of Post Weld Heat Treatment Cracking 78

Soft zone / Overtempered Region 72

MATERIALS 77

EXPERIMENTAL PROCEDURES 86

The "Gleeble Device" 86

Phase Transformations 86

Y-Groove HAC Test 90

Post Weld Heat Treatment Cracking 91

HAZ Soft Zone Evaluation 99

RESULTS AND DISCUSSION 102

Transformation Behavior 102

Transformation Results for the 9Cr-1Mo-V-Nb Materials ... 103

9Cr-1Mo-V-Nb Microstructures 106

Summary of the 9Cr-1Mo-V-Nb Transformation Studies 115

Transformation Results for the Modified

2 1/4Cr and 3Cr Alloys 116

Modified 2 1/4Cr-1Mo and 3Cr-Mo Microstructures 125

Summary of the Modified 2 1/4Cr-1Mo and 3Cr-Mo

Transformation studies 134

Y-Groove Hydrogen Assisted Cracking Test 135

Post Weld Heat Treatment Cracking Behavior 139

Post Weld Heat Treatment Cracking Susceptibility

Evaluation of the 9Cr-1Mo-V-Nb Commercial Heats 140

Fractography of the 9Cr-1Mo-V-Nb Materials 143

Summary of the 9Cr-1Mo-V-Nb PWHT Cracking Behavior 146

Post Weld Heat Treatment Cracking Results for the

Modified 3Cr-Mo and 2 1/4Cr-1Mo Materials by

Gleeble Simulation 146

Post Weld Heat Treatment Cracking Results for the

State-of-the-art Commercial Heats of Modified

2 1/4Cr-1Mo (M10-M50) by Gleeble Simulation 156

Fractography of the 3Cr-Mo and 2 1/4Cr-1Mo Alloys 158

Optical, Scanning Electron and Transmission Electron Microscopy of Gleeble Simulated Post Weld Heat Treatment Specimens 172

C-Ring Test Evaluation of Post Weld Heat Treatment Cracking Susceptibility of the 3Cr-Mo and 2 1/4Cr-1Mo Alloys 186

Results of the C-ring Test for the 3Cr-Mo and 2 1/4Cr-1Mo Materials 190

Metallographic and Fractographic Examination of the 2 1/4Cr-1Mo and 3Cr-Mo C-ring Specimens 196

Results of the C-ring Test for the State-of-the-art Commercial Heats of Modified 2 1/4Cr-1Mo (M10-M50) Materials 200

Problems Encountered with the C-ring Test 203

Summary of PWHT Cracking Results for the 3Cr-Mo and 2 1/4Cr-1Mo Alloys 206

Soft Zone Evaluation 211

Metallographic Examination of Soft Zone 214

CONCLUSIONS 233

Transformation Characteristics 233

Hydrogen Assisted Cracking Susceptibility 235

Post Weld Heat Treatment Cracking Susceptibility 236

Soft Zone Evaluation 242

LIST OF REFERENCES 244

DISTRIBUTION LIST A-1

INTRODUCTION

Ferritic steels alloyed with chromium and molybdenum are utilized in applications where creep behavior or corrosion/oxidation resistance are necessary factors in materials selection. The principle use of these alloys has been in the power generation and process industries. With the advent of the nuclear power industry[1,2] and synfuels development programs[3,4] a world wide effort was initiated to develop materials with improved properties. Further, those industries historically using Cr-Mo alloys seek to employ higher operating temperatures and pressures or larger pressure vessels which would result in increased economy and efficiency.[5,6]

Development of modified alloys with 2 1/4Cr and 3Cr have had the following criteria of principal concern:

1. resistance to high temperature hydrogen attack,
2. minimum variation in hardenability with small changes in composition,
3. a broad range of tempering conditions which will result in a fine bainitic microstructure possessing both strength and toughness,
4. weldability must be as good as or superior to standard 2 1/4Cr-1Mo.[7]

In response to these criteria, Climax Molybdenum Company developed a 3Cr-1Mo-0.1V alloy,[8,9] the University of California-Berkeley proposed a 3Cr-1 1/2Mo alloy with 0.5% Ni added,[10] Japan Steel Works (JSW) developed both 2 1/4Cr-1Mo and 3Cr-1Mo alloys with additions of 1/4% V, 0.02% Ti, and 0.002% B,[11] Nippon Kokan's modified 2 1/4Cr-1Mo and 3Cr-1Mo alloys have

additions of 0.5% Ni, 0.3%V, 0.009% Ti and 0.007%B,[12] Kawasaki's modified 3Cr-1Mo has additions of 0.02%Nb and 0.2%V,[13] while Kobe's modification was to add Ca during melting.

Development of the 9Cr alloys was undertaken to eliminate ferritic to austenitic transition joints, to utilize the increased corrosion resistance compared to 2 1/4Cr and 3Cr materials, to obtain increased resistance to stress-corrosion cracking in caustic and chloride environments compared to type 304 stainless steel, and to reduce the use of strategic materials compared to 304 stainless steel, in particular chromium. The principle criteria for alloy modification were to achieve creep properties that equaled or exceeded those of type 304 austenitic stainless steel up to 1100°F (590°C) and to maintain adequate weldability.[2] These criteria have been addressed by the development of a V-Nb modified 9Cr-1Mo at Oak Ridge National Laboratory (ORNL)[1] and by Sumitomo Metal Industries' duplex, low C 9Cr-2Mo material.[14,15]

The use of these modified alloys for pressure vessel applications requires that they be approved in the appropriate codes and standards. (9Cr-1Mo-V-Nb has recently been approved for use by ASTM, A213-T91 for pipe and ASTM A387-Gr91 for plate.) Therefore the mechanical and fabrication properties must be fully documented. As can be seen from the foregoing criteria, weldability is a significant factor in the acceptance of the these materials for use in pressure vessel fabrication.

Weldability has been defined as "the capacity of a material to be welded under fabrication conditions imposed into a specific, suitably designed structure and to perform satisfactorily in the intended service."[16] In practice, weldability is mainly associated with a materials

resistance to various types of cracking.[17] In Cr-Mo steels susceptibility to postweld heat treatment cracking and hydrogen assisted cracking are most often considered.

Work undertaken in the following described research was primarily concerned with the evaluation of susceptibility to postweld heat treatment (stress-relief or reheat) cracking for the modified, enhanced properties, 9Cr-1Mo, 3Cr-Mo and 2 1/4Cr-1Mo alloys. Work was also performed to determine the heat affected zone transformation temperatures and microstructures, HAC susceptibility of 2 1/4Cr-1Mo and 3Cr-Mo alloys and soft zone studies on the 9Cr-1Mo modified NKK commercial heat are presented.

LITERATURE REVIEW

Phase Transformations

The metallurgical transformations that occur during welding affect the final microstructure and therefore influence many of the potential problems that may develop during and after welding. The coarse grained heat affected zone (HAZ) is the location of maximum susceptibility for postweld heat treatment (PWHT) cracking. It is also the primary region for hydrogen assisted cracking.

The discussion of hydrogen assisted cracking by Linnert[17] indicates that susceptibility increases with increasing hardness of the microstructure. Therefore a martensitic microstructure is more susceptible to hydrogen assisted cracking than a mixed martensitic-bainitic one which, in turn, is more susceptible than an entirely bainitic microstructure. Ito and Nakanishi[18] showed in a study of 1Cr-1/2Mo alloys that a HAZ microstructure consisting of martensite or lower bainite was more susceptible to PWHT cracking than upper bainite. In temper embrittlement, a related materials problem, it was found that a martensitic microstructure is more prone to a loss of ductility and toughness than a bainitic microstructure.[19,20] Thus, the determination of (HAZ) transformation characteristics is a first step in determining the weldability of a material and which may, in turn, provide the key to reducing or eliminating weld HAZ problems.

Easterling[21] has compared the microstructural regions of a weld with the equilibrium phase diagram (Figure 1). However, such a representation is overly simplistic in that it ignores major differences between the weld

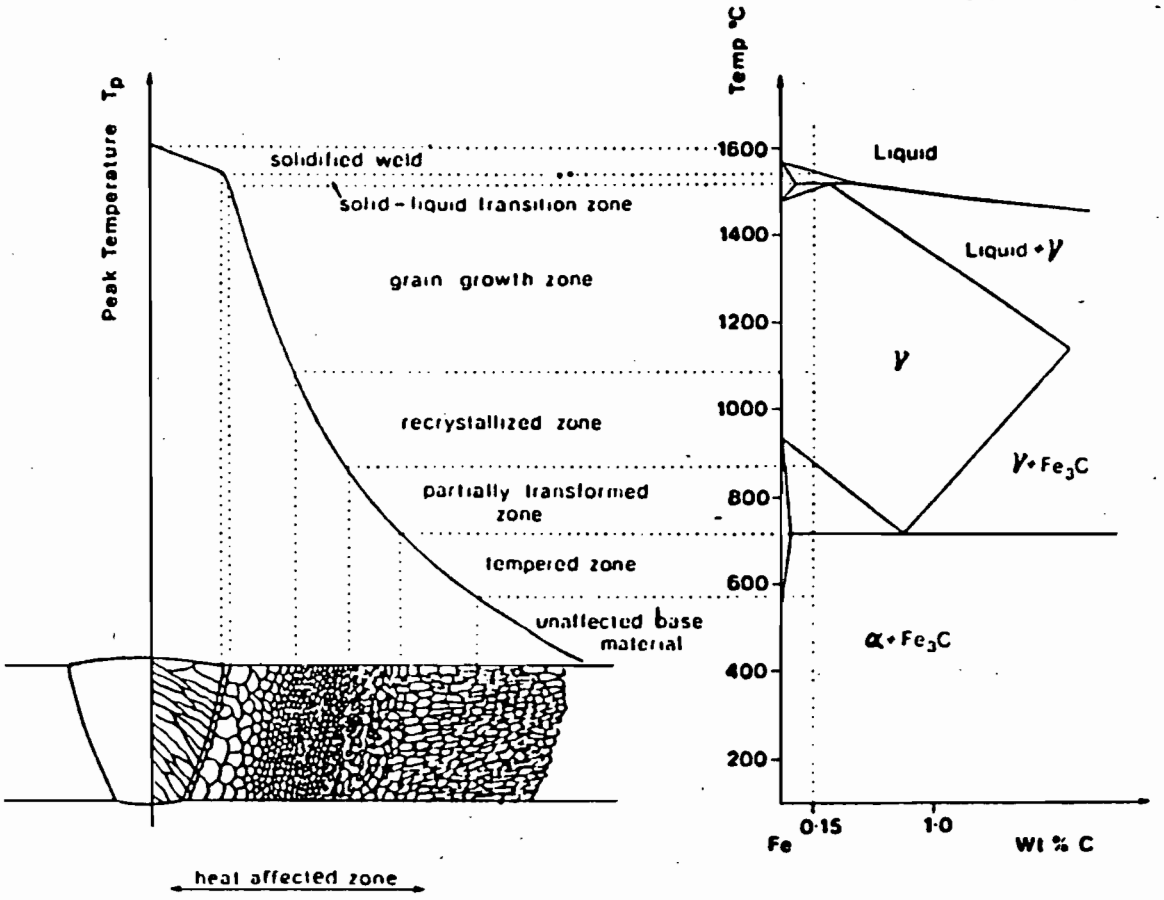

Figure 1. Schematic diagram of the various regions of the HAZ approximately corresponding to the 0.15w/o carbon indicated on the Fe-Fe_3C equilibrium diagram.

Source: Easterling, K., Introduction to the Physical Metallurgy of Welding, Butterworths, 1983.

thermal cycle and the conditions that are utilized in establishing the equilibrium phase diagram. Welding can induce rapid heating (3000F^{o}/sec) and cooling (500°F/sec) rates resulting in conditions far from equilibrium. Furthermore, complete homogenization, required for equilibrium, never exists during welding. Also equilibrium considerations do not include such non-equilibrium constituents such as martensite or bainite.

Many of the objections to the use of the equilibrium diagram to predict weld HAZ transformations also extend to the use of standard continuous cooling transformation diagrams. These diagrams are developed starting with homogeneous austenite. However, in welding the inhomogeneity occurs due to the inability of alloying elements to diffuse uniformly throughout the austenitic microstructure and the incomplete solution of carbides or nitrides as a result of the rapidity of the welding thermal cycle and the concomitant short austenitizing times. In order to accurately predict the on-cooling transformation temperatures and microstructures, weld HAZ continuous cooling transformation diagrams must be derived using the heating and cooling conditions attendant upon welding.[22,23,24]

Figure 2 shows a conventional continuous cooling transformation diagram for 2 1/4Cr-1Mo and Figure 3 illustrates a diagram determined under simulated welding conditions for the coarse grained HAZ in 2 1/4Cr-1Mo.[25] As may be seen by comparing Figures 2 and 3 the depression of the on-cooling transformation temperatures (principally bainite), under welding conditions is approximately 90°F (50°C) due to the rapid heating and cooling rates and short austenitizing times.

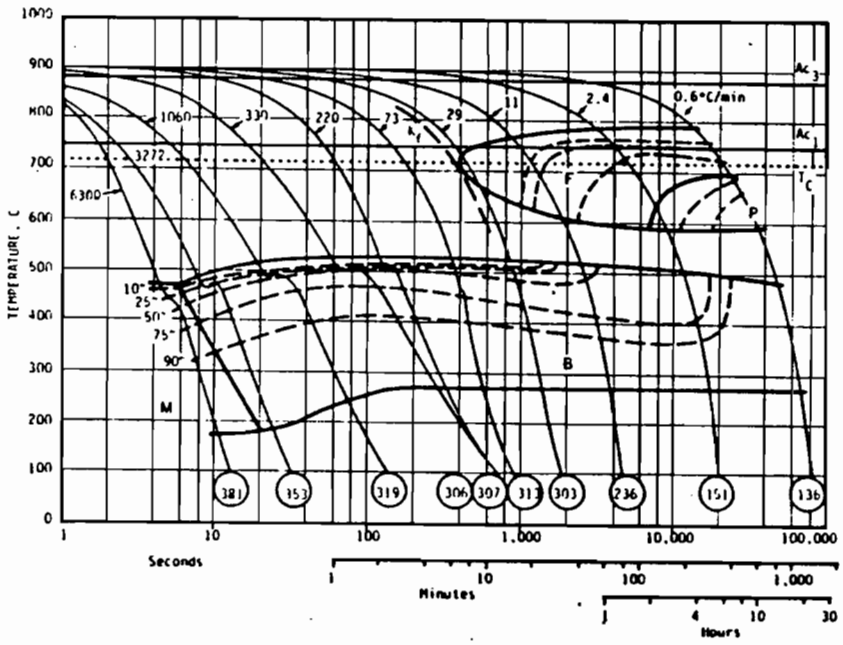

Figure 2. CCT diagram for 2 1/4Cr-1Mo.

Source: Wada, T. and Eldis, Transformation Characteristics of 2 1/4Cr-1Mo Steel, <u>ASTM-STP 755, Applications of 2 1/4Cr-1Mo Steel for Thick Wall Pressure Vessels</u>, Sangdahl and Semchyshen, eds., American Society for Testing and Materials, Philadelphia, 1982.

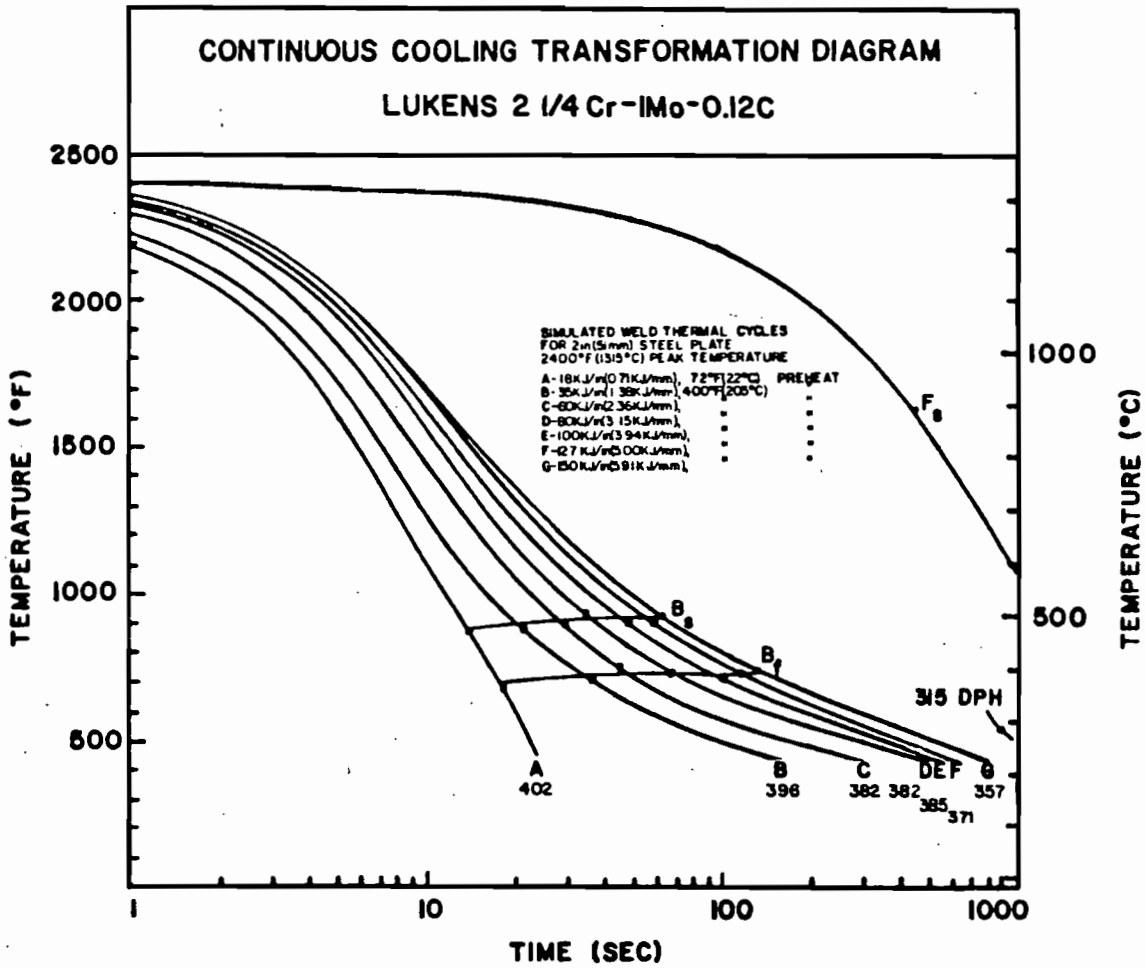

Figure 3. CCT diagram for 2 1/4Cr-1Mo under simulated welding conditions.

Source: Richey, M.W., The Weldability of Cr-Mo Steels for Fossil Energy Applications, M.S. Thesis - University of Tennessee, 1984.

The literature review by Richey[25] reveals that only a few continuous cooling transformation diagrams have been determined under welding conditions for the Cr-Mo materials. However, conventional continuous cooling transformation diagrams are available for many of the modified Cr-Mo alloys. Continuous cooling transformation diagrams for various Cr-Mo steels are shown in Figures 4, 5, 6, and 7. The effects of the additions of vanadium, titanium, and boron to the 2 1/4Cr-1Mo and 3Cr-1Mo alloys on the continuous cooling transformation behavior are shown in Figures 4 and 5 by the superposition of the continuous cooling transformation diagrams for the unmodified and modified materials.

The 2 1/4Cr and 3Cr continuous cooling transformation diagrams, Figures 4, 5 and 6, give clues to the fact that the resulting microstructures under various welding conditions may be complex. Depending on the degree of homogenization and cooling rate (related to the heat input and preheat for a given process and material thickness), the on-cooling transformation microstructures in the weld HAZ may consist of martensite, mixed martensite and bainite, or bainite coupled with retained austenite. However, the continuous cooling transformation diagram for the V-Nb modified 9Cr, Figure 7, indicates that the transformation microstructure will be primarily martensite, martensite + austenite, or martensite + austenite + carbide for cooling rates faster than 11C^{o}/min. (20F^{o}/min.) which is slower than that expected for the usual welding conditions employed in pressure vessel construction.

The microstructure of the 2 1/4Cr and 3Cr steels may be further complicated by the formation of martensite-austenite islands (a martensite-austenite constituent). The formation of a martensite-austenite

	C	Si	Mn	P	S	Cr	Mo	V	Ti	B	Austenitizing Temperature
2¼Cr-1Mo-V-Ti-B	.10	.02	.51	.005	.005	2.20	.94	.30	.022	.0023	950°C (1742°F)
2¼Cr-1Mo	.10	.34	.48	.017	.013	2.18	.96	–	–	–	920°C (1688°F)

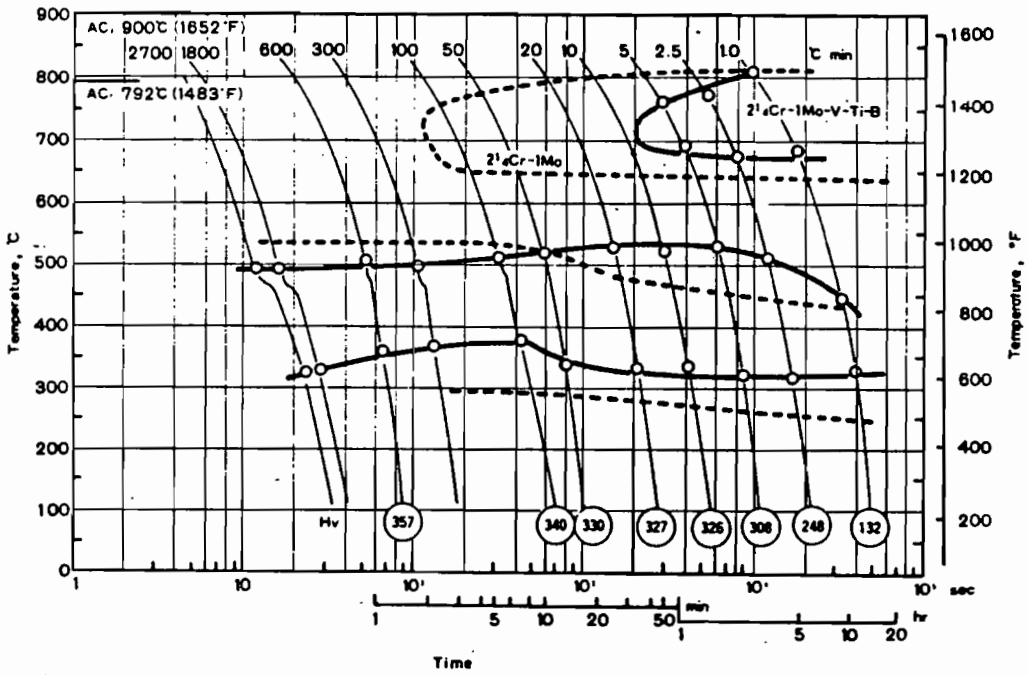

Figure 4. Continuous cooling transformation diagrams for V-Ti-B-modified 2 1/4Cr-1Mo steel and standard 2 1/4Cr-1Mo steel.

Source: T. Ishiguro, et al., A 2 1/4Cr-1Mo Pressure Vessel Steel with Improved Creep Rupture Strength, ASTM-STP 755, Application of 2 1/4Cr-1Mo Steel for Thick Wall Pressure Vessels, Sangdahl and Semchyshen, eds., American Society for Testing and Materials, Philadelphia, 1982.

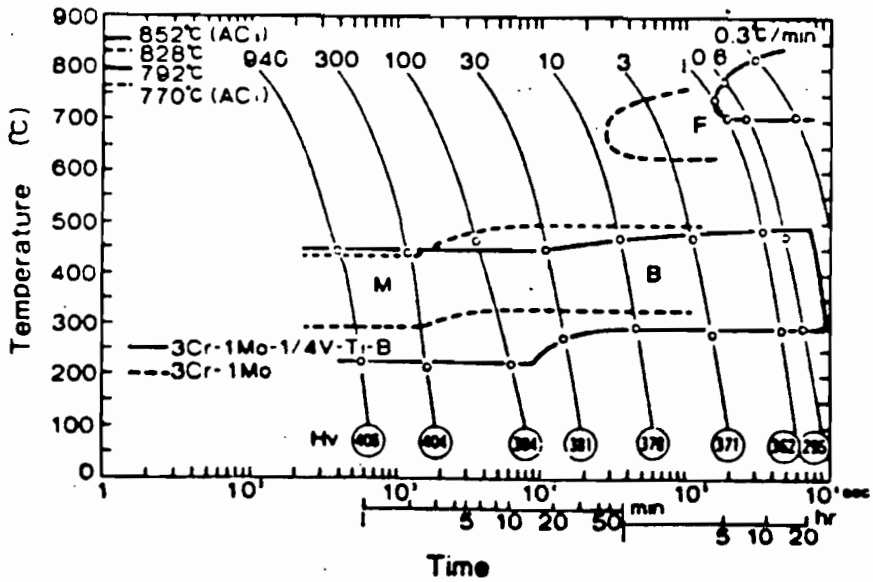

Figure 5. CCT diagrams of a 3Cr-1Mo and a 3Cr-1Mo-1/4V-Ti-B steels.

Source: Ishiguro, T., Murakawi, Y., Ohnishi, K. and Watanabe, J. A 2 1/4Cr-1Mo Pressure Vessel Steel with Improved Creep Rupture Strength, ASTM-STP 755, Application of 2 1/4Cr-1Mo Steel for Thick Wall Pressure Vessels, Sangdahl and Semchyshen, eds., American Society for Testing and Materials, Philadelphia, 1982.

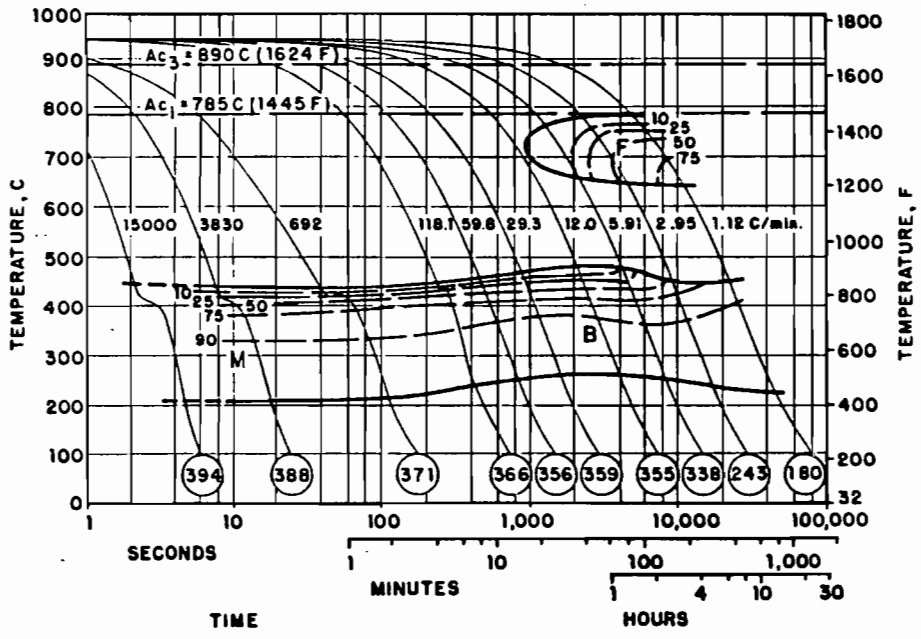

Figure 6. CCT diagram for commercial heat of 3Cr-1.5Mo steel (Heat A9394) Austenite grain size: ASTM No. 5/6.

Source: Wada, T. and Cox, T.B., A New 3Cr-1.5Mo Steel for Pressure Vessel Applications, MPC-21 Research on Chrome-Moly Steels, American Society of Mechanical Engineers, 1984, pp. 77-94.

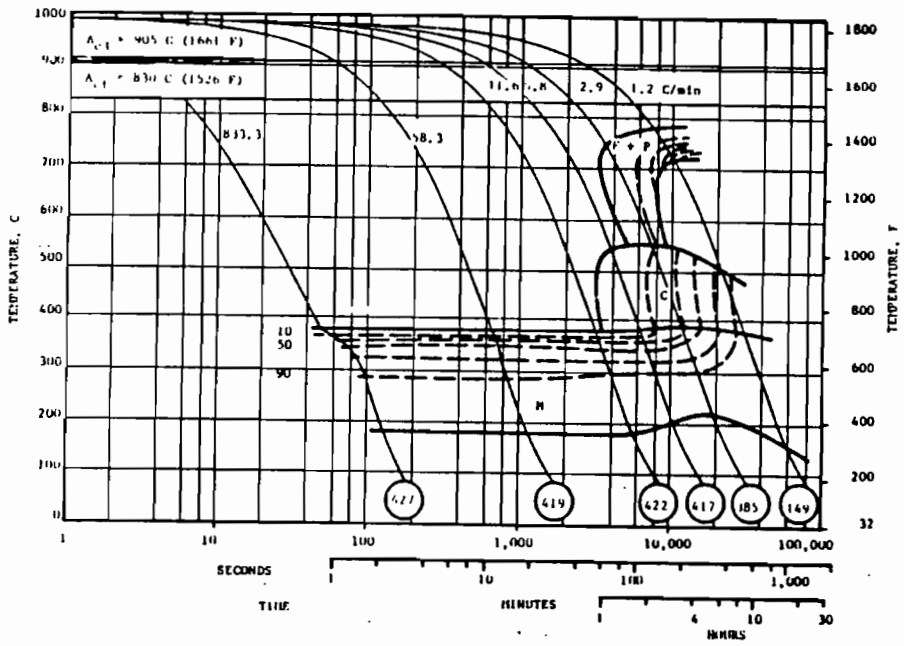

Figure 7. CCT diagram of heat XA 3619, 9Cr-1Mo-0.2V-0.1Nb steel. Austenite grain size: ASTM No. 9.

Source: Wada, T., Climax Molybdenum Company Report J-4617, Climax Molybdenum Company, 1980.

constituent is due to the partitioning of carbon to the austenite during the bainite transformation reaction resulting in locking of dislocations which prevents the shear transformation from occurring[26] or the stabilization of the austenite.[27,28] The last austenite present can be highly enriched in carbon. Carbon contents of the martensite-austenite constituent have been reported by Biss and Cryderman[28] to exceed 0.5 wt%C in a nominal 0.15%C alloy and to be approximately 3 at%C (approximately 0.7 wt%C) in a series of 0.3%C-3Cr-0.5Mo as shown by Thomas et al.[28]

Biss and Cryderman[27] found that slow cooling rates enhanced formation of the martensite-austenite constituent by allowing carbon to diffuse away from the ferrite-austenite interface into the austenite. However rapid cooling rates resulted in higher ferrite-austenite interface carbon content due to carbon diffusion being slower than interface advancement. This results in enhanced cementite precipitation and suppression of the martensite-austenite constituent. Economopoulos and Habraken[26] found that the presence of the martensite-austenite constituent was associated particularly with massive, or granular, bainitic structures formed at slow cooling rates. The cooling rate dependence of martensite-austenite constituent formation probably accounts for the inability of Richey[25] to detect any martensite-austenite constituent in his study of the transformation characteristics of 2 1/4Cr-1Mo steels under simulated welding conditions. However, it is to be noted that Thomas et al.[28] detected thin films of retained austenite along martensite laths by TEM examination. It was claimed that the retention of austenite was due to carbon redistribution during the martensite reaction and that this

diffusion of C was possible due to the high M_s temperature, 300°C (572°F) or higher, and the time to cool through the temperature range for martensite formation.

The as-welded HAZ transformation microstructures may undergo significant changes during subsequent heat treatment. Baker and Nutting[29] have shown that the types of carbides present in 2 1/4Cr-1Mo are dependent on starting microstructure, heat treatment and time at the heat treatment temperature. For bainite and martensite the general sequence for carbide precipitation was found to be:

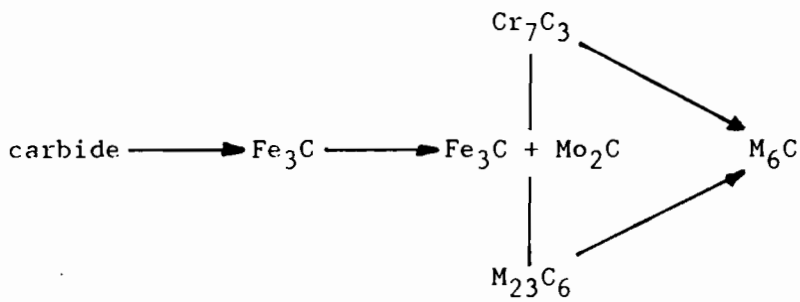

However, in proeutectoid (polygonal) ferrite, formed during slow cooling from the austenitizing temperature, the precipitation sequence during tempering was significantly different. The precipitation sequence in ferrite was found to be:

$$Mo_2C \longrightarrow M_6C$$

Mo_2C, the carbide conferring the greatest resistance to creep deformation, was found to be more stable in ferrite than in the initial microstructures consisting of martensite or bainite. In the martensitic and bainitic microstructures $M_{23}C_6$ grew at the expense of Mo_2C resulting in a degradation of the creep properties with increasing tempering temperature or time at a tempering temperature.

Because of the stability of Mo_2C within the ferrite, Baker and Nutting recommended the use of normalized and tempered 2 1/4Cr-1Mo rather than quenched and tempered 2 1/4Cr-1Mo. However, the presence of proeutectoid ferrite is generally regarded as unfavorable due to its low strength and poor toughness. Current alloy development reflects the need to avoid the formation of ferrite in the microstructure during cooling by making increased hardenability one of the principle criteria in alloy design.[3]

Modification of the 2 1/4Cr and 3Cr alloys by the addition of vanadium results in the precipitation of finely dispersed, slow growing V_4C_3 upon tempering or post weld heat treatment.[30] The precipitation of V_4C_3 occurs directly from the matrix and, unlike Mo_2C, is not dependent on the formation of any other carbides. Vanadium has also been reported to be present in Mo_2C with a metal atom ratio of up to 0.3 in alloys containing more than 0.1%V. Vanadium in Mo_2C results in stabilization of the Mo_2C.[31] The combined effects of precipitation and stabilization result in vanadium being one of the most potent elements in promoting creep resistance.

The nature of carbide formation in the 9Cr-1Mo alloys is substantially different. The general sequence of carbide formation is:[32]

$$Fe_3C \longrightarrow M_7C_3 \longrightarrow M_{23}C_6$$

The addition of niobium and vanadium may alter the kinetics of precipitation and growth of carbides in the 9Cr-1Mo alloys. The presence of niobium and vanadium results in the precipitation of both niobium and vanadium rich MC type carbides.[32] These MC type precipitates, present in a fine, dispersed, form may act as nucleation sites for the precipitation of $M_{23}C_6$ in a fine, dispersed form.[33] The presence of vanadium carbides of

the V_4C_3 or VC type was not found in 9%Cr-0.2%C steels with 0.4%V and 0.97%V by Seal and Honeycombe[34], but it was shown that the presence of vanadium in the alloy restricts the diffusion of chromium in ferrite reducing the rate of carbide growth. This results in a lower rate of softening and minimizes the loss of strength upon tempering or post weld heat treatment.

The effect of vanadium in restricting the mobility of chromium may be an important factor in HAZ softening that occurs in the vanadium-niobium modified 9Cr-1Mo materials. If, during temperature excursions into the intercritical range, chromium mobility in the austenite is restricted while carbon partitions to the austenite, a more rapid rate of tempering may occur during PWHT in the subsequently transformed martensite.

Two factors should be evident from the above discussion of transformation characteristics and resulting microstructure. Since the continuous cooling transformation diagrams are important to the understanding of properties and potential cracking susceptibility, there exists a need to determine the continuous cooling transformation diagrams for welding conditions as the development of the Cr-Mo alloys continues. Also, since the possible role of partial austenite transformation, due to temperature excursions into the intercritical temperature region, on HAZ softening has not been previously addressed, a need exists to evaluate the effect of partial transformation on HAZ softening.

Weldability

The ability of a material or combination of materials to be welded under fabrication conditions into a specific suitably designed structure

and to perform satisfactorily in intended service is defined as its weldability[35]. The concept of weldability requires the careful consideration a large number of variables including the composition and mechanical properties of base metal, welding consumables, energy input, welding sequence, joint design and structure constraint[36]. One of the most common considerations assessing the weldability of a material is whether or not it will be free from cracking under imposed design and fabrication conditions. Coe[37] has drawn a clear distinction between cracking which occurs during service and that which takes place during or shortly after the welding operations. The former is not dealt with in this review but the latter, which may be divided into five categories, is the prime focus in this work:

1. Solidification cracking (weld metal hot cracking)
2. Liquation cracking (HAZ hot tearing)
3. Lamellar tearing
4. Hydrogen induced cracking (HAZ delayed cold cracking)
5. Reheat cracking (post weld heat treatment cracking)

Solidification cracking occurs upon solidification when solute redistribution occurs and both impurities and intentional alloying elements are segregated in concert with the development of solidification substructure. The segregation of these elements lowers the effective solidus temperature of the material in the substructure and grain boundaries and may result in the formation of intergranular or interdendritic film of liquid. These films may not be capable of supporting contractional stresses induced by thermal contractions and a crack may form.

Liquation cracking occurs when partial melting (liquation) takes place near the fusion boundary of the weld. This liquated region is unable to accommodate contractional stresses associated with the weld thermal cycle and a crack develops.

Lamellar tearing occurs in the base metal of a weldment and is the result of low base plate ductility combined with high localized stresses. This form of cracking is associated with restrained corner or "tee" joints, particularly in thick section plate where the fusion boundary of the weld is parallel to the plate surface.

The postulated mechanisms responsible for the first three types of cracking are well accepted and have been confirmed by direct observation. In the case of hydrogen assisted cracking and post weld heat treatment cracking, no single unifying theory has been postulated to explain the presence of cracks under various condition. Because HAC and PWHT cracking are currently not nor may well never be understood in a fundamental manner, this review is aimed towards examining these two types of cracking on a practical welding basis with emphasis on governing factors and necessary precautions.

Hydrogen Assisted Cracking (HAC)

Hydrogen assisted cracking is not confined to welding but may occur in steel during manufacturing, fabrication, or in service. When cracking occurs as a result of welding the cracks are situated either in the HAZ of the parent metal or in the weld metal itself. Cracks in the HAZ are usually situated at the weld toe, the weld root, or in the underbead position as shown schematically in Figure 8 for fillet welds and butt

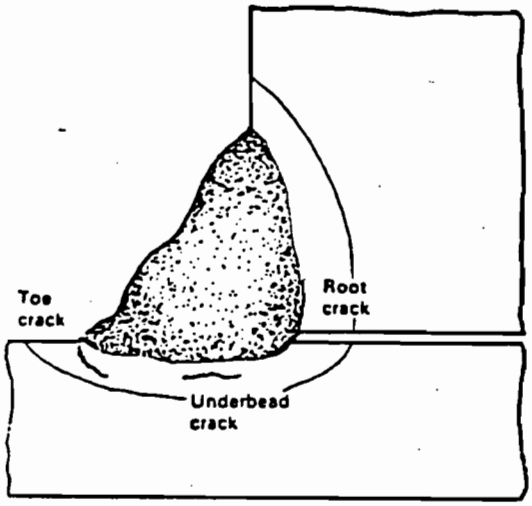

(a)

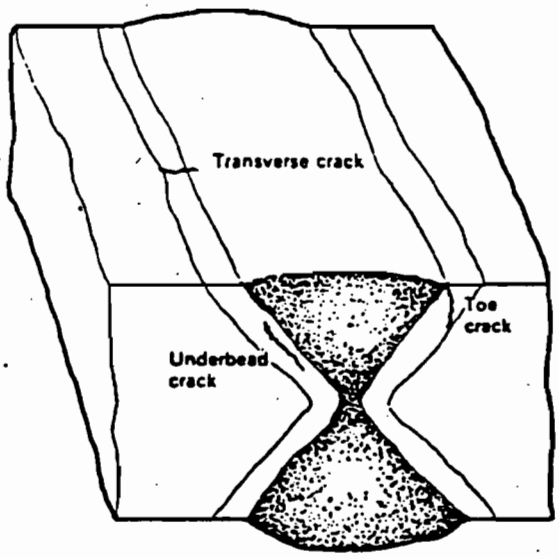

(b)

Figure 8. Heat-affected zone cracks. (a) Fillet weld, (b) Butt weld.

Source: Coe, F. R., Welding Steels Without Cracking, The Welding Institute, 1973.

welds. Usually in the fillet welds the HAZ cracks are oriented along the weld length, but in butt welds subsurface cracks can be transverse to the weld. Intergranular, quasicleavage, or microvoid coalescence fracture modes have all been observed in hydrogen cracks. Beachem[38] has shown that the operating fracture mode depends upon microstructure, the crack-tip stress intensity and the concentration of hydrogen.

As outlined by Coe[39], HAC occurs when the following four conditions occur simultaneously:

1. Hydrogen is present;
2. Tensile stress acts on the weld;
3. A susceptible microstructure is present;
4. A low temperature is reached.

Hydrogen is absorbed by the weld metal from the arc during welding. Although much of the hydrogen may escape during cooling, some may diffuse into the HAZ and the parent metal. The amount diffused depends on the initial amount absorbed, size of the weld and decreasing solubility (Figure 9). Hydrogen is dissociated into atomic hydrogen (H^+) in the weld arc and is dissolved in the metal as an interstitial constituent or as recombined hydrogen gas located in traps. The interstitial solubility of hydrogen in molten steel is governed by Sievert's law[40]:

$$\%[H] = K\sqrt{P_{H2}}$$

where %[H] is the percent of hydrogen dissolved in the molten steel, K is a constant and P_{H2} is the partial pressure of hydrogen in the atmosphere above the molten steel. In steel, hydrogen may also be trapped at grain boundaries, carbides, non-metallic inclusions, dislocations and microvoids. According to Lancaster[41], the total concentration of hydrogen in the traps

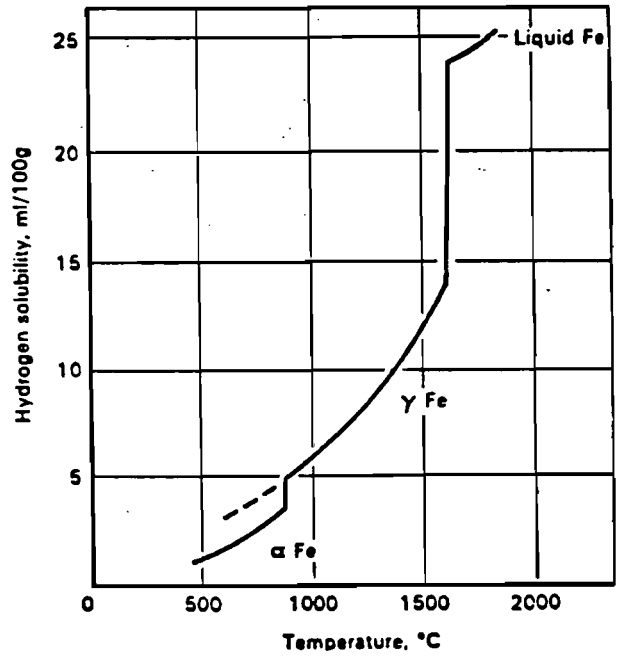

Figure 9. Solubility of hydrogen in weld metal.

Source: Coe, F. R., Welding Steels Without Cracking, The Welding Institute, 1973.

may be up to 10^4 times the interstitial value. The portion of hydrogen which diffuses out of the weld at room temperature is known as diffusible hydrogen and is expressed as ml/100g of deposited metal. Typical weld hydrogen levels range from 30ml/100g of deposited metal in shielded metal-arc covered electrode welds to 2ml/100g of deposited metal in gas shielded metal-arc welds.

Hydrogen is introduced into the arc atmosphere by hydrogen present in the consumables or hydrogen present on the surface of the material to be welded. Coe[39] described the principal sources of hydrogen in welding consumables as:

1. Moisture in electrode coatings or in the fluxes;
2. Any hydrogenous compound in the coating or flux;
3. Oil, dirt, and grease on the surface or trapped in welding wires and electrode wires.

Coe also described the principal sources of hydrogen from the material to be welded as:

1. Oil, grease, dirt and paint on the weld surface;
2. Degreasing liquids employed to clean welding surfaces.

As the weld cools, stresses are developed as a result of thermal contraction and these stresses must be accommodated as strain in the weld. The stresses tend to be concentrated at the toe and root of the weld and at inclusions or any other defect which acts as a notch. Hydrogen appears to lower the stress level at which cracking at the notch occurs.

The region of the HAZ adjacent to the fusion zone experiences a temperature sufficient to produce a coarsened grain size which is more

hardenable and less ductile than regions further away from the fusion boundary. The greatest risk of cracking is therefore in the coarsened region.

As the temperature of the weld decreases after welding the rate of diffusion of hydrogen decreases, thus reducing the amount of hydrogen removed from the weld. As shown in Figure 10, this effect is particularly marked in the range of 68 to 300°F (20 to 150°C). Preheat slows down the cooling rate and allows more time for the escape of hydrogen.

Theory of Hydrogen Assisted Cracking

Although much research, time and effort has been devoted to determine the exact cause and nature of hydrogen assisted cracking in both welding and other metallurgical fields, there is presently no one unifying theory which explains precisely how the presence of hydrogen within a metal structure leads to the formation of cracks under some circumstances and not in others. According to Bernstein[42] all the proposed theories of the role of hydrogen fall into one or more of four general categories:

1. Pressure;
2. Surface adsorption;
3. Binding energy;
4. Dislocation mobility modification.

The oldest, and until recently, the most popular of these theories, has been the pressure theory which was first proposed by Zapffe and Sims[43]. According to this theory molecular hydrogen precipitates into pre-existing mosaic rifts in the lattice resulting in high internal pressures and subsequent failure along mosaic boundaries.

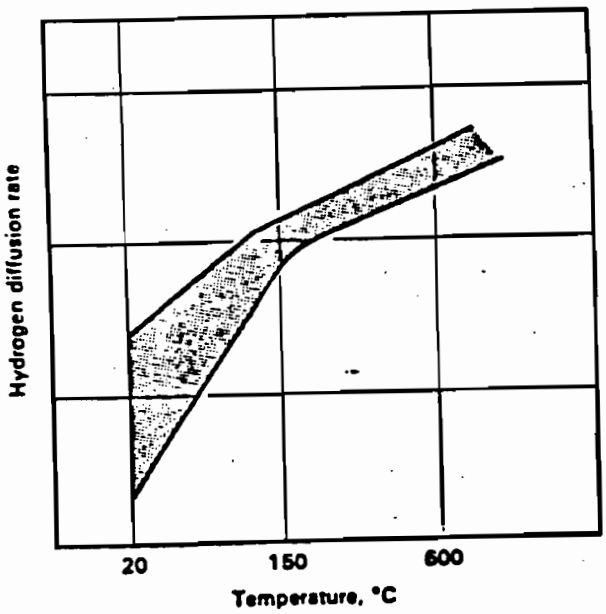

Figure 10. Diffusion rate of hydrogen through ferritic steel.

Source: Coe, F. R., Welding Steels Without Cracking, The Welding Institute, 1973.

In the surface adsorption theory first proposed by Petch and Sables[44], hydrogen upon precipitation from the lattice is adsorbed on the surface of the internal lattice imperfections and microcracks. According to this theory the surface energy at the crack nucleus would be reduced and a lower stress could extend the submicroscopic rift into a major catastrophic crack.

The pressure theory and the surface adsorption theory were advanced before the exact nature of hydrogen cracking was recognized. Both theories were inadequate in explaining many observed details of delayed brittle fracture. For example, in some cases the effect of hydrogen in steel can be completely removed by baking[45]. If the embrittlement of the steel by hydrogen was the result of hydrogen trapped in the microscopic voids, it is difficult to explain how at low baking temperatures this mechanism could operate.

Troiano[46] proposed a cracking theory based on the stress induced diffusion of hydrogen in an effort to more fully explain observed cracking behavior. In this theory, hydrogen distributed in a matrix will diffuse to the area of highest triaxial stress just ahead of a crack tip. When sufficient hydrogen is concentrated in this region a crack will initiate. The hydrogen is considered to reduce the cohesive strength of the lattice by interacting with the electron structure in a way as to lower the binding energy.

The modification of dislocation mobility model of HAC proposed by Beachem[38], unites parts of the previous cracking models to explain the observed decrease in microscopic plasticity and changes in fracture mode associated with some forms of HAC. This model suggests that the presence

of sufficiently concentrated dissolved hydrogen in the lattice just ahead of the crack tip unlocks dislocations, allowing them to multiply or move at reduced stresses. This process aids whatever deformation process the microstructure will permit (intergranular, quasicleavage or microvoid coalescence) and thus explain various fracture features observed in HAC.

Prevention of Hydrogen Assisted Cracking

Crack avoidance in Cr-Mo steels must be accomplished by hydrogen and temperature control. Low hydrogen welding processes and procedures must be used in fabrication of Cr-Mo steels. Temperature control includes both preheat and post weld heating methods of preventing HAC. The general effects of preheating have been summarized by Coe[37] as follows:

1. Reducing cooling rate in the HAZ to produce softer and less susceptible microstructures;
2. Allows "self" tempering of martensite;
3. Promote diffusion of hydrogen away from the HAZ after welding.

Because of the high hardenability of Cr-Mo steels, preheat has little effect on their microstructure and hardness. Apblett et al.[47] showed that in the 2 1/4Cr-1Mo material, softer transformation products could not be produced by increasing preheat temperature (within practical limits). Preheats as high as 600°F (315°C) resulted in only a minor decrease in the maximum HAZ hardness.

In Cr-Mo and other steels, preheat increases the rate of diffusion of hydrogen and thus accelerates its removal from the weld. Preheat requirements are related to chemical composition and thickness (Table 1).

Table 1. Recommended minimum preheat temperatures for welding chromium -molybdenum steels.

Steel[a]	Thickness, in. (mm) Up to 0.5 (13)	0.5 to 1.0 (13 to25)	Over 1.0 (25)
1/2Cr-1/2Mo 1Cr-1/2Mo 1-1/4Cr-1/2Mo	100°F (38°C)	200°F (93°C)	300°F (149°C)
2Cr-1/2Mo 2-1/4Cr-1Mo	150 (66)	200 (93)	300 (149)
3Cr-1Mo	250 (121)	300 (149)	400 (204)
5Cr-1/2Mo 7Cr-1/2Mo 9Cr-1Mo	400 (204)	400 (204)	500 (260)

[a]Maximum carbon content of 0.15%. For higher carbon content, the preheat temperature should be increased 100° to 200°F. Lower preheat temperatures may be used with gas tungsten arc welding.

Source: "Chromium-Molybdenum Steels," Welding Handbook, 7th Edition, Vol. 4, Chap. 1, American Welding Society, 1983.

As thickness and alloy content increases, the preheat temperature to guard against cracking also increases. Carbon content is the most important factor in establishing preheat temperatures. The presence or absence of free ferrite in the structure is a secondary consideration. To keep welding problems to a minimum, Cr-Mo steels are usually manufactured with a maximum carbon content of 0.15%. In addition to alloy content and material thickness, the mass of the joint and degree of restraint must also be considered when determining preheat temperatures.

When preheat cannot remove sufficient hydrogen to prevent cracking, a weld interpass temperature or post heating temperature high enough to avoid cracking must be held for a sufficient length of time to allow hydrogen to diffuse out of the HAZ before the weld is allowed to cool to ambient temperature. The decision as to post heat temperature and time must be based on consideration of the hydrogen concentration at the end of welding and a critical concentration below which cracking will not occur when the weld cools to ambient temperature. There is presently little information on critical hydrogen concentrations for Cr-Mo steels and post heating procedures are generally based on practical experience[48].

Sometimes, for various reasons, it is impossible to preheat or post heat Cr-Mo steels which are to be welded. Under these conditions the only alternative is to use a combination of welding process and consumable which produces a weld metal that is insensitive to hydrogen and has a high solubility for hydrogen, thus preventing the introduction of hydrogen into the crack sensitive HAZ. This can be best achieved by employing austenitic weld metal. At room temperature the austenitic weld metal has a higher solubility for hydrogen and a lower diffusivity than the Cr-Mo HAZ. Thus,

any hydrogen entering the HAZ from the weld can diffuse away faster than it is introduced and there is less chance of the hydrogen concentration reaching a critical level.

Compositional and Microstructural Effects on Hydrogen Assisted Cracking

The HAZ microstructure is one of the most important factors in determining the HAC susceptibility of any steel. Linnert[45] has listed, in order of increasing propensity to HAC, six microstructures commonly found in the HAZ of steel welds:

1. Ferrite and carbides (e.g., pearlite);
2. Bainite;
3. Bainite mixed with martensite;
4. Martensite;
5. Martensite with some ferrite;
6. Martensite with internal twinning.

The microstructure produced in any steel weld is dependent upon the cooling rate through the transformation temperature range of austenite, the austenite grain size and composition (hardenability). The cooling rate is governed by energy input, plate thickness, joint geometry and preheat temperature.

Cr-Mo steels are hardenable in the HAZ under normal welding conditions. The weld HAZ microstructure of a Cr-Mo steel is generally dependent on the alloy content. The weld HAZ of the more common types of Cr-Mo steels can be classified as follows:

1. Low alloy bainitic and/or martensitic microstructures (0.5% to 5% Cr);

2. Martensitic-predominantly martensitic microstructure with some delta ferrite present (5% to 12% Cr);
3. Duplex-martensitic-ferritic microstructure (9% to 12% Cr and 2% Mo).

Smith and his associates[49] have shown that the HAZ structure of 2 1/4Cr-1Mo steel can be classified as follows:

1. Grain coarsened region;
2. Grain refined region;
3. Region of partial transformation;
4. Subcritical region.

The grain coarsened region was found to consist of bainite and/or autotempered martensite.

As the Cr content of Cr-Mo steel increases, the HAZ microstructures change from a bainitic/bainitic-martensitic microstructure to a martensitic-ferritic or fully martensitic microstructure. When the microstructure becomes more martensitic, the HAC susceptibility also increases. The increase in cracking susceptibility of the higher alloy Cr-Mo steels is reflected in Table 1.

Another important factor in determining the HAC sensitivity of Cr-Mo steels is the HAZ hardness. As the hardness of the HAZ increases the susceptibility to HAC increases. In Cr-Mo steels the hardness of the HAZ is primarily dependent on the carbon content[50]. The reduction of C content in martensitic Cr-Mo steels in an effort to improve weldability results in an increase in the amount of delta ferrite present in the normalized and tempered microstructure. The resulting ferritic/martensitic microstructure is characteristic of the duplex Cr-Mo materials.

In addition to affecting the microstructural characteristic of Cr-Mo steels, both Cr and C, as well as Mo and Ni, lower the temperature at which the transformation of austenite to martensite starts and is completed (M_s and M_f temperatures)[45]. From the standpoint of HAC sensitivity it is undesirable to decrease martensitic transformation temperatures because as the martensite transforms the solubility of hydrogen in the matrix is decreased, and at the lower transformation temperatures there is little chance for the hydrogen to diffuse out of the HAZ. Higher transformation temperatures also permit some tempering of martensite to occur which reduces hardness and lowers residual stresses.

Richly alloyed Cr-Mo steels may, on cooling, under welding conditions retain austenite. The retained austenite is able to absorb hydrogen and act as a sink to reduce the amount of hydrogen that can be absorbed by martensite and thus prevent hydrogen embrittlement of the martensite.

Weldability Testing of Chromium-Molybdenum Steels

Although most of the applications of Cr-Mo steels require welding, there is little published work on the weldability of these steels prior to 1969[51]. Smith et al.[49] were some of the first researchers to investigate the HAZ of both stabilized and standard composition 2 1/4Cr-1Mo. The grain coarsened region of samples experiencing a welding thermal cycle were metallographically examined and it was found that the grain coarsened region of the standard material consisted of martensite, while the Nb stabilized material exhibited upper bainite in the HAZ and was less crack sensitive. Thus, the results of this investigation suggested that the

stabilized 2 1/4Cr-1Mo material had improved weldability over the unstabilized material.

Colombe[52] and his associates employed the implant test to compare the relative cracking susceptibilities of stabilized and standard composition 2 1/4Cr-1Mo. The implant test[53] is a weld cracking test that applies a controlled stress on the weld HAZ and evaluates the cracking susceptibility by means of mechanical test parameter. In this test, an actual weld is made over a notched cylindrical test specimen that is inserted into a hole in a test plate (Figure 11). Hydrogen is added to the weld by controlling the arc atmosphere. After the sample cools to a designated temperature (usually 300°F (150°C)), it is stressed to simulate the actual restraint that occurs in a weld during welding. If the specimen does not rupture within 24 hours the test is discontinued. The highest stress level for which no fracture occurs in 24 hours is called the critical stress level. The critical stress level is regarded as a relative measure of the HAC susceptibility of a given material. Materials with a low cracking susceptibility have higher critical stress levels than materials with a high cracking susceptibility. It was the conclusion of Colombe et al. that the risk of HAC in the stabilized 2 1/4Cr-1Mo steel was less than that in the standard composition material.

Terai et al.[54] investigated the HAC susceptibility of standard composition 2 1/4Cr-1Mo-Nb employing both the Y-groove and U-groove restraint cracking tests. The Y-groove test and U-groove test are self restraint cracking tests used to determine the HAC susceptibility of welds. Both plate assemblies are shown in Figure 12. In these techniques, test welds are made at various preheats. The welds are allowed to cool to room

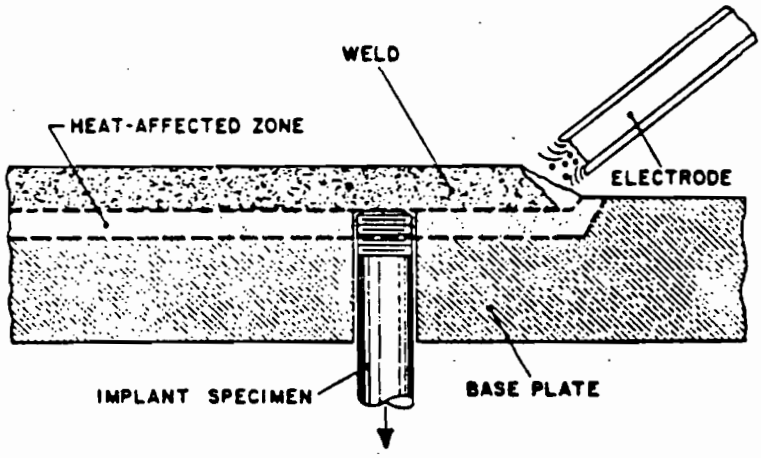

Figure 11. Implant test setup.

Source: Dickenson, D. W. and Ries, G. D., "Implant Testing of Medium to High Strength Steel - A Model for Predicting Delayed Cracking Susceptibility," Welding J., 58(7), 1979, pp. 205s - 211s.

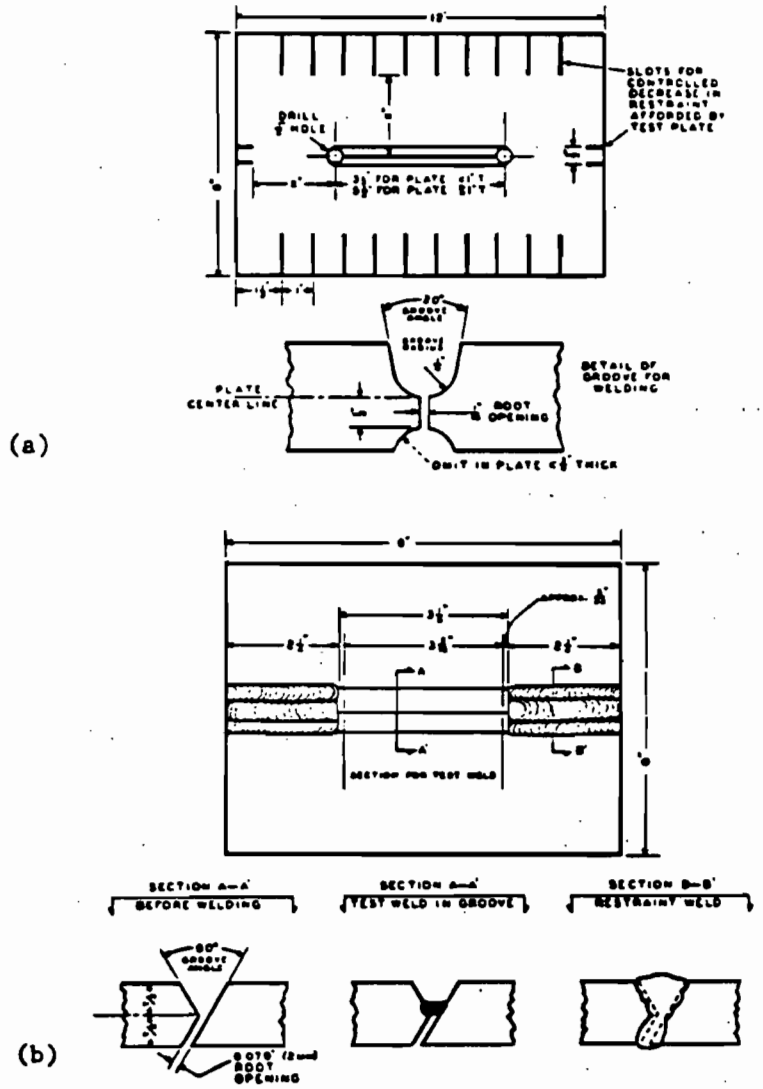

Figure 12. Hydrogen-assisted cracking restraint tests.
(a) U-groove, (b) Y-groove.

Source: Linnert, G. E., Welding Metallurgy, Vol. 2, American Welding Society, 1967.

temperature and sectioned to observe the location and percentage of cracking. The Y-groove test is better suited to evaluate the cracking susceptibility of the base metal while the U-groove is better suited to evaluate the cracking sensitivity of weld metals. The Y-groove test results of Terai et al. showed that the preheat temperature to prevent cracking in the stabilized 2 1/4Cr-1Mo material was 400°F (225°C), 45°F (25°C) higher than that of the standard composition 2 1/4Cr-1Mo material. In contrast the results of the U-groove test showed that the preheat temperature to prevent cracking in the standard composition material was 620°F (325°C), 45°F (25°C) higher than that for the stabilized material. The preheat temperature differences between the two test methods were considered to be small and it was concluded that the weldment crack sensitivity for the stabilized steel was equivalent to that of the standard composition material.

In summary, review of the current literature reveals that a surprisingly limited amount of information exists on the relative HAC sensitivity of Cr-Mo steels, although these materials have been fabricated by welding for a number of years. Most of the studies to date have concentrated on establishing the relative cracking sensitivity of only a few selected materials and little effort has been directed towards explaining the observed cracking behavior on the basis of compositional or microstructural differences. It is therefore apparent that a more broad based investigation of the relative HAC susceptibility of Cr-Mo steels is needed to more adequately address the effects of microstructure and composition on cracking sensitivity.

Postweld Heat Treatment Cracking

Post weld heat treatment (PWHT) cracking, also referred to as reheat or stress-relief cracking, is a problem that occurs in Cr-Mo steels containing less than 3% chromium.[55,56] Cracking is manifested by low rupture ductility and intergranular fracture along prior austenite grain boundaries, typically occurring in the coarse grained HAZ and occasionally in the weld metal, after an initially sound weldment has been subjected to a stress-relief heat treatment.[57] Heat-to-heat variations in stress-relief cracking, indicating a dependence on residual elements, add to the worrisome nature of this problem as bulk chemistry of an alloy may not be a reliable predictor of cracking susceptibility.[58] This type of cracking, if undetected prior to service, may lead to failure of pressure vessels and piping in service.[59]

Through 1975 the mechanism of PWHT cracking was thought to be related solely to the precipitation of alloy carbides and the plastic flow due to stress relaxation at the post weld heat treatment temperature. Temperature excursions experienced in the HAZ above 1200°C (2192°F) result in the rapid solution of carbides and grain growth. The rapid cooling associated with welding results in alloying elements and carbon being retained in martensitic or lower bainitic transformation products above the saturation limit. Subsequent reheating leads to precipitation of intragranular alloy carbides, particularly Mo_2C and V_4C_3, causing an increase in grain matrix strength. Thus, the ratio of the grain matrix strength to the grain boundary strength increases. The relaxation of stress at the post weld heat treatment temperature is accomplished primarily by creep induced plastic flow involving grain boundary sliding

which must be accompanied by general grain deformation if grain boundary cavitation or cracking is be avoided. However, when the grain matrix strength is increased by precipitation, deformation is restricted to the grain boundaries, the area of which has been minimized by grain growth. Although the total strain is small, the locally high strain concentration in the grain boundaries exceeds the ductility of the grain boundaries resulting in cavitation and rupture.[57,59-63]

The type and morphology of precipitates has been a topic of considerable research. Several investigators have contended that the most critical time in PWHT is during the formation of coherent or pre-precipitate clusters at about 500 to 550°C (932 to 1022°F) which corresponds to the maximum in secondary hardening.[62,64-68] Orr et al.[67] have noted that due to the strong lattice correpondance of Mo_2C with bainite or martensite, the nucleation energy is relatively low and therefore Mo_2C forms quickly as a finely divided slow growing precipitate. Swift et al.[62,64-66] have proposed that coherent precipitates, Mo_2C and/or V_4C_3, nucleate in the matrix and at dislocation jogs and intersections. Coherent Mo_2C yields a nonuniform, highly strained matrix with decreased dislocation mobility and dislocation locking and results in a reduction of the ability of the grain interiors in the coarse grained HAZ to plastically deform upon stress-relief.

Temperature is an important factor in that Mo_2C persists for more than 500 hours at 590°C (1100°F) without decomposition to more complex carbides and has a correspondingly long coherency duration. However, at 680°C (1250°F) coherency is quickly lost as evidenced by the formation of visible Mo_2C within one-half hour at temperature[66]. Another factor is the

presence of notches, either surface irregularities or internal defects, at which "stress relief cracking is almost invariably initiated."[60] The notches in the coarse grained HAZ are particularly detrimental, as they act as intense stress concentrators in the very region of the weld already under a high tensile stress and with a low ductility microstructure.[60,63,69,70] The notch acuity further inhibits deformation by the creation of a triaxial stress state.[66]

A carbide denuded zone has also been reported to exist adjacent to the grain boundaries.[31,60,63,71,72] These zones are apparently a result of depletion of alloying elements due to carbide precipitation in the grain boundaries. Several researchers have considered the carbide denuded zones to be detrimental as they provide a narrow soft region in which strain can accumulate preferentially.[72,30] However, Meitzner and Pense[70] found the presence of denuded zones did not contribute to stress-relief cracking, and Swift[66] found that although denuded zones were present they formed only at times beyond those corresponding to the minimum in ductility.

After 1975, interest in the heat-to-heat variability and the development of new techniques, particularly Auger spectroscopy, to study grain boundary compositions led to intense evaluation of residual element effects on stress-relief cracking.[60,61] Segregation of residual elements; phosphorous, sulfur, tin, and antimony, was found to play a critical role by causing embrittlement of grain boundaries.[73-75] The effects of grain boundary embrittlement due to impurity segregation and impurity interactions during precipitation are superposed on the matrix strengthening effects of coherent precipitation.[62] Hippsley et al.[76] have noted that grain boundary segregation of impurities can be due to

equilibrium segregation from the grain matrix or may be due to solute rejection from growing grain boundary carbides, the solubility of impurities being higher in the matrix material than in the carbides. Vinckier and Dhooge[73,75] state that loss of ductility caused by segregation during stress relief heat treatment is certainly a major factor in cracking but "that the true mechanism is almost certainly a combination of these two ideas (segregation and precipitation strengthening) and is more complex."

Other researchers have proposed additional factors that increase the intricacy of the previous PWHT cracking mechanisms. Vinckier[59] proposed that "the decomposition of martensite needles" during heating creates high localized strains at the grain boundary interfaces. These strains plus external restraint can result in the formation of microcavities, particularly when the matrix is strengthened by intragranular precipitation. Hippsley et al.[77] have proposed that segregation of less mobile, embrittling elements, such as phosphorous, tin, and antimony, occurs at elevated temperatures in a fashion similar to that proposed by Troiano[78] for hydrogen. Segregation is locally enhanced in regions of maximum triaxial stresses, such as at the root of a notch or in the region of a crack tip, by diffusion along the strain gradient. Dislocation pile ups at grain boundaries and grain boundary carbides plus the strain induced segregation of impurities reduce the cohesive strength of the grain boundaries and carbide-matrix interfaces sufficiently to allow the development of microcracks. Thus, according to Hippsley et al.[77], the factors involved in cracking are not only segregation and precipitation but also the amount of plastic strain, which for a given load increases as the yield strength falls with increasing temperature.

The necessary factors for stress-relief cracking to occur were summarized by Ito and Nakanishi[18]:

1. the material must have undergone a thermal cycle that results in solution of alloying elements and that retains the elements in solid solution after cooling,
2. grain growth must have occurred as a result of thermal cycling,
3. heat treatment between 450°C and 700°C (850°F and 1300°F) resulting in significant precipitation hardening,
4. grain strength and internal stress must exceed the strength of the grain boundaries,
5. a stress riser must be present to initiate cracking.

In addition to these five the material must be one that has a composition that is susceptible to reheat cracking in alloy content and residual or impurity elements.

Origin of Residual Stresses Responsible for Post Weld Heat Treatment Cracking[17,22]

Residual stresses are developed in the weld HAZ and fusion zone during cooling due to restrained shrinkage and transformation volume changes as a result of austenite decomposition. On-cooling, those areas of the base metal that experienced thermal expansion due to heating must contract or plastically flow. The bulk of the base metal which has experienced no significant heating (and therefore no decrease in strength) prevents or restrains the contraction of the cooling material. Above approximately 1200°F (650°C) the weld fusion zone and those regions immediately adjacent to the weld accommodate the thermal contraction by plastic deformation without developing any significant stress as the yield

strength is low above this temperature. Cooling below 1200°F (650°C) results in significant increases in yield strength with decreasing temperature. Plastic deformation only occurs when the stresses due to thermal contraction exceed the yield stress and therefore cooling to the preheat temperature results in increasing residual tensile stress concomitant with the increased yield strength in the fusion zone and HAZ. The resultant residual tensile stress occuring in the HAZ and fusion zone are in equilibrium with compressive stresses in the bulk of the base material.

Transformation stresses are a result of the volumetric expansion that occurs during the decomposition of austenite. The material being transformed attempts to expand but expansion is hindered by the cooler material not undergoing transformation. The material being transformed therefore experiences a compressive stress and the cooler material a tensile stress. If the transformation temperature is high the transformation stress will be overridden by the effects of subsequent bulk shrinkage. However, if the transformation temperature is low, the transformation stress will lower the overall tensile stress in the HAZ and fusion zone.

Superposition of the components of the residual stress developed during welding leads to an extremely complex final residual stress state. The coarse grained HAZ, that portion of the HAZ adjacent to the fusion zone, is under a significant tensile stress both in the direction of and perpendicular to the weld. This biaxial residual stress state as well as the unfavorable metallurgical characteristics of the grain coarsened zone helps explain the susceptibility of this region to PWHT cracking.

Microstructural Effects on Post Weld Heat Treatment Cracking

Meitzner and Pense[71] have found that martensite and lower bainite are more susceptible to stress-relief cracking than upper bainite although the authors state that the difference is probably due to precipitation processes rather than optically resolved microstructure. Ito and Nakanishi[18] also found that martensitic and lower bainitic microstructures are more susceptible than upper bainite. They related the increased susceptibility to the supersaturation of the bainitic and martensitic microstructures with alloying elements and carbon which results in intense secondary hardening. Debiez and Granjon[79] found that a "bainitic structure seems to be a little more susceptible to cracking than the martensitic" structure under implant testing. However, they do not state whether the bainitic microstructure obtained is upper or lower bainite.

Effects of Composition on Post Weld Heat Treatment Cracking

Meitzner[60] and Dhooge et al.[73], in extensive literature reviews indicate the effects of specific alloying elements. The elements generally considered to be detrimental to PWHT cracking are: carbon, vanadium, molybdenum (in concert with vanadium), columbium, aluminum and the residual elements: tin, antimony, arsenic and phosphorus. The effects of chromium, boron and titanium are not clearly defined. Nickel was found to be the one element that appears to have no effect on cracking. In general, the elements found to be deleterious are either those which promote the formation of carbides of the M_2C or M_4C_3 type or which are known to have general grain boundary embrittling effects.

In 1965 Nakamura et al.[80] attempted to determine the effect of alloy additions on cracking susceptibility in Cr-Mo steels. Variations in the

levels of chromium (0.1-1.5%), molybdenum (0.3-0.6%), nickel (0-3%), and vanadium (0-0.08%) resulted in the ΔG parameter:

$$\Delta G = \%Cr + 3.3(\%Mo) + 8.1(\%V) - 2$$

When ΔG is greater than zero the material is determined to be susceptible to PWHT cracking. In 1972, Ito and Nakanishi[18] extended the work of Nakamura. The alloying elements; manganese (0.5-1.4%), nickel (0.5-1.5%), chromium (0.5-1%), and vanadium (0.05-0.12%), were varied and additions of copper (0.15% and 0.26%), niobium (0.06%) and titanium (0.02% and 0.07%) were made to steels containing nominally 0.3% silicon and 0.5% molybdenum. This work resulted in the development of the cracking parameter, P_{SR}:

$$P_{SR} = \%Cr + \%Cu + 2(\%Mo) + 10(\%V) + 7(\%Nb) + 5(\%Ti) - 2$$

When P_{SR} is greater than zero the material is deemed to be susceptible to cracking. The applicable range of the P_{SR} parameter is limited to alloys containing less than: 2%Mo, 1.5%Cr, 1%Cu, and 0.15% V, Nb and Ti. Ito and Nakanishi also found that chromium contents in excess of 2% eliminated cracking.

Subsequent to development of the P_{SR} and ΔG parameters several investigators have found poor correlation with the parameters and actual susceptibility of different alloys. Pense et al.[81] found that ΔG was a poor predictor of cracking in A535-A, A517-F, and A543 steels. McMahon et al.[82] found that both P_{SR} and ΔG did not accurately predict cracking susceptibility in multiple heats of SA 533-B and SA 508-2. Also, many investigators[55,64-66,77,83-87] have found that 2 1/4Cr-1Mo alloys are susceptible to PWHT cracking although a chromium content of 2% or greater was considered to eliminate stress-relief cracking susceptibility by Ito and Nakanishi.[18]

McMahon et al.[82] have suggested using the CERL parameter with the addition of the percentage chromium in the alloy:

$$CERL = 0.2(\%Cu) + 0.44(\%S) + \%P + 1.8(\%As) + 1.9(\%Sn) + 2.79(\%Sb) + \%Cr$$

The greater the CERL+Cr value the greater the cracking susceptibility. This parameter clearly emphasizes the effects of embrittling elements over the effect of carbide formers. The authors state that individual alloy content will affect the necessary parameters and that increasing the carbide former content may necessitate their inclusion in a manner similar to that of the P_{SR} parameter. Similarly, in reviewing results of cracking susceptibility tests of 2 1/4Cr-1Mo weld metal, Boniszewski[88] recommended use of the MCF (metal composition factor) to rank cracking susceptibility. The MCF factor :

$$MCF = \%Si + \%Cu + 2(\%P) + 10(\%As) + 15(\%Sn) + 20(\%Sb)$$

combines the relative overall potency of grain boundary embrittling elements present in a material. An increase in the MCF factor was found to correlate with a decrease in rupture ductility as measured by elongation in hot tensile tests.

The recent work of Tamaki[56,89-91] attempts to determine the separate effects of chromium and molybdenum on PWHT cracking. His papers represent extensive work on materials of varying chromium (0-5%) and molybdenum (0.3-1.5%) contents. The effects of chromium and molybdenum, independently and in concert, were studied using a modified implant test. The modified implant test was employed to determine the minimum stress which would cause the specimen to fracture within 20 hours while postweld heat treating the specimen at a temperature of 600°C. The susceptibility to reheat cracking

was related to the magnitude of the critical stress to rupture ($\sigma_{AW-crit}$). The lower the minimum critical stress to cause rupture, the greater is the susceptibility to reheat cracking.

Alloys containing chromium over the range tested but low in molybdenum (0.25%) were found to be susceptible to cracking. The 1%Cr-0.25%Mo alloy showed the lowest critical stress for failure and therefore the greatest susceptibility to cracking. Increasing molybdenum at any level of chromium increased susceptibility, but the lowest critical stress for any particular molybdenum level occurred for alloys containing 1% chromium. These data from his studies are shown in Figure 13. Note that for low molybdenum contents (0.25% and 0.5%) when no chromium is present, no cracking occurred over the range of stresses employed indicating that these materials are not susceptible to stress relief cracking.

When the results are expressed as a function of chromium and molybdenum for different stress levels the evaluation shown in Figure 14 results. Susceptibility to PWHT cracking with a change in alloying element content is a maximum on these diagrams where the stress contours are closest together. Susceptibility for a particular alloy may be judged by the magnitude of the critical stress to failure ($\sigma_{AW-crit}$). The plotted data are divided into four regions labeled I, IIa, IIb and III (Figure 14). The materials in region I, those with less than 1%Cr and less than 0.5%Mo, are relatively insensitive to cracking. Materials in region IIa, comprised of alloys with 0-1%Cr and 0.5-1%Mo, have rapidly increasing sensitivity to cracking with increasing chromium or molybdenum content based on the relatively large decreases in the critical stress with small changes in

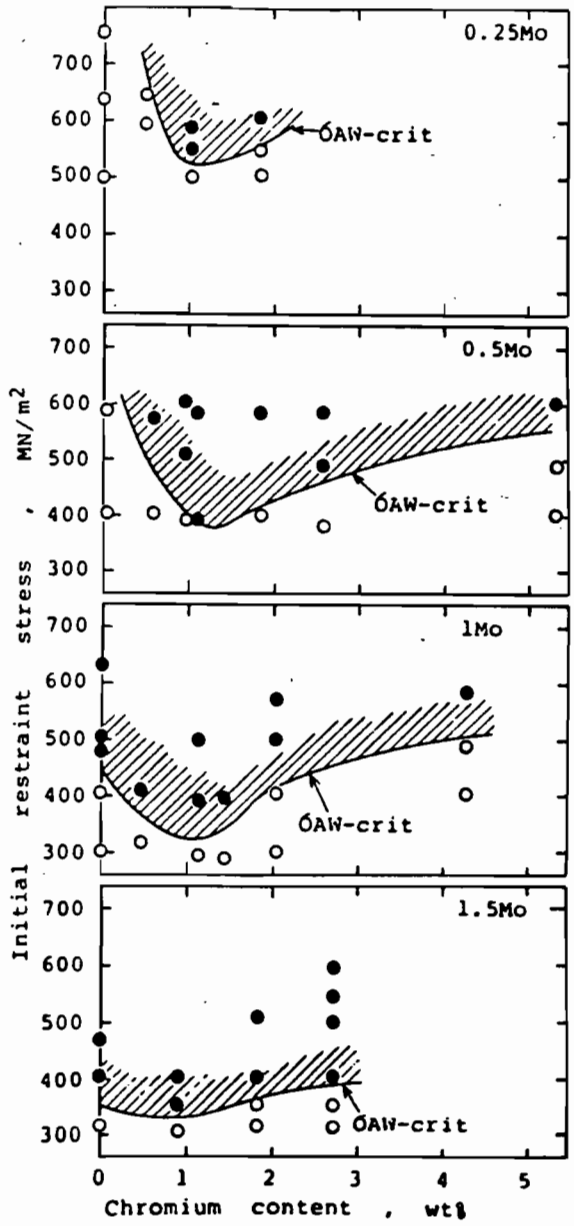

Figure 13. Effect of chromium on the critical restraint stress, $\sigma_{AW\text{-}crit}$

Source: Tamaki, K., and Suzuki, J., Effect of Chromium and Molybdenum on Reheat Cracking Sensitivity of Steels, Transactions of the Japan Welding Society, 15(1), 1984.

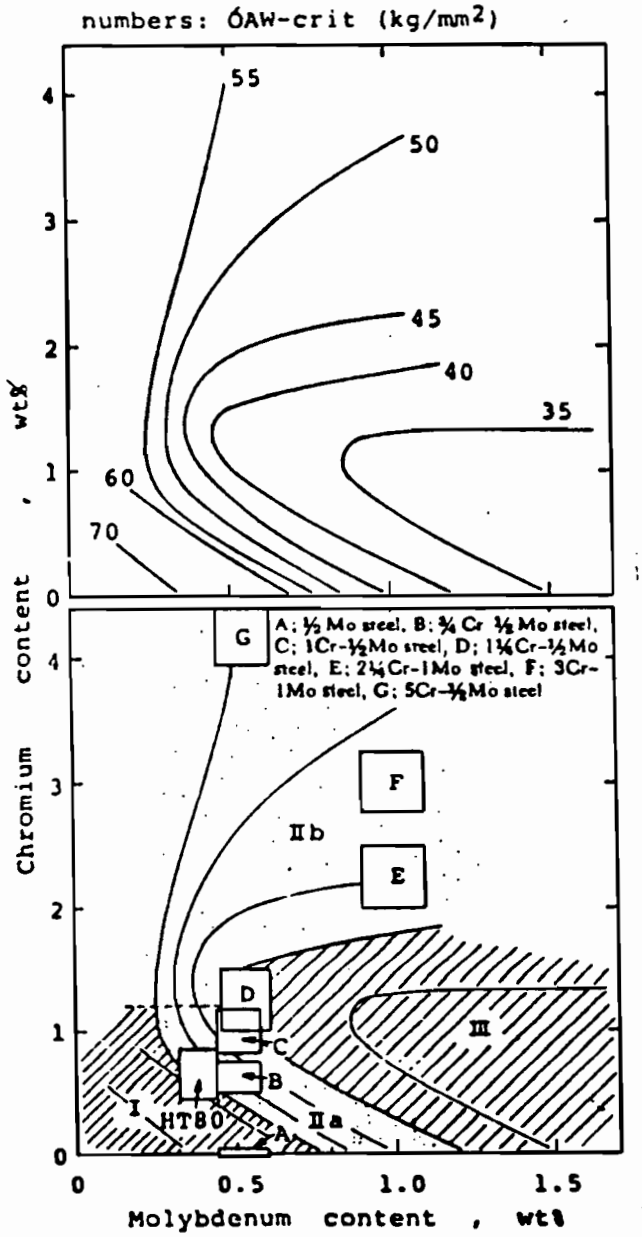

Figure 14. Contour lines of critical restraint stress ($\sigma_{AW\text{-}crit}$) shown on the Cr-Mo content diagram.

Source: Tamaki, K., and Suzuki, J., "Effect of Chromium and Molybdenum on Reheat Cracking Sensitivity of Steels," Transactions of the Japan Welding Society, 15(1), 1983.

alloy content. Region IIb, comprised of alloys with greater than 2%Cr and 0.5-1%Mo, characterizes behavior of decreasing sensitivity with increasing chromium content. Region III, comprised of alloys with approximately 1%Cr and greater than 1%Mo, represents the highest sensitivity to cracking. The Nakamura parameter[60] for PWHT cracking susceptibility, ($\Delta G>0$), was found to predict cracking principally in fields IIa and III extending somewhat in field IIb. The cracking parameter due to Ito[18] predicted cracking, ($P_{SR}>0$), principally in field IIa. (Note: these parameters are limited to chromium contents less than 1.5%.) Since fields IIa and III indicate the alloys of maximum reheat cracking sensitivity, the agreement is excellent, with Tamaki's diagrams being more discriminating than either index (fig. 15).

In order to discern the microstructural causes for the differences in cracking susceptibility for the various materials, Tamaki[91] undertook an extensive study of the carbides in the alloys using x-ray diffraction techniques of extracted carbides and transmission electron microscopy of carbide extraction replicas. It was found that the materials most susceptible to PWHT cracking showed the greatest fraction of M_2C type carbides after post weld heat treatment. With a smaller amount of M_2C, (or a larger amount of M_7C_3 and/or $M_{23}C_6$), the susceptibility to cracking decreased.

Figures 16 and 17 depict these results graphically. Figure 16 shows the relative amounts of carbides present for different alloys on a chromium vs. molybdenum content diagram with the curved lines being constant weight percent M_2C. Figure 17 superimposes these constant weight percent M_2C lines (solid lines-fig. 17) on the chromium vs. molybdenum content diagram

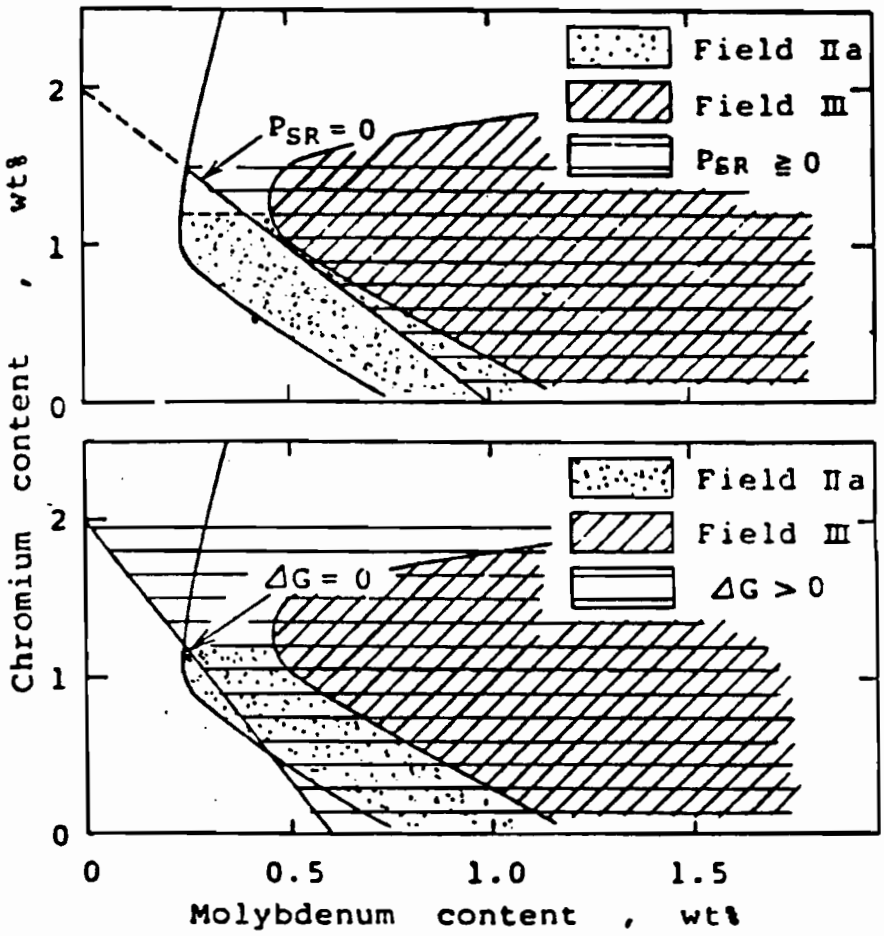

Figure 15. Comparison between the critical restraint stress ($\sigma_{AW\text{-}crit}$) and cracking sensitivity indexes, P_{SR} and ΔG.

Source: Tamaki, K., and Suzuki, J., Effect of Chromium and Molybdenum on Reheat cracking Sensitivity of Steels, Transactions of the Japan Welding Society, 14(2), 1983.

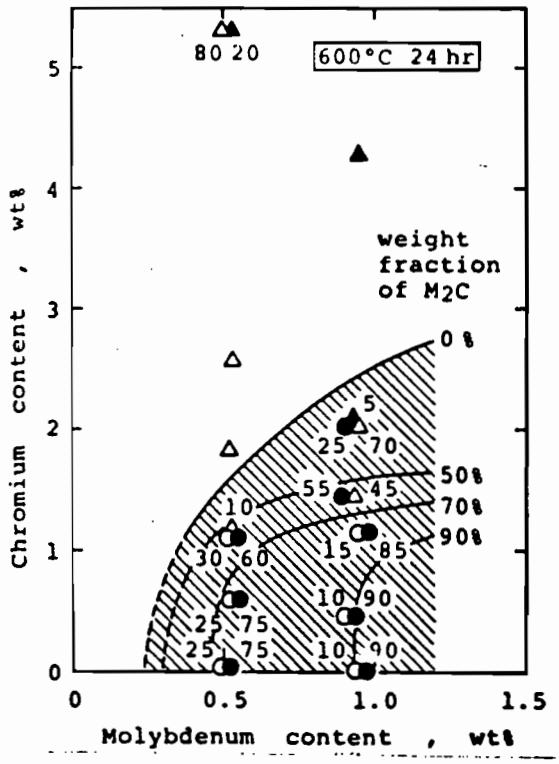

Figure 16. Carbides present in Cr-Mo steels tempered at 600°C for 24 hours. (○M_3C, ●M_2C, △M_7C_3, ▲$M_{23}C_6$)

Source: Tamaki, K., Suzuki, J., Nakaseko, Y., and Tajiri, M., Effect of Carbides on Reheat Cracking Sensitivity, Transactions of the Japan Welding Society, 15(1), 1984.

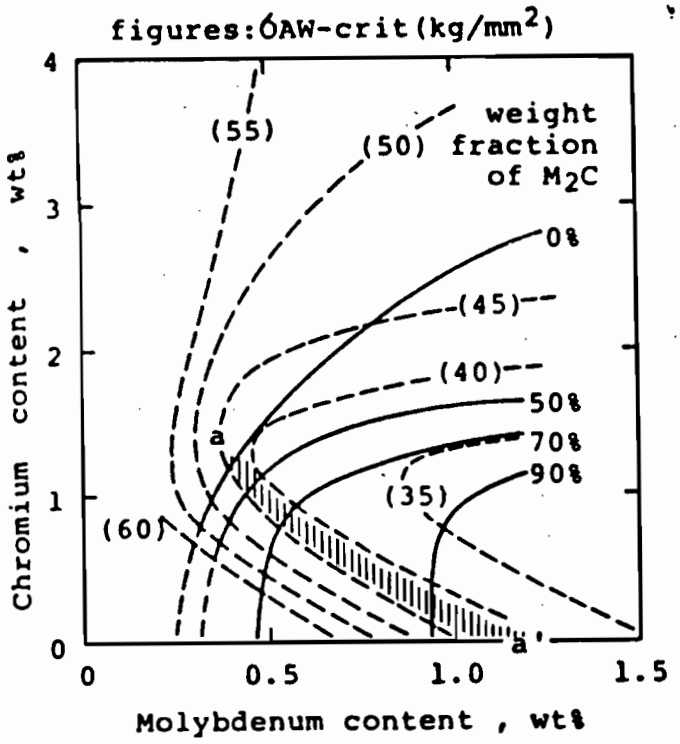

Figure 17. Weight fraction of M_2C shown on the $\sigma_{AW\text{-}crit}$ diagram.

Source: Tamaki, K., Suzuki, J., Nakaseko, Y., and Tajiri, M., Effect of Carbides on Reheat Cracking Sensitivity, Transactions of the Japan Welding Society, 15(1), 1984.

of Figure 14. Figures 16 and 17 thus show that the greatest susceptibility to cracking coincides with the largest fraction of M_2C. The only exception noted is confined to below the a-a_1 line in Figure 17, where, according to Tamaki, in alloys with less than 1%Cr and less than 1%Mo, phosphorus segregation is inhibited.

Since both M_2C and M_7C_3 strengthen the matrix by precipitation, Tamaki investigated the effects of secondary hardening and high temperature hardness by making hardness measurements on samples held at temperature for one hour both at the holding temperature and at room temperature after cooling. While secondary hardening is manifested by an increase in hardness at room temperature, Tamaki found at high temperature the phenomenon is represented only in a delay of softening, ie. softening continues to occur but at a lower rate than that which occurs at lower temperatures. Figure 18 illustrates these results with the room temperature hardness shown as filled circles and the elevated temperature hardness as open circles. This agrees with the findings of Bauford[92]. In hot tensile tests Bauford found that at temperature there is no increase in strength with time but yield strength remains constant over a long period followed by a slow loss in strength.

It was found that in alloys in which the principle precipitate is M_7C_3, the delay in softening occurred at lower temperatures than for those alloys in which the precipitate consists of large fractions of M_2C. Tamaki[90] postulated that the grain boundary embrittlement would be of a similar nature in either type of alloy and therefore embrittlement of the grain boundaries would initiate at the same temperature and proceed in a similar fashion for both types of alloys. As shown schematically in Figure

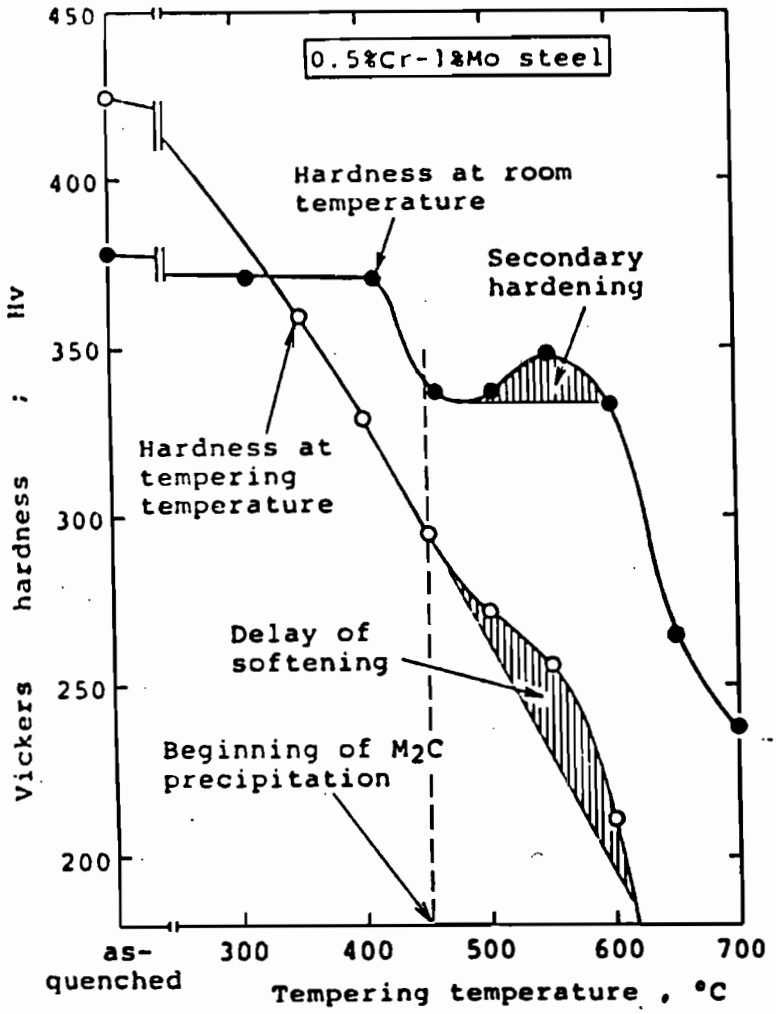

Figure 18. Hot hardness and hardness at room temperature versus tempering temperature.

Source: Tamaki, K., Suzuki, J., Nakaseko, Y., and Tajiri, M., Effect of Carbides on Reheat Cracking Senesitivity, Transactions of the Japan Welding Society, 15(1), 1984.

19a, if a delay in softening occurs at higher temperatures, as for M_2C type precipitation, the embrittlement of the grain boundary may cause the intercrystalline flow stress to be less than the intracrystalline flow stress resulting in fracture. However, as shown in Figure 19b, if a delay in softening occurs at lower temperatures, as with M_7C_3 precipitation, the intercrystalline flow stress exceeds the intracrystalline flow stress at all temperatures and thus intercrystalline fracture does not occur.

In the Cr-Mo alloys vanadium additions dramatically increase the elevated temperature strength. Unfortunately the addition of vanadium to Cr-Mo steels almost universally has been found to result in an equally dramatic increase in PWHT cracking susceptibility.[18,55,59,63,66,68,69,71,79,93,94] The importance of vanadium in increasing cracking susceptibility can be seen in the P_{SR} and ΔG parameters in that the multipliers for vanadium are the largest.[80,18]

The addition of vanadium results, as has been previously indicated, in a uniform and fine precipitation of V_4C_3 in the matrix resulting in significant grain matrix strengthening and accumulation of strain in the grain boundaries.[33,69,93] Bently[68] has noted that early in the heat treatment cycle, intense V_4C_3 precipitation occurs at the ferrite-bainite interfaces due to segregation effects; the bainite having a higher carbon content and the ferrite having a higher vanadium content. At temperatures between 500°C and 550°C (930°F and 1020°F) coherent precipitation of V_4C_3 occurs in the ferrite lattice similar to Mo_2C formation and is concurrent with the development of maximum hardness and strength. At higher

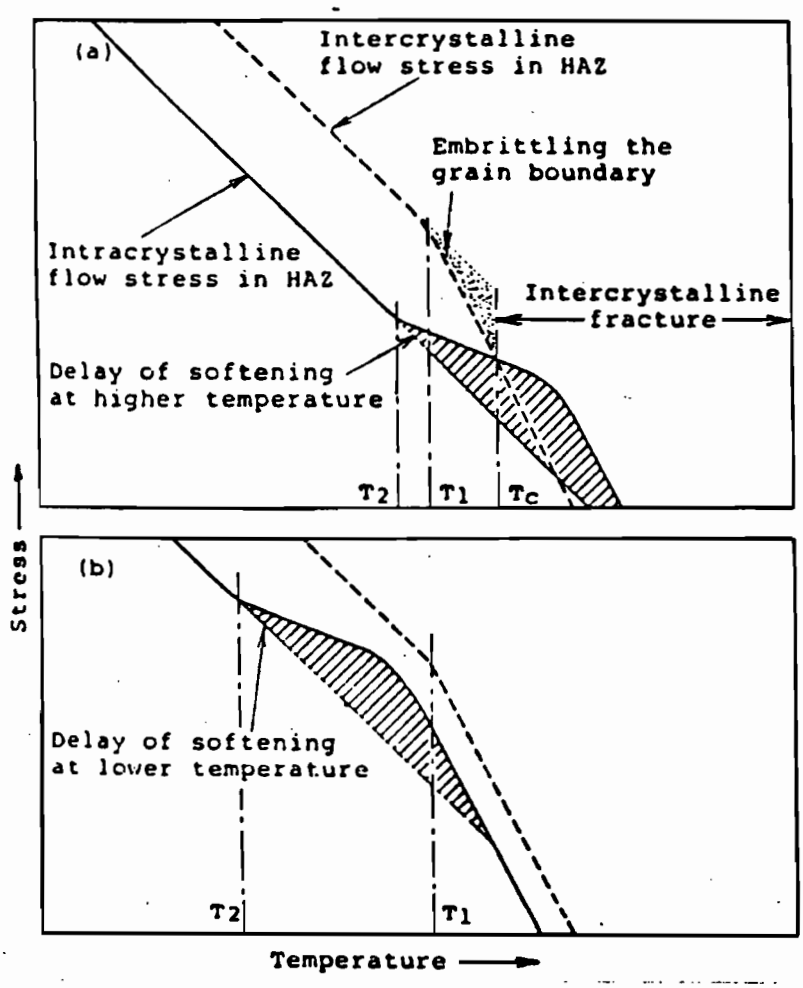

Figure 19. Schematic representation of demonstrating Tamaki's mechanism of reheat cracking.

Source: Tamaki, K., Suzuki, J., Nakaseko, Y., and Tajiri, M., Effect of Carbides on Reheat Cracking Sensitivity, Transactions of the Japan Welding Society, 15(1), 1984.

temperatures, 700°C (1300°F), and longer time, 10 hours, carbide precipitation is transferred to the grain boundaries and large carbides with a grain boundary denuded zone are formed.

Meyers[95], in a study of 1/2Cr-1/2Mo with varying vanadium content, determined that vanadium content below 0.22% to 0.27% did not appreciably increase cracking susceptibility. It was speculated that vanadium content could be increased if residual elements were restricted in order to limit grain boundary embrittlement. However, Meyers noted attention must also be paid to the effects of chromium, manganese, and nickel, which increase initial hardness, and the effect of molybdenum, which increases secondary hardening, and that restrictions may have to be placed on them as well as vanadium.

Jones[96] noted that the vanadium to carbon ratio must be considered. In a study of actual welds in 1Cr-1/2Mo-1/2V materials with a vanadium to carbon ratios between 3.5 and 4.5, a high susceptibility to cracking was found. Stone and Murray[97] noted that a minimum in creep ductility was apparent at vanadium to carbon ratios of 3 to 4 and the reduction of this ratio to 1.5 markedly increased ductility. Thus, a vanadium to carbon ratio of 1.5 to 2 was recommended to prevent PWHT cracking.

Tamaki et al.[91] found that small additions of vanadium (0.06%) reduced the critical stress to fracture in the implant test. The maximum effect was found to occur in low chromium, low to high molybdenum alloys. The increase in cracking susceptibility was said to be related to a decrease in the rate of stress relaxation in a similar fashion to that experienced in the Cr-Mo alloys previously studied.

Nickel is the one element that appears to have the least detrimental effect on the Cr-Mo alloys with respect to PWHT cracking susceptibility. In establishment of the ΔG parameter nickel was varied between 0% and 3.4% without increasing susceptibility to cracking.[80] The same is true of the P_{SR} parameter where nickel was varied between 0% and 1.5%.[18] Thus nickel does not appear in either cracking susceptibility parameter. Tamaki and Suzuki[89] found that nickel content below 1.5% had no effect on the critical stress to fracture but that above 1.5% increasing nickel content greatly increased cracking susceptibility.

The effect of nickel is probably related to the fact that nickel alters the kinetics of carbide precipitation. In a study of the tempering characteristics of 3Cr-1 1/2Mo-Ni alloys Ritchie et al.[10] found that $M_{23}C_6$ replaces M_2C, M_3C and M_7C_3 after only one hour at 700°C (1290°F) as compared to 400 hours for 2 1/4Cr-1Mo. In accordance with Tamaki's model[90], carbides which cause the greatest strengthening of the matrix would form while the overall strength of the grain boundaries is high and before significant embrittlement could occur. The rapid formation of carbides at lower temperatures and the probable very short times of coherency would result in the lowering of PWHT cracking susceptibility.

Boniszewski[88] states the effect of silicon reduction is an increase in ductility and a lower cracking susceptibility. Vinckier[98] found that silicon in excess of 0.5% caused cracking in 2 1/4Cr-1Mo. Increased silicon has been reported to enhance Mo_2C formation in Cr-Mo materials.[94,99] Ratliff and Brown[100] state that increased silicon appears to enhance cementite dissolution and thereby precipitation of alloy

carbides containing chromium, molybdenum, and vanadium resulting in increased secondary hardening which "ultimately impairs stress-rupture ductility."

Research on the effects of titanium on PWHT cracking susceptibility have had mixed results. When titanium has been added for deoxidation purposes (Meyers[101] - 0.016% to 0.055% and Harris and Jones[102] - 0.021% to 0.030%) cracking susceptibility was reported to be diminished in comparison to the same materials deoxidized with other elements, particularly aluminum. Spaeder and Plodder[103] found that addition of 0.048% titanium to T-1 steel did not increase susceptibility while Ito and Nakanishi[18] found that additions of 0.03% to 0.07% titanium in 1Cr-1/2Mo alloys increased susceptibility slightly. Tamaki and Suzuki[91] found that the addition of a small amount of titanium, 0.07%, increased the critical stress to fracture in low chromium high molybdenum alloys. Harris[104] pointed out that, while small amounts of titanium may appear beneficial, larger amounts as deliberate alloying additions may increase cracking susceptibility due to matrix strengthening.

The presence of aluminum, used as a deoxidizer in Cr-Mo steels, has been found to enhance PWHT cracking susceptibility.[74,102] Meyers[101] found that increasing amounts of aluminum, up to 0.035%, used for deoxidation progressively lowered resistance to cracking in a 1/2Cr-1/2Mo-1/4V alloy. Aluminum was thought to prevent grain boundary mobility by the presence of aluminum-nitrogen precipitate clusters rendering the grain boundaries unable to "recrystallize" local regions of strain induced shear. Ratliff and Brown[100] found that when aluminum content exceeded 0.010% in a 1Cr-1/2Mo-1/4V alloy a marked degradation in stress rupture properties

occurred. Aluminum was proposed to reduce the stability of cementite thereby enhancing the formation of Mo_2C and V_4C_3. Edwards et al.[72] found segregation of aluminum, silicon, and nitrogen to have occurred at the grain boundaries by Auger spectroscopy. They speculated that if the combined aluminum and silicon concentration exceeded the austenite loop concentration, the formation of ferrite at the grain boundaries could result causing the rejection of carbon and the creation of a soft, carbide denuded region.

Several researchers have found that the combination of boron and aluminum was particularly detrimental, ie. promoting cracking.[38,52,54] Presser and McPherson[74] speculated that aluminum scavenges nitrogen allowing boron to remain in solution and segregate to the grain boundaries. Boron, segregated to the grain boundaries, forms $M_{23}(C,B)_6$ when held between 1100°F and 1650°F (600°C and 900°C) during cooling or upon reheating above 1200°F (650°C) resulting in deembrittlement. Presser and McPherson[105] also speculated that other strong nitride formers such as titanium or zirconium could enhance embrittlement due to boron. Boron alone has been reported to cause a slight increase in cracking susceptibility.[58,71,74]

Tramp elements have also been reported to affect PWHT cracking susceptibility. Copper and tin were reported to increase susceptibility in 1/2Cr-1/2Mo-1/4V.[102] Copper additions to 2 1/4Cr-1Mo weld metal have been reported by Hunter[106,107] to increase cracking susceptibility. The addition of tin to 1/2Cr-1/2Mo-1/4V was reported by Townsend[104] to significantly lower ductility in weld simulated specimens. However,

Meyers[101] determined that tin additions decreased susceptibility in 1/2Cr-1/2Mo-1/4V while both copper and antimony additions increased cracking susceptibility.

Among the residual elements, phosphorous is the most potent in embrittling the grain boundaries and therefore in enhancing PWHT cracking susceptibility. Auger analysis of fracture surfaces has provided significant evidence of phosphorous segregation in many studies.[77,84,99,108-111] Phosphorous segregation has been reported to be affected by carbide formation and element interaction[19,77,99,111-113], microstructure,[19,113] and grain size.[19]

Phosphorous has been reported by Yu and McMahon[99,111], Hippsley et al.[112,77] and Eyre et al.[19] to interact with molybdenum in solution in the matrix. Molybdenum in solution scavenges or ties up phosphorous in the form of Mo-P clusters or compounds preventing the segregation of phosphorous to the grain boundaries. Precipitation of Mo_2C during heat treatment releases phosphorous allowing segregation to the grain boundaries to occur.

Silicon enhances the formation of Mo_2C and has been reported to have a repulsive interaction with phosphorous similar to that which occurs with carbon. Silicon content was also shown by Auger analysis to be lower at the grain boundaries than within the grains.[99,111] Thus silicon would appear to enhance grain boundary embrittlement by phosphorous.

Precipitation of alloy carbides has also been reported to decrease the activity of carbon in solution thus allowing greater phosphorous segregation.[19,110] The precipitation of molybdenum rich carbides increases the relative amount of chromium in solution and appears to enhance

phosphorous segregation through Cr-P cosegregation.[99,111,113] Also, the formation of carbides in the grain boundaries results in the rejection of phosphorous in to the grain boundaries as phosphorous solubility in the carbides is less than the solubility in the matrix.[19,77,112]

Viswanathan and Joshi[20] and Eyre et al.[19] have found that phosphorous segregation is greater in martensitic microstructures than in bainitic microstructures. Viswanathan and Joshi[20] also reported that segregation increased with increasing hardness for a given microstructure in a 1 1/4Cr-1 1/4Mo-0.3V material. Eyre et al.[19] demonstrated that grain size also affected embrittlement in that increased grain size decreases the area available for segregation.

Tamaki also undertook a study of the effect of phosphorus in Cr-Mo alloys[77]. Several notable results were obtained with Tamaki's study:

(1) Plots similar to those of Figure 17 but made for alloys low in phosphorus (0.010%-0.013%) and higher in phosphorus (0.016%-0.020%) showed that increased phosphorus moved the critical stress curves to lower molybdenum contents.

(2) Phosphorus had already segregated to some extent in the HAZ during the weld thermal cycle.

(3) For a particular alloy there exists a critical phosphorus level below which embrittlement is apparent. The minimum critical value of phosphorus coincides with the 1% Chromium content.

(4) For the range of alloys tested, (0-2%Cr, 0.5%Mo), as long as the phosphorus content was below a critical value for a particular alloy, the critical stress level remained approximately the same.

Thus, phosphorus did indeed adversely affect the cracking susceptibility of the Cr-Mo alloys.

Since phosphorus did not segregate in materials subjected to heat treatments below the A_1 but did segregate when heated above the A_1, Tamaki surmised that the transformation to austenite played a vigorous role in the segregation of phosphorus. It was assumed that the equilibrium distribution of phosphorus was established at the ferrite/austenite interface during the course of transformation and that "the diffusion rate is so small that it (phosphorus) diffuses little from the ferrite/austenite interface to the original ferrite phase."[77] These assumptions combined with the knowledge that the solubility of phosphorus is approximately 2 1/2 times larger in the ferrite than in the austenite, led Tamaki to conclude that phosphorus was carried along on the ferrite/austenite interface. This interface, which is the prior austenite grain boundary on cooling, is therefore enriched with the phosphorus. The welding cycle thus initiates the segregation and embrittling processes.

Sulphur is another residual element that has been found to segregate to fracture surfaces by Auger analysis.[109,110] Imanaka et al.[87] in a study on the effects of sulphur, rare earth metal (REM) and calcium additions in 2 1/4Cr-1Mo found that if "free sulphur" exceeded 25ppm the material showed a high sensitivity to PWHT cracking but below 25ppm exhibited no susceptibility. Free sulphur was calculated by the equation:

$$(S) = [\%S - (32/40)\%Ca - (32/140)\%REM] \times 10^4 \text{ppm}$$

Sulphur in the form of grain boundary sulphides has been linked with the initiation of cavitation on the grain boundaries.[64,94,95]

Hippsley et al.[84,116] have shown that at PWHT temperatures in excess of 600°C (1110°F) materials susceptible to cracking exhibit a change from smooth intergranular fracture surfaces to fracture surfaces with extensive intergranular microvoid coalescence. The microvoids were said to have nucleated on sulphides which were thought to have low interfacial strength with the matrix. The presence of sulphides was thought to be the result of solution of MnS during the thermal cycle and subsequent preferential reprecipitation at grain boundary sites during cooling.

However, Dolby[115] reports that the relationship between grain boundary particles and PWHT cracking is unclear in that some researchers have found that grain boundary particles have no effect on cracking. Further, both Horn and Kunze[110] and Kikuchi and Nakao[109] have found that even in relatively high sulphur materials a reduction in the phosphorous content eliminated cracking in susceptible materials. Thus the effect of sulphur is minor in comparison to that of phosphorous.

In summary, composition is probably the most significant factor in PWHT cracking of the Cr-Mo alloys. Of the alloying elements, molybdenum and vanadium have the greatest effect due to the preferential formation of coherent or fine precipitates in the grain matrix which significantly increase the flow strength of the grain matrix over the that of the grain boundaries. Of the residual elements phosphorous has the greatest effect due to segregation to and embrittlement of the grain boundaries. The effect of composition is complicated by precipitation kinetics, element interactions and the superposition of the effects of other elements such as titanium, tin and copper.

Testing Techniques for Post Weld Heat Treatment Cracking

Baker[104] has enumerated some of the factors that should be included for the ideal PWHT cracking test. - The specimen should include some defect or notch in a microstructure representative of the actual HAZ. The HAZ should be strained, particularly when testing austenitic materials, in a manner similar to that experienced in an actual weld. Finally, the test method employed should preferably incorporate stress relaxation since constant load testing may introduce misleading factors into the evaluation. Dhooge et al.[73] note that the incorporation of all the factors involved in an actual weld into a small specimen would be "difficult".

A common theme among papers reviewing PWHT cracking is that there exists a multitude of tests that have been employed and therefore comparison of test results is difficult and confusing.[60,61,73,98] Dhooge et al[73] cite the use of 26 different testing techniques prior to 1978. In order to simplify the overall number of tests three categories were proposed:

1. Tests on complete weldments
2. Tests on specimens containing a weld
3. Tests on specimens containing thermally simulated heat affected zones

Meitzner[60] in 1975 separated tests into only two categories; direct weldment tests (those containing an actual weld or potions of an actual weld) and simulated weld tests. Vinckier[61,98] in 1974 used three categories to divide some 17 different testing techniques:

1. Tests of a welded specimen
2. Tensile tests at high temperatures on welded or simulated specimens
3. simulation of the PWHT cycle on simulated specimens.

The use of tests on complete weldments or direct weldment tests have the obvious advantage of being directly related to the actual weld and PWHT conditions as well as joint geometry. However, both Meitzner[60] and Dhooge et al[73] note that reproducibility is a significant problem with Meitzner citing erratic results in which one specimen may crack extensively while another may not crack at all. Also a small test specimen will experience a significantly smaller amount of creep strain than a large welded structure.[60,98]

Weld simulation tests have the advantages of reproducibility, known stress level and control of microstructure.[60] The disadvantages are that the strains associated with weld contractional stresses are not duplicated, in general only one region of the HAZ is tested and the effects of adjacent weld metal and base metal are not present.[60,73] Therefore the results of simulation tests must be carefully evaluated before being directly applied to full scale weldments.

The most popular type of tests, although no standard exists, is the tensile or stress rupture test.[73] Several means of evaluating this type of test have been proposed. Vinckier[59] suggested that in hot tensile tests the minimum acceptable reduction in area for an alloy to be considered not susceptible to cracking was 20%. Meyers and Price[117] suggested that, in constant load stress rupture testing, HAZ, base metal and weld metal rupture strengths be compared. If the HAZ rupture strength was lower than

the base metal and weld metal strengths the material was to be considered susceptible and the greater the difference the greater the susceptibility. Spaeder and Plodder[103] have proposed a stress rupture parameter in which the reduction in area was multiplied by the stress to rupture. If the stress rupture parameter was less than $15x10^4$ the material was determined to be susceptible to cracking. Vinckier and Pense[73,98] in extensive Gleeble simulation have determined the following criteria for simulated PWHT at 600°C (1110°F):

1. Extremely susceptible if the reduction of area is less than 5% and peak temperature of the weld simulation exceeds 1200°C (2190°F)
2. Highly susceptible if the reduction of area is below 10% and the peak temperature exceeds 1300°C (2370°F)
3. Slightly susceptible if the reduction of area is below 15% and the peak temperature exceeds 1350°C (2460°F)
4. Not susceptible if the reduction of area exceeds 20% at all peak temperatures.

Thus tensile type or stress rupture tests have been shown to yield a general determination as to the susceptibility of a material to PWHT cracking and allow a ranking of various materials to be determined.[60]

The ideal test previously described can perhaps be accomplished by the use of two or more tests making more efficient use of materials and funds. Utilizing Gleeble simulation to make an initial ranking of a material's stress-relief cracking susceptibility will determine if further testing is indicated. If the material is deemed susceptible to stress relief cracking further testing may be employed with specimens

incorporating a weld or full scale weldments to determine if the material is susceptible under welding conditions or in the actual weldment to be fabricated.

Prevention of Postweld Heat Treatment Cracking.

The most obvious remedy for PWHT cracking, as suggested by Stout[118], is to avoid the use of susceptible alloys. Murray[55] has recommended the use of alloys with limited molybdenum and vanadium. Mullery and Cadman[69] have recommended the use of materials in which the sulphur, phosphorous, and vanadium contents are minimized and manganese content is increased.

When the avoidance of susceptible alloys is not practical process changes may be beneficial. Murray[55] and Pense et al.[81] have recommended using a low strength weld metal with high strength base metals to allow deformation to occur in the fusion zone rather than in the HAZ. Mullery and Cadman[69] have proposed buttering of susceptible alloys to promote the formation of coarser carbides in the coarse grained HAZ of the parent metal. Muraki et al.[86] have suggested welding of the larger side of unsymetric, double V-groove butt joint first.

Increasing heat input and/or preheat has been seen to bring about favorable microstructural changes in the HAZ.[104,86] Higher energy inputs and preheating result in slower cooling rates and softer transformation products,[118] overaging of carbides in the HAZ during cooling,[18] or an "autostress relief".[64] Preheating may also be beneficial in decreasing the temperature range over which internal stresses build up.[119] However, Vinckier[59] reported that higher heat input yielded mixed results. Higher

heat input causes two competing effects to occur: a coarser grain structure results which increases intergranular embrittlement and a softer HAZ is formed which decreases intergranular embrittlement.

An alternative to increasing heat input is to decrease heat input in multiple pass welds. Miller and Batte[85] found that using small gas tungsten arc weld beads in a multipass weld increased the amount of grain refinement due to overlapping of the heat affected zones and that even highly susceptible materials could be welded with this technique with no evidence of cracking after PWHT. Similarly, the use of temper beads, small stringer beads placed over the last pass to refine the grain structure of the HAZ, have been found to be beneficial in eliminating stress-relief cracking.[59]

Complete austenitization after welding[59] or normalizing[79] has been seen to increase the HAZ toughness and prevent cracking. Bentley[68] recommended using low PWHT temperatures and high heating rates to avoid prolonged coherent precipitate formation. However Granjon and Debiez[81] found increasing the heating rate is ineffectual in reducing cracking. Hippsley[121] found high heating rates produced marginal benefit in reducing cracking but speculated that high heating rates might exacerbate cracking in actual weldments due to increased thermal stresses.

Weld dressing to remove discontinuities at weld toes has been found effective in reducing cracking by elimination of crack initiation sites.[55,69,86,118] Peening has also been suggested to eliminate residual tensile stresses at the surface of the weld.[118] Weld stresses can also be reduced by attention to weld sequencing, the use of techniques such as

backstepping, the use of interstage stress relief heat treatments, and simplification of the design of weldments to lower overall levels of restraint.[55]

Thus it may be possible to mitigate PWHT cracking in susceptible alloys by utilizing the techniques described above. Perhaps the most economical means is to eliminate stress risers through careful dressing of the surface of the weld. Temper beading, if correctly performed, combined with weld dressing should provide a microstructure and surface unfavorable to the initiation and propagation of cracks. One important factor, however, is that oxidation during PWHT may provide initiation sites by oxide penetration and wedging along grain boundaries.[79] Therefore inherently susceptible materials may not be prevented from cracking by simple measures and it becomes necessary to know the susceptibility of individual alloys to PWHT cracking in order to ascertain the usefulness of preventative measures.

Figure 20 is a block diagram of the factors affecting the development of PWHT cracking in a material. The complexity of PWHT cracking is demonstrated by the interrelationship of the many factors. As has been shown previously the superposition of several factors may result in the occurrence of cracking but when the same factors are considered alone cracking may not occur.

As vanadium, titanium, and boron are being utilized in the new generation of 3Cr-1 1/2Mo and 2 1/4Cr-1Mo alloys, with vanadium known to increase PWHT cracking susceptibility and the effects of titanium and boron uncertain, it is evident that the susceptibility of these alloys to cracking needs to be investigated. The effect of nickel on PWHT cracking

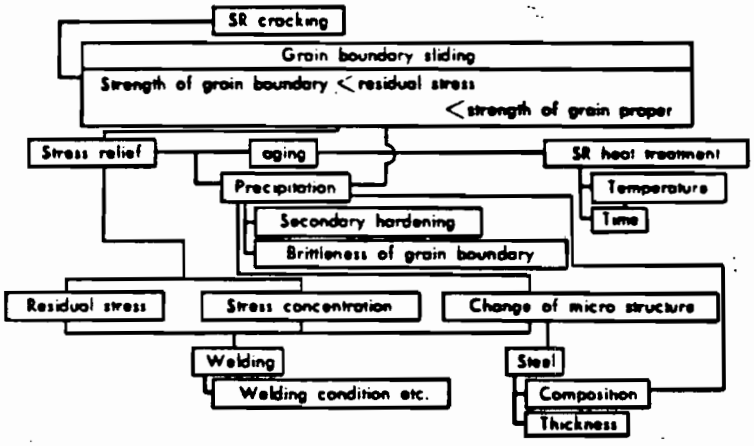

Figure 20. Block diagram showing factors involved in stress relief cracking.

Source: Ito, Y., and Nakanishi, M., Study of Stress Relief Cracking in Welded Low Alloy Steels, The Sumitomo Search, No. 7, 1972.

in the Berkeley 3Cr-1 1/2Mo-1/2Ni material needs to be fully documented. Also additional information on the effect of phosphorous in the 3% chromium alloys needs to be determined.

Soft Zone/Overtempered Region

Any decrease in hardness in the HAZ below the base metal hardness may be deleterious to the creep properties of the material. A loss in hardness may be reflected in shorter times to failure at equivalent stress levels. Thus, the HAZ may control the design of a material for elevated temperature applications.

Softening in the lower temperature regions of the HAZ, those furthest from the fusion line, has been observed in several ferrous materials. Easterling[122] reports that, in plain carbon steels, the region for which the peak temperature is just below the A_1 experiences a transformation of pearlite to spheroidal Fe_3C and a concomitant decrease in hardness. Pogrebnoi[123] has noted a softening in the HAZ of approximately 30 DPH below the base metal, hardness for as welded 11Cr-0.7Mo-0.35V steel. Challenger[124] has shown hardness decrease of 30 to 40 DPH in the HAZ of HY130. King[125] and Biss[126] have shown decreases in hardness in the HAZ below base metal hardness of between 10 and 30 DPH for modified 9Cr-1Mo and similar decrease for HT-9 and 2 1/4Cr-1Mo alloys.

Pogrebnoi[123] and Biss[126] studied the carbide morphology using scanning electron microscopy. They found, when comparing the base metal and the softest region of the HAZ, that carbide coalescence had occurred with preferential carbide growth at grain boundaries and, according to

Biss, at subgrain boundaries. Biss also studied the fusion zone areas of the HAZ that had not softened and found that carbide coalescence was greatest in the softened region.

Challenger, et al.[124] performed the most extensive study. Peak temperatures, heating rates, and cooling rates were measured at various locations in a multiple weld pass HAZ. The locations in the HAZ corresponding to various peak temperatures were examined by optical microscopy, and transmission electron microscopy of carbide extraction replicas and thin foils. The area of minimum softness was determined to correlate with a temperature just below the "rapid heating AC_1-1350°F". At this point both the extraction replicas and thin foils showed the presence of temper carbides.

Thus, the studies to date have led to the conclusion that softening is the result of tempering on the position and/or shape of the carbides present and, while Challenger's study attempted to relate thermal history to the position of the softened region, it appears an exact temperature determination of a particular location is difficult. Further, no attempt to determine the chemical composition or structure of the carbides in the softened region has been attempted.

Studies of the Gleeble simulated soft zones in 9Cr-1Mo-V-Nb, heat 176, at the University of Tennessee has shown that transformations during the weld thermal cycle may play a role in the extent and persistence of the softened region during subsequent heat treatment (PWHT). Samples heated in the Gleeble to approximately 1510°F, a temperature approximately 10°F below the A_1, occasionally showed transformations on a dilatometric trace (the determination of temperature from Gleeble data has an accuracy of

approximately + 15°F). All samples (both which did and did not undergo transformations) showed an initial hardness loss of 10 to 15 DPH. However, after PWHT at 1350°F for 1 hour, the material that did not experience a transformation showed a hardness drop of only 5 DPH while those that transformed showed hardness drops of approximately 30 DPH. The 30 DPH hardness drop was also noted in material heated to a peak temperature of 1550°F, a temperature in excess of the A_1 by approximately 30°F.

When tested for rupture as a function of stress at 1100°F, it was found that the samples that did not experience a transformation exhibited times to rupture equivalent to those for base metal samples that were PWHT but not thermal cycled. However, the samples that had transformed exhibited shorter times to failure at equivalent stresses than the base metal or nontransformed, thermal cycled samples. Although the samples that transformed may have experienced some restraint effects during creep-rupture testing which are not present in the base metal or nontransformed thermal cycled samples, the need to more closely examine the softening effect is strongly suggested.

If the initial work that has been performed is indicative for all 9Cr-1Mo modified materials, it would appear that simple tempering effects, those that occur on heating below the A_1, are essentially overshadowed by PWHT. Thus, it appears that critical softening may occur in that region of the HAZ that experiences peak temperatures in the intercritical region, between the A_1 and A_3, and that a different mechanism, other than simple tempering, is responsible for the softening observed.

One possible mechanism for the observed softening behavior is related to the formation of high carbon austenite and low carbon ferrite by those

areas of the HAZ for which peak temperatures are in the intercritical region. Above the A_1, austenite will begin to form at grain boundaries and subgrain boundaries while carbides, primarily concentrated in the same location, will undergo dissolution. The higher solubility of alloying elements, and in particular, carbon in the austenite, will lead to rapid partitioning of those elements to the austenite. The equilibrium solubility of carbon for the first austenite to form in plain carbon steels is 0.8 w/o and therefore the driving force for the partitioning of carbon is high. Further, carbon can easily diffuse over the distances between carbides in short times thus allowing the partitioning to occur during the relatively short time periods available during the welding thermal cycle.

With carbon and alloying elements being concentrated in the low temperature austenite, in the intercritical range of temperatures, the carbon concentration is lower in the ferrite. Upon cooling the low carbon ferrite is unchanged and is present at room temperature as a soft phase. The austenite transforms to high carbon martensite and/or bainite. The possibility of having some retained austenite, a soft phase, also exists due to a potentially high carbon content in the austenite. Thus, initial HAZ softening would be due primarily to the presence of soft, low carbon ferrite and possibly some retained austenite.

Upon PWHT the low carbon ferrite would experience no change. However, the high carbon martensite/bainite, would temper rapidly. Thus the decrease in hardness would be due to the presence of low carbon ferrite and temper products softer than the constituents present in the normalized and tempered martensitic base material.

The prior discussion has principally been concerned with formation of austenite near the A_1. With the temperatures approaching the A_3, greater amounts of austenite will form until, upon exceeding the A_3, the microstructure would consist of austenite and possibly undissolved carbides. With increasing amounts of austenite at the higher temperatures in the intercritical region, the austenite would have carbon and alloying element concentrations approaching that of the bulk material. The martensite/bainite formed on cooling would be lower in carbon with less alloy segregation resulting in a lower tempering potential and therefore a harder material after PWHT. At, and above the A_3 the austenite would have a carbon concentration of approximately the bulk concentration. Transformation on cooling would yield low carbon martensite/bainite of uniform tempering characteristics. This material would soften more slowly with PWHT than that transformed from the high carbon austenite formed at temperatures near the A_1. Maximum softening would therefore be limited to material that experienced peak temperatures in the intercritical region with maximum softening occurring to material which experience peak temperatures just above the A_1.

MATERIALS

The impetus for development of substitute alloys for 2 1/4Cr-1Mo primarily has been to provide resistance to high temperature and pressure hydrogen attack in synthetic fuels and refining applications and for increased high temperature strength which will permit the production of larger pressure vessels and/or operation at higher temperatures and pressures.[9,128,129] The interest in the modified 9Cr-1Mo alloys is primarily due to the increased corrosion resistance and the possibility of using the material as a substitute for austenitic stainless steel which would eliminate austenitic to ferritic transition joints and result in significant savings both economic and in strategic materials.

The materials that have been studied represent several of the proposed substitutes for 2 1/4Cr-1Mo and several commercial heats of the modified 9Cr-1Mo. Two of the candidate replacement alloys for 2 1/4Cr-1Mo have originated in the United States. The 3Cr-1Mo-0.1V material was conceived by the AMAX (Climax Molybdenum) Materials Research Center[9] and the 3Cr-1 1/2Mo-1/2Ni alloy originated at the University of California, Berkeley.[10,130] The remaining two 2 1/4Cr-1Mo substitutes that were examined, 2 1/4Cr-1Mo-V-Ti-B and 3Cr-1Mo-V-Ti-B, were the result of research performed at the Japan Steel Works (JSW).[4,131]

The alloy developed at the AMAX Materials Research Center has a chromium content of 3% to reduce hydrogen attack susceptibility. Molybdenum and vanadium contents are nominally 1.5% and 0.09% respectively in order to obtain elevated temperature strength. Manganese content of

approximately 1% with a small addition of nickel (approximately 0.2%) is utilized to obtain increased hardenability. Carbon content is limited to 0.1% to promote weldability and prevent any degradation in toughness.[8,9]

The Berkeley alloy, 3Cr-1 1/2Mo-1/2Ni, has higher levels of chromium and molybdenum with respect to 2 1/4Cr-1Mo for the same reasons as the AMAX material. The increased chromium and molybdenum contents are also considered to improve the oxidation resistance in comparison to 2 1/4Cr-1Mo. Nickel is added to increase hardenability and to promote early formation, during tempering, of more stable alloy carbides thus increasing hydrogen attack resistance. However, unlike the AMAX material, manganese is limited to approximately 0.5% in order to prevent temper embrittlement, minimize the amount of retained austenite and prevent banding. Retained austenite and banding are thought to increase susceptibility to hydrogen attack due to non-uniform distributions of unstable alloy carbides. Carbon content is held to a maximum of 0.15% to eliminate the possibility of welding related problems.[10,130]

Development by JSW of the 3Cr-1Mo-V-Ti-B alloy[4,128] followed directly from research performed in the design of the 2 1/4Cr-1Mo-V-Ti-B alloy.[131] The major difference between the two alloys is the chromium content which is increased to provide better resistance to hydrogen attack. Carbon content in the 2 1/4Cr material is 0.10% while the 3Cr material had a maximum content of 0.15%. Silicon content is restricted to a maximum 0.10% in the 3Cr alloy (0.02% - 2 1/4Cr) to minimize temper embrittlement. The addition of 0.25% vanadium is made to increase both tensile and creep strength through the formation of a fine dispersion of vanadium carbides. Boron, 0.001% to 0.003%, is included to increase hardenability and assure

uniformity of mechanical properties throughout thick sections. Titanium additions, 0.015% to 0.035%, are utilized to scavenge nitrogen in order to prevent boron nitride formation and secondarily for grain refinement.

Nippon Kokan (NKK) and Kawasaki, two Japanese steel makers, have also proposed alloys for replacement of 2 1/4Cr-1Mo. Although these steels were not tested, the reasoning behind the alloy modifications provides some background in the different approaches taken in the design of the 2 1/4Cr-1Mo substitutes. Kawasaki[13] obtains the necessary strength and resistance to hydrogen attack with additions of niobium (0.023%) and vanadium (0.20%) to 3Cr-1Mo. Titanium and boron additions are specifically not included due to the degradation of toughness and because adequate hardenability is thought to be obtained by the niobium and vanadium additions. Kawasaki further lowered silicon to 0.08% and sulphur to 0.001% to control hydrogen attack, temper embrittlement and stress-relief cracking. NKK,[5,12] on the other hand, employed low titanium, 0.01% maximum, low boron, 0.0010% maximum, and low nitrogen, 0.004% maximum, to obtain adequate hardenability and toughness and maintain weldability. Although vanadium improves resistance to hydrogen attack and increased creep rupture strength, Nippon Kokan limits additions of vanadium to approximately 0.08%. Vanadium in excess of 0.08% is thought to decrease hardenability substantially. Lower phosphorus, 0.004% maximum, is maintained rather than lowering the silicon content to reduce temper embrittlement. (The proposed silicon level is 0.25%.) Nickel content is 0.15% for the Kawasaki material and 0.5% for the NKK alloy. No discussion of the level of nickel employed was given by either steel maker.

Thus a variety of developmental approaches has been taken. Common among all the materials is the limitation of carbon content to promote weldability. However, beyond that there exists little agreement between the various developers. Weldability and temper embrittlement resistance are thought to be promoted by very lower sulfur content (0.001%) by one steelmaker while temper embrittlement control has been attempted through limiting silicon (below 0.010%) or phosphorus (0.004%) by others. Hardenability has been increased by the addition of boron, high manganese, manganese and nickel additions, or niobium and vanadium additions. Manganese has been increased in one instance to between 1% and 1.2% in order to increase hardenability while in another it has been limited to approximately 0.5% to mitigate hydrogen attack. On the one hand, vanadium additions are limited to 0.08% and niobium not added due to the possible loss of toughness and hardenability while on the other hand, 0.25% vanadium is utilized in one case and 0.20% vanadium plus 0.023% niobium in another. In one alloy nickel is used as the primary alloying addition (other than chromium and molybdenum) to increase both hardenability and eliminate hydrogen attack.

The four alloys that have been studied are representative of those proposed to replace 2 1/4Cr-1Mo. The Berkeley alloy has no additional carbide formers (beyond chromium and molybdenum) and utilizes nickel and a moderate amount of manganese to achieve adequate hardenability. The AMAX (Climax) alloy utilizes high manganese to obtain hardenability and a modest addition of vanadium to increase high temperature strength. The two JSW

materials, both the 2 1/4Cr-1Mo and 3Cr-1Mo, utilize B to increase hardenability and relatively high vanadium content to increase high temperature strength.

In addition to the four modified materials, a standard 2 1/4Cr-1Mo alloy, Lukens 2 1/4Cr-1Mo-0.10C, has been employed in portions of this work. This material has been extensively studied by Richey[25] and the transformation characteristics and sensitivity to PWHT cracking, as determined by Gleeble simulation, have been reported.

Five state-of-the-art heats of modified 2 1/4Cr-1Mo steels made available by the Materials Properties Council were evaluated for the PWHT cracking susceptibility. These were included in this study to compare the results available from the earlier part of this investigation (JSW and Lukens 2 1/4Cr-1Mo). These state-of-the-art heats have been designated as M10 to M50. The various features that can be noted in the composition of these materials are: M10 contains 0.10% carbon and M40 contains 0.15% carbon; M20 has three times more nitrogen than others; M40 has 0.01% P; M50 contains 0.014% Cu; M30 has been treated with Ca during the melting practice. All these heats are modified with different levels of V, Ti, B and Nb. M10 also has 0.48% Ni in addition to V, Ti and B.

Three commercial heats of modified 9Cr-1Mo materials were included in the current work to provide further evaluation of this important alloy. The NKK, Sumitomo and Timken commercial heats of 9Cr-1Mo-V-Nb are quite similar in composition. The NKK heat has very low levels of phosphorus, 0.004%, sulphur, 0.004%, aluminum, 0.006%, and nickel, 0.01%. The Sumitomo heat has the highest phosphorus, 0.014%, and nickel, 0.10%, and

the lowest vanadium, 0.20%, contents. The Timken material had the highest levels of vanadium, 0.31%, aluminum, 0.027%, and sulphur, 0.007%, with an intermediate amount of phosphorus, 0.010%.

The chromium equivalents of the 9Cr-1Mo-V-Nb materials range from 9.59 for ORNL heat 176 (an experimental heat tested by Richey[25]) to a high of 13.42 for the Timken material. The chromium equivalent was determined by the equation:[132]

$$CrE = Cr + 6Si + 4Mo + 1.5W + 11V + 5Nb + 8Ti + 12Al - 40C - 30N - 4Ni - 2Mn - Cu$$

where all elements are in weight percent. The chromium equivalent can be used as a predictor of the degree of delta ferrite present on cooling after welding. For chromium equivalents above 12, substantial amounts of delta ferrite may be formed in the coarse grained heat affected zone, between 10 and 12, some delta ferrite may be formed and below 10, no delta ferrite is expected.[132] Thus, for ORNL heat 176 no delta ferrite would be expected while substantial amounts of delta ferrite may be present in the heat affected zone of the Timken alloy after welding.

The as received material form and heat treatment appear in Table 2. With the exception of the Berkeley 3Cr-1Mo-1/2Ni alloy all materials were tested in the as-received condition. The as-received Berkeley material was given a low temperature, 1125°F (607°C), stress-relief following normalizing and as a result was in a hardened condition. Therefore some of the Berkeley 3cr-1 1/2Mo-1/2Ni material was subsequently heat treated for 24 1/2 hours at 1175°F (635°C) in order to obtain a tensile strength within the limits of those proposed for the new SA 387 grade 22 class 3 classification. Although this classification applies to 2 1/4Cr-1Mo, it

Table 2. As received material condition.

MATERIAL	DESIGNATION	HEAT NO.	FORM	HEAT TREATMENT °F(°C)
9Cr-1Mo-V-Nb	NKK	HT-A-231001	1 in (25mm) plate	Normalized 1900 (1040) Tempered 1400 (760)
9Cr-1Mo-V-Nb	Sumitomo	OYYC-9082	2 in (50mm) OD tube	Normalized 1740 (950) Tempered 1440 (780)
9Cr-1Mo-V-Nb	Timken	82631	3 in (76mm) dia. bar	Normalized 1900 (1040) Tempered 1400 (760)
9Cr-1Mo-V-Nb	ORNL	176	3/8 in (9.5mm) plate	Normalized 1900 (1040) Tempered 1400 (760)
3Cr-1$\frac{1}{2}$Mo-V	AMAX (Climax)	A9349	4 in (102 mm) plate	Austenitized 1750 (955) Water Quenched Tempered 1050 (565)
3Cr-1$\frac{1}{2}$Mo-$\frac{1}{2}$Ni	Berkeley	A9749	4 in (102 mm) plate 1 in (25 mm) plate	Normalized 1750 (955) Tempered 1125 (607)
3Cr-1Mo-V-Ti-B	JSW	---	18 in (450 mm) ring Forging Section	Normalized 1850 (1010) Tempered 1220 (660)
2$\frac{1}{4}$Cr-1Mo-V-Ti-B	JSW	---	10 in (250 mm) forging 1 in (25mm) plate	Normalized 1830 (1000) Tempered 1200 (650)
2$\frac{1}{4}$Cr-1Mo-0.10C	Lukens	3443	13 in (325 mm) plate	Austenitized 1960 (1070) Water Quenched Tempered 1200 (650)
2$\frac{1}{4}$Cr-1Mo-0.12C	Lukens	BP3	3 in (150mm) plate	Austenitized 1780 (955) Water Quenched Tempered 1225 (655)
2$\frac{1}{4}$Cr-1Mo-V-Ti-B (M10)	NKK	JD54015	2 in (50 mm) plate	Quenched Tempered 1275 (690)
2$\frac{1}{4}$Cr-1Mo-V-Ti-B (M20)	JSW	80B0964	2 in (50 mm) plate	Quenched Tempered 1275 (690)
2$\frac{1}{4}$Cr-1Mo-V-Ti-B (M30)	KOBE	TV3951	2 in (50 mm) plate	Quenched Tempered 1275 (690)
2$\frac{1}{4}$Cr-1Mo-V-Ti-B (M40)	NSC	205C-1	2 in (50 mm) plate	Quenched Tempered 1275 (690)
2$\frac{1}{4}$Cr-1Mo-V-Ti-B (M50)	Kawasaki	AP1531B	2 in (50 mm) plate	Quenched Tempered 1275 (690)

was felt that the requirements of this new classification could reasonably be extended to include the alloys proposed to replace 2 1/4Cr-1Mo. It will be noted throughout the following discussions whether the material was in the as received or heat treated condition.

Table 3 shows the chemical compositions of the alloys examined in this study. Analysis of the Lukens 2 1/4Cr-1Mo (2 heats) and all the 9Cr and 3Cr materials were performed by the Metallurgical Laboratory of Combustion Engineering in Chattanooga, Tennessee. JSW 2 1/4Cr-1Mo material was analyzed at ORNL. The five heats supplied by MPC were analyzed by Charles C. Kawin Co., Broadview, Illinois.

Table 3. Chemical compositions of materials studied.

			Composition (Weight %)																							
Heat	Designation	Supplier	C	Mn	P	S	Si	Ni	Cr	Mo	V	Nb	Ti	Co	Cu	Al	B	W	As	Sn	Zr	N	O	Ca	[illegible]
126	9Cr-1Mo-V-Nb	ORNL	0.083	0.37	0.010	0.003	0.11	0.09	8.61	0.89	0.21	0.07	0.01	0.010	0.04	0.007	0.001	0.01	0.001	0.001	0.001	0.055			[illegible]
[illegible]	9Cr-1Mo-V-Nb	NKK	0.10	0.41	0.004	0.004	0.41	0.01	8.26	0.95	0.27	0.07	0.01	0.011	0.02	0.008	0.001	0.02	0.001	0.002	0.001	0.038	0.002		[illegible]
E2631	9Cr-1Mo-V-Nb	Timken	0.095	0.41	0.010	0.007	0.42	0.09	8.76	1.00	0.21	0.09	0.01	0.017	0.09	0.077	0.001	0.07	0.007	0.006	0.001	0.016	0.003		[illegible]
OYYC 9082	9Cr-1Mo-V-Nb	Sumitomo	0.10	0.43	0.014	0.006	0.40	0.10	8.50	0.98	0.20	0.07	0.01	0.018	0.01	0.011	0.001	0.02	0.003	0.002	0.001	0.015	0.003		[illegible]
P2901	3Cr-1½Mo-0.1V	AMAX	0.082	0.86	0.006	0.009	0.16	0.21	3.02	1.43	0.12	0.01	0.01	0.005	0.02	0.005	0.001	0.01	0.001	0.001	0.001	0.010			
A9319-1A	3Cr-1½Mo-0.1V	Lukens	0.11	0.86	0.012	0.001	0.26	0.11	2.94	1.42	0.09	0.03	0.01	0.009	0.02	0.004	0.001	0.01	0.003	0.002	0.001	0.013	0.003		
	3Cr-1Mo-V-Ti-B	JSW	0.14	0.46	0.007	0.008	0.06	0.20	3.11	0.97	0.28	0.01	0.02	0.014	0.09	0.003	0.003	0.01	0.008	0.006	0.001	0.011			
9749	3Cr-1½Mo-½Ni	Berkeley	0.16	0.52	0.010	0.003	0.28	0.51	3.05	1.48	0.007	0.01	0.01	0.010	0.11	0.005	0.001	0.01	0.007	0.001	0.001	0.011			
	2¼Cr-1Mo-V-Ti-B*	JSW	0.12	0.48	0.007	0.006	0.06	0.15	2.31	0.98	0.26	-	0.013	-	0.08	0.016	0.0022		0.008	0.007		0.051			
3443	2¼Cr-1Mo-0.12C	Lukens	0.12	0.41	0.006	0.003	0.22	0.02	2.27	1.05	0.01	0.01	0.01	0.008	0.08	0.008	0.001	0.01	0.007	0.001	0.001	0.015	0.004		
HP3	2¼Cr-1Mo-0.10C	Lukens	0.10	0.44	0.008	0.028	0.19	0.16	2.18	1.02	0.01	0.01	0.01	0.014	0.15	0.003	0.001	0.01	0.006	0.011	0.001	0.007	0.007		
JBK4P15	2¼Cr-1Mo-V-Ti-B	NKK (M10)	0.10	0.54	0.003	0.005	0.06	0.48	2.47	0.93	0.32	0.07	0.01			0.02	0.015					0.0039		0.002	
8010964	2¼Cr-1Mo-V-Ti-B	NSW (M20)	0.13	0.49	0.006	0.007	0.08	0.16	2.27	0.90	0.24	<0.01	0.03			<0.01	0.0022					0.0095		0.002	
TV3951	2¼Cr-1Mo-V-Ti-B	KORE (M30)	0.13	0.52	0.007	0.006	0.08	0.15	2.20	1.10	0.28	0.05	<0.01			0.07	0.0005					0.0018		0.012	
205C-1	2¼Cr-1Mo-V-Ti-B	NIPPON (M40)	0.15	0.50	0.010	0.005	0.08	0.01	2.21	1.20	0.25	0.06	0.03			0.01	0.0011					0.003		0.002	
VP1531H	2¼Cr-1Mo-V-Ti-B	Kawasaki (M50)	0.12	0.52	0.008	0.005	0.09	0.13	2.45	0.98	0.29	0.03	0.01		0.14	0.02	0.0015					0.003			

EXPERIMENTAL PROCEDURES

This investigation incorporated four areas of research: a determination of transformation temperatures and microstructures under welding conditions (for the coarse grained HAZ), an assessment of the PWHT cracking susceptibility, a determination of HAC susceptibility of modified and unmodified 2 1/4Cr and 3Cr alloys and an assessment of the occurrence of soft zone in 9Cr material.

The "Gleeble Device"

The Gleeble is a device that was developed at Rensselaer Polytechnic Institute[133] and allows simulation of the actual thermal cycles experienced at any particular point adjacent to a weld. While a region in the weld HAZ is small, use of the Gleeble permits expansion of the region of interest to a larger volume so that testing may be accomplished on that region alone.

The Gleeble is also capable of applying a tensile load up to 10,000 pounds (44.5kN) at any point in the thermal cycle. At the selected point, the controller energizes a solenoid valve supplying pressure regulated air to a pneumatic cylinder which is affixed to the movable jaw. The load applied is determined from the output of an electrical resistance, strain gauge type of load cell attached to the ram of the pneumatic cylinder. The load cell output is recorded by the light beam oscillograph.

Phase Transformations

On-heating and on-cooling transformation temperatures were determined with the Gleeble utilizing a high speed dilatometer. The dilatometer employs a precision rectilinear potentiometer connected by a mechanical linkage to quartz rods in contact with opposite sides of the specimen

mounted in the Gleeble. Changes in specimen diameter due to thermal expansion/contraction and phase changes result in a change in position of the potentiometer slider and therefore a change in output voltage.

Figure 21 shows a schematic representation of such a dilation versus temperature plot. As indicated in Figure 21 the temperature of transformation is determined by the points at which the trace deviates from linearity with the end points being the start and finish temperatures.

The transformation characteristics of the coarse grained HAZ were determined for welding heat inputs varying from those associated with shielded metal arc welding to submerged arc welding. A peak temperature of 2400°F (1315°C) was utilized with all thermal cycles in order to achieve a microstructure similar to that which occurs immediately adjacent to the weld fusion zone. Figure 22 shows the six welding thermal cycles employed to determine the transformation temperatures. These six thermal cycles simulate weld heat inputs ranging from 18KJ/in (0.7KJ/mm), preheat 72°F (22°C) for a 2in (51mm) thick plate, to 150 KJ/in (59KJ/mm), preheat 400°F (205°C) for a 2in (51mm) thick plate.

The seventh thermal cycle, indicated in Figure 22 as an arc strike, is simulated by interrupting the heating current when the specimen reached the peak temperature and simultaneously blasting the specimen with helium to achieve high radial heat loss as well as the longitudinal conduction heat loss. This cycle was only employed to give a baseline, most rapidly cooled microstructure, for comparison with the microstructures obtained with the six other thermal cycles.

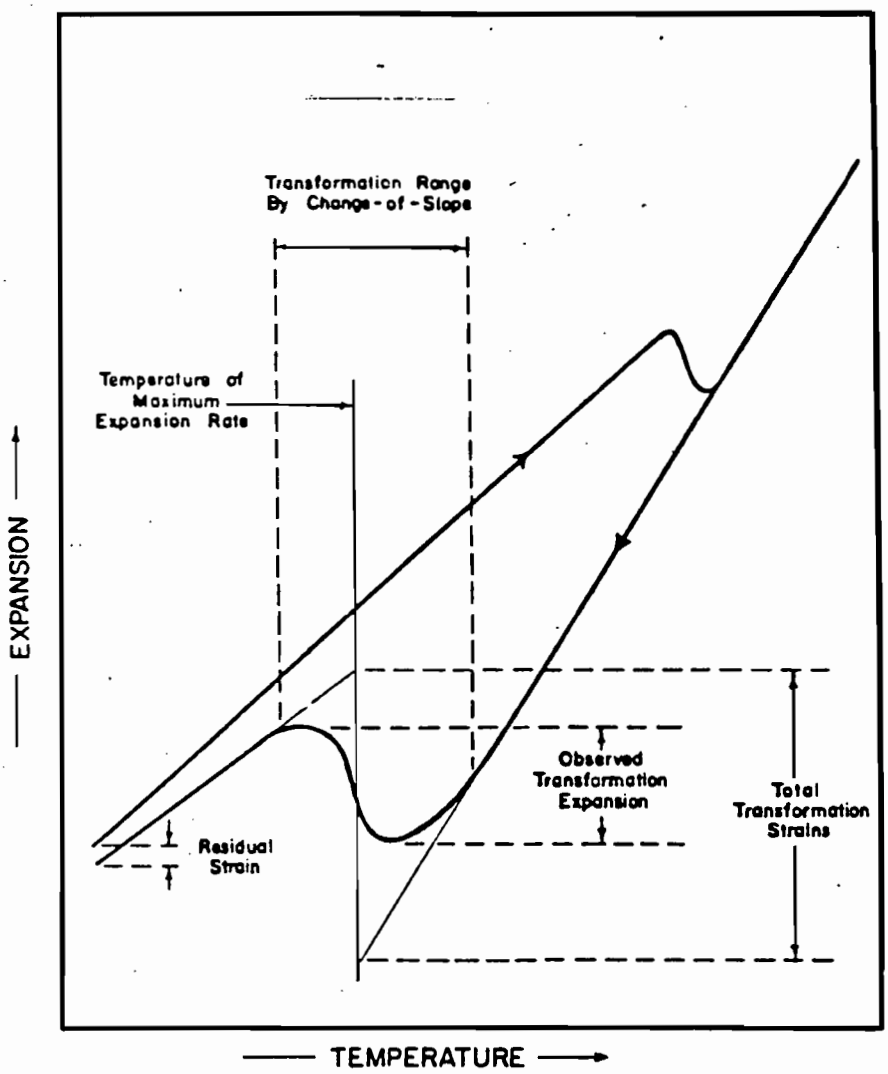

Figure 21. Schematic representation of dilatometric output for the determination of transformation temperatures.

Source: Torok, T.E. and Stout, R.D., Relation of Dilatometric Characteristics of Steels to Delayed Cracking in Welds, Welding Journal, 44(12), 1965.

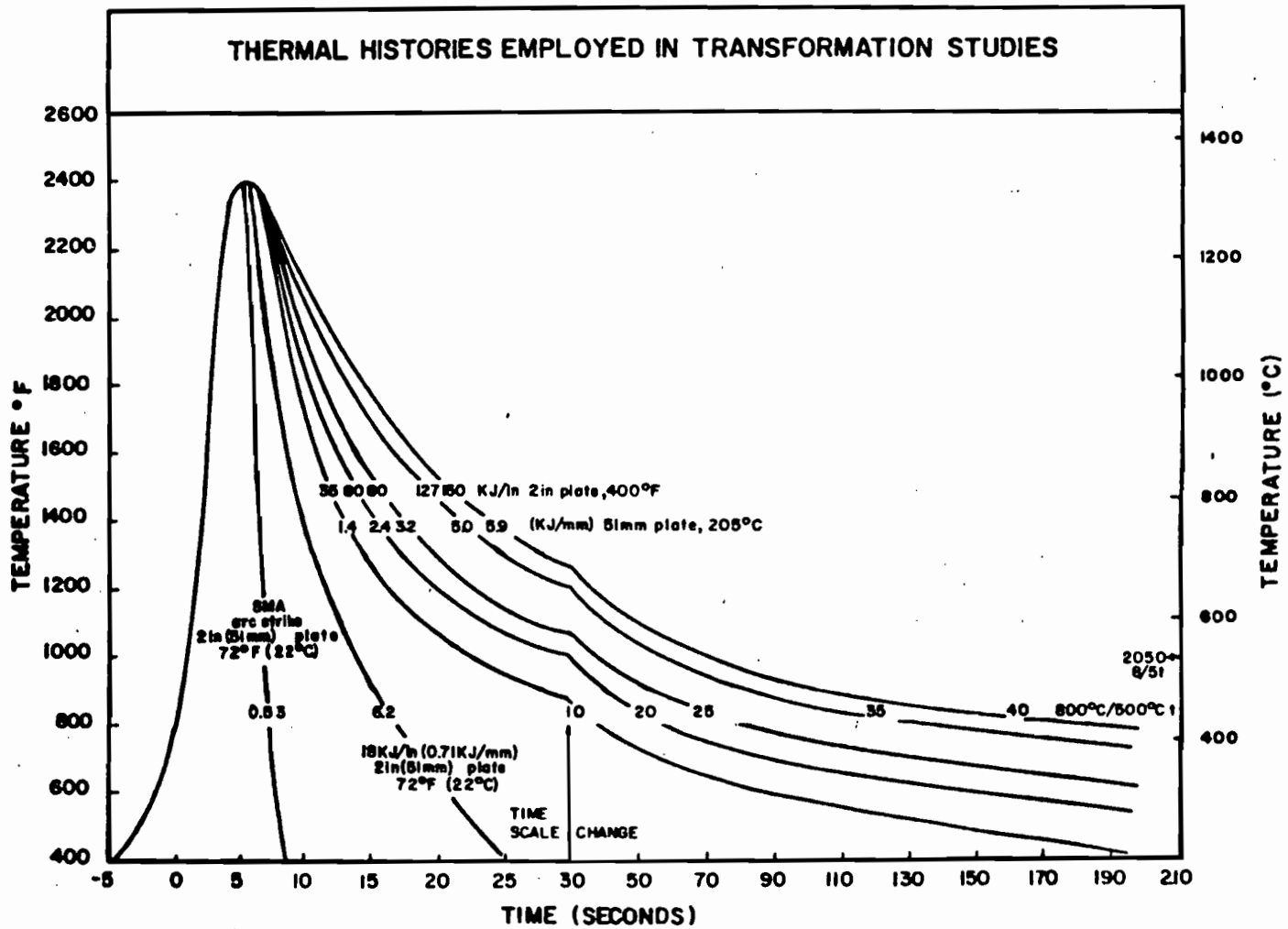

Figure 22. Thermal cycles employed in the determination of transformation temperations for welding conditions.

Y-Groove HAC Test

The oblique Y-groove test is a high restraint test used to evaluate HAC sensitivity of steels and is defined in Japanese Industrial Standard Z 3158. A typical specimen is shown in Figure 12b (in literature section). In this technique, the test welds are made at various preheats. Hydrogen is added to the weld by controlling the arc atmosphere via the moisture in the electrode coating.

The restraint beads are deposited using an electrode of comparable strength under the standard welding conditions when the whole test piece has reached the specified temperature.

The test bead is then deposited at the preheat temperature of interest using an electrode with known diffusible hydrogen content. After 48 hours the the test bead surface is examined for cracks. The surface crack ratio is evaluated by the relation:

Surface crack ratio = (Total cracked length of the test bead/ length of test bead) X 100 %

The portion of the specimen with the test bead is then sectioned into five equal pieces and the section crack ratio is calculated using the following relation:

Section crack ratio = (average of height of root cracks/ Minimum thickness of test bead) X 100 %

Y-groove testing of the 3Cr materials were conducted using electrodes supplied by Combustion Engineering Inc. The Lukens 3Cr-1.5Mo-0.1V and JSW 3Cr-1Mo-V-Ti-B steels were tested using 3Cr-1.5Mo-0.1V electrodes. These electrodes, in the as received condition, had a diffusible hydrogen of 6.94 ml/100g. Baking at 890°F for 2 hours reduced the hydrogen level to 3.71

ml/100g. At these two levels of diffusible hydrogen Y-groove HAC testing was carried out at preheat temperatures above room temperature until a temperature was reached for which no cracking was observed. The Berkeley 3Cr-1.5Mo-0.5Ni was tested with 3Cr-1.5Mo-0.5Ni electrodes also supplied by Combustion Engineering Inc. These electrodes were fully baked and evolved 5.07 ml/100g of diffusible hydrogen. Y-groove testing was carried out at this hydrogen level utilizing preheat temperatures of 275°F to 450°F.

2 1/4Cr-1Mo materials were tested using E9018-B3 electrodes supplied by Teledyne McKay. In the unbaked condition these electrodes had a hydrogen level of 22ml/100g. Baking at 500°F for 2 hours reduced the hydrogen level to 8.04 ml/100g and baking at 890°F for 2 hours reduced the hydrogen level to 2.38 ml/100g. Testing of Lukens, JSW and Kawasaki 2 1/4Cr-1Mo materials were conducted at these two hydrogen levels at preheat temperatures from room temperature to 375°F.

Each specimen was carefully examined for surface cracks on the test bead. If the cracking was not clearly visible, dye penetrant examination was carried out. After measurement of the surface cracks the test bead portion was sectioned into five equal pieces and the through section cracks were measured using a stereo microscope.

Postweld Heat Treatment Cracking

PWHT cracking is intergranular cracking that usually occurs in the coarse grained HAZ of a weld during PWHT or during service at elevated temperatures. This type of cracking is caused by a combination of matrix strengthening as a result of carbide precipitation, embrittlement of the grain boundaries as a result of residual element segregation and both internal residual stress due to welding and externally applied stress.

The Gleeble was utilized to make an initial assessment of cracking susceptibility for all materials. Samples were initially subjected to a 60KJ/in (2.4KJ/mm) thermal cycle with a peak temperature of 2400°F (1315°C). This peak temperature was selected to obtain a microstructure similar to that in the coarse grained HAZ of an actual weld. Subsequent to thermal cycling, the sample is simultaneously loaded in tension to simulate the restraint stress experienced by the coarse grained HAZ and heated to the post weld heat treatment temperature. While the stress is held constant for an individual specimen, a range of stress levels is employed during the testing of a material in order to obtain various times to fracture.

The PWHT temperatures employed in this investigation were 1350°F (730°C) for the modified 9Cr-1Mo materials and both 1250/1275°F (677/690°C) and 1150°F (620°C) for the 2 1/4Cr and 3Cr modified materials. The lower temperature employed for the 2 1/4Cr and 3Cr materials is representative of the trend to lower post weld heat treatment temperatures and higher strengths for these materials.

If the sample did not fracture within the 200 minute period the test was terminated. The reduction in area of the fractured specimens was determined and selected sample fracture surfaces examined for microstructure features in with the scanning electron microscope.

In order to facilitate fractographic examination, several samples of the modified 2 1/4Cr and 3Cr materials were tested in an argon atmosphere. This technique resulted in fracture surfaces essentially free of oxidation.

Samples of the modified 3Cr-Mo and 2 1/4Cr-1Mo were prepared on the Gleeble for transmission electron microscopy examination by thermal cycling

to 2400°F (1315°C) to produce a grain coarsened microstructure followed by a 100 minute simulated PWHT at 1250°F (680°C) with an applied load. The load employed was the highest possible that would not cause fracture or necking of the specimen within the 100 minute hold at the PWHT temperature. The specimens were sectioned at the point of thermocouple attachment with one half mounted and polished for utilization in the replica studies. Four 0.025 inch (0.64mm) thick sections were cut from the thermocouple end of the opposite half of the sample for use as thin foil specimen blanks. The mounted specimens and the thin sections were evaluated by Dr. Judith Todd of the University of Southern California, Los Angeles.

Several objections may be raised to the Gleeble technique employed in the determination of PWHT susceptibility. A major objection is that the Gleeble simulation does not represent the conditions present during PWHT, in that a constant load rather than a time dependent decreasing load is used. Also the effects of surrounding base metal and weld metal on the HAZ are not present in the Gleeble simulation which reproduces only a single portion of the HAZ. Finally, the samples employed were smooth 0.250 inch (6.4mm) round samples although stress-relief cracking is known to be associated with the presence notches at the surface or discontinuities in the interior of the weld.

With these objections in a mind the C-ring test, normally employed in testing for stress corrosion cracking tendency, was selected as a suitable small scale test specimen for verification of the results obtained from the Gleeble testing program. ASTM standard G-38[134] was followed for design of the C-ring specimens and for determination of the deflection necessary to achieve the initial stress state.

To incorporate a weld in the C-ring specimens a 1 inch by 1 inch (25mm x 25mm) square bar is machined with a flat bottomed groove parallel to the rolling direction at the plate surface. Groove geometry is modified in order to accommodate different diameter shielded metal arc welding electrodes. For 5/32 inch (4.0mm) diameter electrodes the groove walls are machined at a 40° angle radial from the center of the bar. For 1/8 inch (3.2mm) diameter electrodes the angle is 30°. In all cases the depth of the groove is 5/32 inch (4.0mm). Figure 23 is a drawing of the cross section of a bar with a 30° angle groove for use with 1/8 inch (3.2mm) diameter electrodes.

A single pass shielded metal arc weld deposit is used to fill the groove (using matching chemistry electrodes whenever possible). The Berkeley 3Cr-1 1/2Mo-1/2Ni material is welded with matching chemistry 1/8 inch (3.2mm) shielded metal arc electrodes. The AMAX (Climax) 3Cr-1 1/2Mo-0.1V material is welded with matching chemistry 5/32 inch (4.0mm) electrodes. These electrodes were manufactured on a special lot basis by Combustion Engineering in Chattanooga, Tennessee. The JSW 3Cr-1Mo-V-Ti-B material is welded with the same electrodes as those used for the AMAX (Climax) 3Cr-1 1/2Mo-0.1V material. The JSW 2 1/4Cr-1Mo-V-Ti-B material and Lukens 2 1/4Cr-1Mo-0.10C material, used for baseline comparison, are welded with 5/32 inch (4.0mm) E9018-B3 electrodes. The M10 to M50 materials were welded with 2 1/4 Cr-1Mo-0.25V electrodes made available by the Amax Materials Research Center.

The welded bars were machined into cylinders and surface ground to a fine, 32 RMS, finish. The cylinders have a nominal 1 inch outside diameter and 0.125 inch wall thickness. Rings, 0.750 inches long, are sectioned

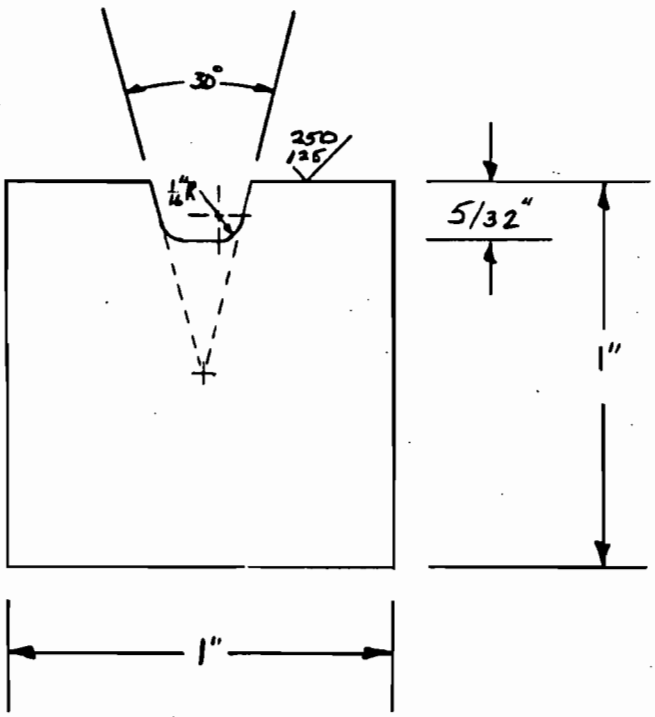

Figure 23. Groove geometry for 1/8" (3.2mm) shielded metal arc electrodes.

from the cylinders. The rings are etched with a 2% solution of hydrofluoric acid in 30% hydrogen peroxide in order to reveal the heat affected and fusion zones. A charpy V type notch, 0.035 inches (0.90mm) deep, is broached into one of the coarse grained heat affected zones and a hole drilled through the ring 90 degrees from the axis of the notch. The back of the ring, away from the notch, is removed in order to allow compression of the ring by tightening of a bolt placed through the drilled holes. Figure 24 schematically shows the successive steps in production of the C-ring specimen from the welded bar to the finished C-ring.

The bolts employed for stressing the C-rings were machined from the Berkeley 3cr-1Mo-1/2Ni material. This was done so that the thermal expansion properties of the bolts would be similar to those of the tested materials. Stress relaxation in the bolts was not found to be a significant factor since elongation of the bolt is only approximately 0.0005 inches (0.01mm) when the C-ring is loaded to a nominal stress of 100ksi (690MPa). This elongation corresponds to approximately 15ksi (103MPa) in the bolt which is not great enough to cause significant stress relaxation in the bolt during PWHT.

Tightening of the bolt through the C-ring results in a constant strain specimen with tensile stresses produced on the exterior of the ring. The amount of deflection of the outside diameter (OD) necessary to produce the desired stress is determined by the equation:[108]

$$\Delta = (f \quad D^2) \ / \ (4EtZ)$$

where: f = the desired stress, D = the mean diameter (OD - t), t = the wall thickness, E = the modulus of elasticity, and Z = a correction factor for curved beams determined from a graph included in ASTM standard G38.

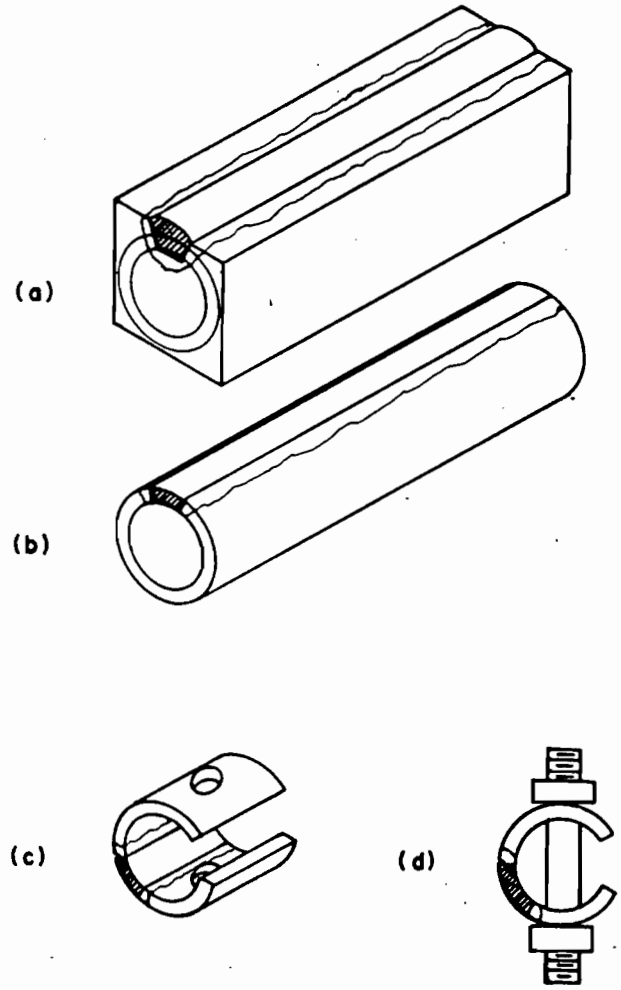

Figure 24. Successive steps in the making of C-rings specimens. (a)bar with weld filled groove, (b)tube machined from square bar stock, (c)portion of the tube notched in the heat affected zone with hole drilled through ring and back removed, and (d) finished C-ring with loading bolt in place.

This equation is modified for the presence of the notch by considering the outer fiber of the ring to be at the root of the notch rather than the outside surface. This results in the OD of the ring and thickness of the ring (t) being reduced by the depth of the notch. The deflection thus calculated is subtracted from the "true" OD to obtain the OD, parallel to the bolt, to which the ring has to be deformed to obtain the nominal stress level desired at the root of the notch.

The stress at the root of the charpy V type notch is considerably higher than the nominal outer fiber stress calculated above due to the induced stress concentration. Utilizing Peterson's[135] curves for the stress concentration factor resulting from bending of a flat bar with a U-shaped notch on one side, the stress concentration factor, K_t, is determined to be approximately 1.7. Thus the stress at the root of the notch for a nominal outer fiber stress of 100ksi (690MPa) would be approximately 170ksi (1200MPa). Based on an average hardness of 400DPH (approximately 380BHN) obtained in the transformation studies for the modified 2 1/4 and 3Cr materials, the coarse grained HAZ has an ultimate strength of approximately 190ksi (1300MPa). A 100ksi (690MPa) applied load should therefore not exceed the ultimate strength of the coarse grained HAZ.

A nominal stress of 100ksi (690MPa) was employed at PWHT temperatures of 1150°F (620°C) and 1250/1275°F (680°C). The initial stress of 100ksi (690MPa) was chosen to insure that plastic deformation had occurred at the root of the notch and therefore that the stress level is of yield stress magnitude. Additional testing was performed at 1150°F (620°C) at stress

levels of 80ksi (550MPa) and 60ksi (410MPa) in order to attempt to discern differences in susceptibility of materials that exhibit cracks at the 100ksi (690MPa) stress level.

C-ring specimens were PWHT in air and under vacuum. The specimens heat treated in vacuum were placed in quartz tubes and the tubes evacuated and sealed. Selected specimens heat treated in vacuum were broken open at liquid nitrogen temperature and examined in the scanning electron microscope. The remaining specimens heat treated in vacuum were sectioned into six pieces, mounted, and examined metallographically. The maximum extent (depth) of cracking in the sections was noted. The samples post weld heat treated in air were cooled in liquid nitrogen and broken open. Oxidation of the C-rings heat treated in air simplifies evaluation of the extent cracking as the intergranular fracture surface is darkened while the cleavage fracture surface is bright. The maximum depth of intergranular fracture was determined and used as the parameter for evaluation of PWHT cracking susceptibility.

HAZ Soft Zone Evaluation

A 50 ton commercial heat of modified 9Cr-1Mo produced by NKK was utilized for the soft zone studies. The material was initially tested in the normalized and tempered condition (normalized 1900°F (1040°C), tempered 1400°C (760°C)), but some material was also tested in the normalized condition to exaggerate the extent of the soft region.

Autogenous single and multipass (five pass) gas tungsten arc (GTA) welds were deposited in the rolling direction using a heat input of 45.2KJ/in (1.6KJ/mm). Hardness measurements were then conducted on transverse sections of these welds to locate and evaluate the extent of the

soft region. The hardness measurements were conducted on specimens in the as welded and in the PWHT (1350°F) 1 hour and 10 hour conditions.

Microhardness profiles were obtained across the HAZ in a direction normal to the weld metal-HAZ-base metal interfaces. A Vickers hardness tester using a 2 Kg load was employed. In addition to the normal section specimens, specimens were also removed at an angular orientation relative to the weld. These specimens enabled the HAZ to be expanded, thus permitting a more detailed examination of individual regions of interest.

Metallographic specimens from cross sections of the weldments were prepared, metallographically polished and etched in modified HCl/picral and modified 5% nital (Table 4). Optical light microscopy, scanning electron microscopy and transmission electron microscopy were utilized to evaluate the microstructure of the weld metal and HAZ. Carbide extraction replicas were prepared from the soft zone detected in the angle cut specimens.

Table 4. Etchants for 9Cr-1Mo steels.

Etchant Composition	Comments
MOD. HCl-Picral	Swab
900 ml Sat'd Picric acid in H_2O	
100 ml Hcl	good for base
20 ml H_2SO_4	metal and general
20 $FeCl_3$	microstructure
20 g $CuCl_2$	reveals solute banding
MOD. 5% Nital	Swab
900 ml Methanol	
50 ml HNO_3	good for weld metal
100 ml H_2O	solidification
20 ml H_2SO_4	substructure
20 g $FeCl_3$	Make two solutions
20 g $CuCl_2$	and mix before using.
20 g HCl	

RESULTS AND DISCUSSION

Transformation Behavior

The formation of cracks in weldments fabricated from the Cr-Mo steels is most often found to occur in the coarse grained heat affected zone. The types of cracking most often associated with welds in these alloys, PWHT cracking hydrogen and assisted cracking, result from the high residual tensile stress state in and metallurgical condition of this region. Therefore, the first step in determining the weldability of these materials is the determination of the transformation characteristics and microstructure of the coarse grained heat affected zone.

The coarse grained heat affected zone in actual welds is a narrow region adjacent to the fusion zone that experiences a gradient of peak temperatures associated with the upper temperature regimes of the austenite region in the equilibrium phase diagram. The limited extent of the coarse grained HAZ and the steep temperature gradient experienced over this region make characterization of the coarse grained heat affected zone in actual welds difficult. Gleeble simulation permits the expansion of this portion of the heat affected zone associated with a single peak temperature to a volume sufficient for mechanical testing and facilitates metallographic examination.

Gleeble simulation of the coarse grained heat affected zone was achieved in the transformation studies by employing a peak temperature of 2400°F (1320°C) and thermal cycles representative of a variety of welding conditions. The transformation temperatures associated with welding conditions were determined by the use of a high speed dilatometer in

contact with the specimen during the thermal cycle. When the dilatometer output is coupled by the appropriate electronic circuitry to an X-Y chart recorder, a relative dilation versus temperature plot is obtained from which the transformation temperatures may be determined. Selected thermal cycled samples were sectioned at the point of thermocouple attachment, mounted, polished, and examined by both optical microscopy and scanning electron microscopy to determine the on-cooling transformation microstructures over the range of simulated welding conditions employed.

Transformation Results for the 9Cr-1Mo-V-Nb Materials.

The V-Nb modified 9Cr-1Mo alloys have been shown to possess high hardenability in Jominy tests, exhibiting uniform hardness over the length of the Jominy bar.[114] Bodine et al.[132] have shown that the modified 9Cr-1Mo alloys "invariably transform to martensite on cooling after normalization, irrespective of the cooling rate used." Based on these observations and the continuous cooling transformation diagram for a 9Cr-1Mo-V-Nb alloy (Figure 7), it was anticipated that a martensitic microstructure would result in the coarse grained heat affected zone for all thermal cycles employed in the transformation investigation. Therefore, only three weld thermal cycles were utilized to characterize the transformation behavior of the three commercial 9Cr-1Mo-V-Nb heats. The three thermal cycles employed were the nominal 18KJ/in (0.71KJ/mm), 35KJ/in (1.4KJ/mm), and 150KJ/in (5.9KJ/mm) heat input weld simulations.

The on-heating transformation temperatures, A_{C1} and A_{C3}, for the NKK 9Cr-1Mo-V-Nb, Sumitomo 9Cr-1Mo-V-Nb, and Timken 9Cr-1Mo-V-Nb are shown in Table 5. For these materials the A_{C1} temperatures range from 1620 to 1640°F (880 to 895°C) and the A_{C3} temperatures range from 1750 to 1770°F

Table 5. Summary of the on-heating transformation temperatures for the 9Cr-1Mo-V-Nb alloys.

Material	Supplier	A_{C1}		A_{C3}	
		°F	(°C)	°F	(°C)
9Cr-1Mo-V-Nb-0.10C	NKK	1640	(895)	1750	(950)
9Cr-1Mo-V-Nb-0.095C	Timken	1620	(880)	1750	(950)
9Cr-1Mo-V-Nb-0.10C	Sumitomo	1630	(890)	1770	(940)

Table 6. Summary of the on-cooling transformation temperatures for the 9Cr-1Mo-V-Nb alloys.

Material	Supplier	18KJ/in		35 KJ/in		150 KJ/in	
		M_s °F (°C)	M_f °F (°C)	M_s °F (°C)	M_f °F (°C)	M_s °F (°C)	M_f °F (°C)
9Cr-1Mo-V-Nb	NKK	755 (400)	520 (270)	710 (375)	495 (260)	730 (390)	530 (275)
9Cr-1Mo-V-Nb	Timken	720 (380)	530 (275)	735 (390)	540 (280)	740 (395)	535 (280)
9Cr-1Mo-V-Nb	Sumitomo	735 (390)	535 (280)	715 (380)	515 (270)	730 (390)	520 (270)

(940 to 950°C). A comparison of the A_{C1} and A_{C3} temperatures obtained for the three commercial heats with the A_{C1} and A_{C3} temperatures (1526°F (830°C) and 1661°F (905°C) respectively) shown on the continuous cooling transformation diagram (Figure 7) shows that the fast heating rate associated with welding has resulted in an increase of the on-heating transformation temperatures. The A_{C1} temperatures have been increased between 94 and 124F° (52 and 69C°) and the A_{C3} temperatures have been increased between 89 and 109F° (50 and 65C°).

The on-cooling transformation temperatures, M_s and M_f, for the NKK, Timken, and Sumitomo 9Cr-1Mo-V-Nb materials are shown in Table 6. The M_s temperatures range from 755 to 710°F (400 to 375°C) and the M_f temperatures range from 540 to 495°F (280 to 260°C). The M_s and M_{f90} temperatures obtained from the continuous cooling transformation diagram (Figure 7) are 716°F (380°C) and 545°F (285°C) respectively. Thus, the M_s and M_f temperatures obtained for the NKK, Timken, and Sumitomo under welding conditions agree reasonably well with those from the conventional continuous cooling transformation diagram. The M_s temperatures are within +36 to -9F° (+20 to -5C°) and the M_f temperatures are within +9 to -45F° (+5 to -25C°) of the M_s and M_{f90} temperatures shown in Figure 7.

Figure 7 shows that the last 10% of the austenite to martensite transformation occurs between 716°F (380°C), the M_{f90} temperature, and 536°F (280°C), the M_f temperature. This small amount of transformation over a relatively large temperature range is not likely to have been detected in the Gleeble transformation studies. System sensitivity, electronic noise and small variations that occur in the slope of the dilation versus temperature trace combine to obscure a minor amount of

transformation over a wide temperature range. However, in a practical sense, the M_f for the modified materials obtained by Gleeble simulation is sufficiently accurate for the purpose of weldability assessment.

9Cr-1Mo-V-Nb Microstructures.

Optical micrographs of the Gleeble simulated 18KJ/in (0.71KJ/mm) and 150KJ/in (5.9KJ/mm) weld thermal cycle specimens of the NKK 9Cr-1Mo-V-Nb, Sumitomo 9Cr-1Mo-V-Nb, and Timken 9Cr-1Mo-V-Nb are shown in Figures 25 through 30. Scanning electron micrographs of the 150KJ/in (5.9KJ/mm) for the three 9Cr-1Mo-V-Nb heats are shown in Figures 31 through 34.

The optical micrographs (Figures 25-30) reveal little about the microstructure of the 9Cr-1Mo-V-Nb materials. A comparison of the 150KJ/in micrographs (Figures 25, 27, and 29) with the 18KJ/in (0.71KJ/mm) micrographs (Figures 26, 28, and 30) shows a modest amount of grain coarsening which would be anticipated with the longer time above the grain coarsening temperature associated with the higher energy input thermal cycle. Delta ferrite is present in both of the Timken 9Cr-1Mo-V-Nb optical micrographs (Figures 29 and 30) with the delta ferrite in the 150KJ/in (5.9KJ/mm) specimen present in larger and more widely spaced pools.

The scanning electron micrographs of the NKK 9Cr-1Mo-V-Nb (Figure 31)and Sumitomo 9Cr-1Mo-V-Nb (Figure 32) materials show microstructures consisting of acicular martensite and autotempered martensite. The autotempered martensite appears more clearly at the lower magnification, 2000X, (Figures 31a and 32a) as irregular, roughened, lenticular structures. Similar microstructures are shown in De Ferri Metallographia[110] for quenched 2 1/4Cr-1Mo (900°C to 500°C in 0.7sec) and 5Cr-1Mo (oil quenched from 950°C) with the lenticular, roughened structures

Figure 25. NKK 9Cr-1Mo-V-Nb CCT specimen, 18KJ/in. Modified Wazu's etch, OLM 200X.

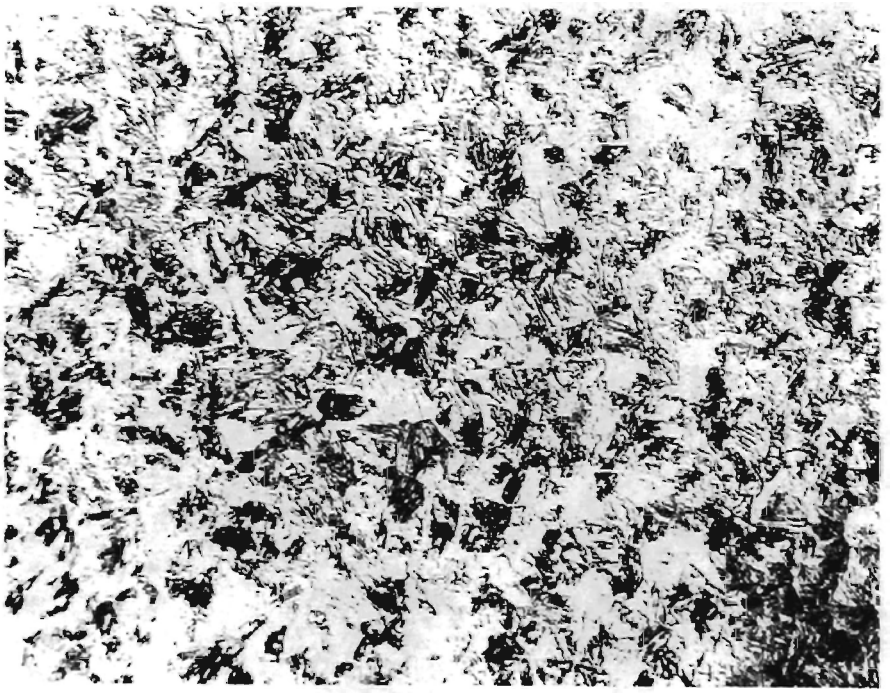

Figure 26. NKK 9Cr-1Mo-V-Nb CCT specimen, 150KJ/in. Modified Wazu's etch, OLM 200X.

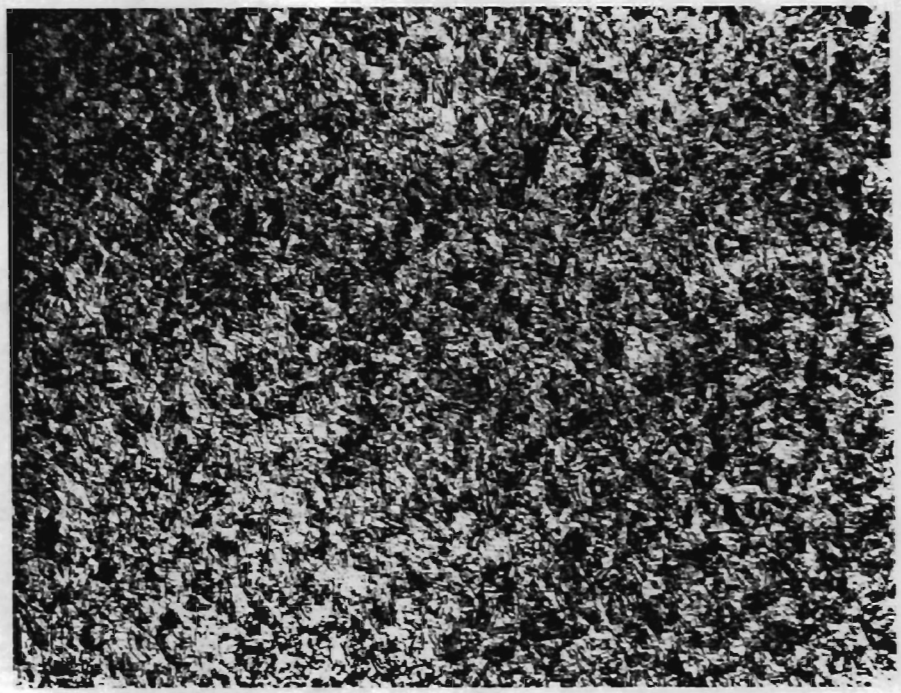

Figure 27. Sumitomo 9Cr-1Mo-V-Nb CCT specimen, 18KJ/in. Modified Wazu's etch, OLM 200X.

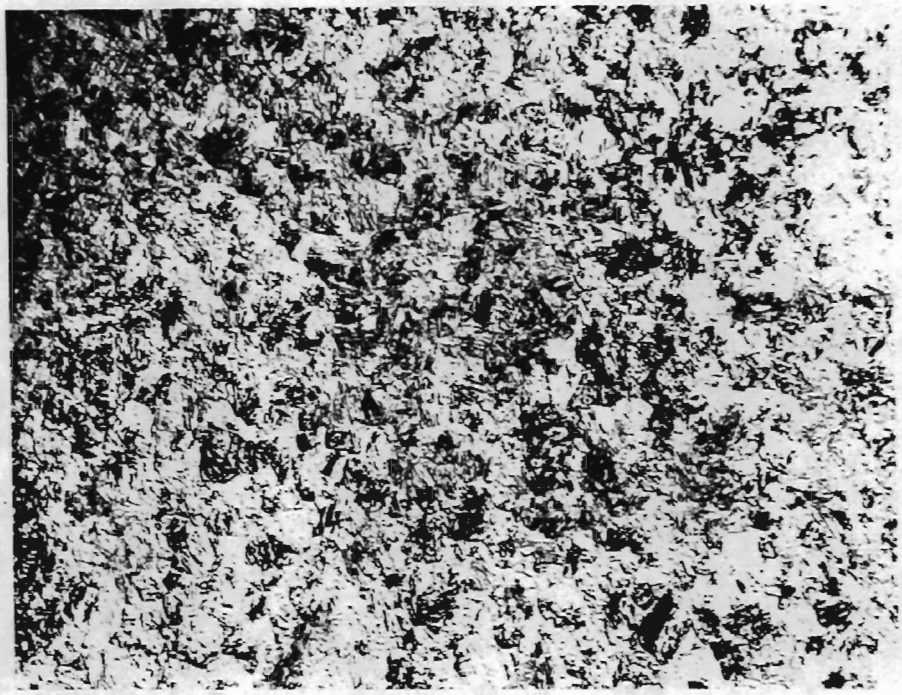

Figure 28. Sumitomo 9Cr-1Mo-V-Nb CCT specimen, 150KJ/in. Modified Wazu's etch, OLM 200X.

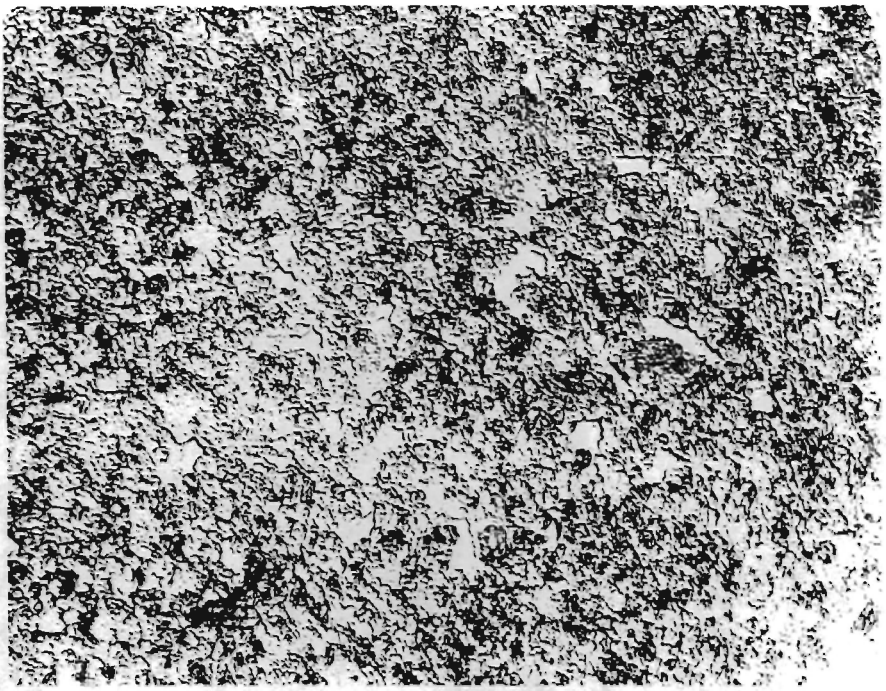

Figure 29. Timken 9Cr-1Mo-V-Nb CCT specimen, 18KJ/in. Modified Wazu's etch, OLM 200X.

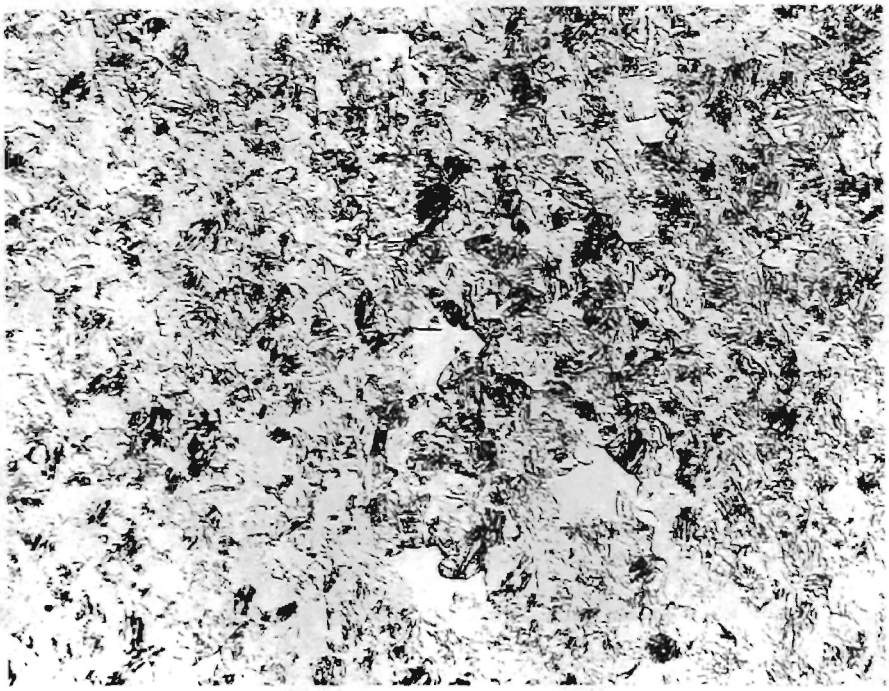

Figure 30. Timken 9Cr-1Mo-V-Nb CCT specimen 150KJ/in. Modified Wazu's etch, OLM 200X.

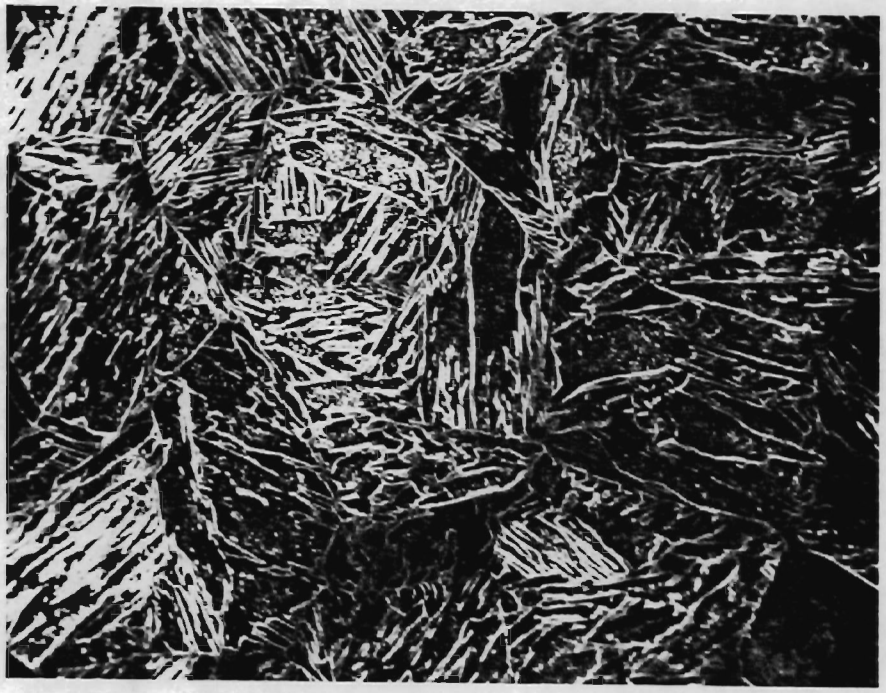

A

B

Figure 31. NKK 9Cr-1Mo-V-Nb CCT specimen, 150KJ/in. Modified Wazu's etch, SEM. a) 2,000X, b) 10,000X.

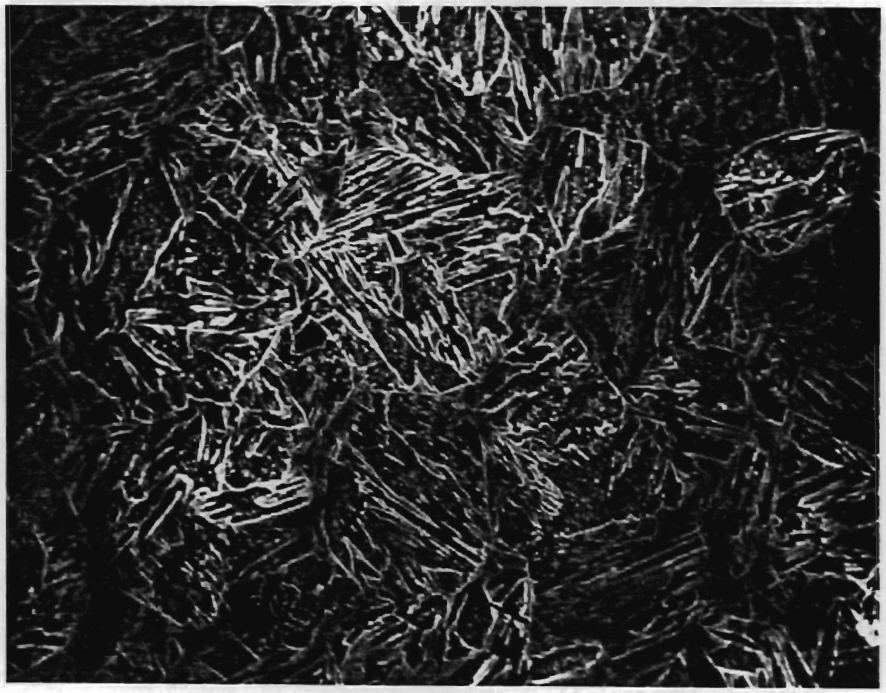

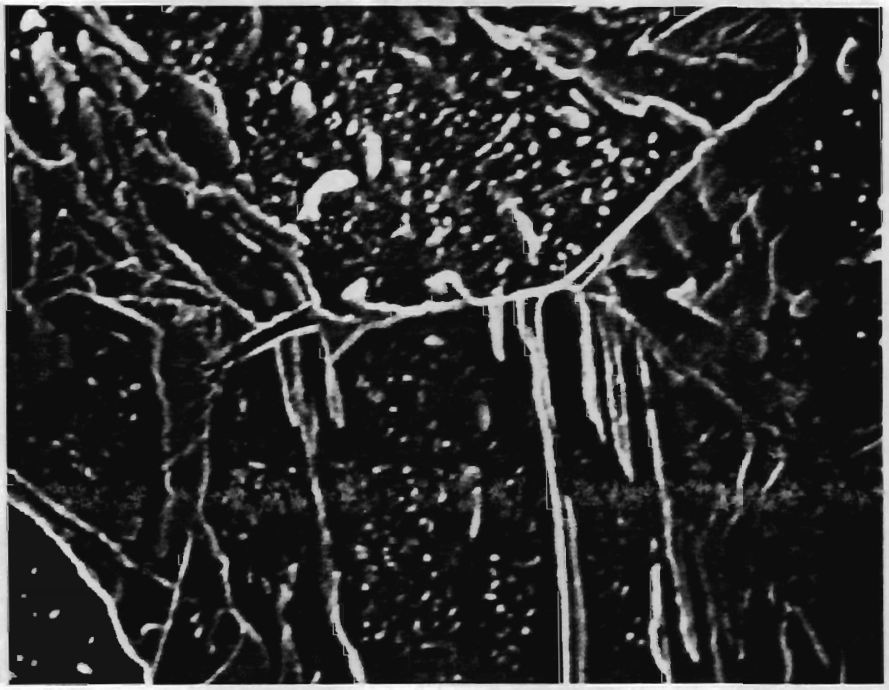

Figure 32. Sumitomo 9Cr-1Mo-V-Nb CCT specimen, 150KJ/in. Modified Wazu's etch, SEM. a) 2,000X, b) 10,000X.

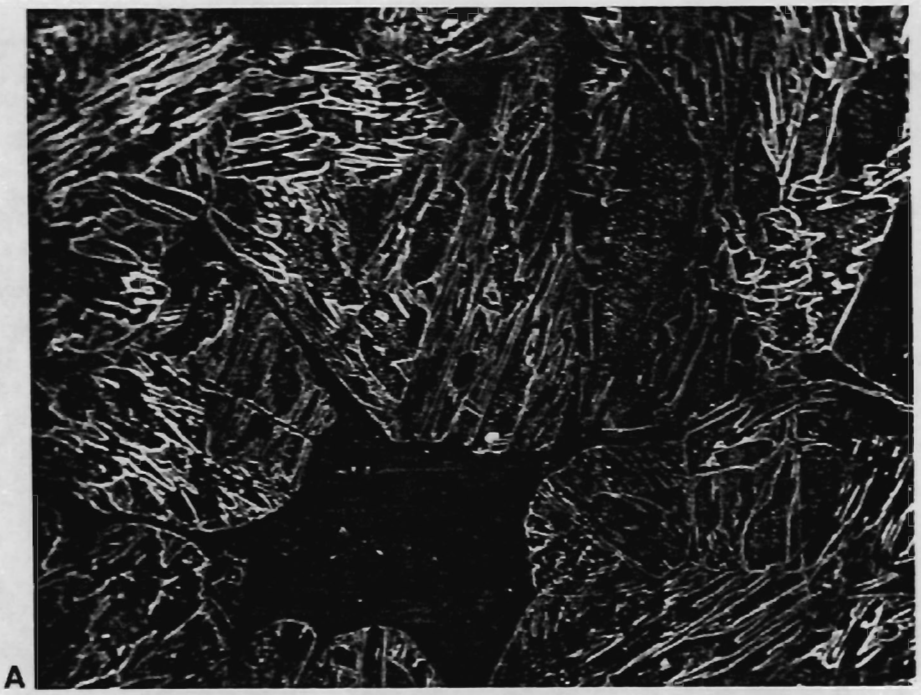

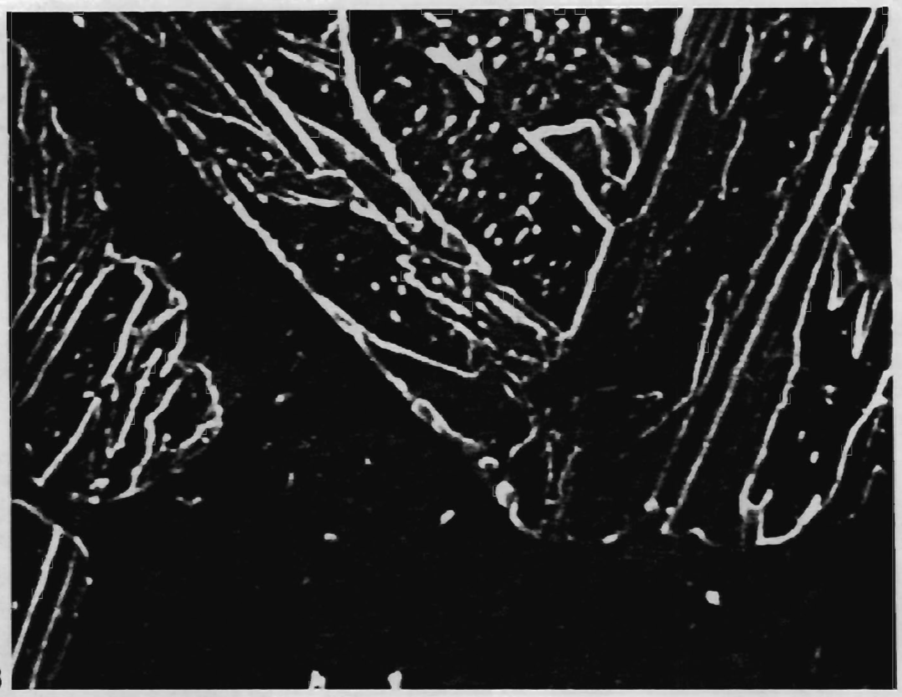

Figure 33. Timken 9Cr-1Mo-V-Nb CCT Specimen, 150KJ/in. Modified Wazu's etch SEM. a) 2,000X, b) 10,000X.

Figure 34. Timken 9Cr-1Mo-V-Nb CCT specimen, 150KJ/in. Modified Wazu's etch. SEM 10,000X.

described as being due to autotempering of the first martensite formed from the austenite. The roughening of the plate like structures is said to result from the formation of carbides during autotempering. At higher magnification, 10,000X, (Figures 31b and 32b) the roughening in the plate like structures observed at lower magnification can clearly be seen to be due to the formation of carbides within the autotempered martensite.

The scanning electron micrographs of the Timken 9Cr-1Mo-V-Nb material (Figures 33 and 34) show the microstructure to consist of martensite, autotempered martensite and delta ferrite. The large pool of delta ferrite shown in Figure 33 was located at a triple point in the prior austenite microstructure. The narrow regions of delta ferrite extending from the main pool are disposed along the prior austenite grain boundaries. The presence of residual scratches, from polishing, within the pool may be used as additional evidence that this structure consists of ferrite, as ferrite is an inherently softer constituent than martensite.

The retention of delta ferrite, the elevated temperature body centered cubic phase, is a result of stabilization of the high temperature ferrite phase. 9Cr-1Mo alloys have a composition near the austenite-ferrite phase boundary of the iron-chromium equilibrium phase diagram. The addition of ferrite stabilizing elements such as silicon, molybdenum, vanadium and niobium may result in an alloy that exists in the two phase region over a large temperature range. Since the decomposition of ferrite to austenite is a diffusion controlled process, rapid cooling and a low ferrite to austenite transformation temperature combine to result in retention of delta ferrite in the ambient temperature microstructure.[25] Work performed at ORNL has shown that for normalizing heat treatments, the

chromium equivalent equation (equation 3.1) can be utilized to predict the retention of delta ferrite in the microstructure.[132] For chromium equivalents in excess of 12 normalizing was found to result in the retention of substantial amounts of delta ferrite. The Timken 9Cr-1Mo-V-Nb alloy, with a chromium equivalent of 13.4, had delta ferrite retained in the Gleeble simulation microstructures as would be anticipated from the work performed at ORNL. The NKK and Sumitomo heats, with chromium equivalents of 11.7 and 10.6, did not exhibit delta ferrite retention in the optical or scanning electron micrographs although the work at ORNL indicated that delta ferrite might be present for 9Cr-1Mo-V-Nb alloys with chromium equivalents between 10 and 12.

Figure 34 is a scanning electron micrograph of a region well removed from the delta ferrite in the Timken 9Cr-1Mo-V-Nb material. The microstructure is similar to that of the NKK 9Cr-1Mo-V-Nb and the Sumitomo 9Cr-1Mo-V-Nb (Figures 31b and 32b). The microstructure consists of both acicular martensite and autotempered martensite. Figure 34 again shows that the roughening of the auto tempered martensite is due to the formation of carbides within the plate like structures.

Summary of the 9Cr-1Mo-V-Nb Transformation Studies.

The on-heating and on-cooling transformation temperatures for the NKK 9Cr-1Mo-V-Nb, Sumitomo 9Cr-1Mo-V-Nb, and Timken 9Cr-1Mo-V-Nb alloys were found to be approximately the same as would be expected from their similar chemical compositions. The A_{C1} and A_{C3} temperatures were found to be higher under the rapid heating of the simulated welding thermal cycle in comparison to those determined by Wada et al. (Figure 7). This elevation of the on-heating temperatures was expected as the formation of austenite

is diffusion controlled. The on-cooling transformation temperatures are in substantial agreement with those shown on the continuous cooling transformation diagram (Figure 7). The formation of martensite occurs by a diffusionless, shear process and therefore depression of the transformation temperature would not be expected to be significant. With the exception of the Timken material the microstructures of the weld simulated specimens were martensitic as was predicted by the continuous cooling transformation diagram. The microstructure of the Timken alloy contained retained delta ferrite due to the increased amount of ferrite stabilizing elements which was reflected in the higher value of the chromium equivalent in comparison to the NKK and Sumitomo materials. The presence of delta ferrite in the Timken material was in agreement with work performed at ORNL with normalized 9Cr-1Mo-V-Nb alloys.

Transformation Results for the Modified 2 1/4Cr and 3Cr Alloys.

The on-heating transformation temperatures for the AMAX (Climax) 3Cr-1 1/2Mo-0.1V (heat A9349), Berkeley composition 3Cr-1 1/2Mo-1/2Ni, JSW 3Cr-1Mo-V-Ti-B, and JSW 2 1/4Cr-1Mo-V-Ti-B alloys appear in Table 7. The on-cooling transformation temperatures determined for the modified 2 1/4Cr and 3Cr materials appear in Table 8. Figures 35 through 38 are continuous cooling transformation diagrams determined under simulated welding conditions for the AMAX (Climax) 3Cr-1 1/2Mo-0.1V, Berkeley 3Cr-1 1/2Mo-1/2Ni, JSW 3Cr-1Mo-V-Ti-B, and JSW 2 1/4Cr-1Mo-V-Ti-B materials.

The A_{C1} and A_{C3} temperatures for the Berkeley 3Cr-1 1/2Mo-1/2Ni material (Table 7) are dramatically increased by the additional heat treatment given to the as received material. The as received material,

Table 7. Summary of the on-heating transformation temperatures for the modified 3Cr and 2 1/4Cr alloys.

Material	A_{C1}		A_{C3}	
	°F	(°C)	°F	(°C)
Amax (Climax) 3 Cr-1½Mo-0.1	1490	(810)	1660	(905)
Berkeley 3 Cr-1½Mo-½Ni	1325	(720)	1570	(850)
Berkeley heat treated to Class III	1515	(825)	1630	(890)
JSW 3 Cr-1Mo-V-Ti-B	1480	(805)	1620	(880)
JSW 2¼ Cr-1Mo-V-Ti-B	1500	(815)	1670	(910)

Table 8. Summary of the on-cooling transformation temperatures for the modified 3Cr and 2 1/4Cr alloys.

Thermal Cycle (KJ/in)		Climax (A9349) 3 Cr-1½ Mo-0.1V		Berkeley 3 Cr-1½ Mo - ½ Ni		Berkeley Heat Treated to Class III		JSW 3Cr-1Mo-V-Ti-B		JSW 2¼ Cr-1Mo-V-Ti-B	
		°F	(°C)	°F	(°C)	°F	(°C)	°F	(°C)	°F	(°C)
18	S	820	(435)	790	(420)	790	(420)	830	(440)	880	(470)
	F	620	(325)	620	(325)	575	(300)	840	(340)	640	(340)
35	S	820	(435)	770	(410)	780	(415)	800	(425)	880	(470)
	F	680	(360)	650	(345)	850	(345)	660	(350)	670	(355)
60	S	820	(435)	770	(410)	775	(415)	810	(430)	890	(475)
	F	710	(375)	630	(330)	630	(330)	690	(365)	680	(360)
80	S	810	(430)	790	(420)	-	-	800	(425)	900	(480)
	F	720	(380)	710	(375)	-	-	690	(365)	700	(370)
127	S	840	(450)	820	(435)	-	-	840	(450)	900	(480)
	F	730	(385)	710	(375)	-	-	750	(400)	740	(395)
150	S	850	(455)	830	(445)	840	(450)	860	(460)	940	(505)
	F	740	(395)	730	(385)	715	(300)	760	(405)	770	(410)

S - Martensite or bainite start temperatures.

F - Martensite or bainite finish temperatures.

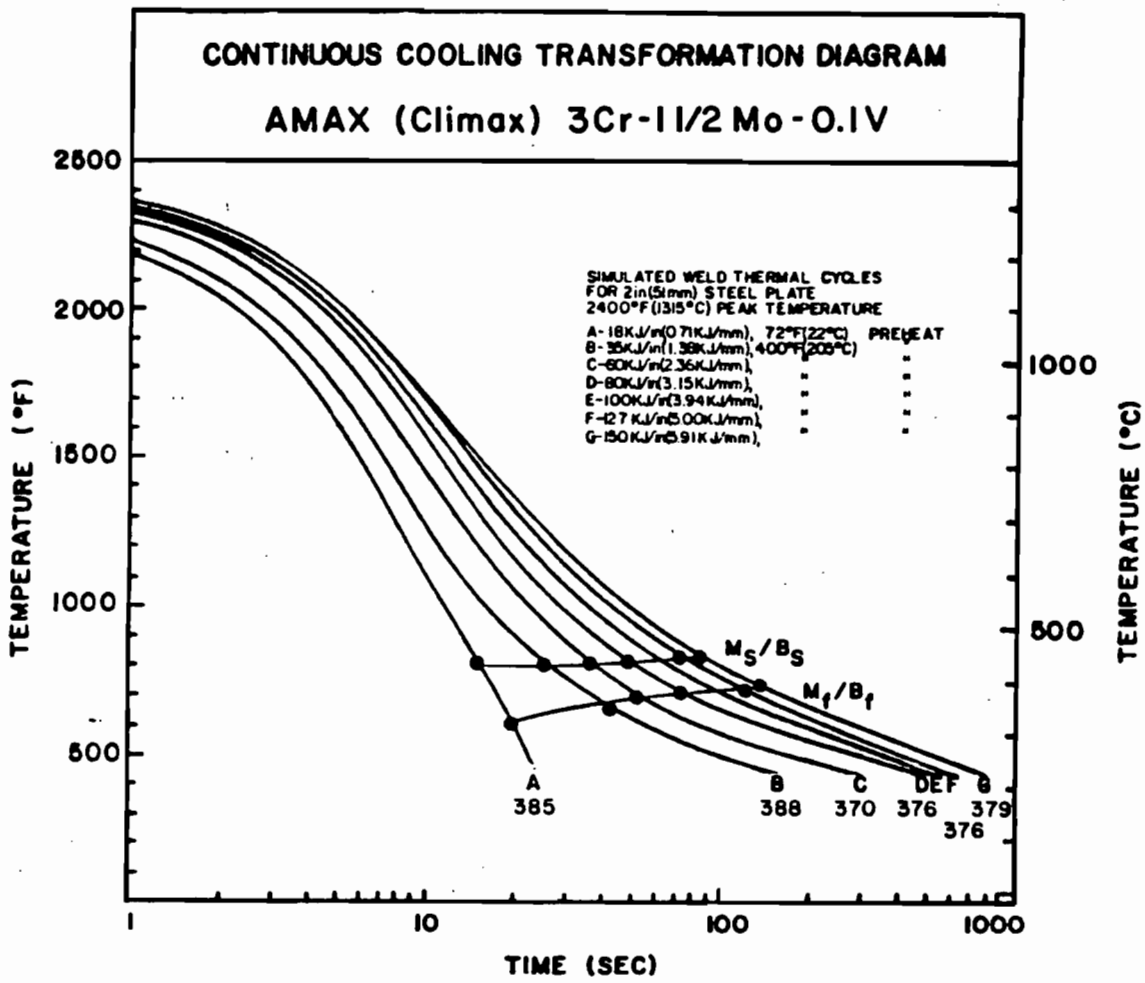

Figure 35. CCT diagram for AMAX (climax) 3Cr-1 1/2Mo-0.1V, determined for welding conditions.

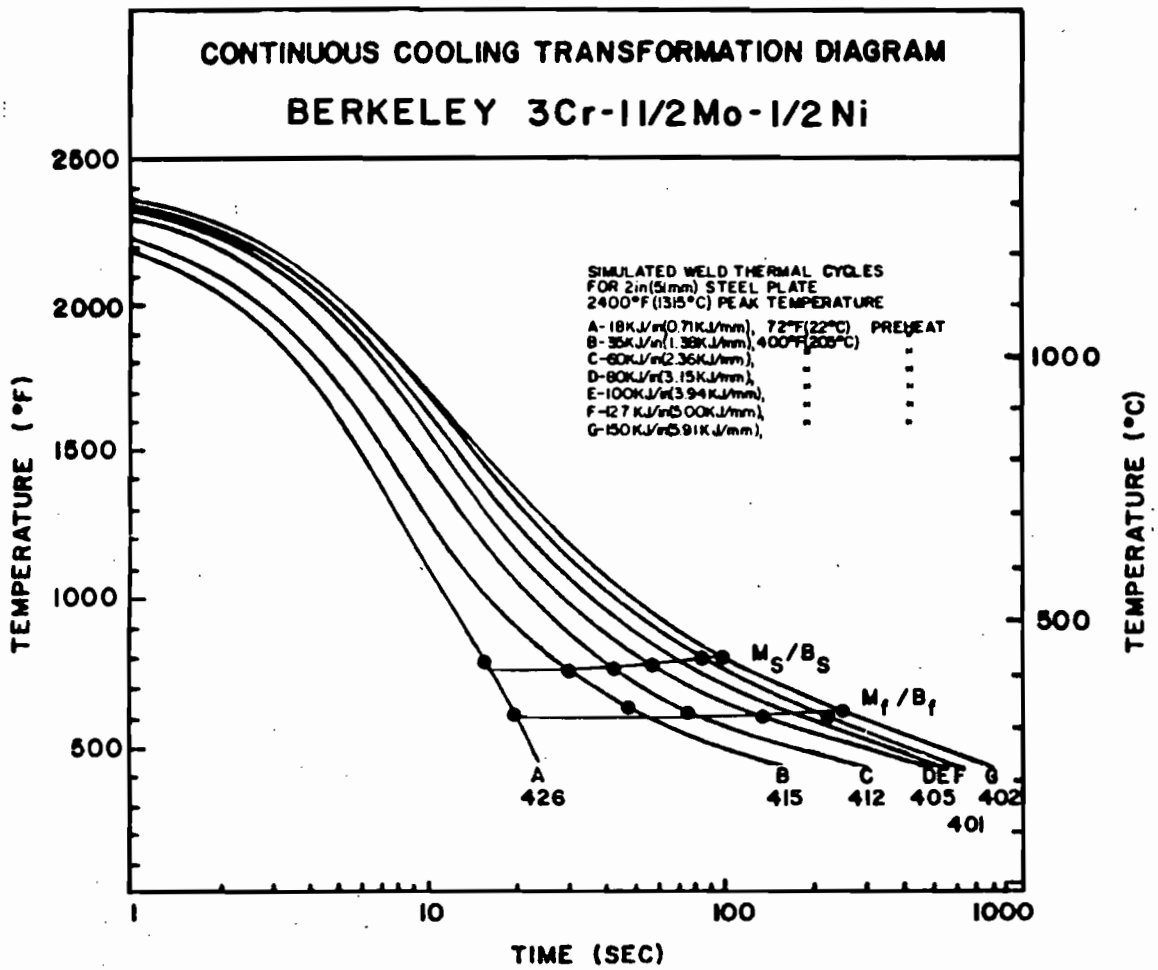

Figure 36. CCT diagram for Berkeley composition 3Cr-1 1/2Mo-1/2Ni, determined for welding conditions.

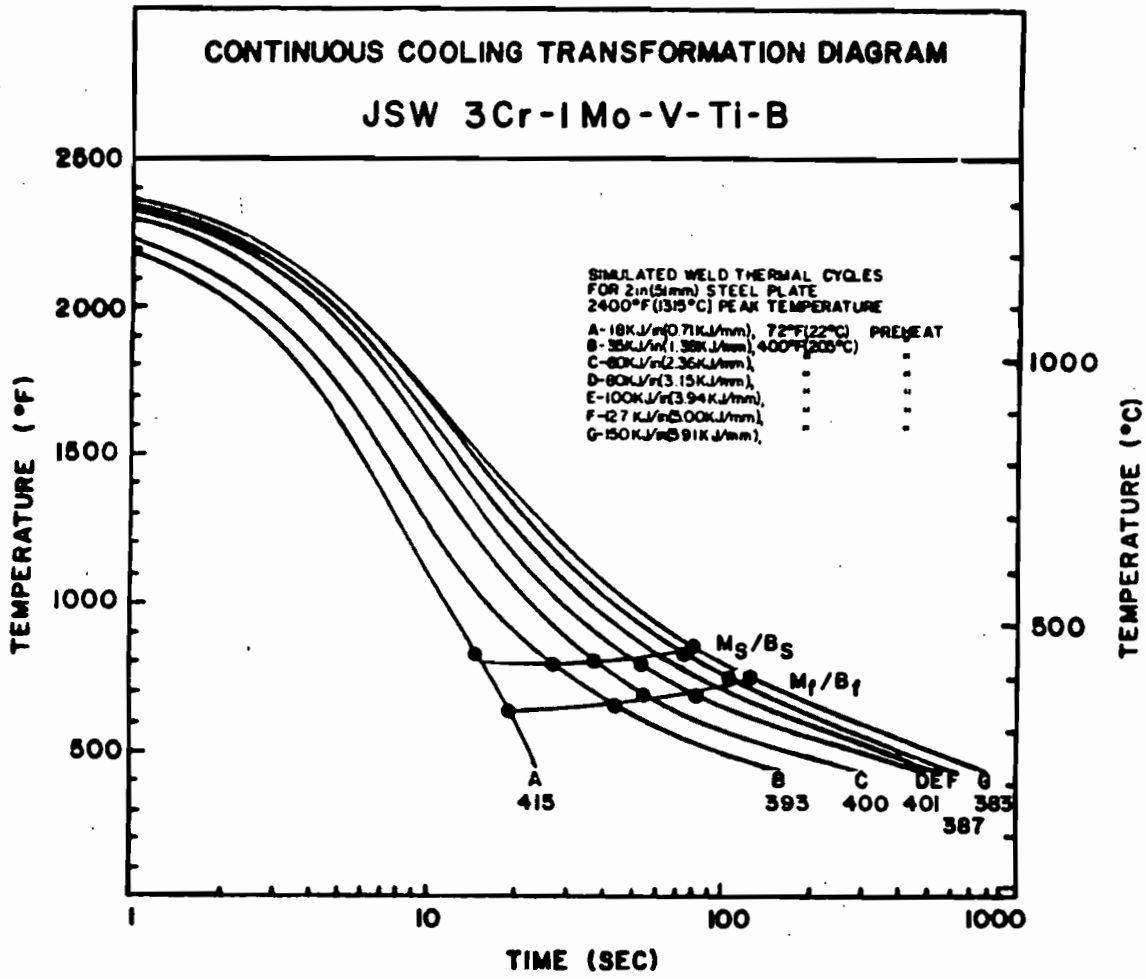

Figure 37. CCT diagram for JSW 3Cr-1Mo-V-Ti-B, determined for welding conditions.

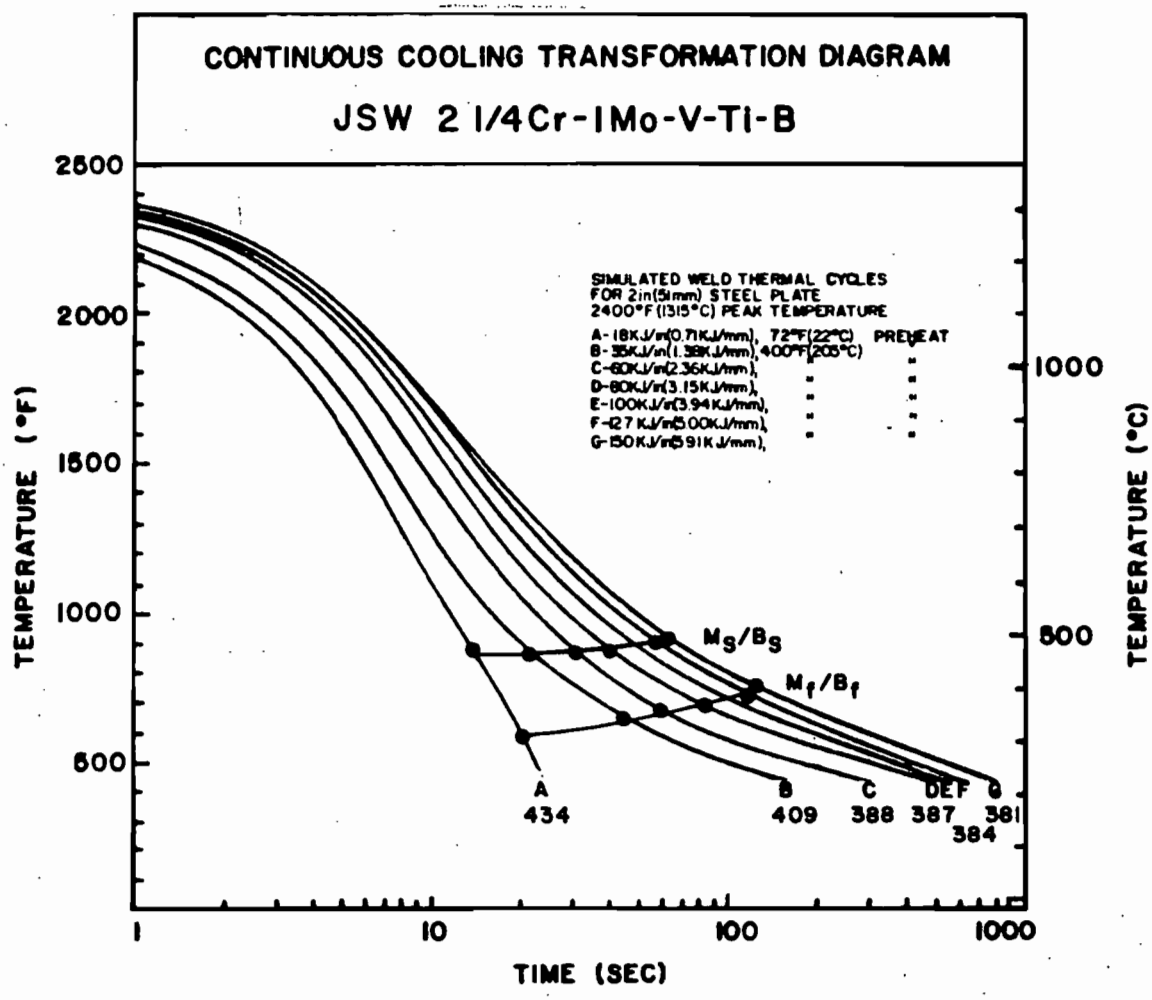

Figure 38. CCT diagram for JSW 2 1/4Cr-1Mo-V-Ti-B, determined for welding conditions.

which had been given only a short time, low temperature stress-relief heat treatment, exhibited A_{C1} and A_{C3} temperatures of 1325°F (720°C) and 1570°F (850°C) respectively. After heat treatment to obtain a strength level concomitant with the proposed class III strength level, the A_{C1} and A_{C3} temperatures were determined to be 1515°F (825°C) and 1630°F (890°C).

Higher heat treatment temperatures and longer times at the heat treatment temperature result in carbide coarsening. Coarser carbides dissolve more slowly and therefore inhibit the transformation to austenite by limiting the amount of carbon available. Under welding conditions, where the rate of heating is rapid, the sluggish dissolution of carbides results the in elevation of the transformation temperatures.

The A_{C1} temperatures for the AMAX (Climax) 3Cr-1 1/2Mo-0.1V, heat treated Berkeley 3Cr-1 1/2Mo-1/2Ni, and JSW 2 1/4Cr-1Mo-V-Ti-B materials range from 1490 to 1515°F (810 to 825°C) and A_{C3} temperatures range from 1620 to 1670°F (880 to 910°C). The A_{C1} and A_{C3} temperatures obtained from the Gleeble weld simulation studies for the AMAX (Climax) 3Cr-1 1/2Mo-0.1V, JSW 3Cr-1Mo-V-Ti-B, and JSW 2 1/4Cr-1Mo-V-Ti-B materials (Table 7) are higher than those reported on the continuous cooling transformation diagrams (Figures 4-6) between 22 and 45F° (12 and 25C°) and 18 and 54F° (10 and 28C°) respectively. The increase in the transformation temperature is the result of the carbide dissolution kinetics and diffusion control of austenite formation and the rapid heating rate associated with welding conditions.

The on-cooling transformation temperatures in Table 8 are reported as start (S) and finish (F) and in Figures 35-38 as M_s/B_s and M_f/B_f as no discernible separate finish for the bainite transformation (B_f) or start

for the martensite transformation (M_s) could be detected on the dilation versus temperature traces. For the Berkeley 3Cr-1 1/2Mo-1/2Ni no significant difference in the on-cooling transformation temperatures was observed between the as received or heat treated material with the exception of the 18KJ/in transformation finish temperature.

A comparison of the transformation start temperatures for the AMAX (Climax) 3Cr-1 1/2Mo-0.1V, JSW 3Cr-1Mo-V-Ti-B, and JSW 2 1/4Cr-1Mo-V-Ti-B under simulated welding conditions with the continuous cooling transformation diagrams for these materials (Figures 4-6) show, in general, a lowering of the transformation start by approximately 45F^{o} (25C^{o}) due to the fast cooling rate under welding conditions. Table 7 and Figures 35 through 38 show that the highest on-cooling transformation start temperatures were exhibited by the JSW 2 1/4Cr-1Mo-V-Ti-B material and the lowest on-cooling transformation start temperatures were exhibited by the Berkeley 3Cr-1 1/2Mo-1/2Ni material. The higher transformation temperatures of the JSW 2 1/4Cr-1Mo-V-Ti-B material is due to the lower carbon (0.12%) and overall lower alloying element content of this material. The lower transformation start temperatures of the Berkeley 3Cr-1 1/2Mo-1/2Ni material is due to the relatively high carbon (0.16%) and nickel (0.51%) content compared to the other three modified alloys.

A comparison of the transformation finish temperatures obtained for the AMAX (Climax) 3Cr-1 1/2Mo-0.1V material and the continuous cooling transformation diagram for the same material (Figure 6) shows a general agreement between the finish temperatures obtained under Gleeble simulated weld conditions and transformation temperatures corresponding to 90% completion of the austenite to martensite or bainite transformation. The

transformation finish temperatures obtained under Gleeble simulated welding conditions range from 620 to 740°F (324 to 395°C) and M_{f90}-B_{f90} temperatures range from 617 to 740°F (325 to 393°C). As was the case with the 9Cr-1Mo materials, the last 10% of transformation occurs over a large temperature range (approximately 225°F (125°C)) and therefore was not detectable. Similarly, the finish transformation finish temperatures for the JSW 3Cr-1Mo-V-Ti-B and JSW 2 1/4Cr-1Mo-V-Ti-B shown in table 7 are higher than the transformation finish temperatures shown in Figures 4 and 5, continuous cooling transformation diagrams for materials of similar composition.

Modified 2 1/4Cr-1Mo and 3Cr-Mo Microstructures.

Optical and scanning electron micrographs of the JSW 3Cr-1Mo-V-Ti-B alloy for the helium quench, 35 KJ/in (1.38 KJ/mm), 60 KJ/in (2.36 KJ/mm), and 150 KJ/in (5.91 KJ/mm) heat input simulated weld thermal cycles are shown in Figures 39 through 42. Since the microstructures for all the materials; AMAX (Climax) 3Cr-1 1/2Mo-0.1V, Berkeley 3Cr-1 1/2Mo-1/2Ni, JSW 3Cr-1Mo-V-Ti-B, and JSW 2 1/4Cr-1Mo-V-Ti-B, are similar only one representative set of microstructures for the range of thermal cycles employed is shown. Figures 43 through 45 are optical and scanning electron micrographs of the AMAX (Climax) 3Cr-1 1/2Mo-0.1V, Berkeley 3Cr-1 1/2Mo-1/2Ni, and JSW 2 1/4Cr-1Mo-V-Ti-B for the 60 KJ/in (2.36 KJ/mm) heat input weld simulation samples. The similarity of the microstructures obtained from the same heat input thermal cycle may be seen in the micrographs of the 60 KJ/in (2.36 KJ/mm) specimens.

As was the case with the modified 9Cr-1Mo continuous cooling transformation specimens, the optical micrographs (Figures 39a-45a) of the

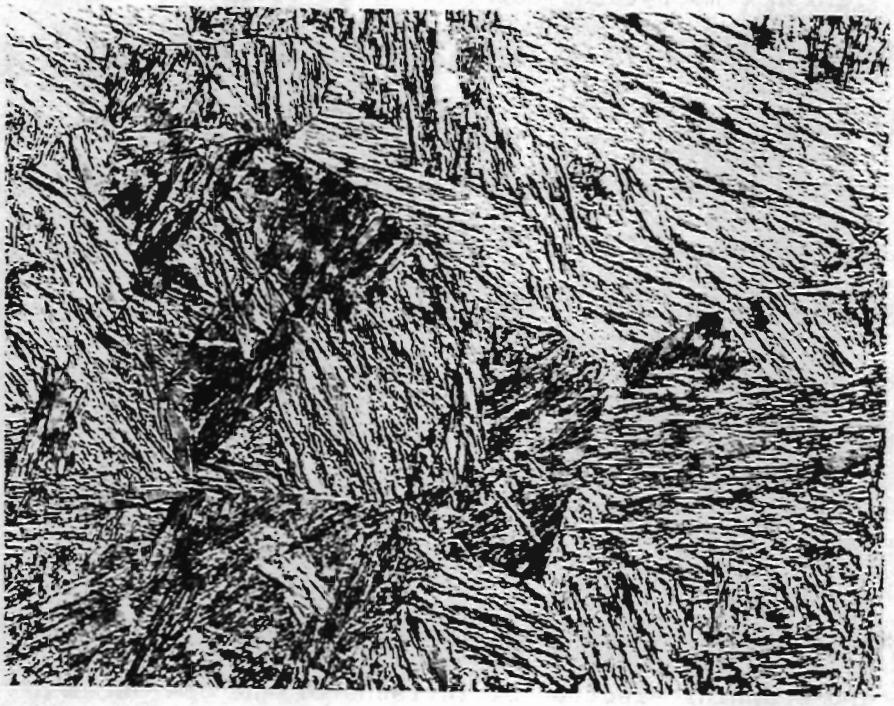

A

B

Figure 39. JSW 3Cr-1Mo-V-Ti-B, CCT specimen, helium quenched. Nital-Picral, a) 500X OLM, b) 10,000X SEM.

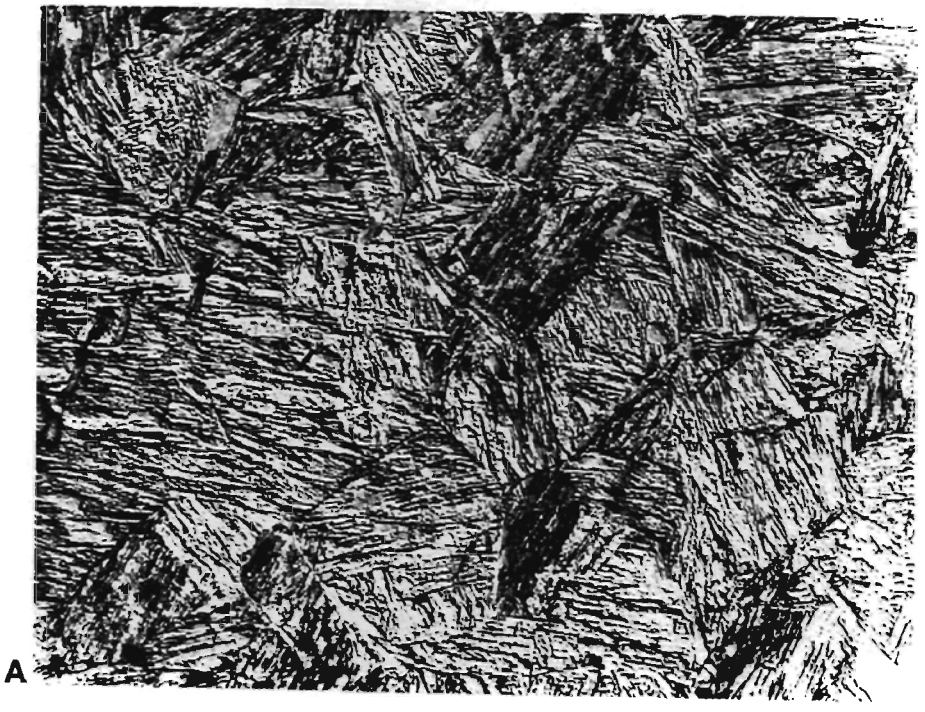

Figure 40. JSW 3Cr-1Mo-V-Ti-B, CCT specimen, 35KJ/in. Nital-Picral, a) 500X OLM, b) 10,000X SEM.

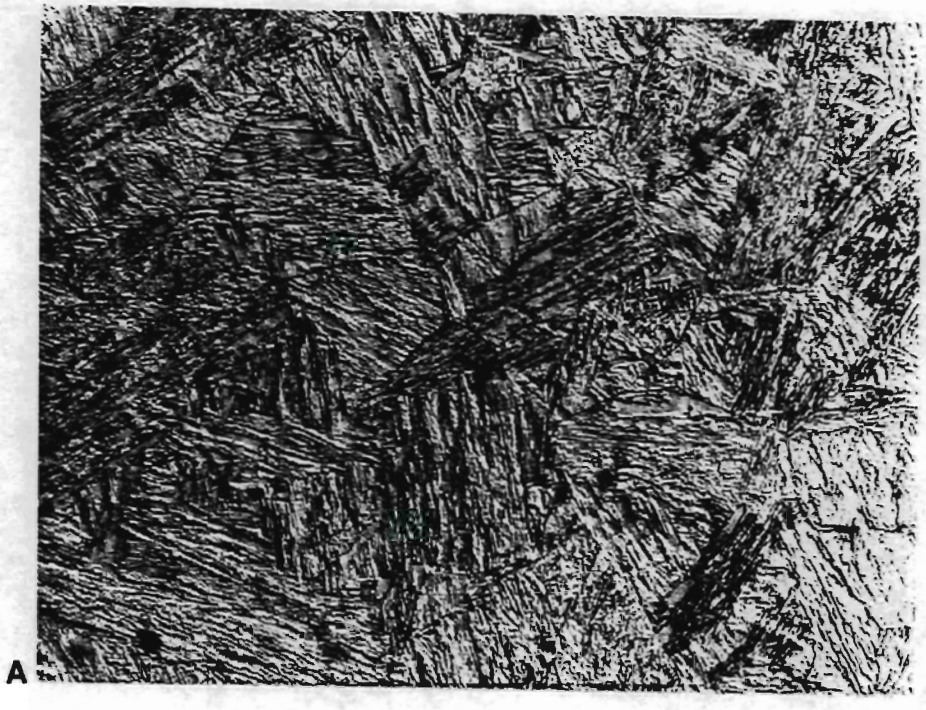

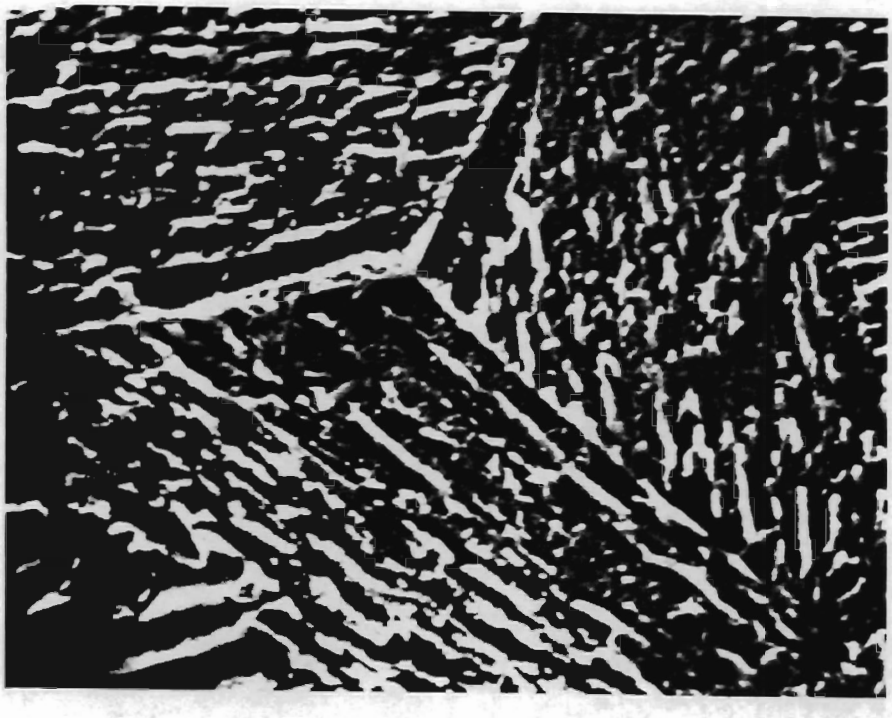

Figure 41. JSW 3Cr-1Mo-V-Ti-B, CCT specimen 60KJ/in. Nital-Picral, a) 500X OLM, b) 10,000X SEM.

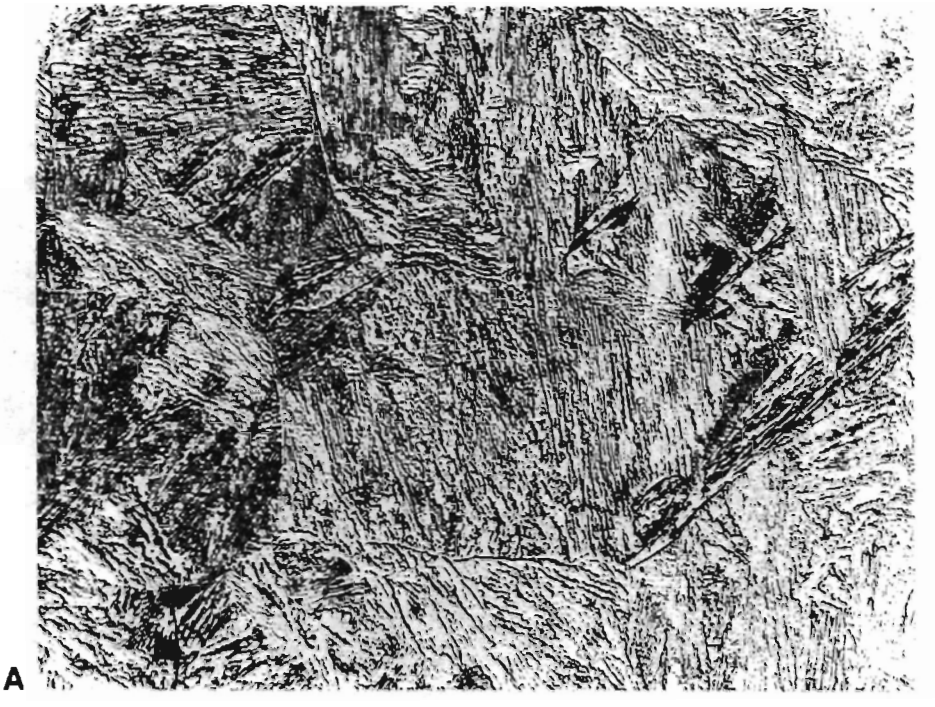

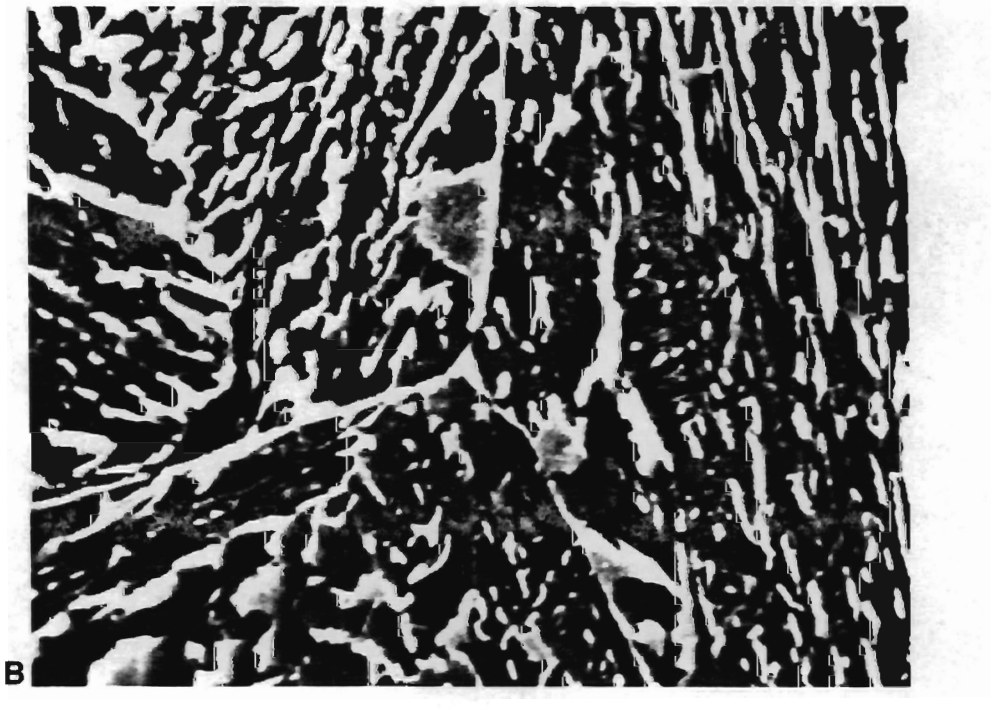

Figure 42. JSW 3Cr-1Mo-V-Ti-B, CCT specimen, 150KJ/in. Nital-Picral, a) 500X OLM, b) 10,000X SEM.

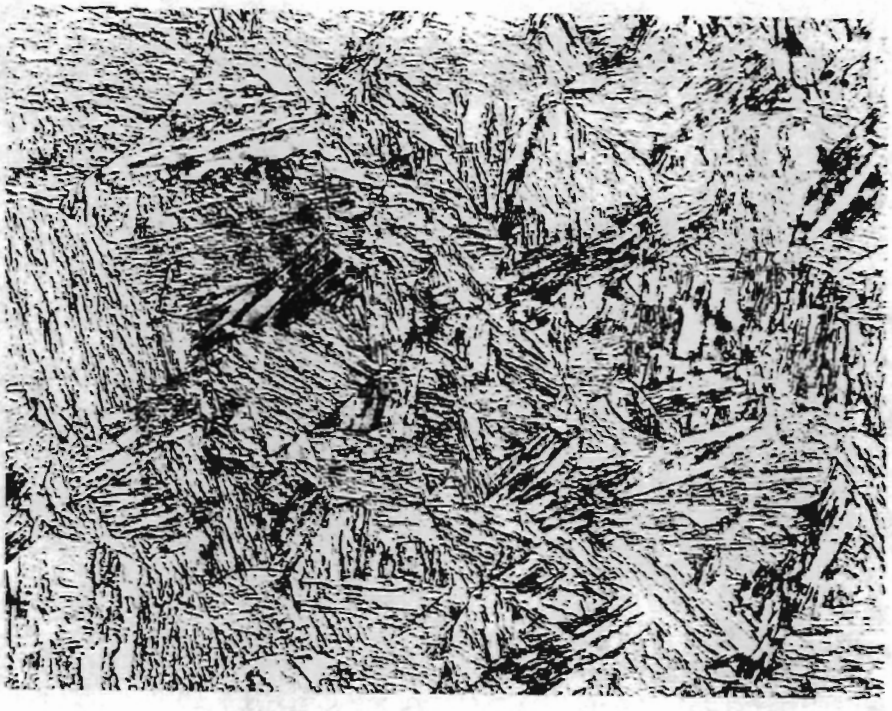

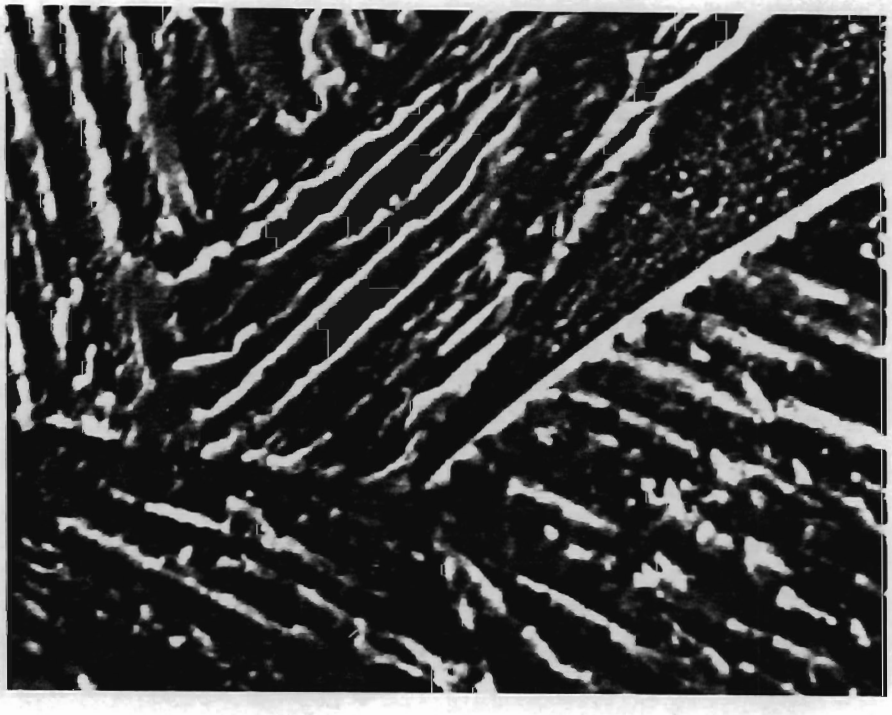

Figure 43. AMAX (Climax) 3Cr-1 1/2Mo-0.1V, CCT specimen, 60KJ/in. Nital-Picral, a) 500X OLM, b) 10,000X SEM.

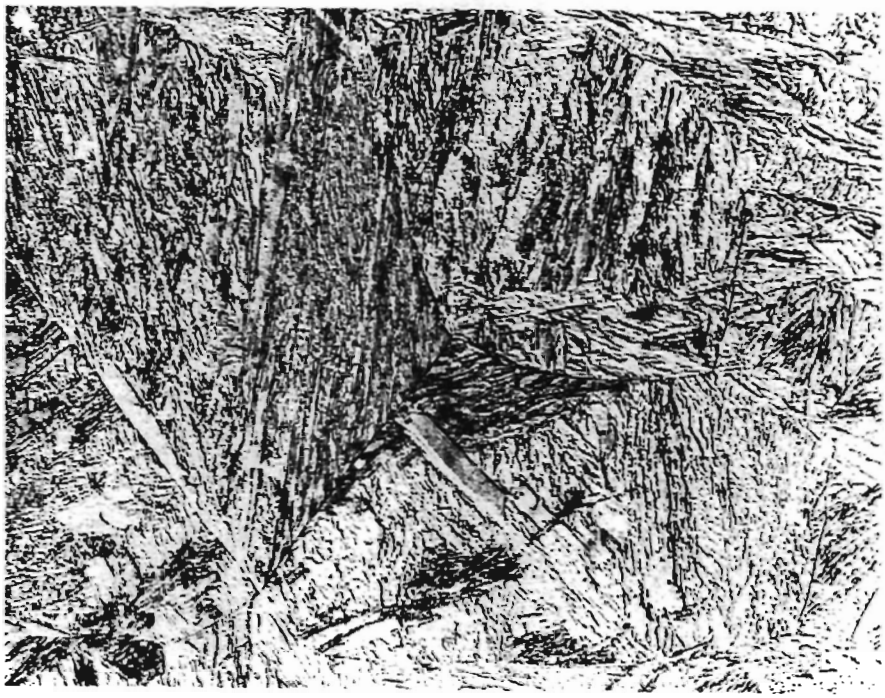

A

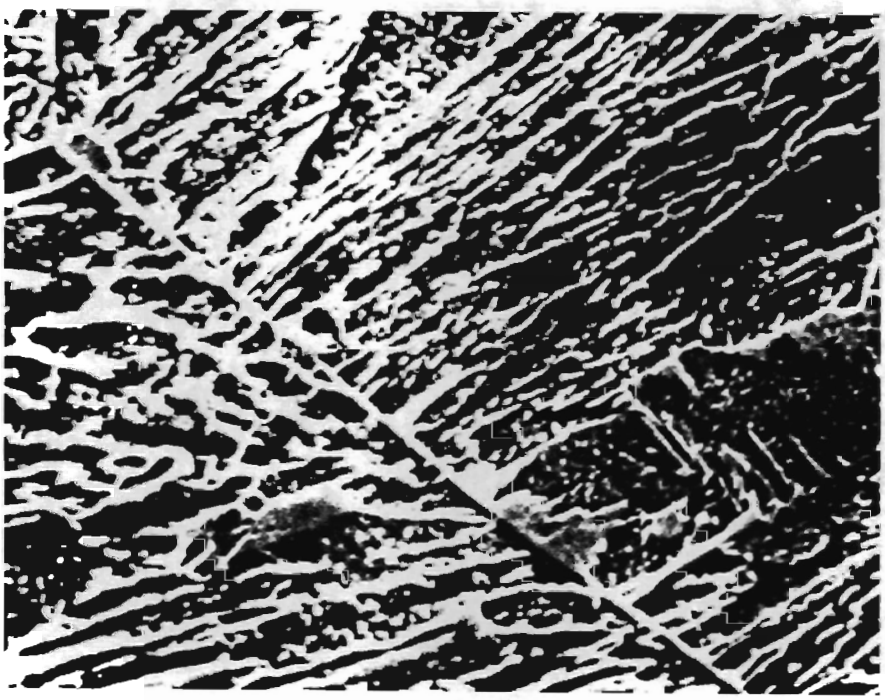

B

Figure 44. Berkeley 3Cr-1 1/2Mo-1/2Ni CCT Specimen, 60KJ/in. Nital-Picral, a) 500X OLM, b) 10,000X SEM.

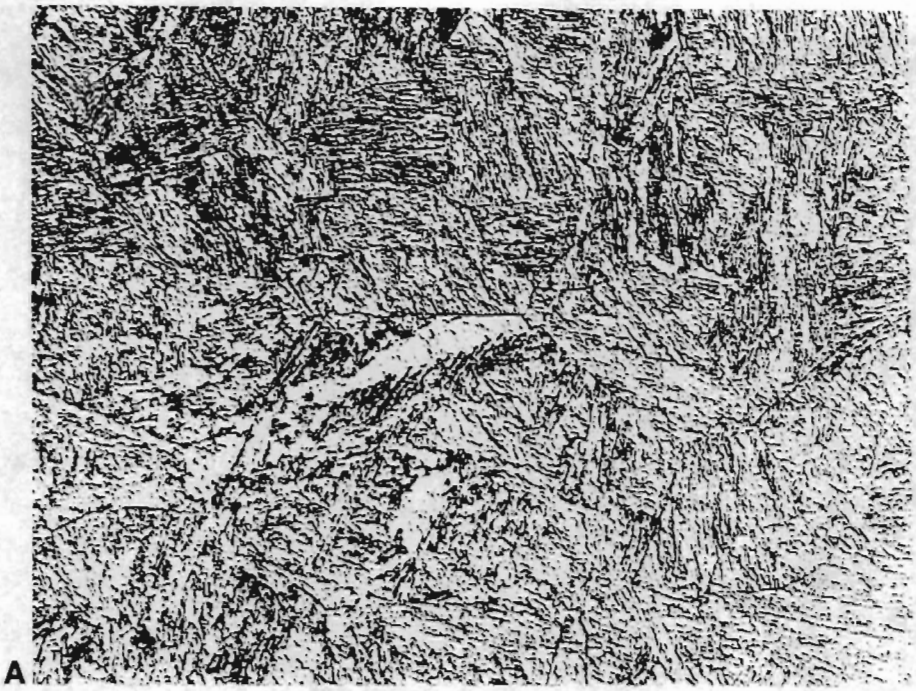

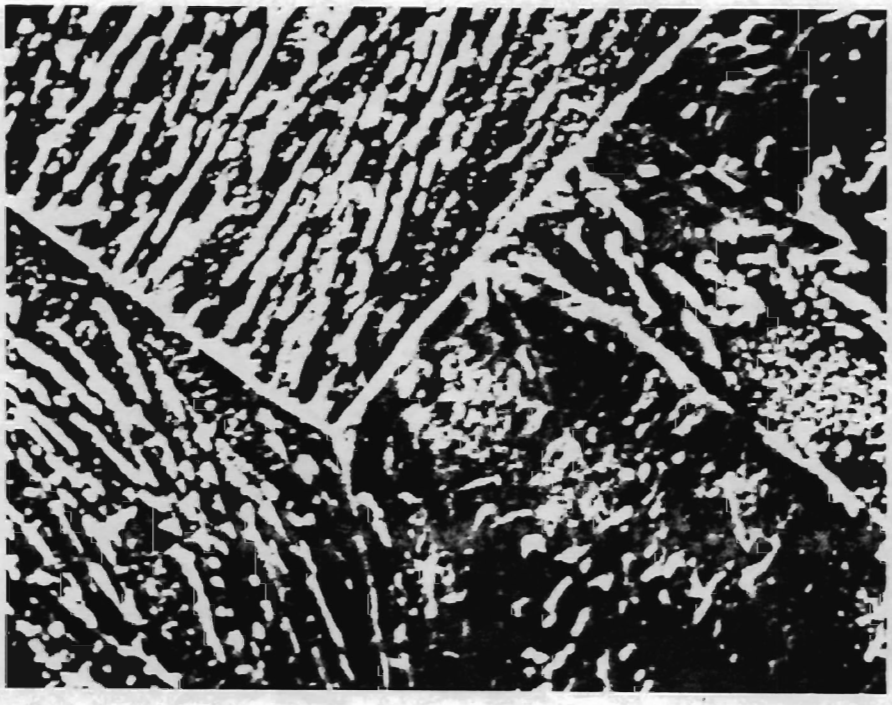

Figure 45. JSW 2 1/4Cr-1Mo-V-Ti-B. CCT specimen, 60KJ/in. Nital-Picrl, a) 500X OLM, b) 10,000X SEM.

modified 2 1/4Cr and 3Cr materials reveal little information about the microstructures. A modest amount of coarsening of the prior austenite grains with increasing heat input (longer times above the grain coarsening temperature) is evident in Figures 39a through 42a. The acicular aspect of the microstructure also becomes less marked with increasing energy input.

The scanning electron micrographs (Figures 39b through 42b) for the JSW 3Cr-1Mo-V-Ti-B specimens show a change in the microstructure with increasing energy input from autotempered martensite and martensite, to lower bainite and autotempered martensite and, finally, to a transition microstructure consisting of lower bainite and granular bainite. Figure 39b, the helium quenched JSW 3Cr-1Mo-V-Ti-B specimen, shows a microstructure that consists of autotempered martensite and martensite. Figures 40b, the JSW 3Cr-1Mo-V-Ti-B 35 KJ/in (1.38 KJ/mm) specimen, and Figures 41b, and 43b through 45b, the 60 KJ/in (2.36 KJ/mm) specimens of the JSW 3Cr-1Mo-V-Ti-B, AMAX (Climax) 3Cr-1 1/2Mo-0.1V, Berkeley 3Cr-1 1/2Mo-1/2Ni, and JSW 2 1/4Cr-1Mo-V-Ti-B show microstructures that consist of lower bainite and autotempered martensite. The 150 KJ/in (5.91 KJ/mm), JSW 3Cr-1Mo-V-Ti-B specimen (Figure 42b) exhibits a breaking up of the lower bainite, lath like microstructure into granular bainite and, since both structures are present, this is termed a transitional bainitic microstructure. The sequence of microstructures with increasing energy input is consistent with that determined by Richey[25] for 2 1/4Cr-1Mo alloys.

The presence of mixed microstructures consisting of bainite and martensite in alloy steels has been observed previously. Brown et al.[137] have predicted from the continuous cooling transformation diagram for

2 1/4Cr-1Mo that fast cooling rates would result in martensitic or mixed martensitic-bainitic microstructures. Autotempered martensite present with bainite has been reported in 2 1/4Cr-1Mo simulated weld HAZ's by Smith et al.[138] and in quenched 2 1/4Cr-1Mo and 5Cr-1Mo in De Ferri Metallographia.[136] Ishigiro et al.[131] have observed microstructures consisting of martensite, mixed martensite and bainite, and bainite in JSW 2 1/4Cr-1Mo-V-Ti-B simulated weld HAZ's. Bonizewski et al.[139] have reported mixed martensite and bainite in both actual and simulated weld HAZ's for 5Cr-1/2Mo, 9%Ni, 2%Mn and 3%Mn steels. The microstructures containing martensite or autotempered martensite reported in the literature are similar in appearance to the roughened, lenticular structures observed in the helium quenched, 35 KJ/in (1.38 KJ/mm), and 60 KJ/in (2.36 KJ/mm) microstructures (Figures 39-41, 43-45). These structures are also similar to those observed in the 9Cr-1Mo-V-Nb microstructures (Figures 31-34) shown previously. Therefore, there is little question that these lenticular structures are auto tempered martensite.

Summary of the Modified 2 1/4Cr-1Mo and 3Cr-Mo Transformation Studies

As was expected with the rapid heating rate employed and the diffusion controlled nature of austenite formation, the on heating transformation temperatures of the AMAX (Climax) 3Cr-1 1/2Mo-0.1V, JSW 3Cr-1Mo-V-Ti-B, and JSW 2 1/4Cr-1Mo-V-Ti-B materials were higher than those shown on the continuous cooling transformation diagrams for these materials. The on cooling transformation temperatures were found to be depressed by approximately 45F^{o} (25C^{o}) with respect to the transformation temperatures shown on the continuous cooling transformation diagrams. The depression of the on-cooling transformation temperatures is due to the

rapid cooling and limited amount of diffusion that must occur during the lower bainite bainite transformation. The JSW 2 1/4Cr-1Mo-V-Ti-B had the highest transformation start temperatures which is a result of the lower alloy and carbon content. The Berkeley 3Cr-1 1/2Mo-1/2Ni material had the lowest transformation start temperatures due to this alloys high carbon and nickel content.

The microstructures which were observed in the AMAX (Climax) 3Cr-1 1/2Mo-0.1V, Berkeley 3Cr-1 1/2Mo-1/2Ni, JSW 3Cr-1Mo-V-Ti-B, and JSW 2 1/4Cr-1Mo-V-Ti-B materials over the range of thermal cycles employed were consistent with those found by Richey[25] for 2 1/4Cr-1Mo. As the energy input increased, the microstructures changed from martensite and autotempered martensite to bainite and autotempered martensite and, at the highest energy input employed, to a transitional microstructure consisting of lower bainite and granular bainite. No retained austenite was observed in any of the microstructures in the modified 2 1/4Cr-1Mo and 3Cr-Mo materials as is expected with the fast cooling rates in welding.

Y-Groove Hydrogen Assisted Cracking Test

In order to evaluate the hydrogen assisted cracking susceptibility of the unmodified and modified 3Cr and 2 1/4Cr materials Y-groove testing was carried out. The results of Y-groove tests are given in Table 9 for the 3Cr materials and are given in Table 10 for the 2 1/4Cr-1Mo materials. The testing procedure is given in the experimental procedures part in detail. The different weld metals hydrogen levels were obtained by using electrodes which have undergone a controlled baking to develop a specified moisture content.

Table 9. Results of Y-groove HAC tests on 3Cr steels.

Material	Preheat Temp.	Electrode used	Diffusible Hydrogen (ml/100 gms.)	Surface Crack Ratio %	Section Crack Ratio %
Lukens 3Cr-1.5Mo-0.1V	275°F (235°C)	3Cr-1.5Mo-0.1V (0.21% moisture)	6.94	81	94
Lukens 3Cr-1.5Mo-0.1V	375°F (191°C)	3Cr-1.5Mo-0.1V (0.21% moisture)	6.94	0	0
Lukens 3Cr-1.5Mo-0.1V	450°F (232°C)	3Cr-1.5Mo-0.1V (0.09% moisture + baked 890°F-2hrs)	3.71	0	0
Lukens 3Cr-1.5Mo-0.1V	375°F (191°C)	3Cr-1.5Mo-0.1V (0.09% moisture + baked 890°F-2hrs)	3.71	0	0
Lukens 3Cr-1.5Mo-0.1V	275°F (135°C)	3Cr-1.5Mo-0.1V (0.09% moisture + baked 890°F-2hrs)	3.71	0	0
Berkeley 3Cr-1/2Mo-1/2Ni	275°F (135°C)	3Cr-1.5Mo-1/2Ni (Fully baked)	5.07	68	80
Berekeley 3Cr-1/2Mo-1/2Ni	375°F (191°C)	3Cr-1.5Mo-1/2Ni (Fully baked)	5.07	91	100
Berekeley 3Cr-1/2Mo-1/2Ni	450°F (232°C)	3Cr-1.5Mo-1/2Ni (Fully baked)	5.07	0	0
JSW 3Cr-1Mo-V-Ti-B	375°F (191°C)	3Cr-1.5Mo-0.1V (0.09% moisutre + baked 980°F-2hrs.)	3.71	0	0
JSW 3Cr-1Mo-V-Ti-B	275°F (135°C)	3Cr-1.5Mo-0.1V (0.09% moisutre + baked 980°F-2hrs.)	3.71	0	0
JSW 3Cr-1Mo-V-Ti-B	80°F (26°C)	3Cr-1.5Mo-0.1V (0.09% moisutre + baked 980°F-2hrs.)	3.71	100	100
JSW 3Cr-1Mo-V-Ti-B	150°F (65°C)	3Cr-1.5Mo-0.1V (0.09% moisutre + baked 980°F-2hrs.)	3.71	100	100

Table 10. Results of Y-groove HAC tests on 2 1/4Cr-1Mo steels.

Material	Preheat Temp.	Electrode used	Diffusible Hydrogen (ml/100 gms.)	Surface Crack Ratio %	Section Crack Ratio %
Lukens 2 1/4 Cr-1MO	80°F (26°C)	E 9018-B3 Baked 980°F-2hrs.	2.38	100	100
Lukens 2 1/4 Cr-1MO	150°F (65°C)	E 9018-B3 Baked 980°F-2hrs.	2.38	0	0
Lukens 2 1/4 Cr-1MO	300°F (149°C)	E 9018-B3 Baked 980°F-2hrs.	2.38	0	0
Kawasaki 2 1/4Cr-1Mo	300°F (149°C)	E 9018-B3 Baked 980°F-2hrs.	2.38	0	0
JSW 2 1/4Cr-1Mo-V-Ti-B	300°F (149°C)	3Cr-1.5Mo-1/2Ni (Fully baked)	2.38	0	0
Kawasaki 2 1/4Cr-1Mo	300°F (149°C)	E 9018-B3 Baked 980°F-2hrs.	8.04	70	91
Kawasaki 2 1/4Cr-1Mo	375°F (191°C)	E 9018-B3 Baked 980°F-2hrs.	8.04	0	0

At relatively low levels of diffusible hydrogen (3.71 ml/100g) HAC can be avoided using a preheat temperature of 275°F in 3Cr materials. A preheat of 275°F appears to be the minimum required since testing at room temperature as well as 150°F at the hydrogen level of 3.71 ml/100g resulted in 100% cracking for tests conducted on JSW 3Cr. There was no decernable difference in behavior between the modified and the unmodified 3Cr steels tested. However, the susceptibility to HAC appears to be extremely sensitive to the diffusible hydrogen contents of the welds deposited. This fact is made clear from the results of tests on the Berkeley 3Cr-1.5Mo-1/2Ni steel. A preheat temperature of 450°F (232°C) was required to prevent HAC in this steel when the diffusible hydrogen level was increased to 5.07 ml/100g. The Berkeley material also has the highest C content among the 3Cr steels tested and this may account for its sensitivity to diffusible hydrogen content.

For 2 1/4Cr-1Mo steels the tests were conducted at diffusible hydrogen levels of 2.38 and 8.04 ml/100g. At the low diffusible hydrogen level of 2.38 ml/100g HAC can be avoided by using a preheat temperature of 150°F. However, at the hydrogen level of 8.04 ml/100g a preheat temperature of 375°F is necessary before HAC can be avoided. Thus, it can be seen that HAC is extremely sensitive to the diffusible hydrogen content of the weld metal and preheats must be adjusted accordingly.

The results of Y-groove testing indicates that for 2 1/4Cr and 3Cr steels tested, preheat temperatures required to prevent HAC are commensurate with those recommended as standard practice for these

materials. Further, there appears to be no decernable difference in the behavior between the modified and the unmodified materials as far as the susceptibility to HAC is concerned.

Postweld Heat Treatment Cracking Behavior

PWHT cracking is defined as intergranular cracking in the weld HAZ or weld metal that occurs during heat treatment or high temperature service.[60] This type of cracking is of particular concern for fabricators of Cr-Mo steels since no adequate predictor of susceptibility exists. To compound the difficulty, heat to heat variations in susceptibility may result in cracking of alloys with nominally equivalent compositions to those previously successfully welded.[58,60,61]

PWHT cracking involves a synergistic interaction of many metallurgical changes coupled with the high residual tensile stresses in the coarse grained HAZ.[18] A primary factor is the precipitation of M_2C, MC and M_4C_3 type carbides within the matrix resulting in an increase of the matrix flow stress relative to the grain boundary flow stress. The difference in relative flow stress between the grain matrix and grain boundaries prevents plastic deformation from occurring in the grain matrix during stress relaxation and gives rise to strain accumulation in the grain boundaries. If the strain accumulation exceeds the grain boundary ductility, cavitation and subsequent rupture occur.[57,59-63]

Grain boundary ductility may be decreased by the segregation of residual embrittling elements, particularly phosphorus, during PWHT.[62,73-76] Carbides, nitrides or sulphides located at the grain boundaries may be initiation sites for grain boundary cavitation.[15,78,84,138,142] The rapid

growth of grain boundary carbides may result in the formation of a weak, carbide denuded, zone immediately adjacent to the grain boundary in which strains may accumulate and thus initiate rupture.[30,72] Grain coarsening, associated with the high peak temperature regions closest to the weld, exacerbates the foregoing effects by limiting the grain boundary area available to accommodate slip and for accommodating segregation of residual elements.[3,19] In general, any mechanism which results in an increase in the grain matrix to grain boundary strength ratio or decreases grain boundary ductility during PWHT may be contributory to PWHT cracking.

The 9Cr-1Mo, 3Cr-Mo, and 2 1/4Cr-1Mo modified alloys are designed to have high strength, high hardenability and good resistance to loss in strength during tempering or elevated temperature service. In general, these attributes have been conferred by the addition of strong carbide forming elements, vanadium and/or niobium, which form highly stable MC or M_4C_3 type carbides. (Hardenability has been increased by boron, manganese and/or nickel additions in the 3Cr and 2 1/4Cr modified alloys.) However, the addition of strong carbide forming elements is known to increase PWHT cracking susceptibility and therefore the present work was undertaken to assess the susceptibility of the modified Cr-Mo alloys to this type of cracking.

Postweld Heat Treatment Cracking Susceptibility Evaluation of the 9Cr-1Mo-V-Nb Commercial Heats.

Susceptibility of the NKK 9Cr-1Mo-V-Nb, Timken 9Cr-1Mo-V-Nb, and Sumitomo 9Cr-1Mo-V-Nb materials was determined by Gleeble simulation. Cylindrical specimens, 1/4in diameter by 4in long (6mm diameter by 102mm long), were subjected to a 60KJ/in (2.36KJ/mm) heat input thermal cycle

(2in (51mm) thick plate, 400°F (205°C) preheat) with a peak temperature of 2400°F (1315°C) followed by simultaneous loading to a predetermined stress and heating to the PWHT temperature, 1350°F (732°C). Samples were held at the PWHT temperature under load until fracture occurred. While the stress is held constant for an individual specimen, a range of stress levels is employed during the testing of a material in order to obtain various times to fracture. The reduction of area (RA) was determined, and a scanning electron microscopy examination of the fracture surfaces was conducted.

Figure 46 shows the RA as a function of the time to fracture for the three commercial heats of the modified 9Cr-1Mo-V-Nb material. The RA for the NKK 9Cr-1Mo-V-Nb material range between 30 and 37%, for the Timken 9Cr-1Mo-V-Nb material between 35 and 46%, and for the Sumitomo 9Cr-1Mo-V-Nb between 15 and 31%. In comparison, the RA obtained by Richey[25] for the experimental 9Cr-1Mo-V-Nb heat, ORNL 176, a forerunner to the commercial heats, was between 35 and 56% and for the unmodified 9Cr-1Mo-0.11C material was in excess of 70% under the same test conditions.

The lower ductility of the V-Nb modified 9Cr-1Mo in relation to the unmodified 9Cr-1Mo material is the result of differences in carbide evolution. Vitek and Klueh[32] found that the addition of niobium and vanadium to 9Cr-1Mo provides a fine dispersion of Nb/Vcarbo-nitrides. These fine, dispersed MC type carbides act as nucleating sites for $M_{23}C_6$ resulting in more finely dispersed $M_{23}C_6$ carbides than exist in the unmodified 9Cr-1Mo material which does not have the fine precursor distribution.[33] Further, the addition of vanadium alters the mobility of

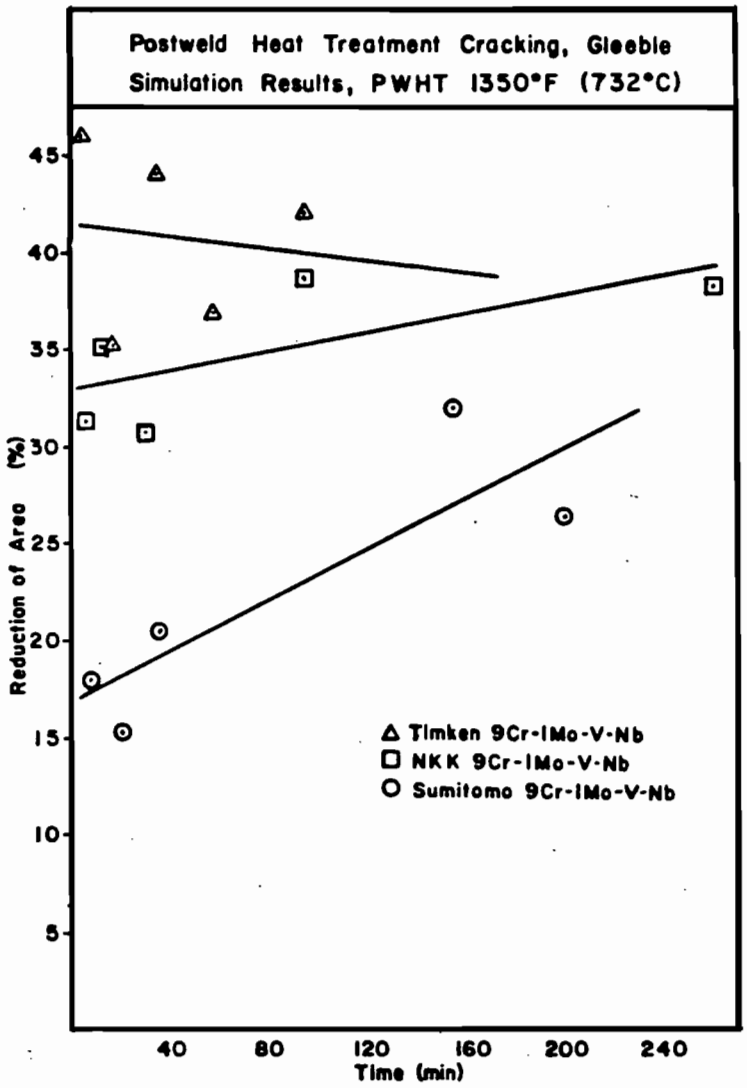

Figure 46. 9Cr-1Mo-V-Nb alloys' Gleeble stress-rupture behavior for simulated PWHT at 1350°F (732°C). Reduction of area vs. time to rupture produced by testing at different stress levels.

chromium, slowing the growth of $M_{23}C_6$ carbides.[34] The presence of fine, dispersed carbides results in increased rupture strength and lower ductility compared to the unmodified 9Cr-1Mo material.

The generally lower rupture ductility of the Sumitomo 9Cr modified alloy may be the result of the higher phosphorus content compared to the NKK and Timken materials. The Sumitomo material has a phosphorus content of 0.014% while the NKK and Timken materials have phosphorus contents of 0.004 and 0.010% respectively. The increase in rupture ductility with increasing time to rupture exhibited by the Sumitomo material may be the result of carbide evolution (overaging affects).

Assuming that the Vinckier and Pense[73,98] criteria can be extended to the PWHT temperature employed for the 9Cr-1Mo materials, the NKK 9Cr-1Mo-V-Nb and Timken 9Cr-1Mo-V-Nb materials, having rupture ductilities in excess of 30%, would not be considered susceptible to PWHT cracking. The Sumitomo 9Cr-1Mo-V-Nb, which exhibits lower rupture ductilities compared to the NKK and Timken materials, has a minimum ductility of 15% and may be considered marginally susceptible to PWHT cracking by the Vinckier and Pense criteria.

Fractography of the 9Cr-1Mo-V-Nb Materials.

Figures 47, 48 and 49 are scanning electron fractographs of NKK 9Cr-1Mo-V-Nb, Timken 9Cr-1Mo-V-Nb, and Sumitomo 9Cr-1Mo-V-Nb Gleeble simulated PWHT specimens. The primary mode of fracture of the 9Cr-1Mo-V-Nb materials is microvoid coalescence. The Sumitomo alloy, which exhibited the lowest ductilities, clearly shows an underlying intergranular character

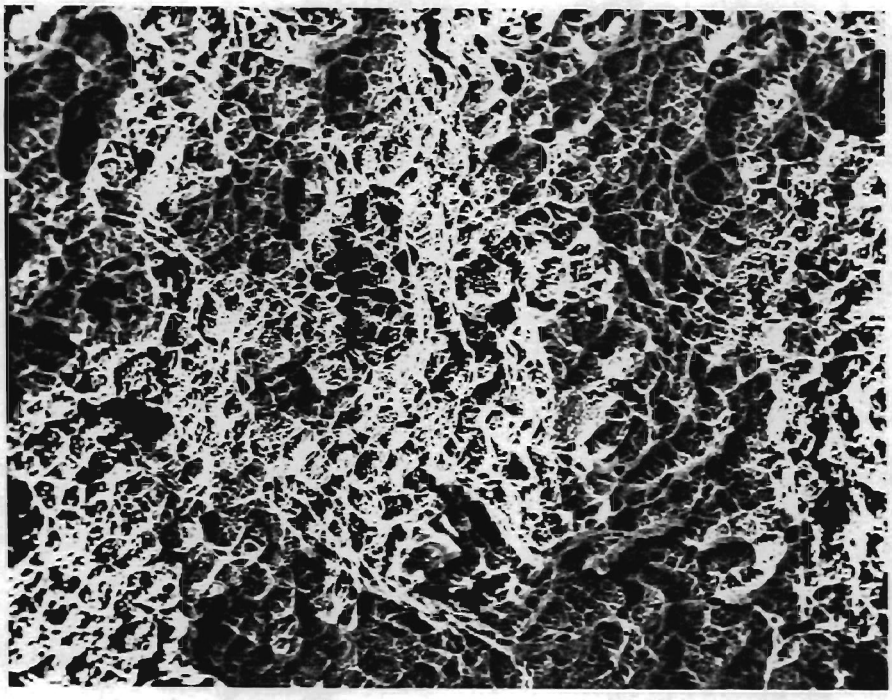

Figure 47. Fractograph of NKK 9Cr-1Mo-V-Nb. 34.2 KSI, 12.8 min. to fracture, 35.3% R/A, SEM 200X.

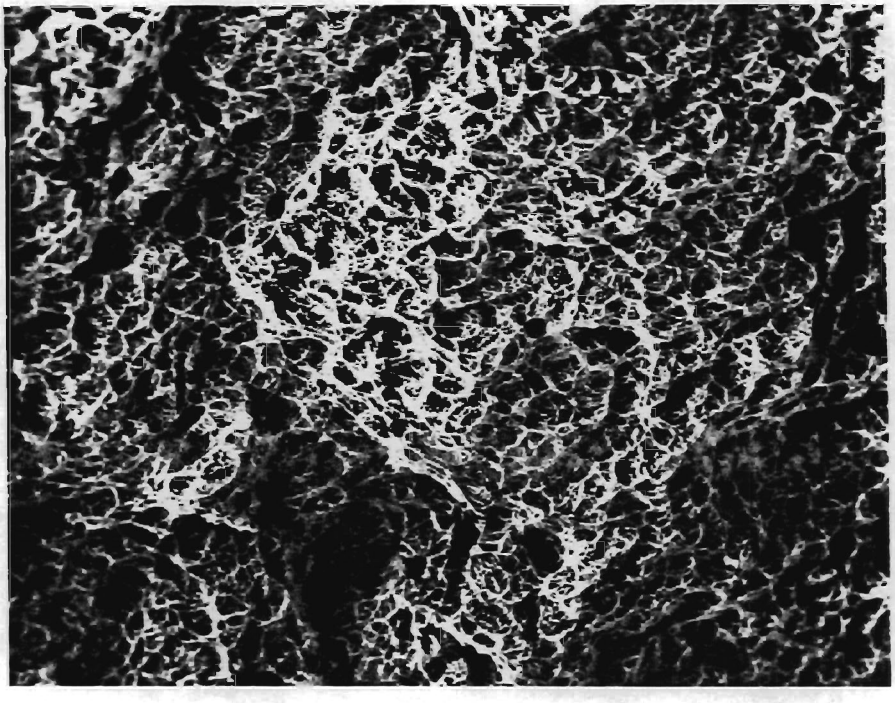

Figure 48. Fractograph of Timken 9Cr-1Mo-V-Nb. 35.0 KSI, 16.7 min. to fracture, 35.3% R/A, SEM 200X.

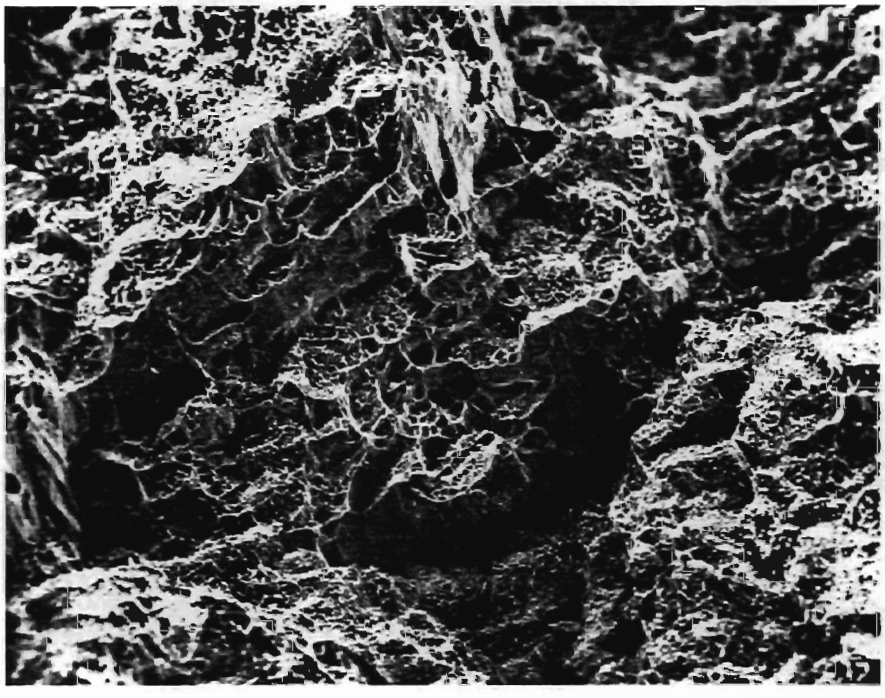

Figure 49. Fractograph of Sumitomo 9Cr-1Mo-V-Nb. 22KSI, 20.9 min. to fracture, 15.4% R/A, SEM 200X.

to the fracture. The extent of microductility in these alloys is concomitant with the measured macroductility and indicates that PWHT cracking should not be a problem.

Summary of the 9Cr-1Mo-V-Nb PWHT Cracking Behavior.

The addition of vanadium and niobium lowers the rupture ductility of 9Cr-1Mo from over 70% to between 15 and 56% in gleeble simulated PWHT testing. The decrease in ductility is a result of the precipitation of fine, dispersed V/Nb-carbo-nitrides, the nucleation of $M_{23}C_6$ on the V/Nb precipitates resulting in a fine, dispersed precipitation of $M_{23}C_6$, and reduction of the rate of growth of the $M_{23}C_6$ precipitates due to the lowering of chromium mobility by vanadium. However, both macroscopic and microscopic ductility are sufficient to preclude PWHT cracking as a significant fabrication problem in these materials. The relatively high phosphorus of the Sumitomo heat may be the primary causal factor for the lower rupture ductilities observed for this alloy and may indicate a need to carefully control residuals in the modified 9Cr-1Mo alloys.

Postweld Heat Treatment Cracking Results for the Modified 3Cr-Mo and 2 1/4Cr-1Mo Materials by Gleeble Simulation.

The PWHT cracking susceptibility of the AMAX (Climax) 3Cr-1 1/2Mo-0.1V, Berkeley 3Cr-1 1/2Mo-1/2Ni, JSW 3Cr-1Mo-V-Ti-B, JSW 2 1/4Cr-1Mo-V-Ti-B and M10 to M50 alloys was determined by Gleeble simulation in the same manner as that used with the modified 9Cr-1Mo materials. Two PWHT temperatures were employed, 1250/1275°F (680/690°C) and 1150°F (620°C) for evaluation of cracking susceptibility of the

modified 2 1/4Cr and 3Cr materials. The lower temperature was utilized to be representative of the trend toward lower PWHT temperatures and thus higher strength levels.

Figures 50 and 51 present the RA of the fractured Gleeble specimens as a function of time to fracture at the 1250°F (680°C) and 1150°F (620°C) PWHT temperatures respectively. At 1250°F (680°C) the RA ranges from 0.3 to 1.4% for AMAX (Climax) 3Cr-1 1/2Mo-0.1V, from 21 to 29% for Berkeley 3Cr-1 1/2Mo-1/2Ni, from 4 to 14% for JSW 3Cr-1Mo-V-Ti-B, and from 2.3 to 10% for JSW 2 1/4Cr-1Mo-V-Ti-B. At 1150°F (620°C) the RA ranges from 0.1 to 1.3% for the AMAX (Climax) 3Cr-1 1/2Mo-0.1V, from 10 to 20% for Berkeley 3Cr-1 1/2Mo-1/2Ni, from 1.6 to 7.0% for JSW 3Cr-1Mo-V-Ti-B, and from 1.8 to 3.9% for JSW 2 1/4Cr-1Mo-V-Ti-B.

Clearly there is a marked decrease in ductility for all four modified materials tested at 1150°F (620°C) compared to 1250°F (680°C). The decrease in ductility may be due to the increased duration of coherency of Mo_2C, slower growth and the increased time for the formation of the higher order carbides ($M_{23}C_6$, M_7C_3, M_6C) at the lower PWHT temperature. These changes reduce plastic flow especially in the grain matrix as opposed to the grain boundaries.

Figures 50 and 51 clearly show a separation in the response of the Berkeley 3Cr-1 1/2Mo-1/2Ni and the three vanadium modified alloys. The RA of the Berkeley alloy, which has no vanadium addition, is significantly higher than the RA of the AMAX (Climax), JSW 3Cr, or JSW 2 1/4Cr alloys. This is consistent with the literature which indicates that the addition of vanadium to the Cr-Mo alloys is detrimental with respect to PWHT cracking susceptibility.[18,66,69,79,93]

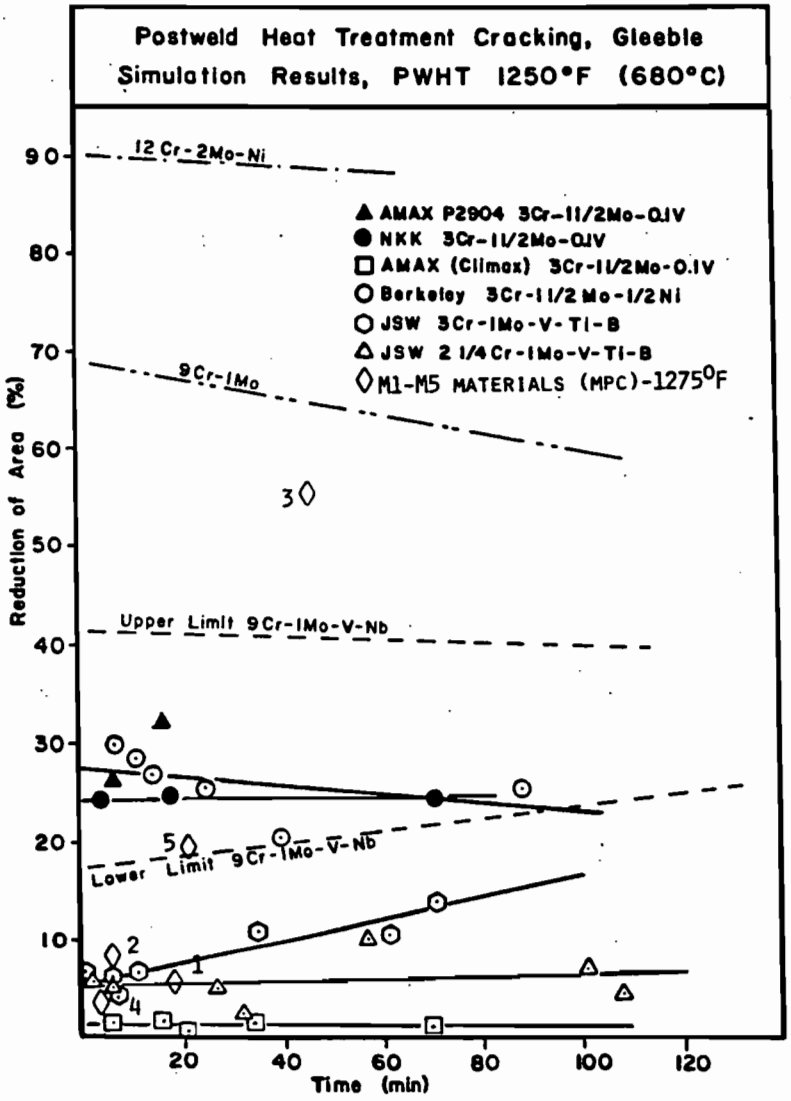

Figure 50. Modified 3Cr and 2 1/4Cr alloys' Gleeble stress-rupture behavior for simulated PWHT at 1250°F (680°C). Reduction of area vs. time to rupture produced by testing at different stress levels.

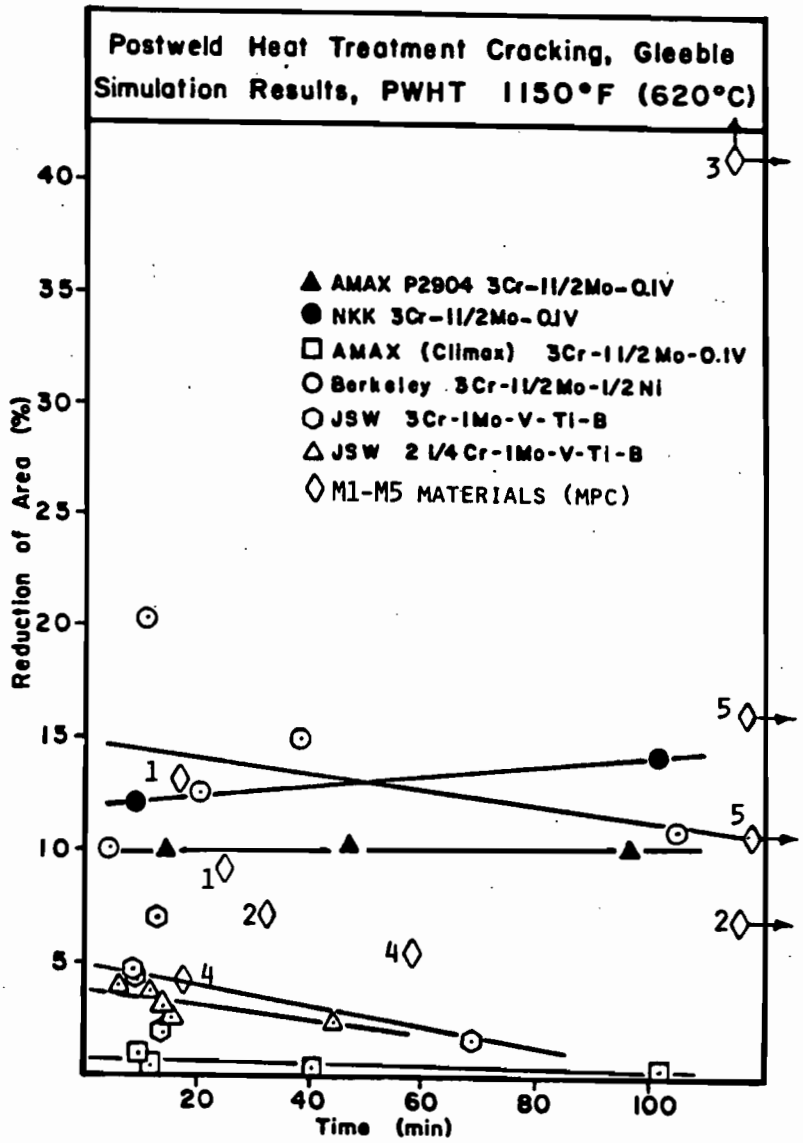

Figure 51. Modified 3Cr and 2 1/4Cr alloys' Gleeble stress-rupture behavior for simulated PWHT at 1150°F (620°C). Reduction of area vs. time to rupture produced by testing at different stress levels.

The Berkeley 3Cr-1 1/2Mo-1/2Ni material exhibits relatively high ductility at both 1150°F (620°C) and 1250°F (680°C) which probably is the result of the high nickel (0.52%) content and the absence of strong carbide formers (vanadium, niobium). Increased nickel has been shown to increase the rate of dissolution of Fe_3C and Mo_2C and speed the precipitation of $M_{23}C_6$, M_7C_3 and M_6C.[10] The rapid formation of carbides at lower temperatures and the concomitant very short times of coherency would result in the greatest strengthening of the matrix while the overall strength of the grain boundaries is high and before significant embrittlement could occur in accordance with Tamaki's model.[90] It is to be noted that although the Berkeley 3Cr-1 1/2Mo-1/2Ni material has the highest carbon (0.16%) and silicon (0.28%) and relative high phosphorus (0.010%), this material appears to be significantly resistant to PWHT cracking.

The relatively low rupture ductilities exhibited by the JSW 3Cr-1Mo-V-Ti-B and JSW 2 1/4Cr-1Mo-V-Ti-B is probably due to the high vanadium content (0.28 and 0.26%) of these materials. Both materials have particularly low phosphorus (0.007%) and silicon (0.06%) and therefore these elements would not significantly affect susceptibility. Although the aluminum content of the JSW 2 1/4Cr-1Mo-V-Ti-B material (0.016%) is at least three times greater than the other modified alloys investigated, the similarity in response of the JSW 3Cr-1Mo-V-Ti-B would appear to rule out aluminum as being significant in regard to the low ductility of the JSW 2 1/4Cr-1Mo-V-Ti-B material. The increase in rupture ductility with increasing time to fracture at 1250°F (680°C) for the JSW 3Cr-1Mo-V-Ti-B

alloy may be the result of carbide coarsening which, in turn, may be related to the higher Cr to Mo ratio for this material compared to the other modified 2 1/4Cr-1Mo and 3Cr-Mo alloys.

The limited rupture ductility of the AMAX (Climax) 3Cr-1 1/2Mo-0.1V material (in comparison to the other V-Ti-B modified materials) was not anticipated. A nominally similar composition experimental heat of the AMAX (Climax) material (P2904), tested previously by Richey[25], exhibited higher rupture ductility (from 27 to 36% RA at 1250°F (680°C) and from 8.5 to 10% RA at 1150°F (620°C)). It should be noted that the composition of the AMAX (Climax) 3Cr-1 1/2Mo-0.1V material is higher in phosphorus (0.012%) and silicon (0.26%) and lower in nickel (0.11%) than the other vanadium modified alloys including the experimental AMAX (Climax) heat, P2904. (Heat P2904 has phosphorus, silicon and nickel contents of 0.006%, 0.016% and 0.21% respectively.) As discussed in the literature review, phosphorus can cause grain boundary embrittlement, lower rupture ductility and increase susceptibility to PWHT cracking,[77,84,109,112] silicon can enhance the formation of Mo_2C[94,99,100] and aid phosphorus segregation,[99,111] and increasing nickel appears to accelerate the kinetics of carbide formation.[10] Thus, the high susceptibility of the AMAX (Climax) 3Cr-1 1/2Mo-0.1V material may be due to a combination of embrittlement, enhanced formation of Mo_2C and a slower rate of formation of more stable (and less detrimental) carbides such as $M_{23}C_6$, M_7C_3 and M_6C (due to the lower nickel content). Tamaki's[77,91] work has shown that the formation and persistence of Mo_2C at high temperatures combined with embrittlement due to elevated phosphorus levels is extremely detrimental with respect to cracking susceptibility.

Overall susceptibility of the modified 3Cr-Mo and 2 1/4Cr-1Mo alloys may be made using the Vinckier and Pense Criteria[73,98] (page 51). According to this criteria, an alloy that exhibits a RA of less than 5% is "extremely" susceptible, between 5 and 10% is "highly" susceptible, between 10 and 15% is "slightly" susceptible, and above 20% is "not" susceptible. The AMAX (Climax) 3Cr-1 1/2Mo-0.1V material would be considered "extremely" susceptible at both PWHT temperatures. The JSW 2 1/4Cr-1Mo-V-Ti-B and JSW 3Cr-1Mo-V-Ti-B materials would both be considered "highly" susceptible at 1250°F (680°C) and "extremely" susceptible at 1150°F (620°C). The Berkeley 3Cr-1 1/2Mo-1/2Ni material would be considered "not" susceptible at 1250°F (680°C) and only "slightly" susceptible at 1150°F (620°C).

An alternative approach used by Spaeder and Plodder[103] is to multiply the RA by the stress to cause fracture for a time to fracture of ten minutes. This value, called the stress rupture parameter (SRP) indicates susceptibility to PWHT cracking when less than $15(X10^4)$. The values of the SRP and the stress rupture index (SRI), a normalized value of the SRP with the highest SRP being equal to 100, are presented in Table 11. The SRP values indicate that only the AMAX (Climax) 3Cr-1 1/2Mo-0.1V at 1250°F (680°C) and 1150°F (620°C) and the JSW 2 1/4Cr-1Mo-V-Ti-B at 1150°F (620°C) are susceptible to PWHT cracking. However, the SRI shows the great difference in the response of the V and V-Ti-B modified alloys compared to the Berkeley 3Cr-1 1/2Mo-1/2Ni material with no addition of strong carbide forming elements. The Berkeley 3Cr-1 1/2Mo-1/2Ni has a SRI value at least four times the SRI value of the modified alloys containing deliberate additions of vanadium.

Table 11. Stress-rupture parameter and stress rupture index for the modified 3Cr and 2 1/4Cr alloys.

Material	PWHT Temperature		Stress		Reduction in Area %	SRP ($x10^4$)	SRI
	°F	(°C)	KSI	(MPa)			
AMAX 3Cr-1½Mo-0.1V (Climax)	1250 1150	(680) (620)	42 64	(289) (441)	1.5 0.8	6.4 4.8	6 4
Berkeley 3 Cr-1½Mo-½Ni	1250 1150	(680) (620)	36 61	(248) (420)	31.0 16.0	110.0 97.0	100 88
JSW 3 Cr-1Mo-V-Ti-B	1250 1150	(680) (620)	44 55	(303) (379)	5.7 3.9	25.0 21.0	23 19
JSW 2¼ Cr-1Mo-V-Ti-B	1250 1150	(680) (620)	47 49	(324) (338)	6.0 3.0	28.0 14.0	25 13

In order to ascertain that the grain coarsened region of the HAZ exhibited the lowest ductility during PWHT samples were subjected to several different thermal cycles and simulated PWHT. Further, grain refinement of the coarse grained HAZ by overlapping HAZ's in multiple pass welds has been proposed as one method of preventing PWHT cracking[59,85] and this also was evaluated. Samples of the AMAX (Climax) 3Cr-1 1/2Mo-0.1V, JSW 3Cr-1Mo-V-Ti-B, and JSW 2 1/4Cr-1Mo-V-Ti-B materials were subjected to two consecutive thermal cycles; the first to 2400°F (1315°C) to produce a coarse grained HAZ, the second to 1700°F (927°C) to produce a grain refined HAZ from the coarse grained material, and then subjected to simulated PWHT at 1150°F (620°C). With only a grain coarsening thermal cycle prior to PWHT all three materials exhibited severe embrittlement with rupture ductilities less than 5%. However, when a grain refining thermal cycle was superposed on the material after a grain coarsening cycle, rupture ductilities were found to be 12% for the JSW 3Cr-1Mo-V-Ti-B and JSW 2 1/4Cr-1Mo-V-Ti-B materials and 15% for the AMAX (Climax) 3Cr-1 1/2Mo-0.1V material after PWHT at 1150°F (620°C). By the Vinckier and Pense criteria,[73,98] the grain refining has resulted in change in ranking to "slightly" susceptible from the "extreme" susceptibility of the coarse grained regions. Therefore, the small bead, half bead technique[85] or temper beading[59] methods, which result in refinement of the coarse grained HAZ, may prove successful in preventing PWHT cracking in these alloys.

The cracking susceptibility of the grain refined region was determined for comparison with the results obtained from the multiple pass simulation (grain coarsening followed by grain refinement) for the JSW 2 1/4Cr-1Mo-V-Ti-B alloy. This material was thermal cycled to 1700°F

(927°C) and then PWHT at 1150°F (620°C) with an applied stress of 62ksi (430MPa). The RA was found to be 54%, significantly higher than the 12% RA obtained for the multiple thermal cycle sample.

The stress to cause fracture was higher for the multiple thermal cycle specimens, 84ksi (580MPa), than for the grain refined specimens, 62ksi (430MPa), or the grain coarsened specimen, 52ksi (360MPa). This result indicates that load shedding to the grain refined region or fusion zone may occur if the coarse grained region is fully refined by subsequent passes. However, if some coarse grained material remains in the HAZ after the use of welding techniques to refine the coarse grained region of the HAZ, strain accumulation may occur in the coarse grained material, due to it's lower strength, resulting in an increase in PWHT cracking susceptibility.

In addition, samples of the modified 2 1/4Cr-1Mo and 3Cr-Mo materials were subjected to simulated PWHT in the Gleeble with no prior thermal cycle. The JSW 3Cr-1Mo-V-Ti-B and Berkeley 3Cr-1 1/2Mo-1/2Ni materials were were PWHT at 1250°F (680°C) with applied stresses of 39ksi (270MPa) and 37ksi (260MPa) respectively, and a sample of the JSW 2 1/4Cr-1Mo-V-Ti-B was PWHT at 1150°F (620°C) with an applied stress of 52ksi (360MPa). The RA values obtained were 91% for the JSW 3Cr-1Mo-V-Ti-B, 86% for the Berkeley 3Cr-1 1/2Mo-1/2Ni, and 74% for the JSW 2 1/4Cr-1Mo-V-Ti-B. Thus, these studies show that the grain coarsening thermal cycle is indeed a precursor to the metallurgical events which result in the embrittlement of the modified Cr-Mo steels observed at both PWHT temperatures.

Post Weld Heat Treatment Cracking Results for the State-of-the-art Commercial Heats of Modified 2 1/4Cr-1Mo (M10-M50) by Gleeble Simulation

Five additional heats of 2 1/4Cr-1Mo materials were introduced in the later part of this program. These heats constitute commercial state-of-the-art materials and hence it was felt necessary to test these materials and compare the results with the data already available from 2 1/4Cr and 3Cr alloys in the base program.

The Gleeble simulation test results for M10-M50 are given in Table 12. These data are also shown in Figures 50 and 51 for comparison with all other materials. It can be seen that the M10-M50 heats exhibited better PWHT cracking resistance than all the other 2 1/4Cr and 3Cr materials which may show that there has been continuous improvement in the production process and chemistry of 2 1/4Cr-1Mo class of materials over a short time period in order to attain better properties with respect to both strength and PWHT cracking susceptibility.

Among the M10 to M50 materials M30 showed far superior PWHT cracking resistance than the remaining of the materials. This heat was calcium treated during the production process (residual Ca 0.012%). Ca is known to modify the sulphide inclusion morphology and distribution. So it can be concluded that the inclusion morphology and distribution also plays an important role in the ability of the material to resist PWHT cracking (in addition to the changes in behavior attained through modifications by changing the composition (addition of Ti, V, B, Nb, Ni), and controlling the residual elements (S, P, As, Sb)).

The M50 alloy can be ranked next in the series. The only marked difference in the composition for this alloy is the presence of 0.014% Cu.

Table 12. Results of PWHT cracking tests on state-of-the-art commercial 2 1/4Cr-1Mo alloys.

Material	Peak Temp. (°F)	PWHT Temperature (°F)	Stress (KWI)	Time to Rupture (Min)	RA %
M10	2400	1150	75.0	23.33	9.5
	2400	1150	70.9	16.33	13.0
	2400	1275	57.8	18.08	5.7
M20	2400	1150	75.0	33.25	7.3
	2400	1150	70.9	183.25	6.9
	2400	1275	57.8	6.00	7.8
M30	2400	1150	75.0	65.33	12.2
	2400	1150	70.9	207.20	68.7
	2400	1275	57.8	48.75	55.9
M40	2400	1150	75.0	18.33	3.8
	2400	1150	70.9	60.10	5.5
	2475	1150	75.0	15.90	5.6
	2400	1275	57.8	4.25	2.9
M50	2400	1150	75.0	170.90	15.6
	2400	1150	70.9	285.25	11.5
	2475	1150	75.0	156.40	8.6
	2400	1275	57.8	21.16	19.8

The effect of Cu on PWHT cracking is not very clearly defined in the literature. The effect of Cu has been thought to be slightly harmful by various investigators[18,82,88]. The effect of high nitrogen (0.0095%) in M20 is also not very clear.

The testing conducted at 1150°F and 1275°F which constitutes the range of PWHT temperatures commercially used shows similar relative results although the PWHT cracking susceptibility is less at 1275°F than 1150°F for this series of alloys.

Fractography of the 3Cr-Mo and 2 1/4Cr-1Mo Alloys.

Fractographs of representative Gleeble simulated PWHT cracking specimens are shown in Figures 52 through 59 for the AMAX (Climax) 3Cr-1 1/2Mo-0.1V, Berkeley 3Cr-1 1/2Mo-1/2Ni, JSW 2 1/4Cr-1Mo-V-Ti-B, and JSW 3Cr-1Mo-V-Ti-B materials. The samples for the fractographic examination were thermal cycled and PWHT in an argon atmosphere chamber mounted in the Gleeble. The specimens were essentially free of oxidation on the fracture face.

Two modes of fracture are clearly evident in Figures 52 through 59 and are similar to those described by Hippsley[84] as low ductility intergranular fracture (LDIGF) and intergranular microvoid coalescence (IGMVC). LDIGF is characterized by intergranular fracture along the prior austenite grain boundaries that is smooth and free of any microductility. However, IGMVC is characterized by fracture along the prior austenite grain boundaries that exhibits extensive microductility.

The AMAX (Climax) 3Cr-1 1/2Mo-0.1V material (Figures 52 and 53) and the JSW 2 1/4Cr-1Mo-V-Ti-B material (Figures 56 and 57) exhibit LDIGF at both PWHT temperatures, 1250°F (680°C) and 1150°F (620°C). The low

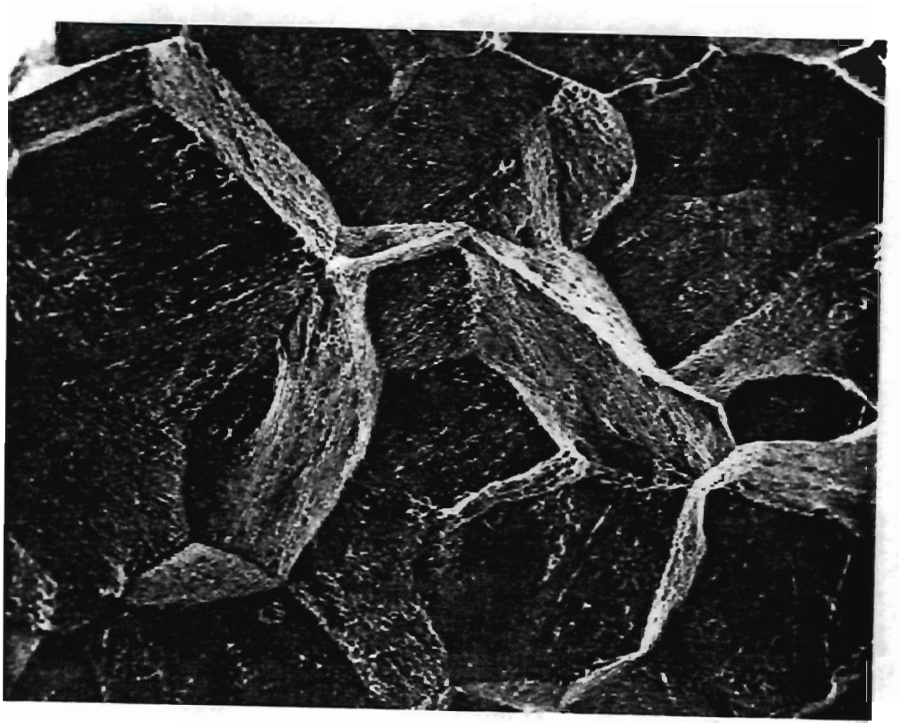

Figure 52. Fractograph of AMAX (Climax) 3Cr-1 1/2Mo-0.1V, 1250°F (680°C) PWHT. 43.4KSI (229MPa), 7.9min. to fracture, 3.8% RA, SEM 500X.

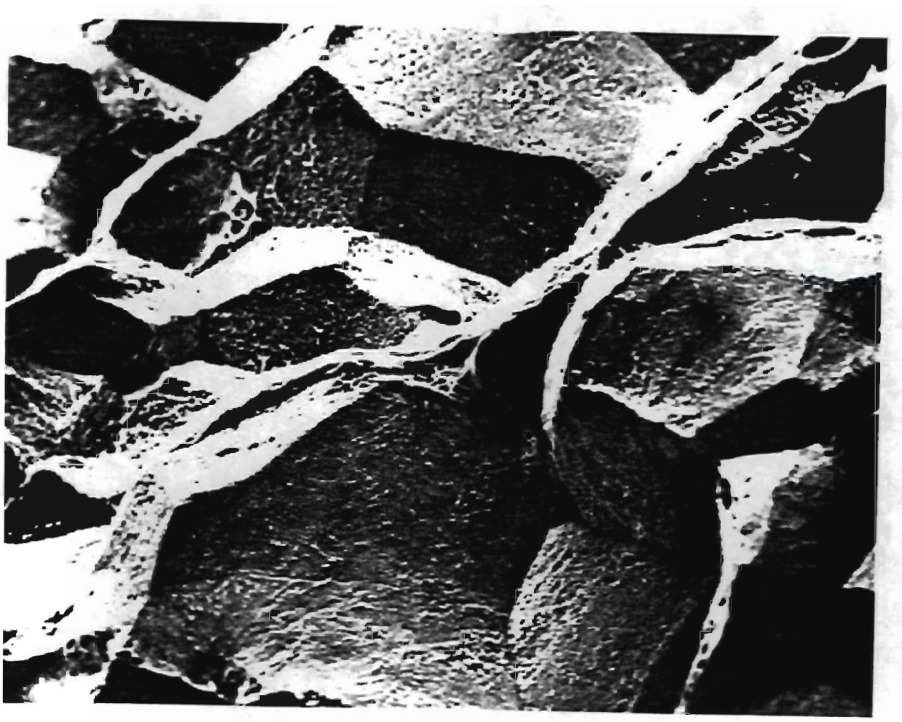

Figure 53. Fractograph of AMAX (Climax) 3Cr-1 1/2Mo-0.1V, 1150°F (620°C) PWHT. 65.1KSI (449MPa), 8.9min. to fracture, 1.3% RA, SEM 500X.

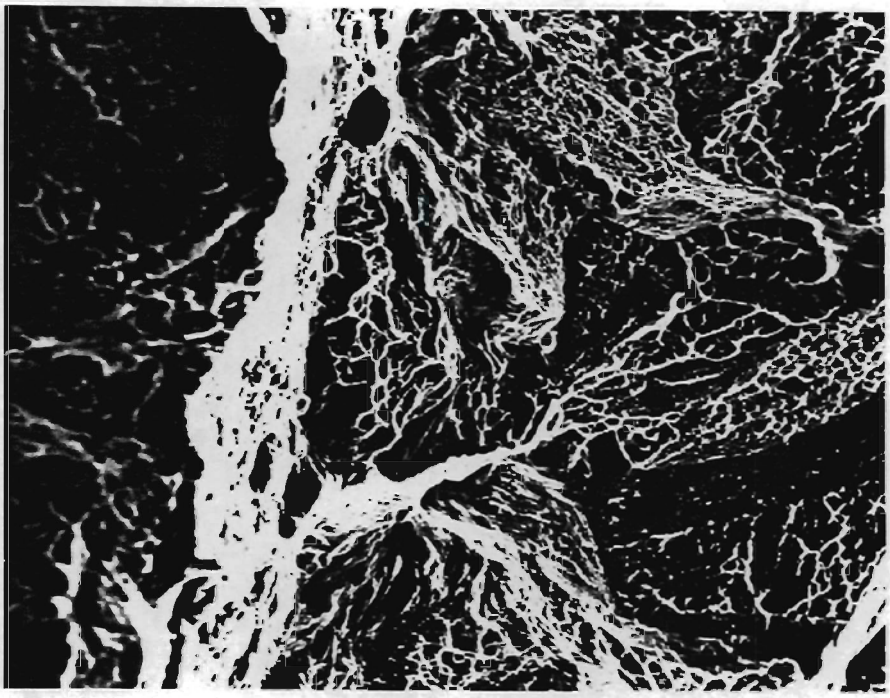

Figure 54. Fractograph of Berkeley 3Cr-1 1/2Mo-1/2Ni, 1250°F (680°C) PWHT. 39.3KSI (271MPa), 9.9min. to fracture, 21% RA, SEM 500X.

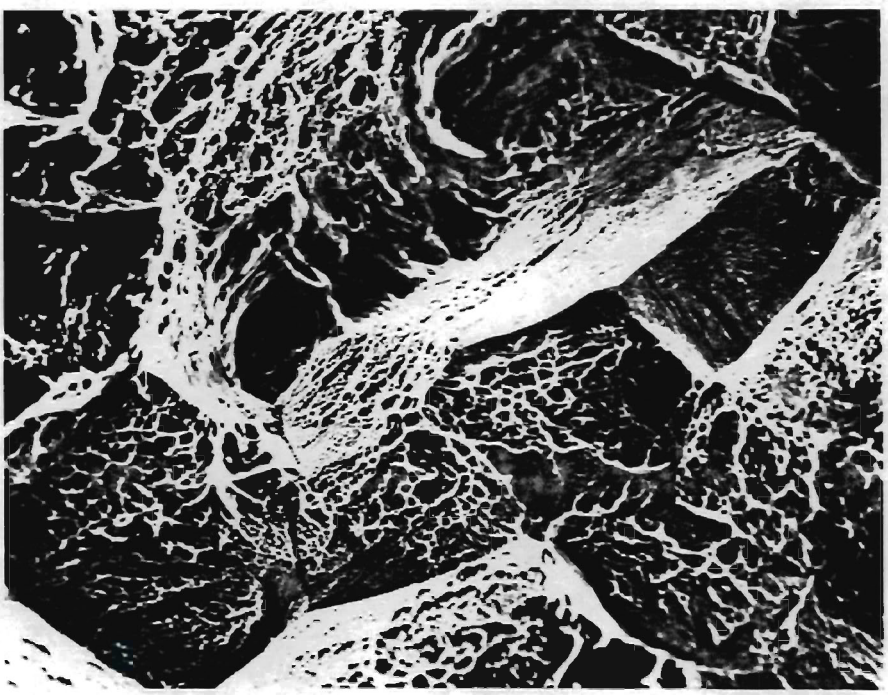

Figure 55. Fractograph of Berkeley 3Cr-1 1/2Mo-1/2Ni, 1150°F (620°C) PWHT. 64.2KSI (442MPa), 2.7 min. to fracture, 11% RA, SEM 500X.

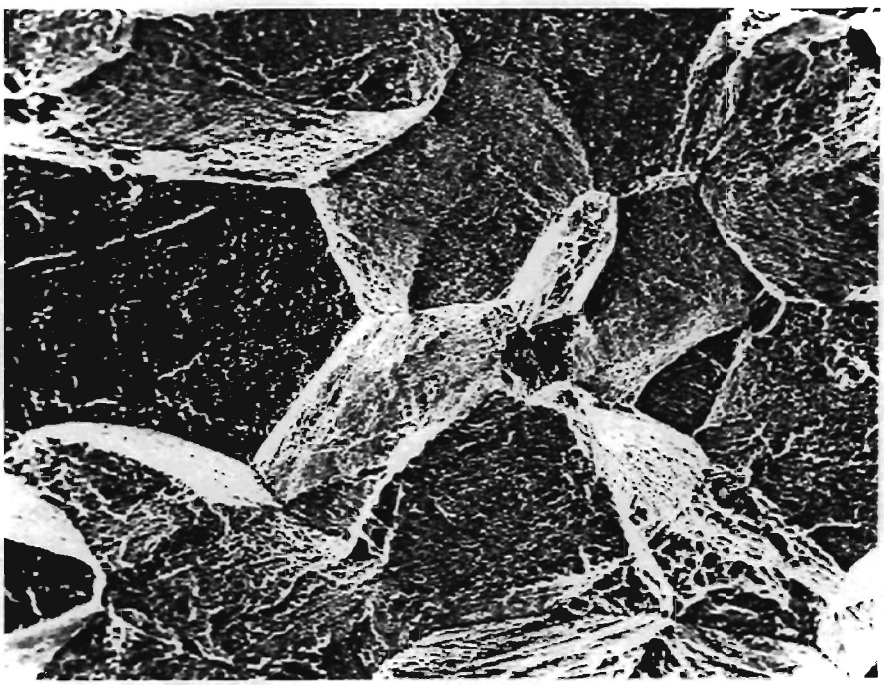

Figure 56. Fractograph of JSW 2 1/4Cr-1Mo-V-Ti-B, 1250°F (680°C) PWHT. 51.9ksi (358MPa), 5.5 min. to fracture, 5.1% RA, SEM 500X.

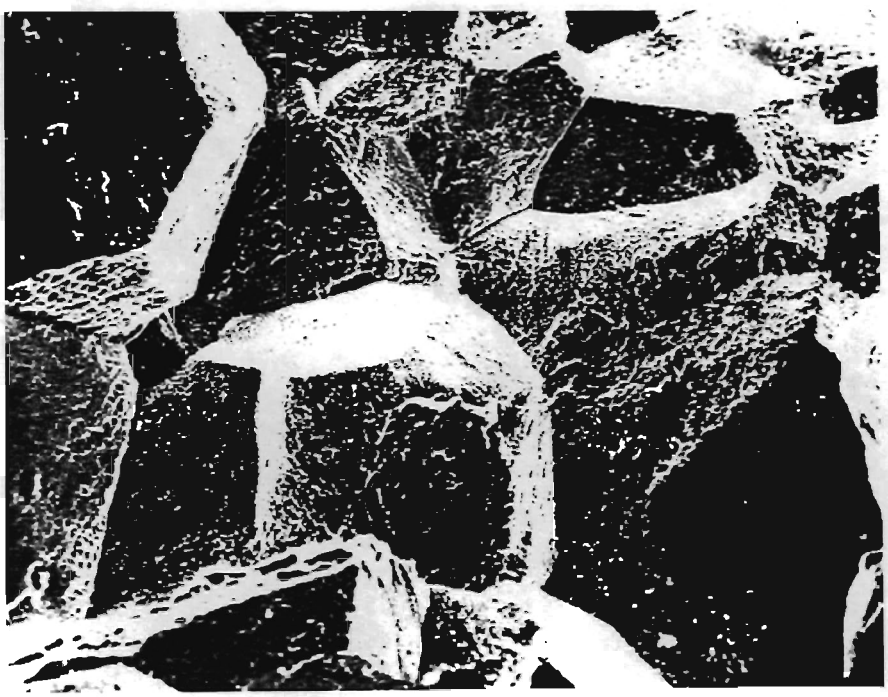

Figure 57. Fractograph of JSW 2 1/4Cr-1Mo-V-Ti-B, 1150°F (620°C) PWHT. 47.2ksi (325MPa), 44.6 min. to fracture, 1.8% RA, SEM 500X.

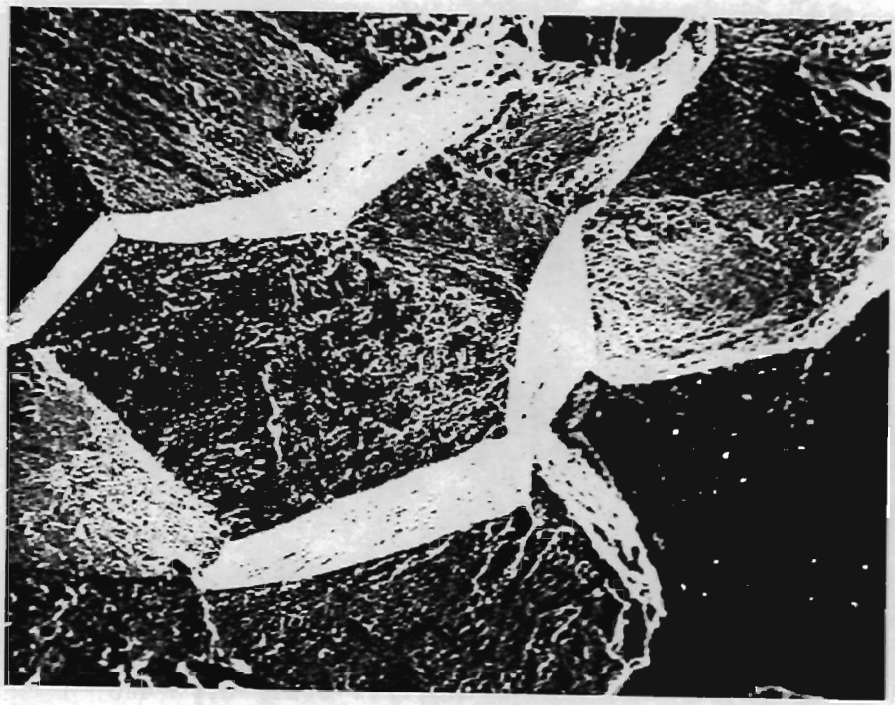

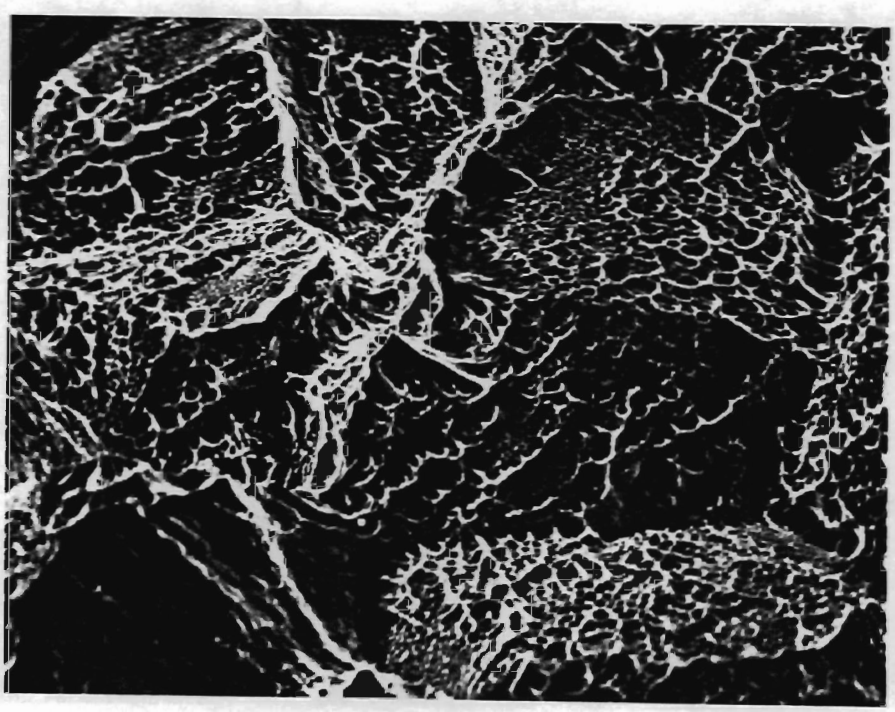

Figure 58. Fractographs of JSW 3Cr-1Mo-V-Ti-B, 1250°F (680°C) PWHT. 34.6ksi (239MPa), 16.3 min. to fracture, 7.7%RA, SEM 500X, a) LDIGF region, b) IGMVC region.

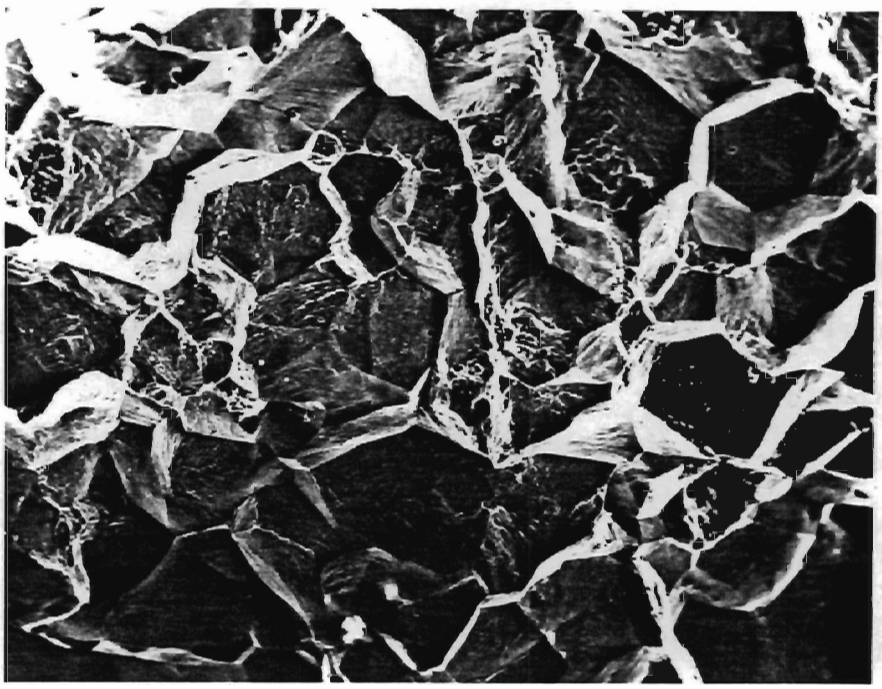

A

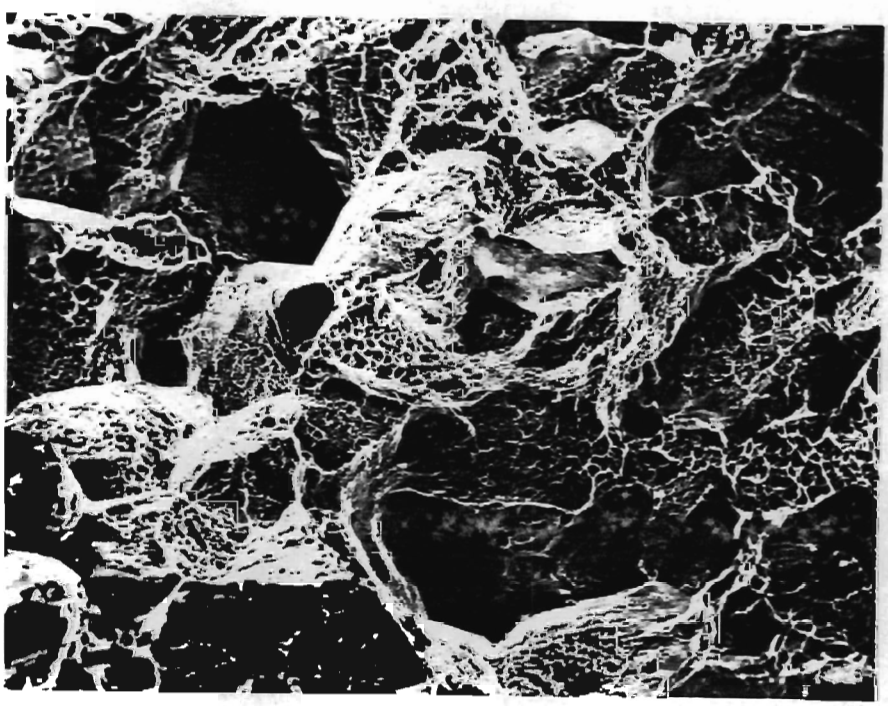

B

Figure 59. Fractographs of JSW 3Cr-1Mo-V-Ti-B, 1150°F (620°C) PWHT. 64.8ksi (446MPa), 8.6 min. to fracture, 1.8%RA, SEM 200X, a) LD1GF region, b) IGMVC region.

macroductility, 3.8 and 1.3% respectively for the AMAX material and 5.1 and 1.8% respectively for the JSW 2 1/4Cr material, correlates with the lack of microductility in the fractographs.

The Berkeley 3Cr-1 1/2Mo-1/2Ni material (Figures 54 and 55) primarily shows the IGMVC mode of fracture at both PWHT temperatures. Figure 55, the 1150°F (620°C) PWHT specimen fractograph, shows a lesser amount of microvoid formation with several grain faces devoid of any microductility. This corresponds with a decrease in macroductility, RA, from 21% at 1250°F (680°C) to 11% at 1150°F (620°C).

The JSW 3Cr-1Mo-V-Ti-B material exhibited a dual fracture mode at both PWHT temperatures. Figures 58a and 58b show the LDIGF and IGMVC regions observed on the sample PWHT at 1250°F (680°C). Comparison of Figure 58b and Figure 54, the Berkeley 3Cr-1 1/2Mo-1/2Ni, 1250°F (680°C) PWHT specimen, shows that the IGMVC regions of the JSW 3Cr-1Mo-V-Ti-B material exhibit less microvoid formation than the Berkeley type. The presence of the LDIGF region and the lesser extent of microvoid formation correspond to a lower ductility, 7.7% RA, compared to the Berkeley alloy, 20% RA.

Figures 59a and 59b show the LDIGF and IGMVC regions of the JSW 3Cr-1Mo-V-Ti-B type PWHT at 1150°F (620°C). (Note, the magnification has been reduced in Figure 59 to 200X) The IGMVC region, Figure 59b, contains some smooth grain faces, free of any microductility. The increase in the amount of LDIGF surface is seen in the reduction of the observed macroductility to 1.8% RA compared to 7.7% RA for the 1250°F (680°C) PWHT JSW 3Cr-1Mo-V-Ti-B specimen.

The dual mode of fracture has been observed by Granjon[79] in PWHT cracking susceptibility determinations employing the implant testing technique. Granjon found that at lower temperatures or higher stresses the LDIGF mode predominates on the fracture surface while at higher temperatures or lower stresses IGMVC is the mode of fracture. In Gleeble testing, where a constant load is maintained, it is possible that the fracture may initiate by IGMVC when the stress is lowest and change to LDIGF as microvoid formation occurs. The formation of microvoids would decrease the load bearing cross sectional area effectively increasing the stress, driving the change in fracture mode to LDIGF.

Figure 60 shows a region of LDIGF on the Berkeley 3Cr-1 1/2Mo-1/2Ni, 1150°F (620°C) PWHT sample. Energy dispersive x-ray analysis (EDAX) for the small inclusion, the region immediately adjacent to the inclusion (region A in Figure 60b) and the smooth grain boundary well removed from the inclusion (region B in Figure 60a) are shown in Figures 61a through 61c. (Figure 61c superposes the EDAX spectrum for region B, the lower spectrum, and the EDAX spectrum for the inclusion.) The EDAX spectra show the presence of aluminum in the inclusion and on the grain boundaries. Although the aluminum content on the fracture surface well removed from the inclusion (region B, Figure 60a) is greatly reduced, the presence of aluminum in the EDAX spectrum can still be discerned in Figure 61c. The literature review indicated that aluminum has been found to increase PWHT cracking susceptibility in several studies.[74,100-102] The presence of aluminum on the LDIGF surfaces in the Berkeley 3Cr-1 1/2Mo-1/2Ni alloy, for which the predominant fracture mode is IGMVC, indicates that aluminum

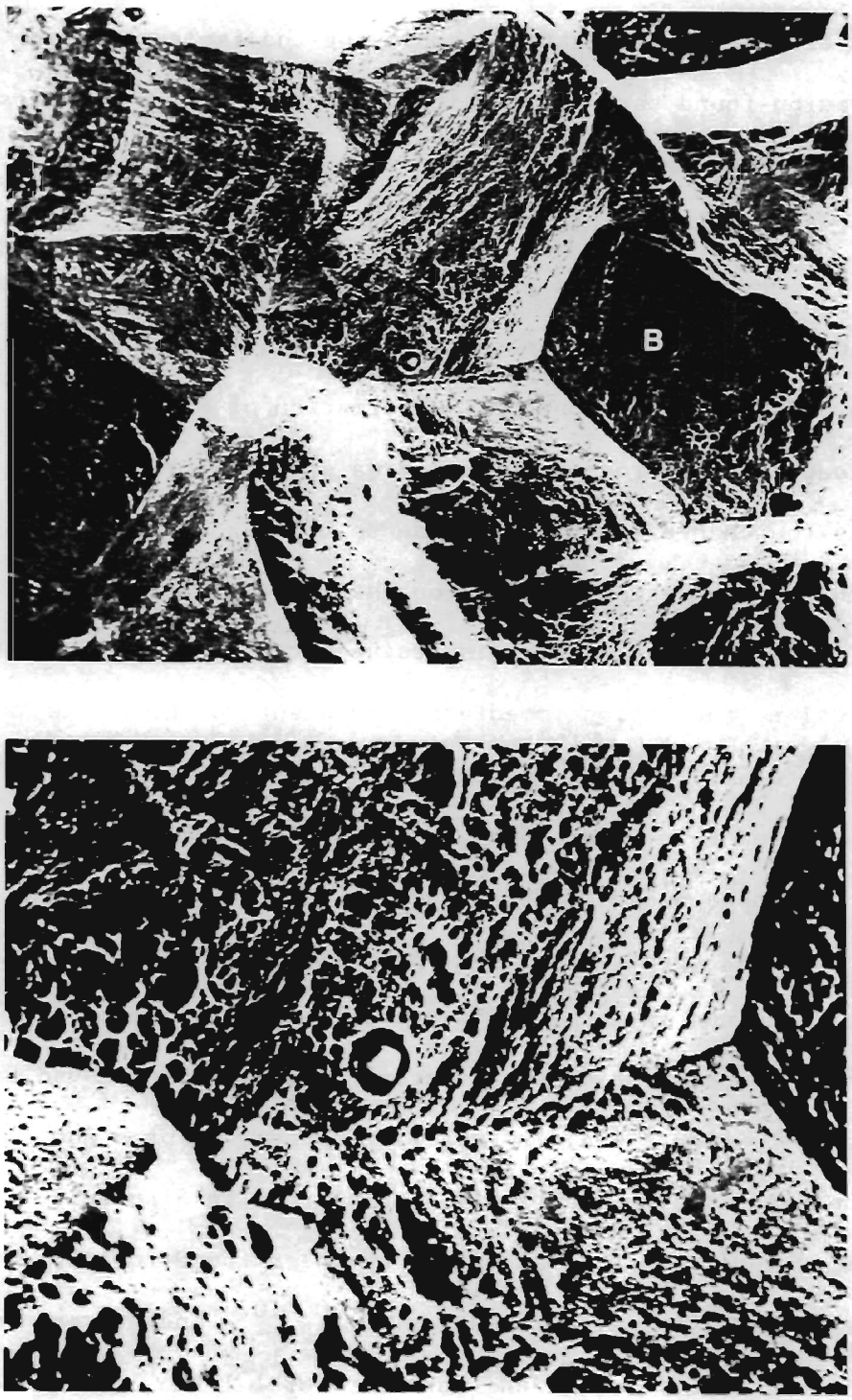

Figure 60. Fractographs of Berkeley 3Cr-1 1/2Mo-1/2Ni, 1150°F (620°C) PWHT. 64.2ksi (442MPa), 2.7 min. to fracture, 11% RA, a) SEM 500X, b) SEM 2000X.

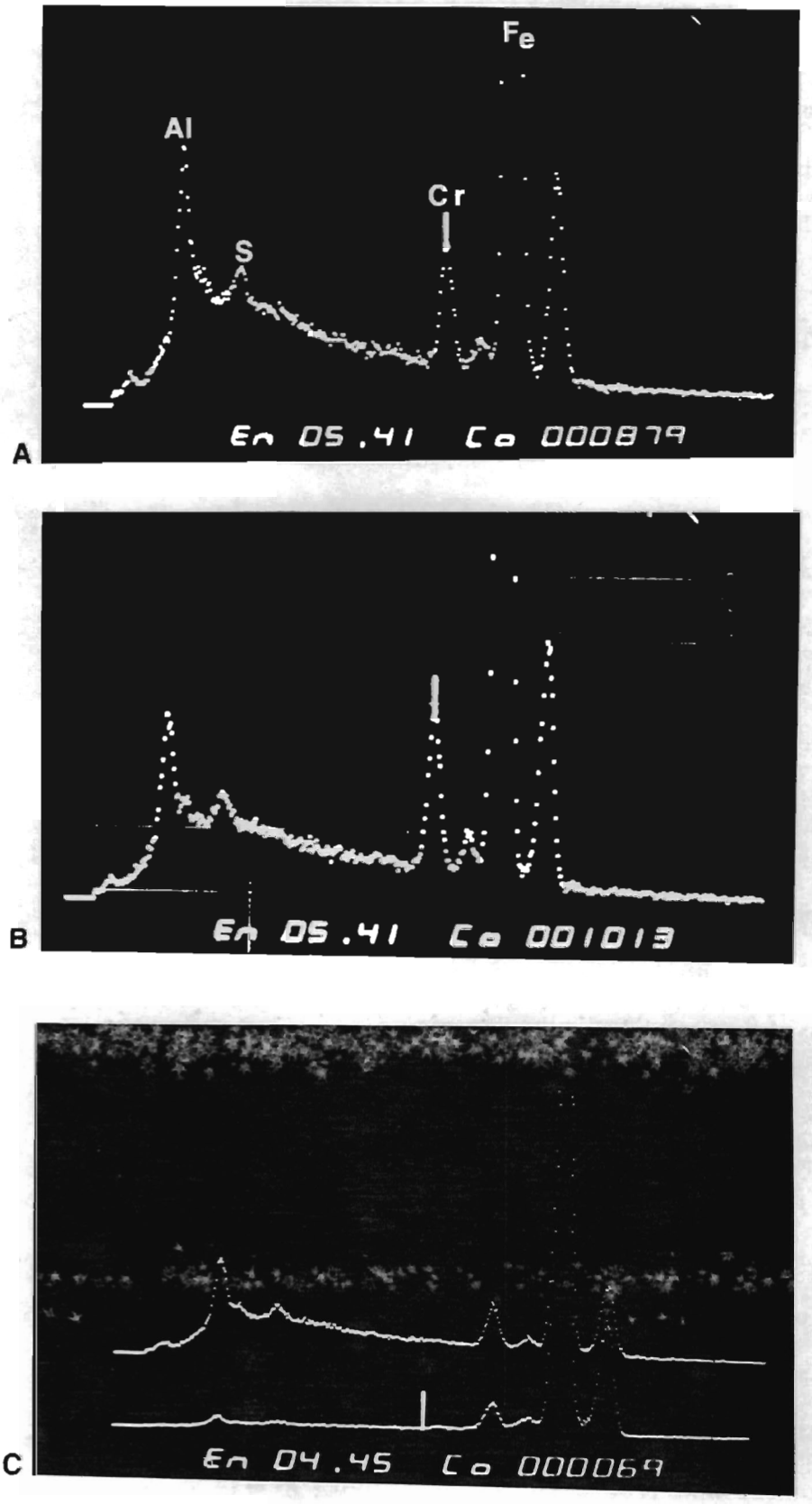

Figure 61. Energy dispersive X-ray analysis (EDAX) of; a) inclusion, b) region A, c) region B vs. inclusion shown in Figure 60.

segregation to the prior austenite grain boundaries or partial dissolution of aluminum rich particles during the weld thermal cycle may be a factor in the loss of ductility during PWHT.

Aluminum bearing grain boundary particles were also found in the JSW 3Cr-1Mo-V-Ti-B material (Figure 62a). (Figure 62 is a fractograph of an IGMVC region taken from the same sample as shown in Figure 58.) The EDAX spectra for the particle and region immediately adjacent to the particle are shown in Figures 62b and 62c respectively. The limited ductility of the area immediately adjacent to the particle, which also showed aluminum in the EDAX spectrum, is evident in Figure 62a. However, unlike the Berkeley material shown in Figure 60, the region devoid of significant microvoid formation is limited to the area immediately adjacent to the particle. To some extent this may be the result of the lower PWHT temperature, 1150°F (620°C), of the Berkeley 3Cr-1 1/2Mo-1/2Ni sample as opposed to the 1250°F (680°C) PWHT temperature of the JSW 3Cr-1Mo-V-Ti-B sample as the ductility is greater at the higher temperature microvoid formation is enhanced.

Grain boundary particles in the JSW 3Cr-1Mo-V-Ti-B material were found to be present in greater number and were most often found to be initiation sites for the formation of microvoids (Figure 63). The EDAX spectra for the three typical particle compositions are shown in Figure 64. The particles labeled 1 on Figure 63a and 63b consist primarily of chromium, manganese and iron (Figure 64a) and are probably carbides. The particles labeled 2 and 3 both contain sulphur with type 2 being rich in manganese and iron with lesser amounts of titanium and chromium while type 3 particles are rich in titanium with lesser amounts of manganese,

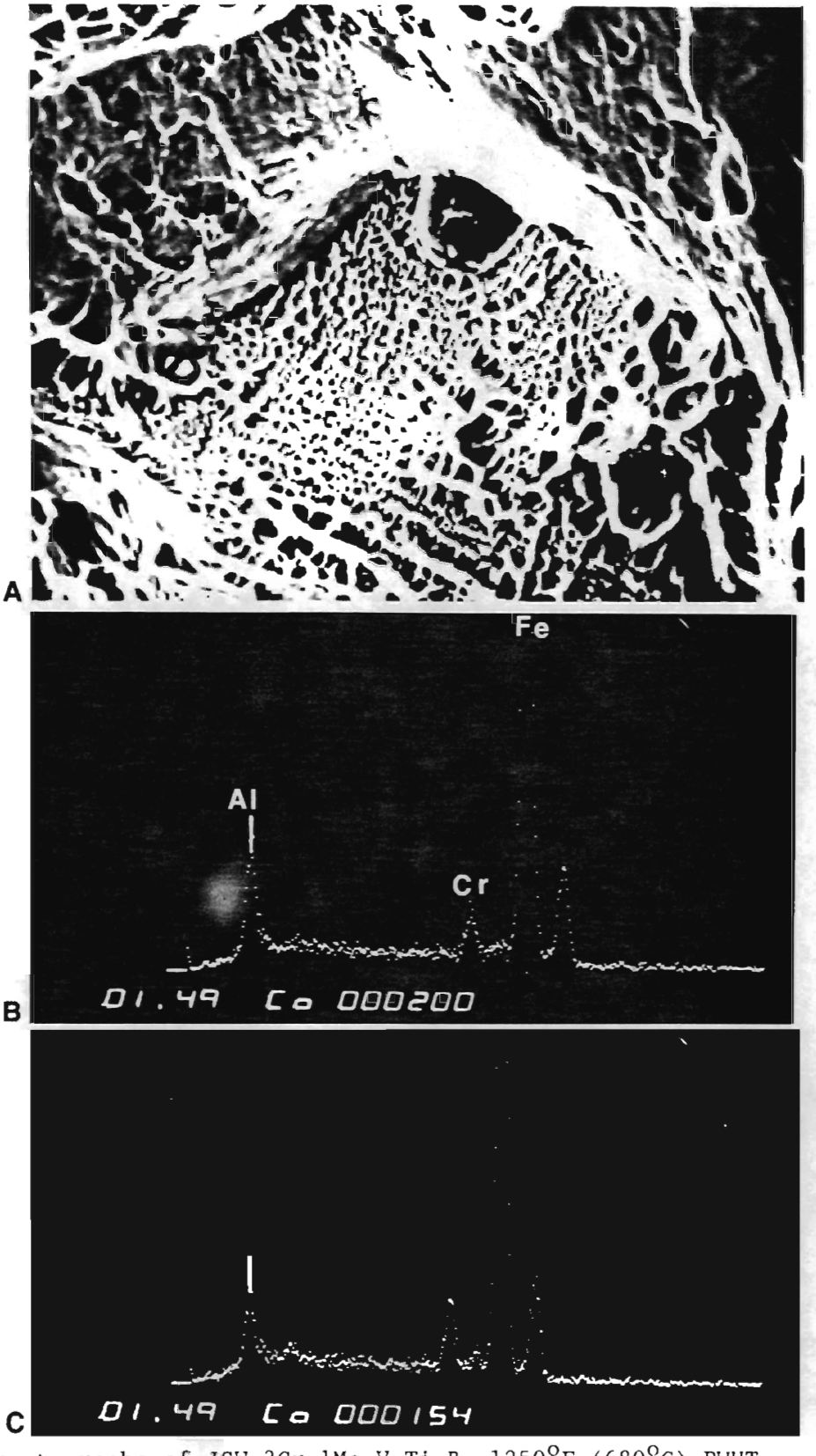

Figure 62. Fractographs of JSW 3Cr-1Mo-V-Ti-B, 1250°F (680°C) PWHT. 34.6ksi (239MPa), 16.3 min. to fracture, 7.7% RA, a) SEM 2000X, b) EDAX of grain boundary particle, c) EDAX of area immediately adjacent to the particle.

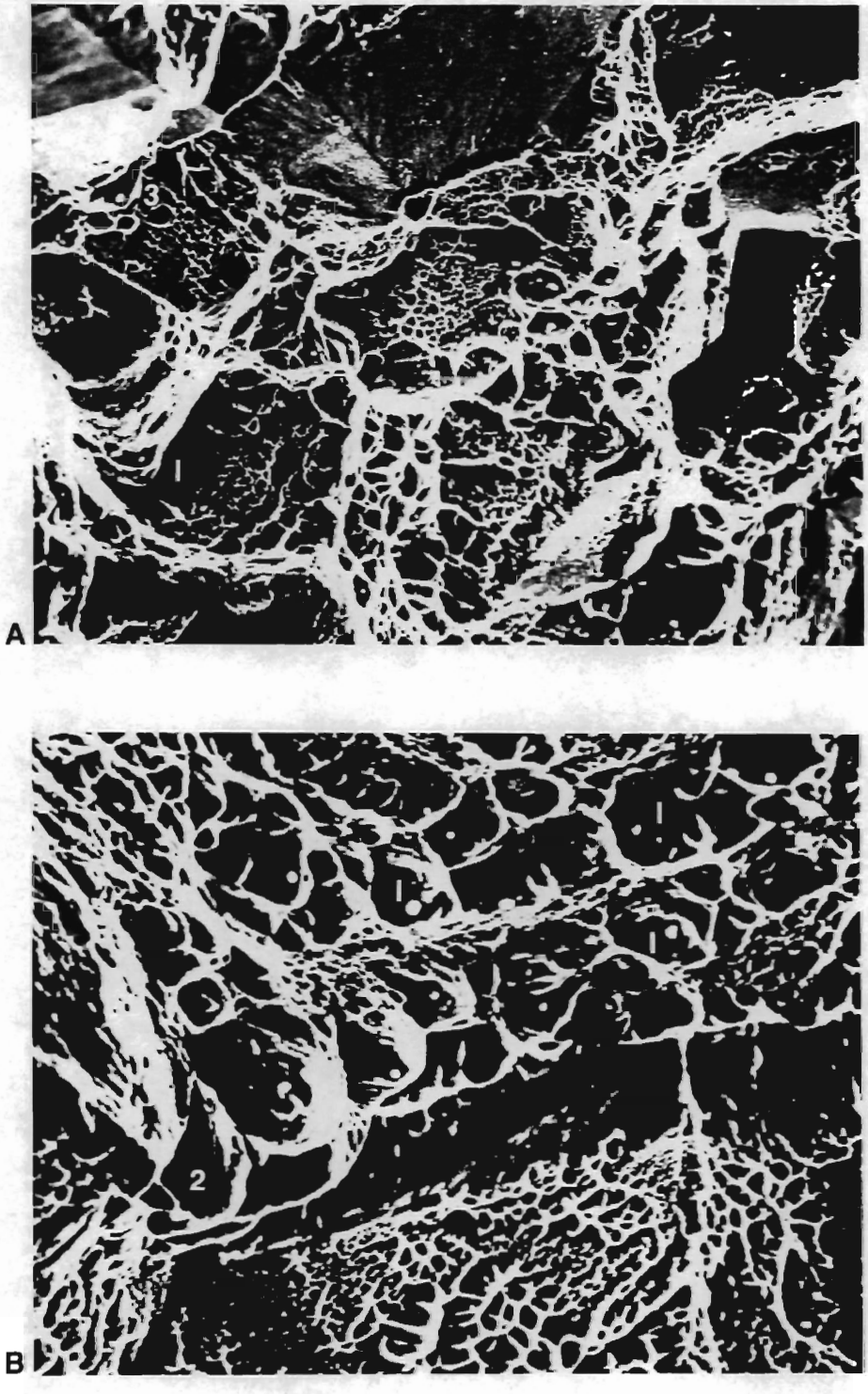

Figure 63. Fractographs of JSW 3Cr-1Mo-V-Ti-B, 1150°F (620°C) PWHT. 64.8ksi (446MPa), 8.6 min. to fracture, 1.8% RA, a)SEM 500X, b)SEM 1000X.

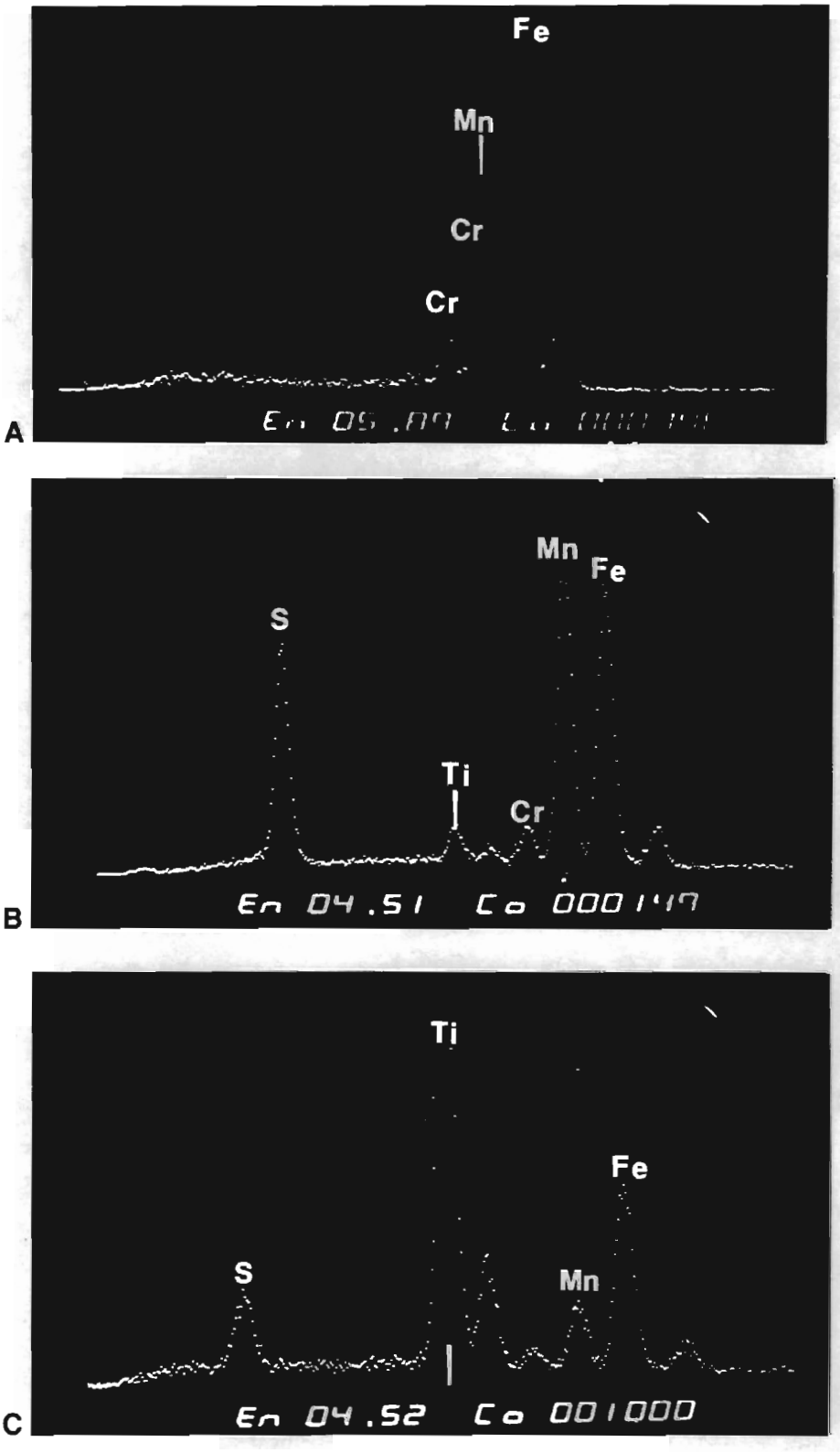

Figure 64. EDAX analysis of grain boundary particles initiating cavitation in JSW 3Cr-1Mo-V-Ti-B (Figure 63), a) type 1, b) type 2, c) type 3.

chromium, and iron.(The aluminum bearing particles discussed previously were found only rarely.) The nucleation of microvoids on sulphides, nitrides and carbides has been observed by several researchers.[15,76,84,116,140] Hippsley[84] has stated that low interfacial strength may be the cause of cavitation or microvoid formation about grain boundary particles.

The fractographic study therefore shows that the two fracture modes reported in the literature[79,84,116], LDIGF and IGMVC, are observed in the present study and, in agreement with Granjon[79], may in fact be present on a single specimen. The presence of aluminum and aluminum bearing particles in the prior austenite grain boundaries has been shown to be a possible factor contributing to LDIGF. However, in the JSW 3Cr-1Mo-V-Ti-B, where an abundance of grain boundary particles are present, cavitation initiating on the grain boundary particles may have a greater overall effect on rupture mode than the presence of a limited number of aluminum rich particles per se.

Optical, Scanning Electron and Transmission Electron Microscopy of Gleeble Simulated Postweld Heat Treatment Specimens.

Figures 65 through 68 are optical and scanning electron micrographs of the region near the fracture surface of AMAX (Climax) 3Cr-1 1/2Mo-0.1V, Berkeley 3Cr-1 1/2Mo-1/2Ni, JSW 3Cr-1Mo-V-Ti-B, and JSW 2 1/4Cr-1Mo-V-Ti-B Gleeble simulated PWHT cracking specimens. The specimens employed for study were the longest time to fracture (88, 88.5, 71, and 100.9 minutes respectively), lowest stress, 1250°F (680°C) PWHT specimens for each alloy.

The microstructure, shown by both optical and scanning electron microscopy, has changed substantially from the as-cycled (as welded and no

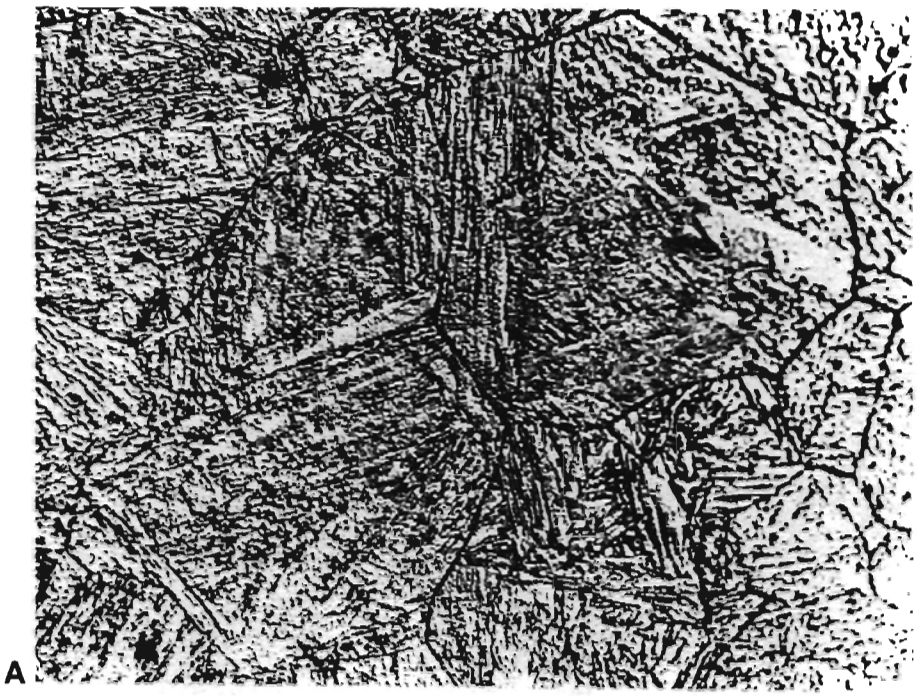

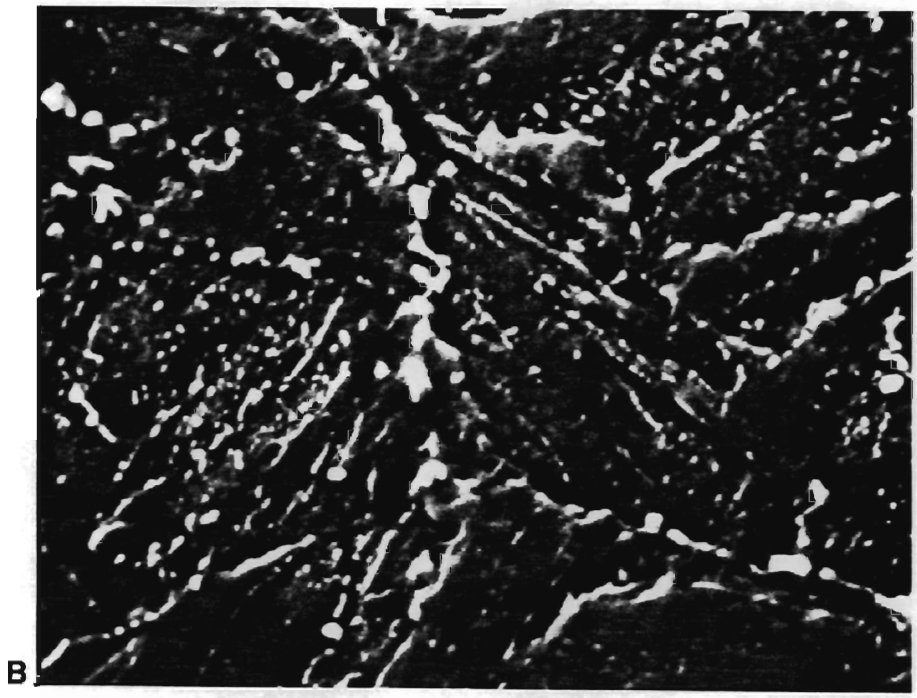

Figure 65. AMAX (Climax) 3Cr-1 1/2Mo-0.1V Gleeble simulated PWHT cracking specimen, 1250°F (680°C) PWHT. 25.5ksi (176MPa), 5% RA, 88 min. to fracture, a)500X OLM, b) 10,000X SEM.

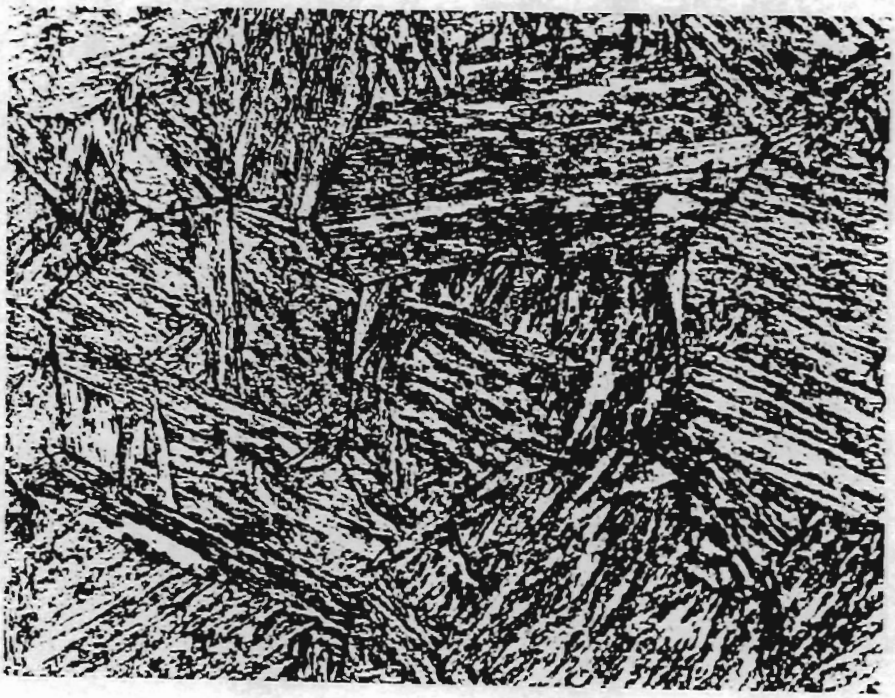

A

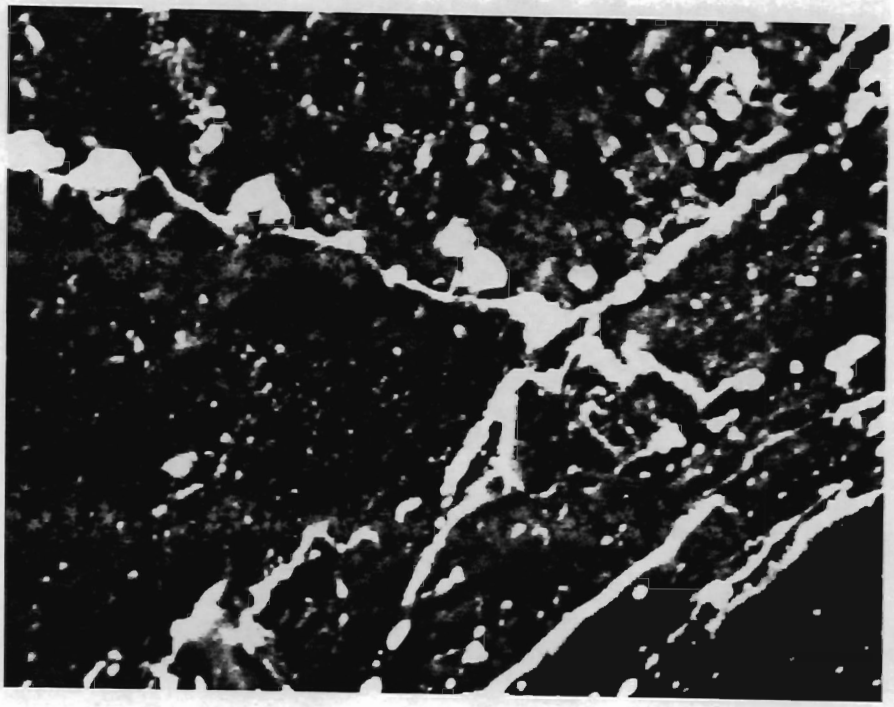

B

Figure 66. Berkeley 3Cr-1 1/2Mo-1/2Ni Gleeble simulated PWHT cracking specimen, 1250°F (680°C) PWHT. 21.4ksi (147MPa) 88.5 min. to fracture, 26% RA, a) 500X OLM, b) 10,000X SEM.

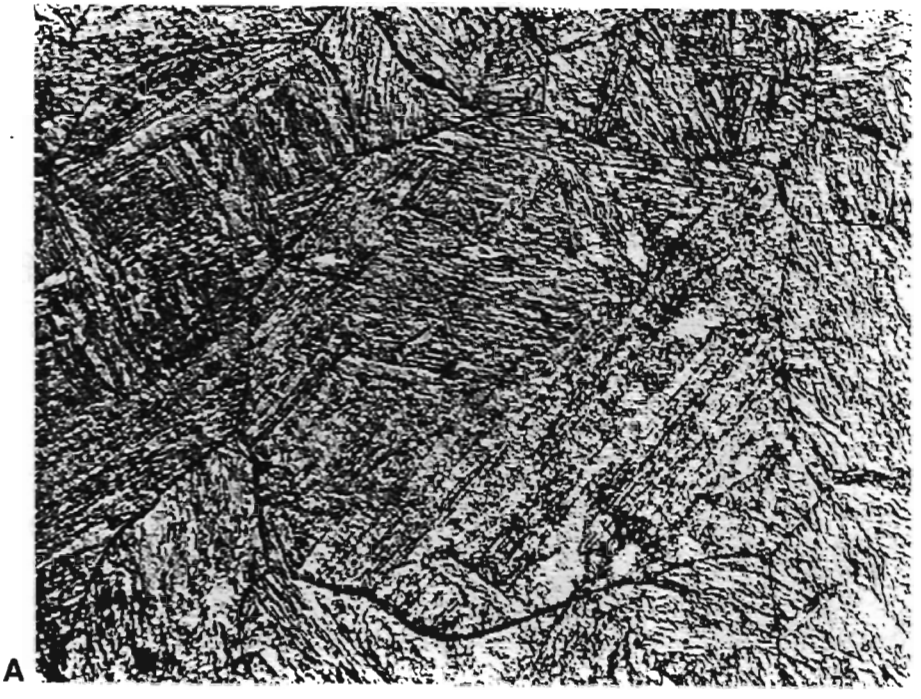

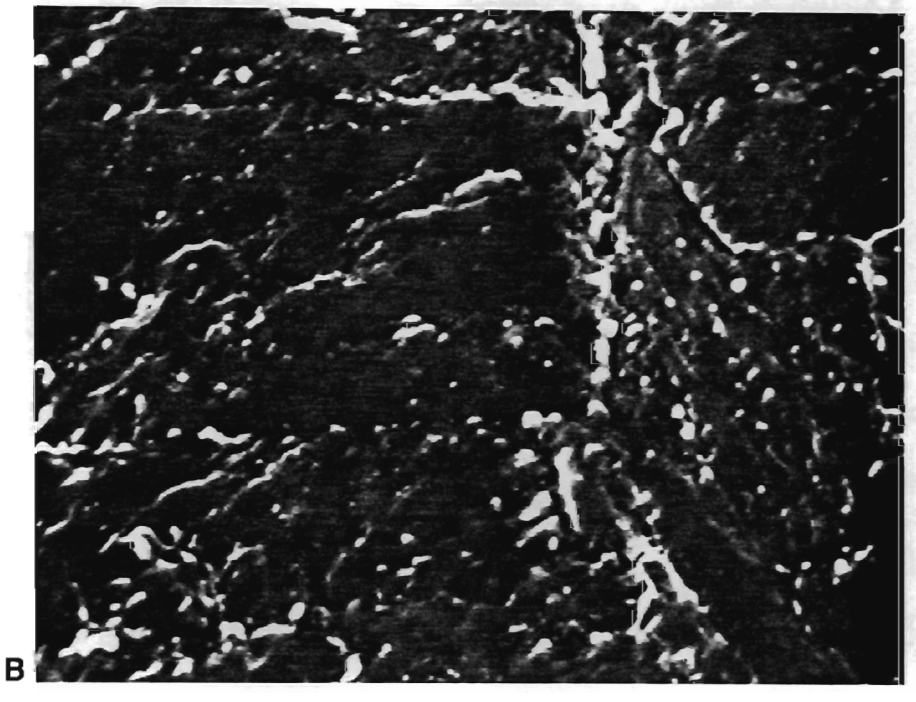

Figure 67. JSW 3Cr-1Mo-V-Ti-B Gleeble simulated PWHT cracking specimen, 1250°F (680°C) PWHT. 39.1ksi (269MPa), 14% RA, 71 min. to fracture, a) 500X OLM, b) 10,000X SEM.

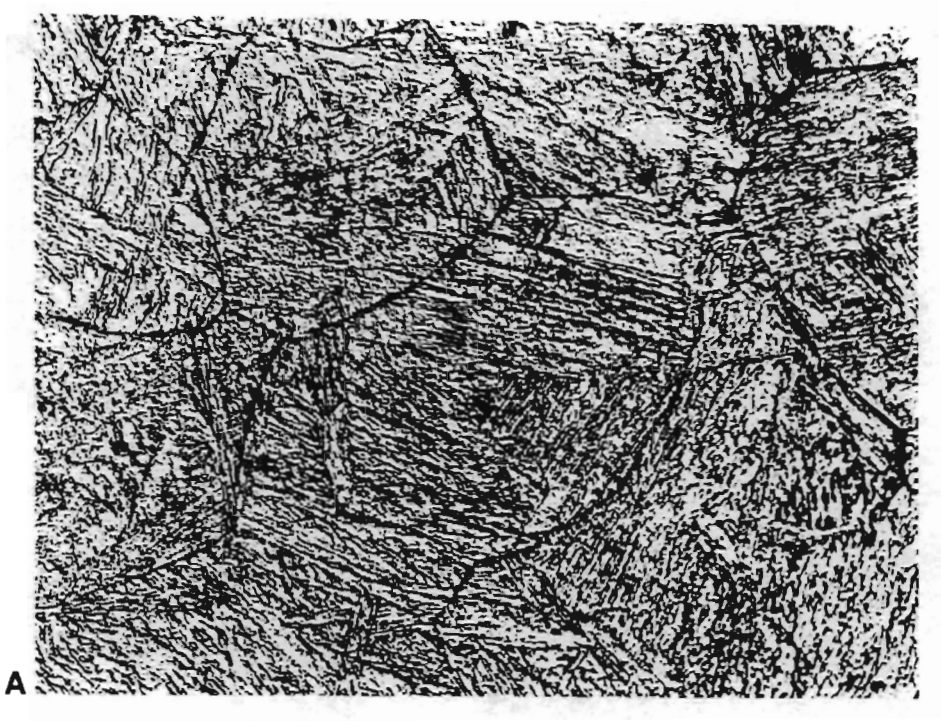

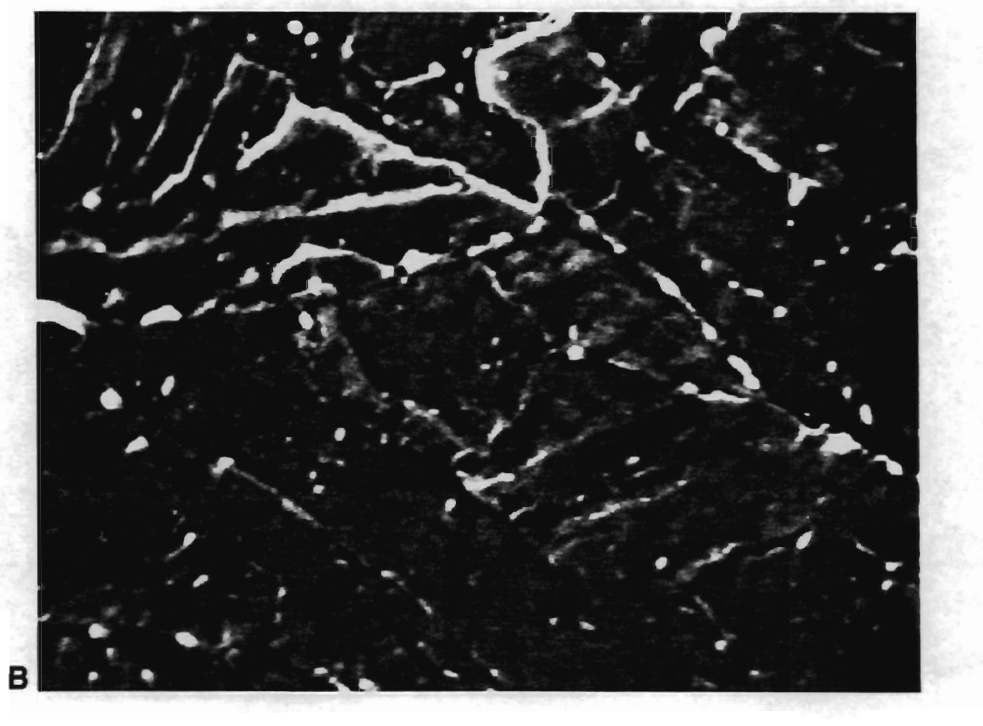

Figure 68. JSW 2 1/4Cr-1Mo-V-Ti-B Gleeble simulated PWHT cracking specimen, 1250°F (680°C) PWHT. 34.3ksi (236MPa), 7.1% RA, 101 min. to fracture, a) 500X OLM, b) 10,000X SEM.

PWHT) microstructure shown in the transformation section (Figures 41 and 43 through 45). The optical microstructures (Figures 65a through 68a) show that after PWHT the prior austenite grain boundaries are more clearly delineated and the acicular aspect of the microconstituents are less well defined in comparison to the as cycled microstructures. The scanning electron micrographs (Figures 65b through 68b) show an almost complete break down of the lath type constituents observed in the as cycled condition with extensive carbide precipitation along the prior austenite grain boundaries. Fine carbide precipitation has occurred within the grain matrix with the carbides in the Berkeley 3Cr-1 1/2Mo-1/2Ni material coarser than in the AMAX (Climax) 3Cr-1 1/2Mo-0.1V, JSW 3Cr-1Mo-V-Ti-B, or JSW 2 1/4Cr-1Mo-V-Ti-B alloys.

The presence of observable carbides in the matrix and extensive precipitation along the grain boundaries is concomitant with a loss in hardness or strength. The as cycled hardnesses, shown in Figures 35 through 38, were 370, 412, 400, and 388DPH for the AMAX (Climax) 3Cr-1 1/2Mo-0.1V, Berkeley 3Cr-1 1/2Mo-1/2Ni, JSW 3Cr-1Mo-V-Ti-B, and JSW 2 1/4Cr-1Mo-V-Ti-B materials respectively. After Gleeble simulated PWHT at 1250°F (680°C), the hardnesses were 253, 227, 268, and 256DPH for the AMAX (Climax), Berkeley, JSW 3Cr, and JSW 2 1/4Cr alloys respectively. The Berkeley 3Cr-1 1/2Mo-1/2Ni material exhibited the greatest change in hardness, a 185DPH decrease, and the lowest hardness value, 227DPH, after PWHT which is indicative of a greater progression of carbides toward the end of the evolutionary chain.

Figures 69 through 72 show the transmission electron micrographs of the carbide extraction replicas of the AMAX (Climax) 3Cr-1 1/2Mo-0.1V,

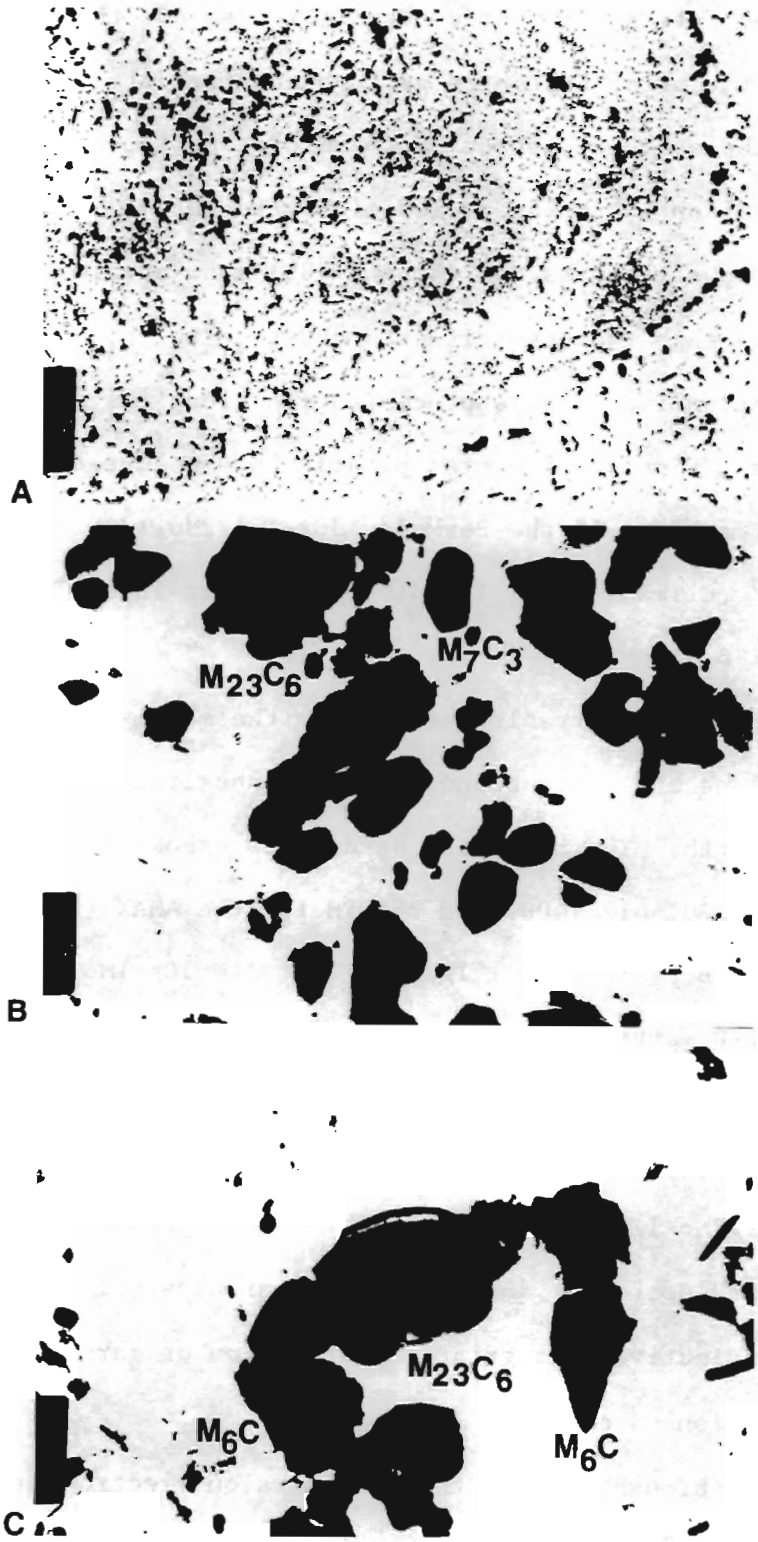

Figure 69. Transmission electron micrographs of AMAX (Climax) 3Cr-1 1/2Mo-0.1V. thermal cycled and PWHT at 1250°F (680°C) for 100 min. a) 3,300X, b) 36,000X, c) 49,000X.

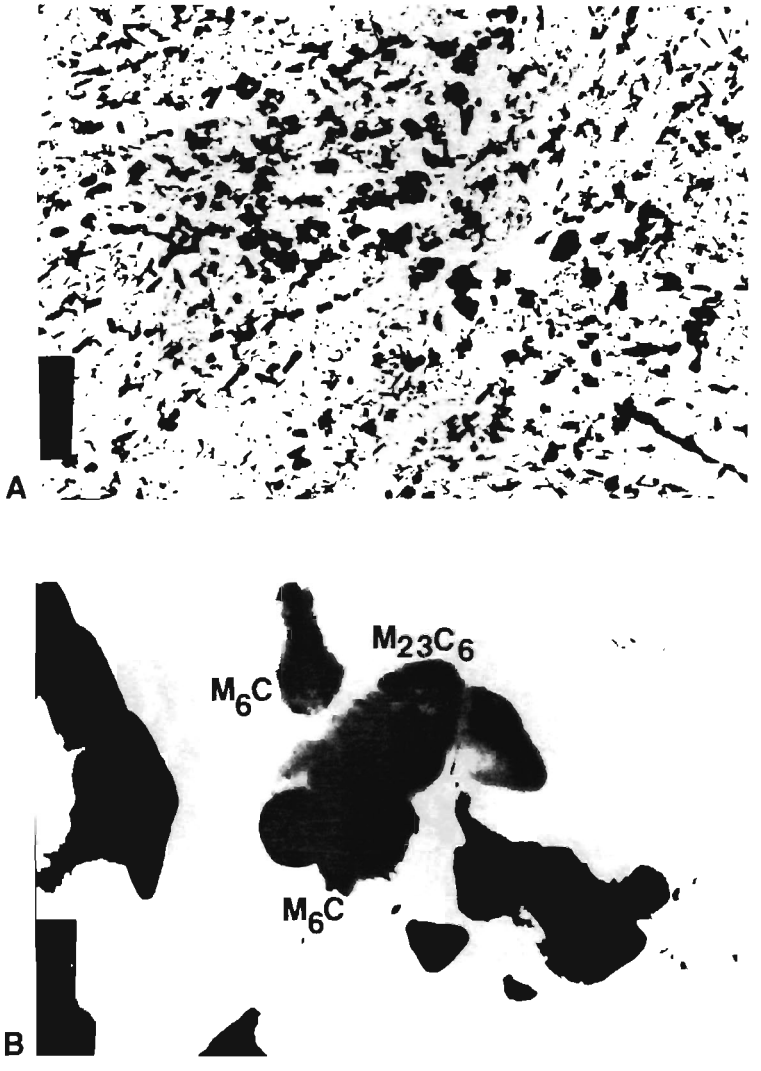

Figure 70. Transmission electron micrographs of Berkeley 3Cr-1 1/2Mo-1/2Ni, thermal cycled and PWHT at 1250°F (680°C) for 100 min. a) 6,350X, b) 82,000X.

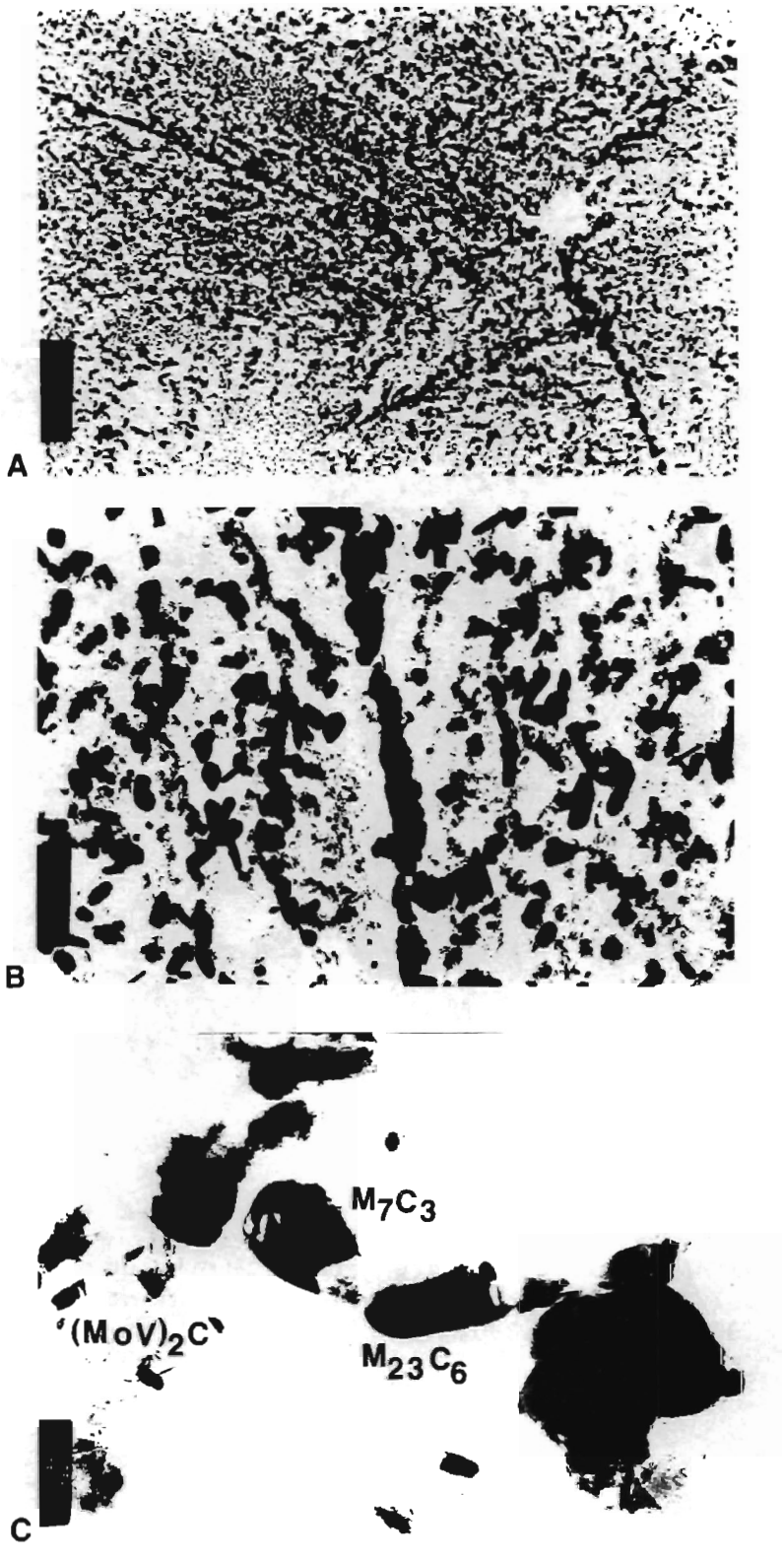

Figure 71. Transmission electron micrographs of JSW 3Cr-1Mo-V-Ti-B, thermal cycled and PWHT at 1250°F (680°C) for 100 min. a) 3,300X, b) 18,500X, c) 175,000X.

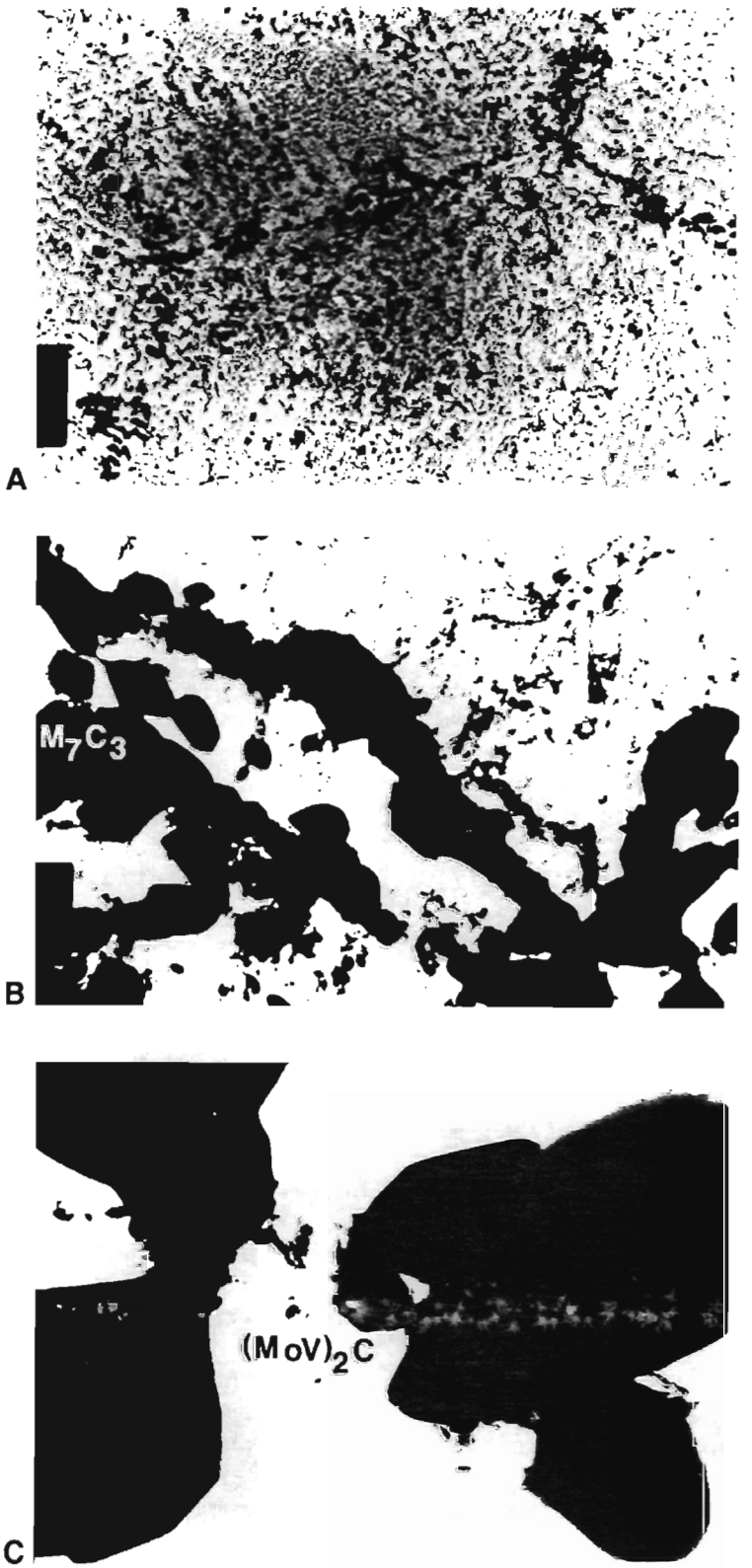

Figure 72. Transmission electron micrographs of JSW 2 1/4Cr-1Mo-V-Ti-B, thermal cycled and PWHT at 1250°F (680°C) for 100 min. a) 3,300X, b) 49,000X, c) 230,000X.

Berkeley 3Cr-1 1/2Mo-1/2Ni, JSW 3Cr-1Mo-V-Ti-B, and JSW 2 1/4Cr-1Mo-V-Ti-B from a cooperative effort undertaken at the University of Southern California, Los Angeles.[141] Table 13 summarizes the results of the carbide identification performed on extraction replicas for specimens thermal cycled on the Gleeble and PWHT at 1250°F (680°C) for 100 minutes (with applied stress). Table 13 also shows the approximate width of a carbide denuded zone observed adjacent to the prior austenite grain boundaries for the AMAX (Climax) 3Cr-1 1/2Mo-0.1V, Berkeley 3Cr-1 1/2Mo-1/2Ni, JSW 3Cr-1Mo-V-Ti-B, and JSW 2 1/4Cr-1Mo-V-Ti-B specimens. The width of the carbide denuded zone in the Berkeley 3Cr-1 1/2Mo-1/2Ni material was not determined.

The precipitates found within the grain matrix for all four materials was primarily M_2C with some MC type carbides in the vanadium modified alloys. The matrix precipitates in the AMAX (Climax) 3Cr-1 1/2Mo-0.1V, JSW 3Cr-1Mo-V-Ti-B, and JSW 2 1/4Cr-1Mo-V-Ti-B materials (Figures 69a, 71a and 72a) appear to be finer than in the Berkeley 3Cr-1 1/2Mo-1/2Ni material (Figure 70a). It is also apparent that the AMAX (Climax) 3Cr-1 1/2Mo-0.1V alloy had a higher volume fraction of precipitates in comparison to the Berkeley 3Cr-1 1/2Mo-1/2Ni material. The smaller size and greater amount of precipitates in the vanadium modified materials would result in a generally higher matrix strength than that of the Berkeley 3Cr-1 1/2Mo-1/2Ni alloy. The slower growth of the precipitates in the vanadium modified alloys also indicates that the duration of the period of coherency during PWHT is also probably longer. The combined effect of the delayed carbide evolution and the carbide morphology for the vanadium

Table 13. Carbide analysis for the modified 3Cr and 2 1/4Cr alloys; Gleeble simulated PWHT at 1250°F (680°C) for 100 minutes.

Carbide	Berkeley 3 Cr-1½Mo-0.1V	AMAX (Climax) 3 Cr-1½Mo-0.1V	JSW 3 Cr-1Mo-V-Ti-B	JSW 2½ Cr-1Mo-V-Ti-B
M_3C	NF	NF	NF	NF
M_2C	M	M	M	M
M_7C_3	NF	B (0.3-0.6μm)	B* (0.3-0.6μm)	B (0.3-0.6μm)
$M_{23}C_6$	B,LB (0.3-0.6μm)	B (0.3-0.6μm)	B (0.3-0.6μm)	B* (0.3-0.6μm)
M_6C	B (0.3-0.6μm)	B (0.3-0.6μm)	NF	NF
Denuded zone width	NR	~0.3μm	~0.1μm	<0.1μm

M - Matrix
B - boundary
LB - Lath boundary

* - predominate species
NF - not found
NR - not reported

modified materials is to extend the period of maximum matrix strengthening to longer times and higher temperatures which is considered a major factor in PWHT cracking susceptibility as discussed by Tamaki.[90]

The TEM micrographs (Figures 69 through 72) show clearly the presence of coarse grain boundary carbides in all four alloys (approximately 0.3 to 0.6 μm in size). However, the scanning electron micrographs (Figures 65 through 68) show that the grain boundary carbides in the Berkeley 3Cr-1 1/2Mo-1/2Ni material tend to be larger in size than the grain boundary carbides in the AMAX (Climax) 3Cr-1 1/2Mo-0.1V, JSW 3Cr-1Mo-V-Ti-B, or JSW 2 1/4Cr-1Mo-V-Ti-B materials. The presence of only $M_{23}C_6$ and M_6C carbides in the grain boundaries (Table 13) of the Berkeley 3Cr-1 1/2Mo-1/2Ni material clearly demonstrates the accelerated kinetics of carbide precipitation in this alloy with respect to the other vanadium modified alloys. In the AMAX (Climax) 3Cr-1 1/2Mo-0.1V material, the presence of M_7C_3 in addition to $M_{23}C_6$ and M_6C indicates that carbide evolution is somewhat more sluggish in this alloy compared to the Berkeley alloy. However, the lack of any M_6C in the JSW 3Cr-1Mo-V-Ti-B or the JSW 2 1/4Cr-1Mo-V-Ti-B materials, with 0.28% and 0.26% vanadium respectively, shows the significant retardation of carbide evolution in these alloys with respect to the Berkeley alloy. The effect of vanadium in stabilizing carbides[31] and restricting diffusion of chromium in ferrite[34] was discussed in the literature review. The retardation of carbide evolution and growth with the increased vanadium content is clearly evident from the data in Table 13.

The formation of the grain boundary carbides is accompanied with the formation of carbide denuded zones in the AMAX (Climax) 3Cr-1 1/2Mo-0.1V,

JSW 3Cr-1Mo-V-Ti-B, and JSW 2 1/4Cr-1Mo-V-Ti-B materials. (The presence of and extent of a carbide denuded zone in the Berkeley 3Cr-1 1/2Mo-1/2Ni material has not been defined.) The rapid formation and growth of carbides along the prior austenite grain boundaries depletes the surrounding material of carbon and alloying elements and results in the formation of a weak region devoid of carbides. Several researchers have considered this narrow, soft region to be the site of strain accumulation and, ultimately, the region in which fracture occurs.[30,72]

The denuded zone widths were reported to be approximately 0.3 μm in the AMAX (Climax) 3Cr-1 1/2Mo-0.1V, 0.1 μm in the JSW 3Cr-1Mo-V-Ti-B, and not as pronounced in the JSW 2 1/4Cr-1Mo-V-Ti-B as in the JSW 3Cr-1Mo-V-Ti-B. It has been stated in the literature that as the denuded zone width increases the zone should be more able to accommodate the strain associated with creep induced plastic flow and therefore more resistant to cavitation and rupture.[55,62,66] However, the Gleeble results for the PWHT cracking study show that the AMAX (Climax) 3Cr-1 1/2Mo-0.1V material, with the greatest extent of the denuded zone, was more susceptible to cracking than the JSW 3Cr-1Mo-V-Ti-B or JSW 2 1/4Cr-1Mo-V-Ti-B materials. The higher phosphorus content (0.012%) in the AMAX (Climax) material than the JSW 3Cr or JSW 2 1/4Cr materials (0.007%) may result in embrittlement being more potent in increasing susceptibility than the increase in the denuded zone width is in decreasing susceptibility. It is important to remember at this point that the effect of the denuded zone is disputed in the literature with both Swift[66] and Meitzner and Pense[70] arguing that the denuded zone is not a factor in PWHT cracking.

C-Ring Test Evaluation of Postweld Heat Treatment Cracking Susceptibility of the 3Cr-Mo and 2 1/4Cr-1Mo Alloys.

No single test for evaluating PWHT cracking susceptibility has been universally accepted although a great number of tests have been used and the results reported in the literature.[73,60,61,98] An ideal test for evaluating PWHT cracking susceptibility should have the following characteristics:[104] the specimen should include a notch or defect in a microstructure representative of the actual HAZ, the HAZ should be strained in a manner similar to that experienced in an actual weld, and the specimen should experience stress relaxation analogous to that experienced in actual welds since multiaxial stress in welds may produce a lower relaxation rate and higher triaxial stress state than is typical of uniaxial bars. To find a single test that incorporates all the factors involved in an actual weld into a small specimen has been said to be "difficult".[73]

The Gleeble test for determining susceptibility is certainly not an ideal test. A major objection is that a constant load is normally employed rather than a time dependent, decreasing load as is actually experienced during PWHT. (A paper was presented at the 1986 American Welding Society Annual Convention on a new test method for evaluating PWHT cracking.[132] The method employs the new Gleeble 1500 which is capable of applying a preprogrammed load and incorporates feed back control for these parameters which makes possible a simulation of the variable stress state present during PWHT.) Since Gleeble simulation reproduces only a single portion of the HAZ the constraint effects of the surrounding base metal and weld metal are not included.[60,63] Also, since the specimens normally employed do not

include a notch, the test does not simulate actual conditions, in that a notch or internal defect invariably is the initiation site for cracking.[60,18]

The C-ring test, normally employed for evaluating susceptibility to stress-corrosion cracking, was determined to be a suitable, small scale test to evaluate PWHT cracking susceptibility. This test incorporates all aspects of the ideal test outlined by Baker.[60] It is possible to incorporate an actual weld, to introduce a notch into the coarse grained HAZ, to load the coarse grained HAZ to any level of stress and, most importantly, since the C-ring is an approximately constant strain type test, the stress decreases with time at temperature in a manner similar to that of an actual weldment.

The procedure employed in making the C-rings was presented in the experimental procedure section, however, several points deserve further discussion. The walls of the weld groove are made along radial lines from the center of the bar in order to obtain an HAZ which is oriented perpendicular to the walls of the machined C-ring. Therefore, the plane of maximum stress will be aligned through the HAZ and, therefore, crack propagation will not be forced to deviate from the plane of maximum stress in order to remain in the coarse grained HAZ as is the case with the Y-groove test.

The shielded metal arc welds that were performed to fill the groove in the bar were made at heat inputs ranging from 55 to 84KJ/in (2.17 to 3.31KJ/mm) as shown in Table 14. The high heat input was employed so that the microstructures in the HAZ would be similar to that obtained with the 60KJ/in (2.36 KJ/mm) thermal cycle employed in the Gleeble test and to

Table 14. Weld parameters and heat input utilized in C-ring specimen preparation.

Material	Volts	Amps	Time (min)	Length of Weld		Heat Input	
				(in)	(mm)	KJ/m	(kJ/mm)
AMAX 3Cr-1⅛Mo-0.1V (Climax)	23	150	1.13	2 7/8	73	82	3.2
	23	150	1.30	3 3/4	95	72	2.8
	29	145	2.43	7 1/2	190	82	3.2
	30	165	1.07	3 3/4	95	84	3.3
	30	165	0.95	3 1/2	89	81	3.2
Berkeley 3 Cr-1⅛Mo-⅛Ni	30	120	1.50	4	100	81	3.2
	30	120	1.38	4	100	74	2.9
	30	120	1.45	4	100	78	3.1
JSW 3Cr-1Mo-V-Ti-B	25	150	2.38	6 5/8	170	81	3.2
	30	165	0.83	4 1/4	110	58	2.3
	30	165	1.02	4 1/4	110	71	2.8
	30	165	1.00	4 1/4	110	70	2.8
	30	165	0.88	4 1/8	105	64	2.5
	30						
JSW 2¼ Cr-1Mo-V-Ti-B	25	150	2.12	5 5/8	140	85	3.3
	30	165	1.12	5	130	66	2.6
	30	165	0.92	4 7/8	125	56	2.2
	30	165	0.90	4 7/8	125	55	2.2
	30	165	1.03	4 3/4	120	65	2.5
	30	165	1.12	4 3/4	120	70	2.8
Lukens 2¼Cr-1Mo-0.10C	24	160	1.28	4 3/4	120	62	2.4
	24	160	1.32	4 3/4	120	64	2.5

obtain a HAZ with a reasonable width. A wide HAZ is desirable as more tolerance exists for placement of the notch in the coarse grained region. Although higher energy input welds may reduce cracking susceptibility[18,64,86,106,114] the ability to place the notch consistently in the coarse grained HAZ is a critical factor in the test.

Four test conditions were employed for C-ring testing, utilizing two PWHT temperatures, 1150°F (620°C) and 1250°F (680°C), and three stress levels, 100ksi (690MPa), 80ksi (550MPa) and 60ksi (410MPa). The amount of deflection to produce the nominal stress was determined using equations from ASTM standard G 38.[134] The 100ksi (690MPa) stress was used at both PWHT temperatures in order to determine the effect of temperature on cracking. All three stress levels were used at the lower PWHT temperature, which was associated with greater susceptibility in the Gleeble test, in order to examine the effects of stress level and also to try and develop a greater degree of accuracy in the ranking of the materials.

Evaluation of the C-ring test is based on the maximum extent of crack propagation through the ring thickness (the maximum depth of the crack). This parameter was chosen as the manually performed, shielded metal arc welds do not always produce linearly uniform HAZ's. Therefore, the notch does not always lie within the coarse grained HAZ along the entire specimen width with the result that cracking was not uniform within the section.

The maximum depth of the crack can be determined in a number of ways depending on how the sample was prepared and PWHT. Some C-rings were cut into six sections along the notch (approximately 1/8 inch (3mm) thick), and metallographically prepared. The crack length was measured in each of the six sections with the maximum crack length used for comparison. The

remaining C-ring specimens, whether heat treated in air or vacuum, were cooled to liquid nitrogen temperatures and fractured. The extent of intergranular fracture through the section was determined with a low power microscope. The samples PWHT in air were the more easily evaluated than those PWHT in vacuum as the intergranular fracture surface was discolored due to oxidation as opposed to the bright cleavage fracture surface. The fracture surfaces of the samples PWHT in vacuum were examined in the scanning electron microscope for fracture characteristics .

Results of the C-ring Test for the 3Cr-Mo and 2 1/4Cr-1Mo Materials.

The Berkeley 3Cr-1 1/2Mo-1/2Ni and Lukens 2 1/4Cr-1Mo-0.10C materials did not crack when stressed to 100ksi (690MPa) and PWHT at 1150°F (620°C) or 1250°F (680°C). Both the Lukens 2 1/4Cr-1Mo-0.10C and Berkeley 3Cr-1 1/2Mo-1/2Ni were predicted to be "not" susceptible at 1250°F (680°C) and only "slightly" susceptible at 1150°F (620°C) using the Gleeble technique. However all three vanadium modified materials, predicted to be "highly susceptible" or "extremely" susceptible by the Gleeble test, cracked at both PWHT temperatures at all stress levels employed in the C-ring test. Thus, the C-ring test confirms the general ranking of materials as either susceptible or not susceptible.

One sample of the AMAX (Climax) 3Cr-1 1/2Mo-0.1V material was tested without a notch in the coarse grained HAZ but with the HAZ oriented in the same manner. The unnotched specimen was stressed to 100ksi (690MPa) and PWHT at 1150°F (620°C) for eight hours. No cracking was found in mounted and polished cross sections indicating the necessity of imperfections (stress concentrators) in initiating PWHT cracking.

The results of the C-ring test program appear in Figure 73 and Table 15. Figure 73 and Table 15 show the average value of the depth of section cracked as a percentage of the total section height for each vanadium modified alloy at each test condition. Table 15 also includes the maximum deviation (range) from the average value. The average deviation (ignoring the large deviations for the AMAX(Climax) 3Cr-1 1/2Mo-0.1V material PWHT at 1150°F (620°C) and stress to 100ksi (690MPa)) is approximately ± 6%.

A comparison of results at 1250°F (680°C) and 1150°F (620°C) with an applied stress of 100ksi (690MPa)shows a decrease in the depth of section cracked for all three materials. The decrease in crack depth indicates a lower susceptibility to cracking at the higher PWHT. The Gleeble test results also showed a lower susceptibility to cracking at 1250°F (680°C) compared to 1150°F (620°C). Thus the general trend toward lower susceptibility with higher PWHT temperatures is confirmed by both the C-ring and Gleeble simulation tests.

As would be anticipated, cracking diminished as the applied stress was decreased. Since the stress is the driving force for crack propagation, as the stress decreases less cracking occurs. An apparent exception to this trend occurs with the JSW 3Cr-1Mo-V-Ti-B stressed to 80ksi (550MPa) and 60ksi (410MPa). However, with the average deviation in cracking being ±6%, the 1% increase in crack depth with a decrease in stress from 80ksi (550MPa) to 60ksi (410MPa) is not significant.

As the stress was decreased, at 1150°F (620°C), the magnitude of the difference in crack depth between the alloys decreased. At 60ksi (410MPa), considering the average deviation of ±6%, the difference in the response of the AMAX (Climax) 3Cr-1 1/2Mo-0.1V, JSW 3Cr-1Mo-V-Ti-B, and JSW

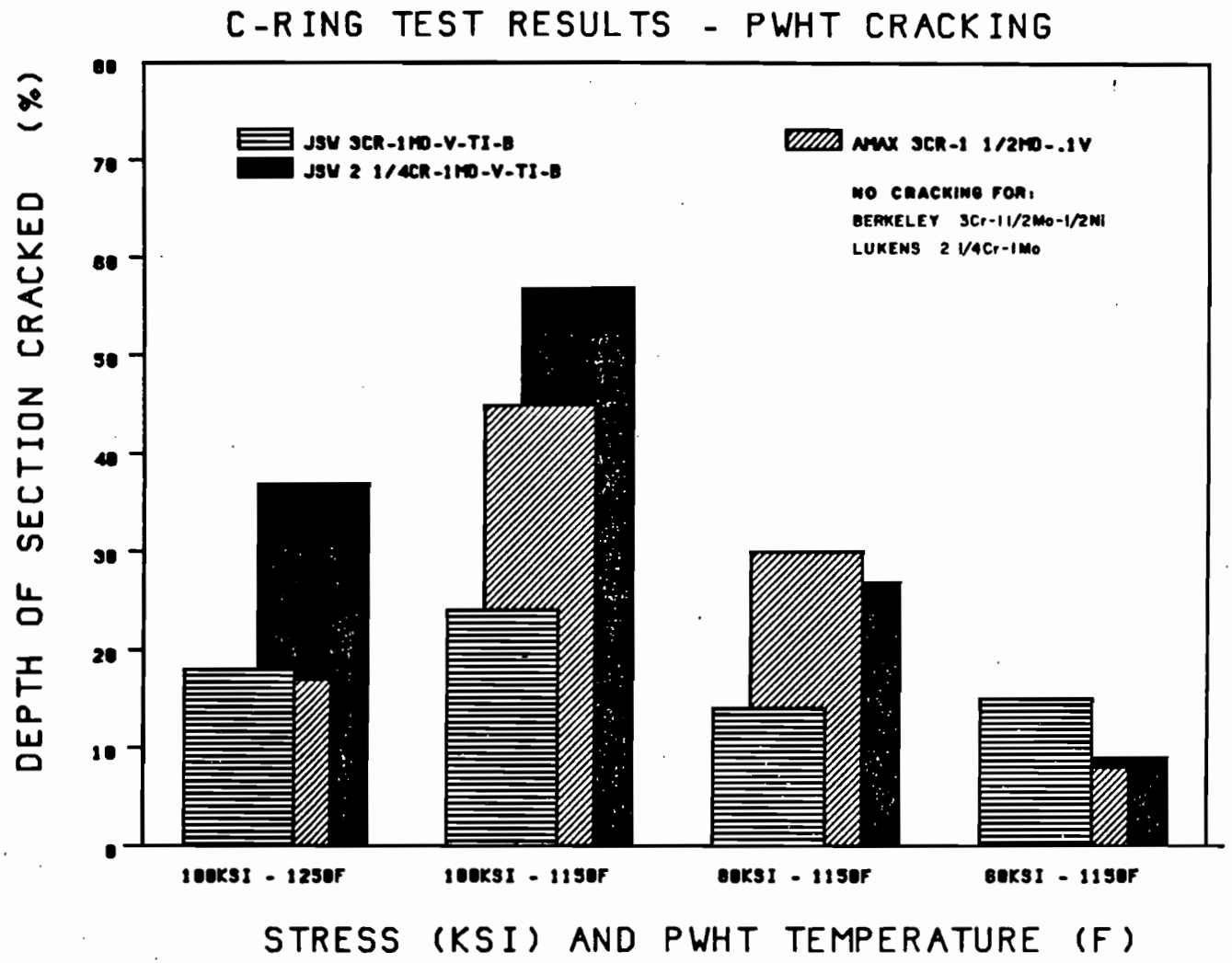

Figure 73. PWHT cracking results for the C-ring test.

Table 15. PWHT cracking results for the C-ring test.

PWHT Temperature		Stress		% Depth of Section Cracked		
°F	(°C)	KSI	(MPa)	AMAX (Climax) 3Cr	JSW 3Cr	JSW2¼Cr
1250	(680)	100	(690)	17 (Range +4,-2)	18 (± 3)	37 (± 13)
1150	(620)	100	(690)	45 (+34,-20)	24 (± 11)	53 (+15,-12)
1150	(620)	80	(550)	30 (± 1)	14 (± 1)	27 (± 12)
1150	(620)	60	(410)	8 (± 4)	15 (± 6)	9 (± 4)

2 1/4Cr-1Mo-V-Ti-B alloys observed in Figure 73 and Table 15 has little significance. The same reasoning can be applied to the results for the AMAX (Climax) and JSW 2 1/4Cr materials tested at 80ksi (550MPa) and 1150°F (620°C) where the difference in the depth of cracking is 3% and to the results for the AMAX (Climax) and JSW 3Cr materials tested at 1250°F (680°C) where the difference in the depth of section cracked is only 1%.

Based on the test results at 1150°F (620°C) and 1250°F (680°C) with an applied stress of 100ksi (690MPa) the JSW 2 1/4Cr-1Mo-V-Ti-B material may be ranked as the most susceptible of the three vanadium modified materials. Based on the test results at 1150°F (620°C) with applied stresses of 100ksi (690MPa) and 80ksi (550MPa) the next most susceptible material is the AMAX (Climax) 3Cr-1 1/2Mo-0.1V. The least susceptible material is the JSW 3Cr-1Mo-V-Ti-B alloy.

The greater susceptibility of the JSW 2 1/4Cr-1Mo-V-Ti-B material with respect to the JSW 3Cr-1Mo-V-Ti-B material may be the result of the smaller Cr:Mo and Cr:V ratios. The relatively higher Cr content of the the JSW 3Cr-1Mo-V-Ti-B alloy results in the preferential precipitation and growth of chromium rich M_7C_3 in the grain boundaries (which was found to be the predominate grain boundary species, Table 13) as opposed to the preferential precipitation and growth of molybdenum rich $M_{23}C_6$ in the grain boundaries of the JSW 2 1/4Cr-1Mo-V-Ti-B alloy. The growth of M_7C_3 in the grain boundaries would leave more molybdenum available in solution and may permit a relatively faster growth rate of Mo_2C during PWHT resulting in a shorter period of Mo_2C coherency.

The lower susceptibility of the JSW 3Cr-1Mo-V-Ti-B material with respect to the JSW 2 1/4Cr-1Mo-V-Ti-B material at both PWHT temperatures

and with respect to the AMAX (Climax) 3Cr-1 1/2Mo-0.1V material at 1150°F (620°C) are the points of agreement between the C-ring test and the Gleeble simulation test in the ranking of the individual vanadium modified alloys. The major discrepancy in ranking of materials for the two tests is in the rating of the AMAX (Climax) 3Cr-1 1/2Mo-0.1V material. In the Gleeble test the AMAX (Climax) material was ranked as the most susceptible material at both PWHT temperatures. However, in the C-ring test the AMAX (Climax) material is less susceptible to cracking than the JSW 2 1/4Cr-1Mo-V-Ti-B alloy at both PWHT temperatures and equivalent to the JSW 3Cr-1Mo-V-Ti-B alloy at 1250°F (680°C).

The improvement in the relative susceptibility of the AMAX (Climax) 3Cr-1 1/2Mo-0.1V material with respect to the JSW 3Cr-1Mo-V-Ti-B and JSW 2 1/4Cr-1Mo-V-Ti-B materials observed in the C-ring test may possibly be related to a lesser degree of segregation (and embrittlement) during the critical period when the residual stress (applied stress in the C-ring test) is high. Since stress relief and segregation occur simultaneously in the C-ring test, as the stress decreases the effect of grain boundary embrittlement on cracking susceptibility may be attenuated in comparison to the Gleeble simulation test where the stress is artificially maintained at high levels for the duration of the test. Additionally, if Hippsley's[77] model of stress induced transport of residual embrittling elements is considered, the constant stress employed in the Gleeble simulation test may result in a significant increase in the degree of embrittlement compared to the C-ring test in which the stress decreases with time at temperature.

The difference in the 1250°F (680°C) and 1150°F (620°C) C-ring test results for the AMAX (Climax) 3Cr-1 1/2Mo-0.1V alloy appears to

substantiate the foregoing argument. At 1150°F (620°C), when the persistence of coherent Mo_2C inhibits relaxation of stress, the stress level is maintained for longer times and the relative embrittlement, as shown by the extent of cracking, is high (Figure 73). However, at 1250°F (680°C), where stress relaxation may occur more rapidly due to the shorter coherency times of Mo_2C, the relative embrittlement of the AMAX (Climax) material is lower. The decrease in the extent of cracking from 1250°F (680°C) to 1150°F (620°C) is approximately twice the amount observed for the JSW 2 1/4Cr-1Mo-V-Ti-B material and four times the amount observed for the JSW 3Cr-1Mo-V-Ti-B material. This greater decrease in the extent of cracking in the AMAX (Climax) material would appear to be related to more than just a change in carbide morphology which would be expected to produce approximately equivalent decreases in the extent of cracking. Further, the Gleeble test results indicate that the AMAX (Climax) 3Cr-1 1/2Mo-0.1V material should be substantially more susceptible to cracking at 1250°F (680°C) than either the JSW 3Cr-1Mo-V-Ti-B or JSW 2 1/4Cr-1Mo-V-Ti-B. The time dependency of residual stress and embrittlement due to segregation, with high stress early in PWHT concomitant with limited embrittlement and lower stress (due to stress relaxation) later in PWHT concomitant with significant embrittlement, appears to be a plausible explanation of the AMAX (Climax) 3Cr-1 1/2Mo-0.1V material behavior.

Metallographic and Fractographic Examination of the 2 1/4Cr-1Mo and 3Cr-Mo C-ring Specimens.

Figures 74 through 76 show the optical light micrographs of the C-ring cross sections and scanning electron fractographs of the AMAX (Climax) 3Cr-1 1/2Mo-0.1V, JSW 3Cr-1Mo-V-Ti-B, and JSW 2 1/4Cr-1Mo-V-Ti-B

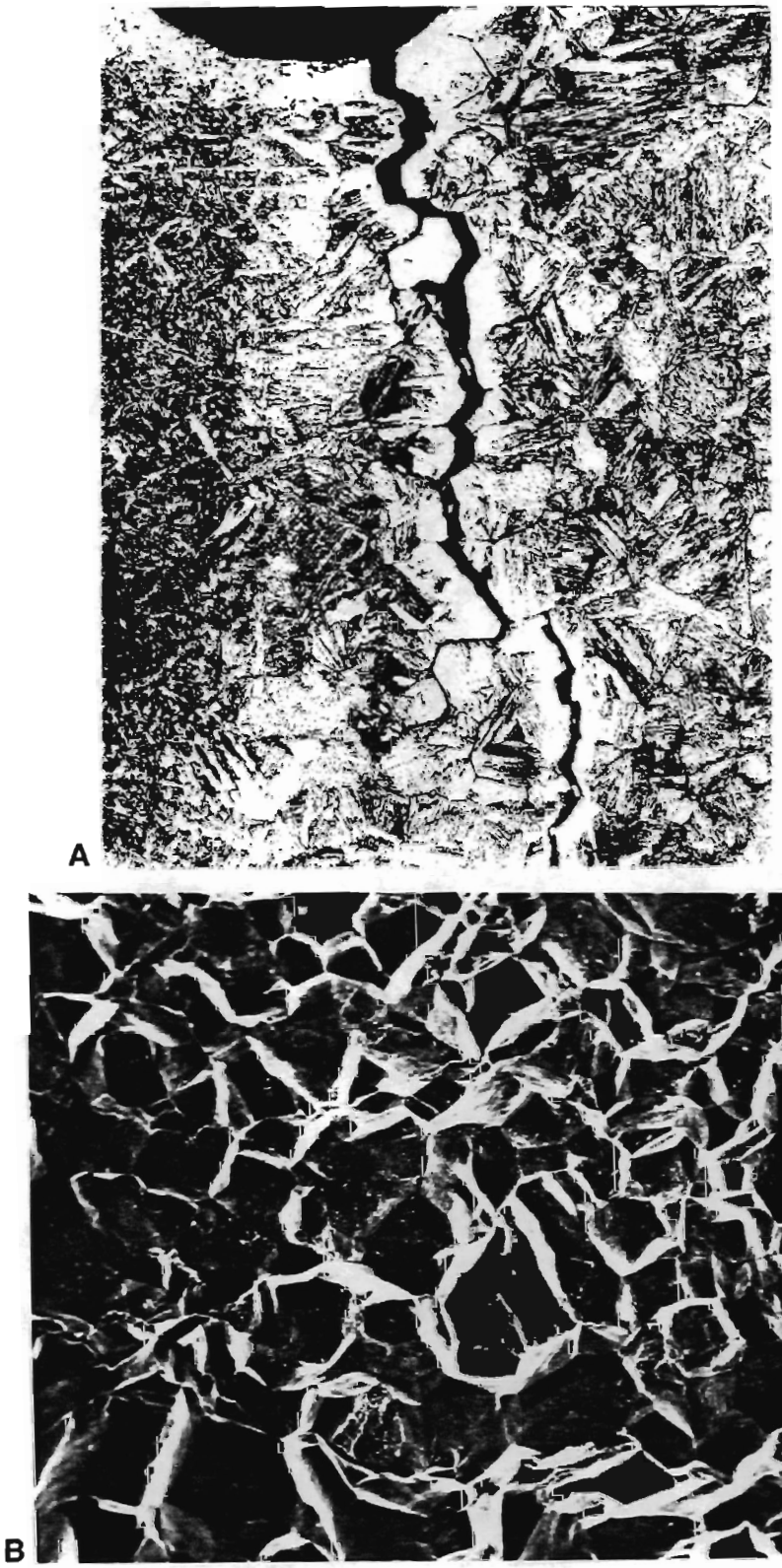

Figure 74. AMAX (Climax) 3Cr-1 1/2Mo-0.1V C-ring specimen. 1150°F (620°C) PWHT, 100ksi (690MPa), a) Noren's reagent, 100X OLM, b) 200X SEM.

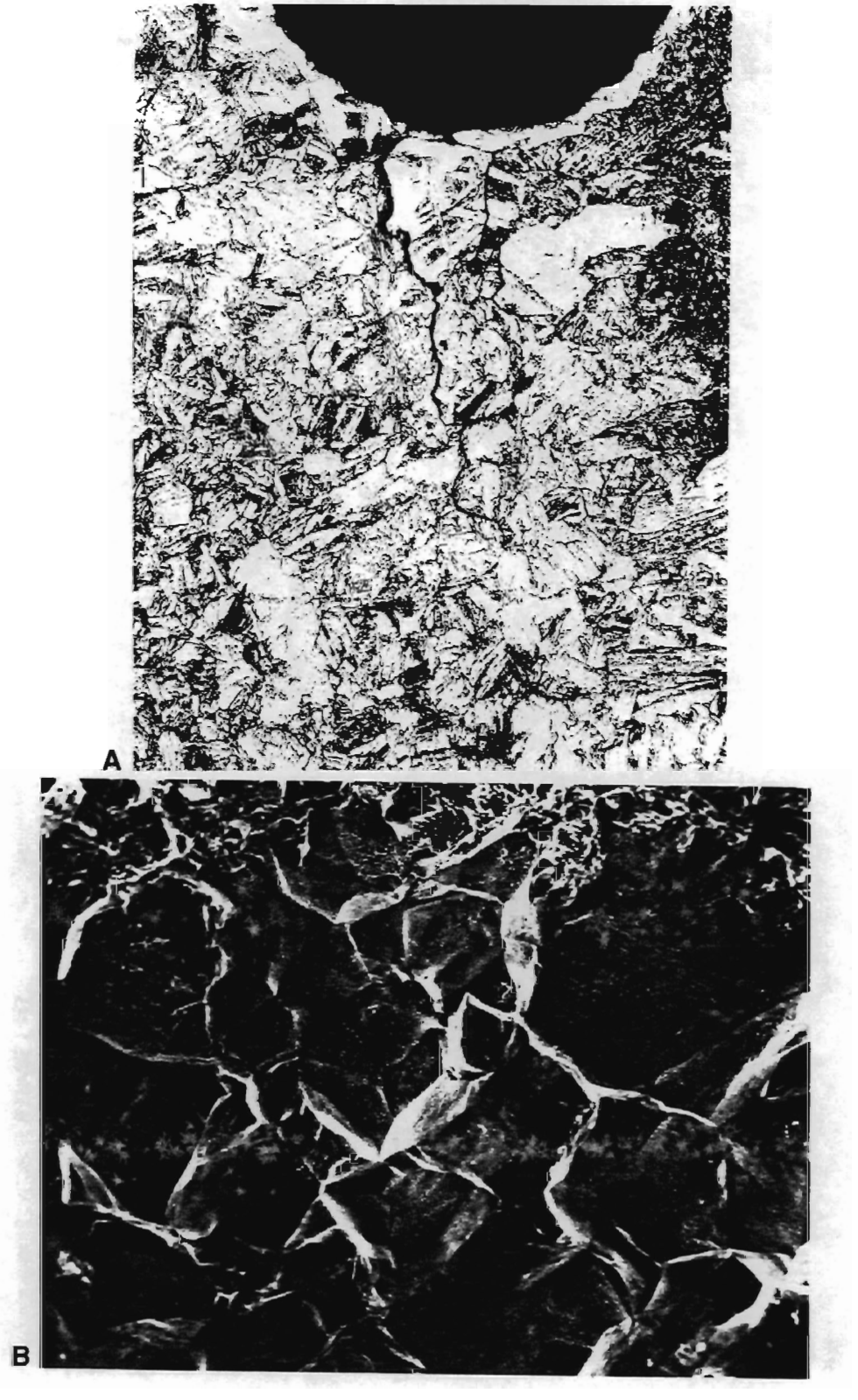

Figure 75. JSW 3Cr-1Mo-V-Ti-B C-ring specimen. 1150°F (620°C) PWHT. 100ksi (690MPa), a) Noren's reagent, 100X OLM, b) 200X SEM.

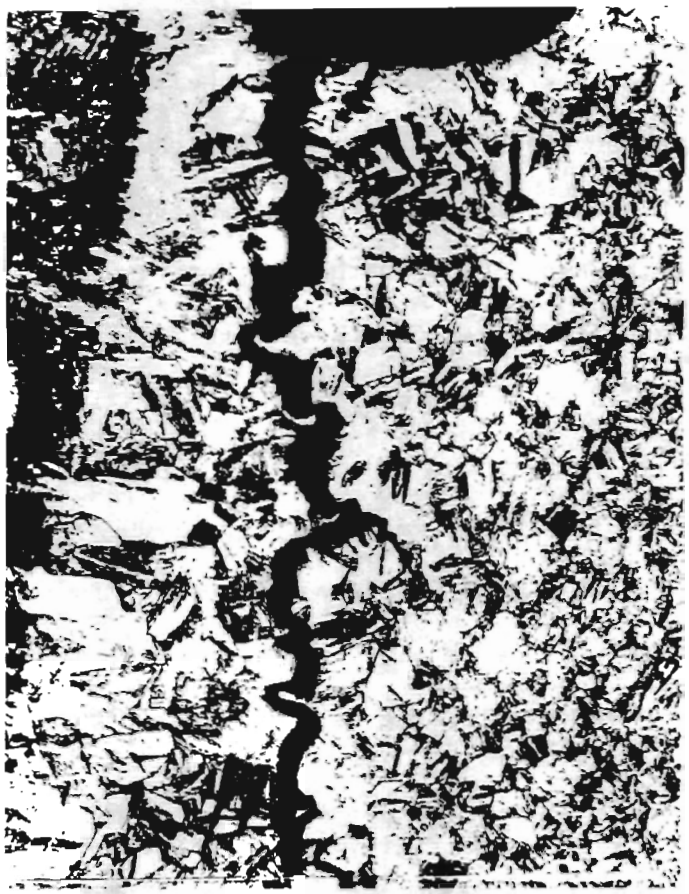

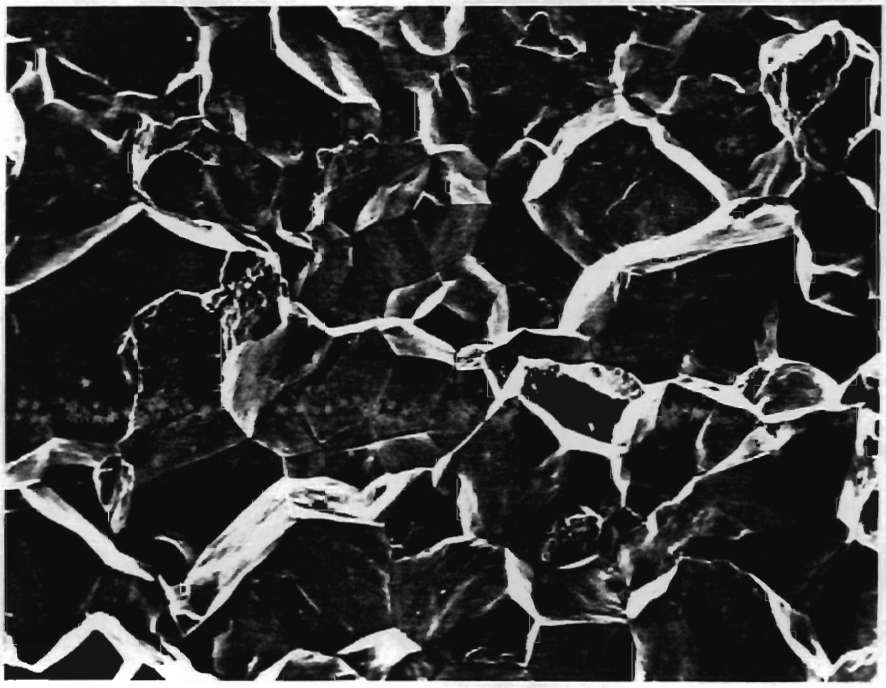

Figure 76. JSW 2 1/4Cr-1Mo-V-Ti-B C-ring specimen. 1150°F (620°C) PWHT, 100ksi (690MPa), a) Noren's reagent, 100X OLM, b) 200X SEM.

C-rings stressed to 100ksi (690MPa) and PWHT at 1150°F (620°C). The optical light micrographs clearly show the intergranular morphology of cracking with the crack propagating along the prior austenite grain boundaries in the coarse grained region of the HAZ. The fractographs (Figures 74b through 76b) show the characteristic LDIGF along the prior austenite grain boundaries for these materials. No evidence of any microductility was observed on the grain faces in the fractographic examinations.

Figure 77 is a higher magnification (1000X) fractograph of the JSW 2 1/4Cr-1Mo-V-Ti-B C-ring specimen. Figure 77 is representative of the smooth fracture surface obtained with all three vanadium modified materials. Secondary cracking is exhibited in the lower right portion of fractograph.

Evidence of microductility was observed only at the crack tip or the boundary of the intergranular and cleavage fracture regions. Figure 78 is typical of that observed under creep conditions. Note that the cavitation does not appear to be associated with particles on the grain boundaries.

Results of the C-ring Test for the State-of-the-art Commercial Heats of Modified 2 1/4Cr-1Mo (M10-M50) Materials

The C-ring testing of M10-M50 alloys was also conducted in the same manner as that of the Climax and JSW materials. The test results are given in Table 16. From the test results it can be seen that M30 exhibits the best resistance to PWHT cracking at both the PWHT temperatures (1150 and 1275°F). This observation is in accordance with the Gleeble test results. M50 is ranked second among the five heats.

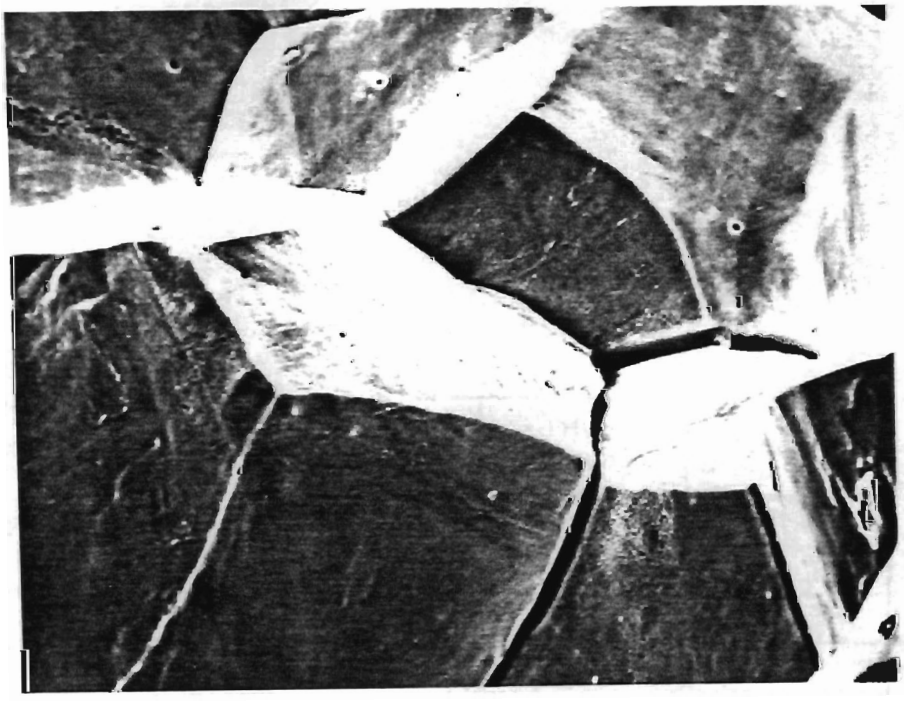

Figure 77. Higher magnification fractograph of the JSW 2 1/4Cr-1Mo-V-Ti-B C-ring specimen. 1150°F (620°C) PWHT, 100ksi (690MPa), 1,000X SEM.

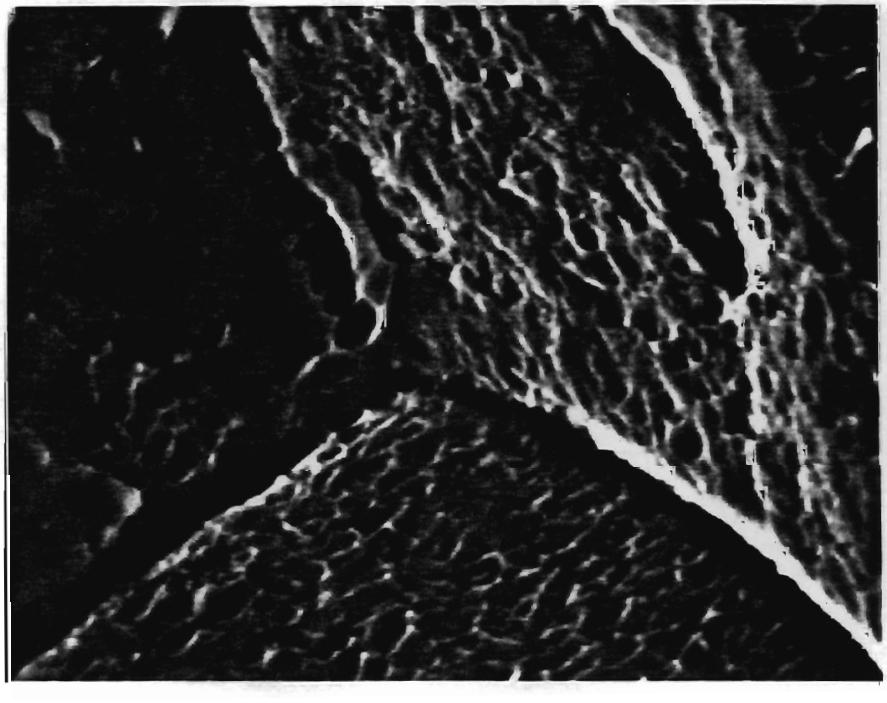

Figure 78. Grain boundary cavitation at the intergranular-cleavage fracture interface in the AMAX (Climax) 3Cr-1 1/2Mo-0.1V C-ring specimen. 1150°F (620°C) PWHT, 100ksi (690MPa), 5,000X SEM.

Table 16. PWHT cracking results for the C-ring test conducted on the state-of-the-art commercial 2 1/4Cr-1Mo alloys.

Material	PWHT Temp. (°F)	Applied Stress (KSI)	Depth Cracked (%)
M10	1150	100	81.8
	1150	100	86.3
	1150	100	89.9
	1275	100	74.21
M20	1150	100	19.1
	1150	100	54.5
	1150	100	76.9
	1275	100	39.8
M30	1150	100	Not Cracked
	1150	100	Not Cracked
	1150	100	Not Cracked
	1275	100	Not Cracked
M40	1150	100	85.9
	1150	100	95.2
	1150	100	93.1
	1275	100	77.5
M50	1150	100	76.0
	1150	100	52.2
	1150	100	68.8
	1275	100	59.2

The high Ca in the M30 material may be the key to the improved behavior (modifies inclusion morphology and distribution). Thus, the inclusion morphology may play an important role on the behavior of 2 1/4Cr-1Mo materials with respect to PWHT cracking. All the materials exhibited a higher resistance to PWHT cracking at 1275°F than at 1150°F.

From these results and the previously described C-ring test data it is apparent that the C-ring test is viable in the determination of PWHT cracking susceptibility and can be used successfully to rank individual heats and compare different materials.

Problems Encountered with the C-ring Test.

The problems encountered in making and using the C-ring specimens were, as indicated previously, primarily the result of the irregular HAZ due to the manually performed shielded metal arc welds. Figure 79 shows a macrograph of a notched C-ring not employed in testing. Note the unequal HAZ width and the deviation of the notched HAZ from a perpendicular to the ring wall. The arc in this case clearly favored one side wall of the notch at this point which resulted in the HAZ distortion.

Figure 80 shows several notch positions in the HAZ that were encountered during testing. The correct placement of the notch, at the fusion line, is shown darkened in on the figure. Displacement of the notch either into the fusion zone or towards the fine grained HAZ is shown in Figure 81 with the displacement being between 0.02 to 0.04 inches (0.5 to 1mm). If the notch is displaced into the fusion zone either no cracking occurs or, if the displacement is small, cracking may initiate at the root of the notch, traverse into the coarse grained region and propagate along the coarse grained HAZ as shown in Figure 81. If, on the other hand, the

Figure 79. Unequal, non-linear HAZ's as a result of welding in a C-ring specimen.

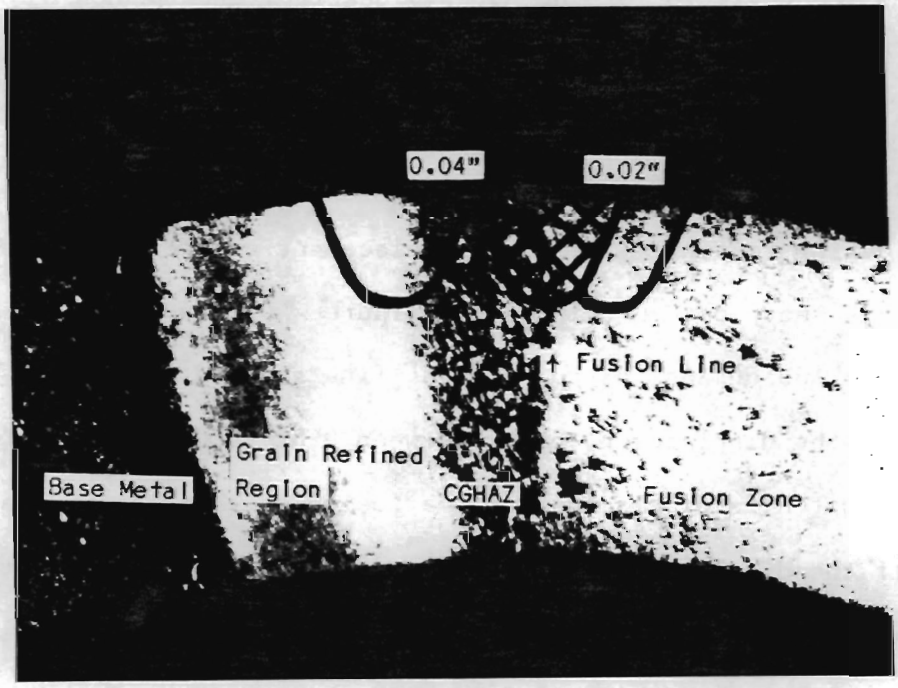

Figure 80. Schematic of ideal notch placement and two sites of notch misplacement in the C-ring test specimen.

Figure 81. Notch displaced into the fusion zone in a AMAX (Climax) 3Cr-1 1/2Mo-0.1V C-ring specimen. 1150°F (620°C) PWHT, 100ksi (690MPa), Noren's reagent, 100X OLM.

notch is displaced from the fusion line towards the fine grained HAZ, any cracking which initiates at the root of the notch propagates only a short distance before being stopped as shown in Figure 82. Several small cracks along the fusion zone may also be observed in Figure 82.

One improvement in the preparation of the C-rings would be to perform the welds automatically and thus obtain more uniform HAZ's. If the HAZ is linear over the sample width and perpendicular to the ring wall, an assessment of susceptibility based on the percentage of total area cracked might be employed and the scatter in the data reduced.

Summary of PWHT Cracking Results for the 3Cr-Mo and 2 1/4Cr-1Mo Alloys.

The vanadium modified alloys; AMAX (Climax) 3Cr-1 1/2Mo-0.1V, JSW 3Cr-1Mo-V-Ti-B, and JSW 2 1/4Cr-1Mo-V-Ti-B, have been found to more susceptible to PWHT cracking than the Berkeley 3Cr-1 1/2Mo-1/2Ni or the unmodified 2 1/4Cr-1Mo alloys. The vanadium modified alloys exhibited low rupture ductilities at PWHT temperatures of 1150°F (620°C) and 1250°F (680°C) in the Gleeble simulation test and would be considered as either "highly" susceptible or "extremely" susceptible to cracking by the Vinckier and Pense criteria.[73,98] In the C-ring test the vanadium modified alloys exhibited cracking at both PWHT temperatures and at all stress levels employed while the Berkeley 3Cr-1 1/2Mo-1/2Ni and the unmodified Lukens 2 1/4Cr-1Mo-0.10C materials did not crack at either PWHT temperature when stressed to 100ksi (690MPa), the highest stress utilized.

Both the Gleeble test and the C-ring test results show that a higher PWHT temperature results in a lower susceptibility to cracking. In the Gleeble simulation test the RA was greater at the higher PWHT temperature,1250°F (680°C), than at the 1150°F (620°C) PWHT temperature for

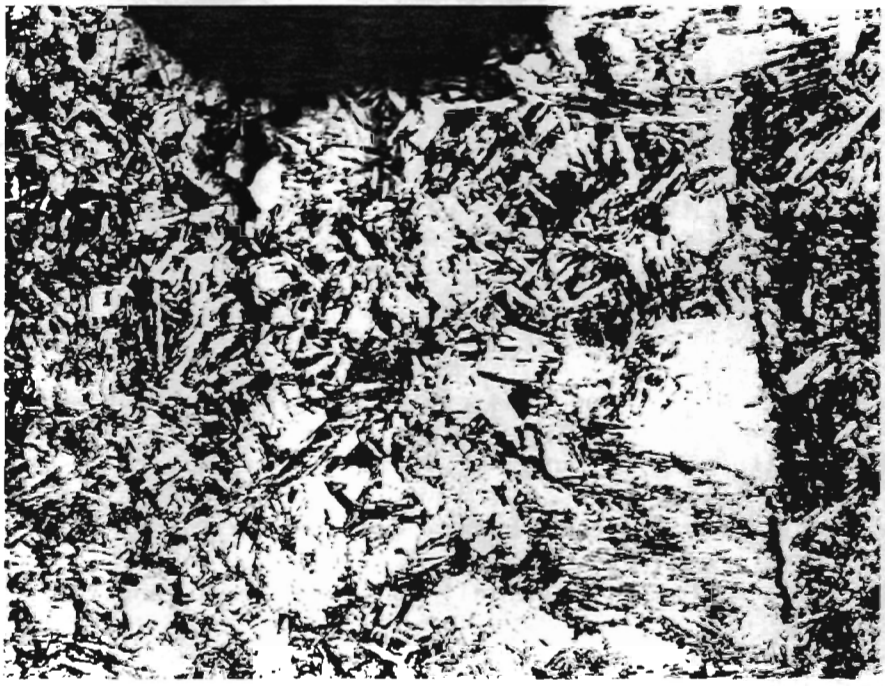

Figure 82. Notch displaced towards the fine grained HAZ in a JSW 2 1/4Cr-1Mo-V-Ti-B C-ring specimen. 1150°F (620°C) PWHT, 100ksi (690MPa), Noren's reagent, 100X OLM.

all materials tested. In the C-ring test the depth of section cracked decreased at the higher PWHT in comparison to the lower PWHT temperature for the vanadium modified materials.

The greater susceptibility of the vanadium modified alloys with respect to the Berkeley 3Cr-1 1/2Mo-1/2Ni and unmodified 2 1/4Cr-1Mo alloys is primarily related to the retarded carbide evolution in the alloys with vanadium additions. Scanning transmission electron microscopy and scanning electron microscopy have shown that the Berkeley 3Cr-1 1/2Mo-1/2Ni alloy has large grain boundary carbides of the $M_{23}C_6$ and M_6C type after thermal cycling to 2400°F (1315°C) and a PWHT at 1150°F (620°C) for 100 minutes. However, the AMAX (Climax) 3Cr-1 1/2Mo-0.1V, JSW 3Cr-1Mo-V-Ti-B, and JSW 2 1/4Cr-1Mo-V-Ti-B specimens all have smaller grain boundary carbides than the Berkeley material for the same PWHT conditions with the Climax material having M_6C, $M_{23}C_6$, and M_7C_3 grain boundary carbides and the JSW 3Cr and 2 1/4Cr alloys having only $M_{23}C_6$ and M_7C_3 carbides in the grain boundaries. The matrix carbides have been identified by Todd[140] as $(CrMo)_2CN$ in the Berkeley and AMAX (Climax) alloys and as Mo_2C containing chromium, molybdenum, and vanadium in the JSW 3Cr and JSW 2 1/4Cr alloys. The delay in grain boundary carbide evolution and the lower order matrix carbides may be related to longer times of coherency and slower growth of Mo_2C or $(CrMo)_2CN$ in the matrix resulting in greater strengthening over longer times in comparison with the unmodified materials. As was shown in the literature review, the longer the duration of significant matrix strengthening the greater the susceptibility of the material to PWHT cracking.[56,89,90]

The greater susceptibility of the JSW 2 1/4Cr-1Mo-V-Ti-B material in comparison with the JSW 3Cr-1Mo-V-Ti-B alloy, particularly in the C-ring test, may be related to the lower chromium to molybdenum ratio of the JSW 2 1/4Cr alloy. The predominant grain boundary carbide in the JSW 2 1/4Cr alloy was molybdenum rich $M_{23}C_6$ whereas the predominant grain boundary carbide in the JSW 3Cr alloy was chromium rich M_7C_3. The preferential formation of $M_{23}C_6$ in the JSW 2 1/4Cr alloy may lower the level of molybdenum in solution and increase the time of Mo_2C coherency as compared to the JSW 3Cr alloy. A longer period of coherency and slower growth of Mo_2C will result in an overall greater susceptibility to cracking.

The width of the carbide denuded zone may also be a factor in the greater susceptibility of the JSW 2 1/4Cr-1Mo-V-Ti-B alloy in comparison to the JSW 3Cr-1Mo-V-Ti-B alloy. Strain accumulation in the soft, denuded zone has been cited as one of the factors in PWHT cracking.[30,72] The JSW 2 1/4Cr was found to have a smaller denuded zone width than the JSW 3Cr alloy with the result that strain accumulation will occur over a smaller "width" of boundary and thus, higher local strains will develop.[72]

The AMAX (Climax) 3Cr-1 1/2Mo-0.1V alloy was found to be "extremely" susceptible to PWHT cracking in the Gleeble simulation test and cracked in the C-ring test. The susceptibility to cracking in this material appears to be a synergistic combination of precipitation strengthening of the matrix and grain boundary embrittlement due to phosphorus segregation. (We have no direct evidence for the phosphorus segregation but the majority of the research literature shows that phosphorus is indeed a major contributor to PWHT cracking.) The Climax alloy had the highest phosphorus content (0.012%) of the vanadium modified alloys tested (0.007%) and twice the

phosphorus content of an experimental heat, P2904, (0.006%) of similar composition which exhibited significantly higher rupture ductilities.[25] This material exhibited the most extensive denuded zone and only a moderate retardation in precipitate evolution (some M_6C was found along the grain boundaries) in comparison to the JSW 3Cr-1Mo-V-Ti-B and JSW 2 1/4Cr-1Mo-V-Ti-B alloys which would suggest that the Climax material should be less susceptible to cracking than the other vanadium modified alloys. Thus, the susceptibility of this material is probably due to a combined precipitation and segregation effect exacerbated by the relatively high phosphorus content.

Gleeble simulation has also shown that susceptibility to cracking may be lowered by refinement of structure in the grain coarsened region through the overlapping effect of the HAZ's of subsequent passes in a multiple pass weld. Thermal cycling samples to 1700°F (927°C) after a grain coarsening thermal cycle increased the rupture ductility to above 12% from less than 5% for the vanadium modified alloys. Thus, the small bead, half bead technique[85] or temper beading[59] methods may prove to be successful in preventing PWHT cracking. However, due to the higher elevated temperature rupture strength of both the multiple thermal cycled and the grain refined region (experiencing only a single thermal cycle to 1700°F), complete refinement of all coarse grained HAZ regions must be accomplished in order to prevent strain accumulation in any lower strength coarse grained material left unrefined.

From the study of the M10-M50 materials it is clear that residual Ca has a beneficial effect on the PWHT cracking susceptibility apparently to a greater extent than any other single element or combination of minor

elements. Thus Ca treatment may be considered for as a regular part of the processing of the Cr-Mo materials (Ca treatment also has shown to have a significant effect on the properties of HSLA steels through modification of inclusion morphology and distribution). Cu also appears to be beneficial in materials and its effects needs to be fully documented.

Soft Zone Evaluation

Hardness Traverses

The hardness profiles in the HAZ of the normalized and tempered modified 9Cr-1Mo-V-Nb steel for single pass and five pass autogenous welds are shown in Figure 83 and 84 respectively. It appears that a soft region exists near the HAZ in a temperature regime heated to just below the Ac_1, 3-3.5 mm from the fusion line. The hardness of the soft region is 25 to 30 DPH lower than that of the base metal. It also appears that PWHT at 1350°F (730°C) for 1 hour and 10 hours almost completely eliminates this soft region. The minimum hardness in the soft zone appears to be 20 DPH lower in case of the five pass weld when compared to the single pass weld.

Similar weld and hardness tests as those described above were conducted on the NKK material in the normalized condition so as to exaggerate the extent and magnitude of the soft region. Hardness traverses on the single pass and five pass specimens are shown in Figure 85 and Figure 86 respectively.

The hardness profile of the modified 9Cr-1Mo-V-Nb steel in the normalized condition exhibits a pronounced saw tooth effect in the weld metal and transformation zone area (high temperature part of HAZ) reflecting the varying amounts of tempering at each location produced by the welding process. The hardness of the soft zone of the five pass weld

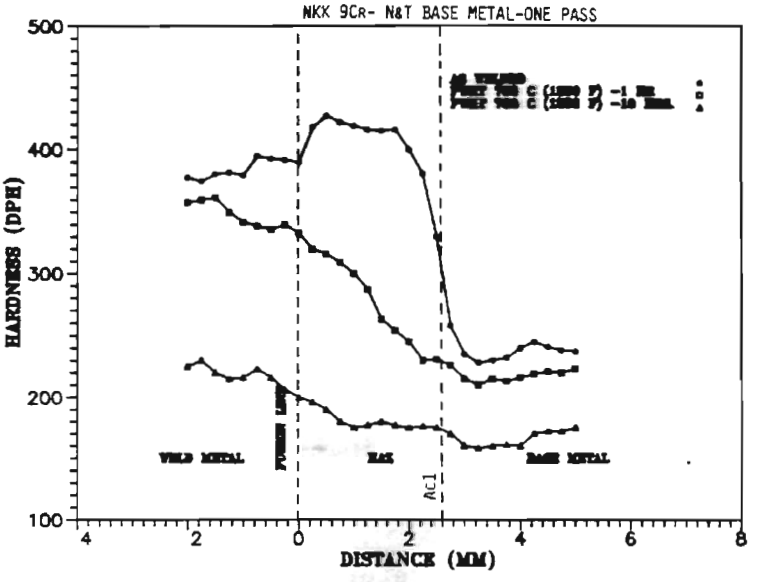

Figure 83. Hardness distributions in transverse sections of single pass autogenous welds in NKK 9Cr-1Mo in the normalized and tempered condition.

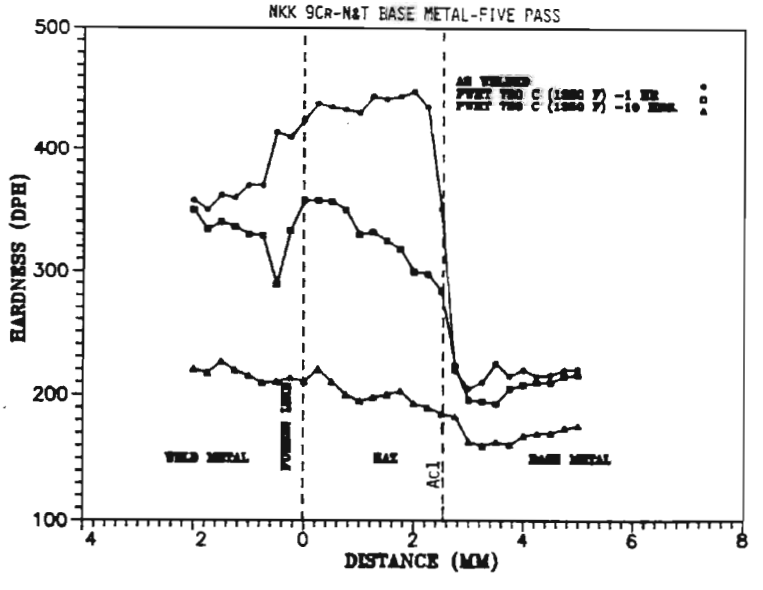

Figure 84. Hardness distributions in transverse sections of five pass autogenous welds in NKK 9Cr-1Mo in the normalized and tempered condition.

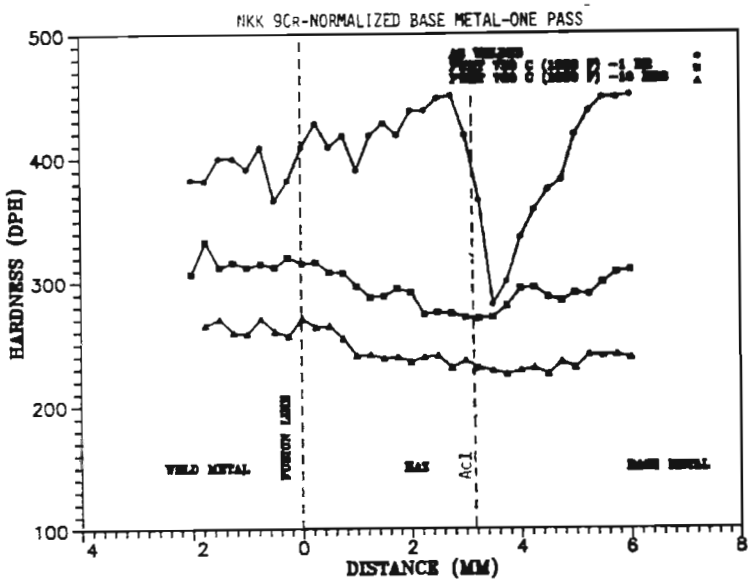

Figure 85. Hardness distributions in transverse sections of single pass autogenous welds in NKK 9Cr-1Mo in the normalized condition.

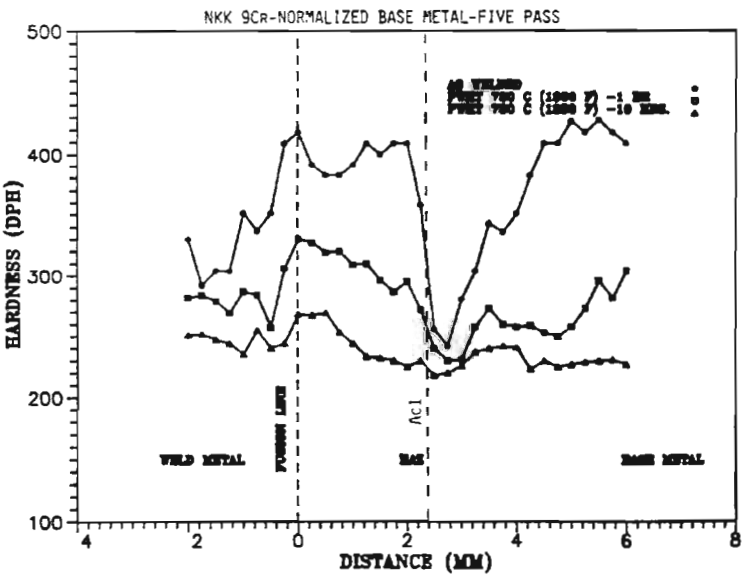

Figure 86. Hardness distributions in transverse sections of five pass autogenous welds in NKK 9Cr-1Mo in the normalized condition.

in the as welded condition drops sharply to a low value of 250 DPH followed by a gradual hardness increase to the base metal hardness of over 420 DPH. The hardness of the soft region measures approximately 170 DPH and 200 DPH below that of the base metal in the single pass and five pass welds respectively. The location of the soft region appears to be closer to the fusion line in the case of the five pass weld when compared to the single pass weld. The location of the lowest hardness was in a region heated just below the Ac_1 (as in the case of the normalized and tempered samples). PWHT at 1350°F (730°C) -1hour completely eliminated the soft zone in case of the single pass weld. However, for the five pass weld the soft zone disappeared only after a PWHT at 1350°F (730°C) for 10 hours. Figures 87 and 88 show hardness profiles in the HAZ of the angle cut specimens removed from five pass autogenous welds in the normalized and tempered and normalized base materials respectively. Figures 87 and 88 can be compared to Figures 84 and 86 respectively. The hardness data from the angle cut specimens also confirms the existence of the soft zone in the region of the HAZ that is heated to a temperature just below the Ac_1. The general trend in hardness data and the magnitudes of hardnesses are similar to those noted in the normal cut specimens.

Metallographic Examination of Soft Zone

Base material in the normalized and tempered condition:

SEM micrographs of five pass autogenous welds deposited with base material in the normalized and tempered condition at a magnification of 5000X are shown in Figures 89b-f. Figure 89e locates the soft zone and in

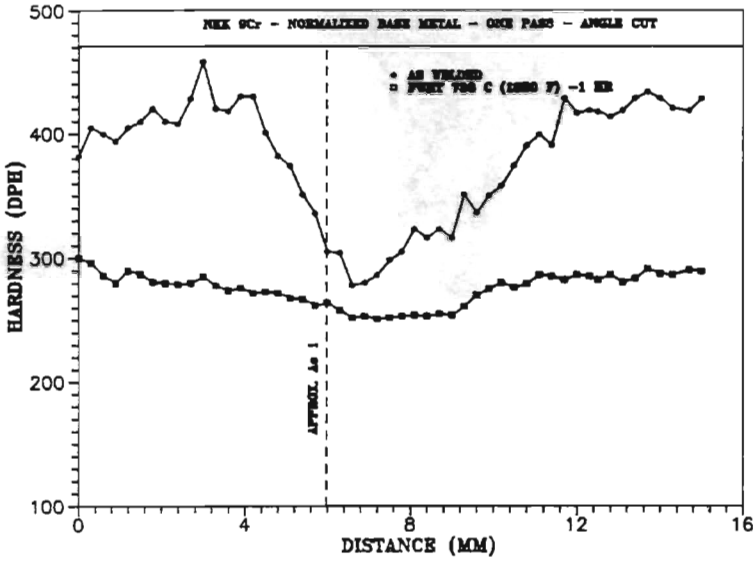

Figure 87. Hardness distributions in angle cut section of five pass autogenous welds in NKK 9Cr-1Mo in the normalized and tempered condition.

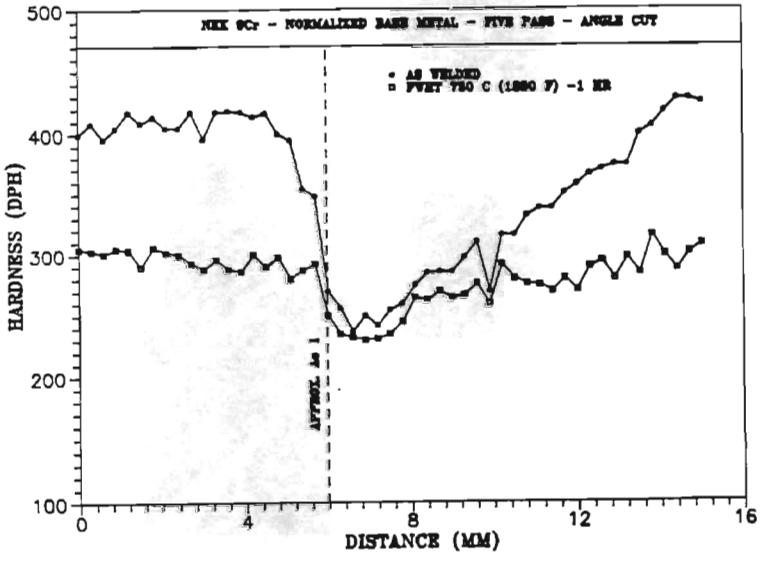

Figure 88. Hardness distributions in angle cut sections of five pass autogenous welds in NKK 9Cr-1Mo in the normalized condition.

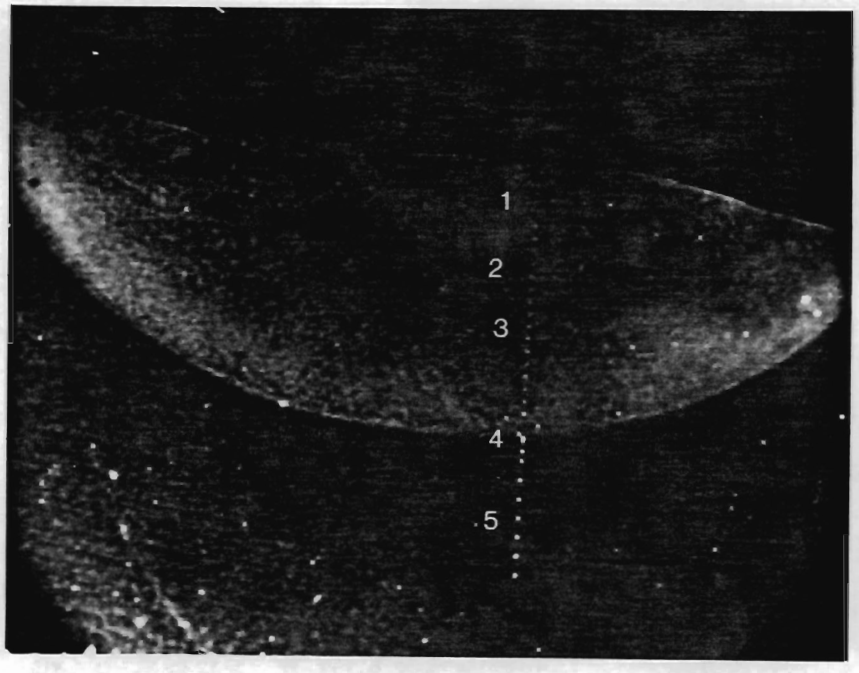

(a) SEM micrograph of 9Cr-1Mo-V-Nb autogenous weld, five passes, as-welded, 12X.

(b) Location 1, Weld Metal, 5000X.

Figure 89. As-welded SEM micrographs of normalized and tempered 9Cr-1Mo-V-Nb NKK steel weldment at various locations along the hardness profile marked in (a).

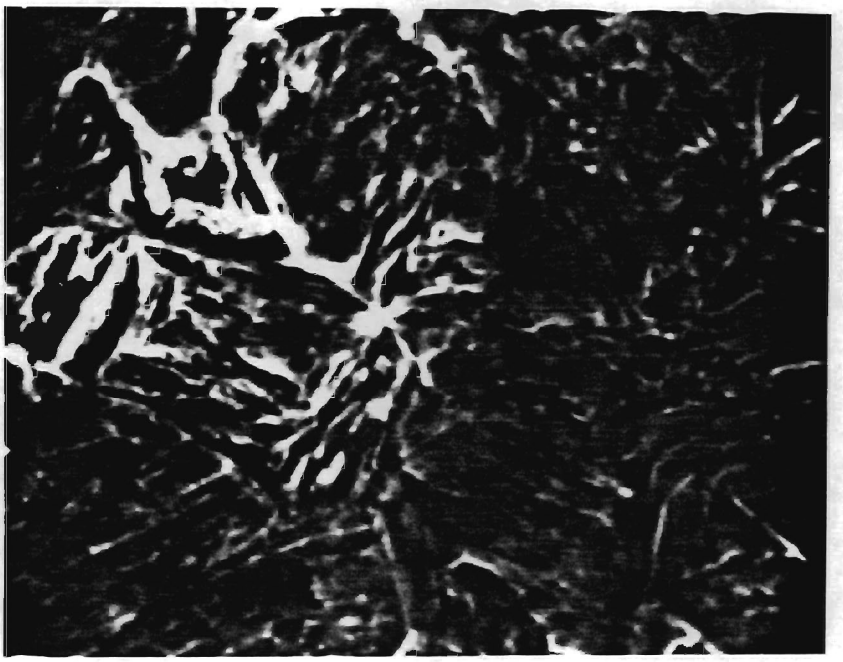

(c) Location 2, Coarse grained region, 5000X.

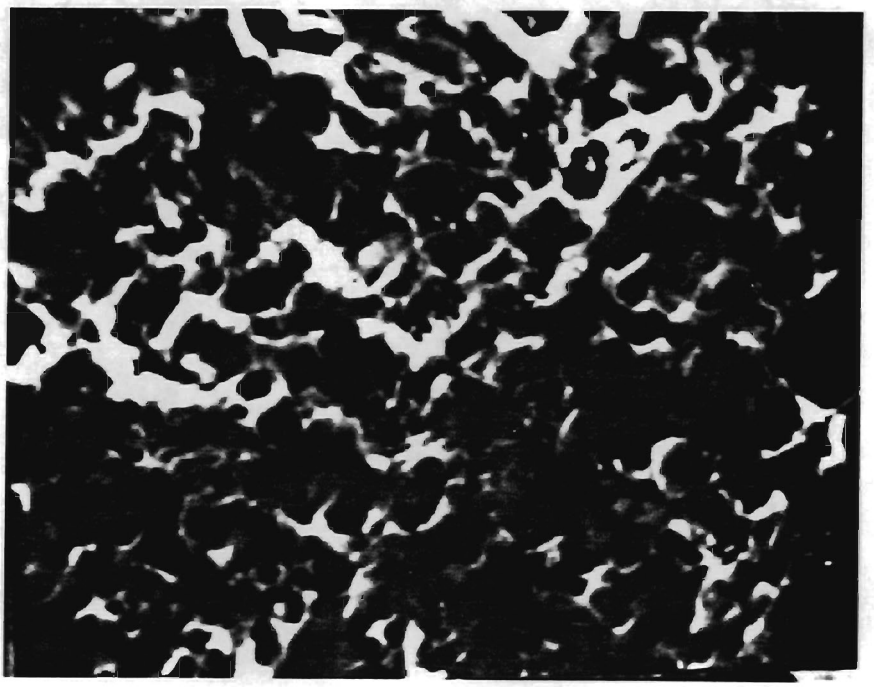

(d) Location 3, Refine grained region, 5000X.

Figure 89. -Continued

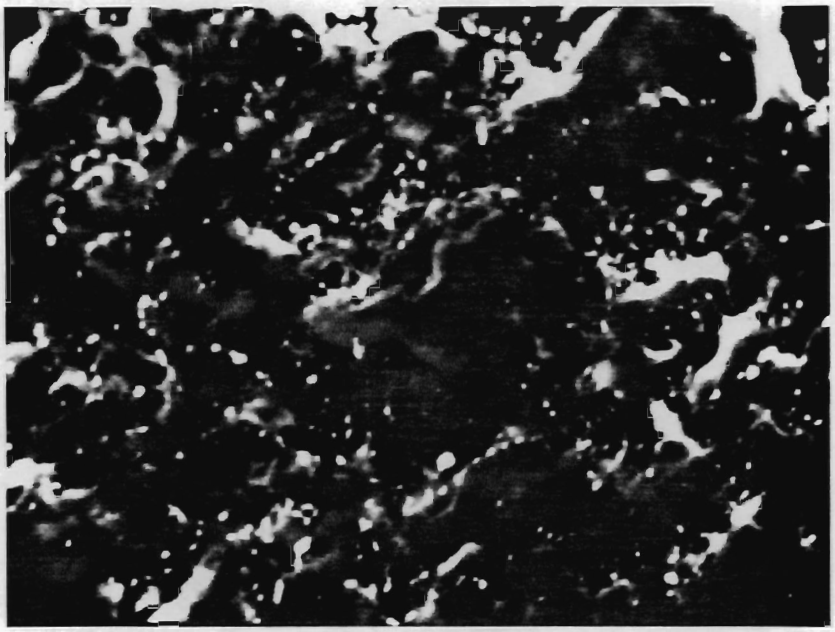

(e) Location 4, Base Metal near HAZ, 5000X.

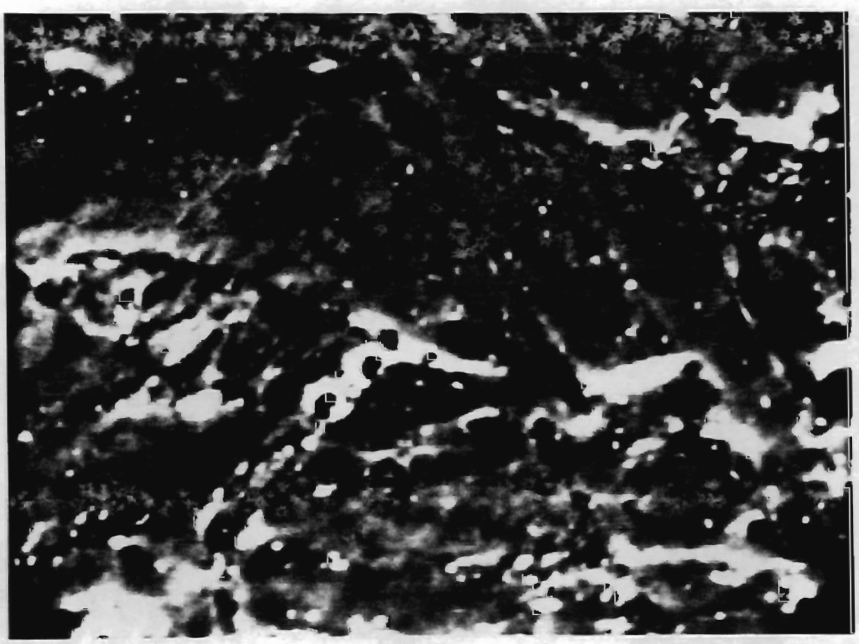

(f) Location 5, Base Metal, 5000X.

Figure 89. -Continued

comparison with the other regions examined in the HAZ. The soft region appears to have undergone a significantly greater extent of carbide precipitation and precipitate coarsening. This results in low hardness.

In the PWHT condition (1350°F (730°C) - 10 hours) SEM micrographs at similar locations in the five pass weld are shown in Figure 90. The SEM micrographs (Figure 90) show that a significant amount of precipitation has occurred in all regions of the HAZ thus resulting in an overall lower hardness.

Base material in the normalized condition

A set of micrographs similar to the ones for the base material in the normalized and tempered condition appears in Figures 91 and 92. In the as welded condition, the SEM micrographs in Figure 91e reveals that the soft zone is where significant precipitation of carbides has occurred. In the PWHT condition, extensive precipitation occurs in all regions of the HAZ, thus resulting in an uniformly low hardness.

Transmission Electron Microscopy

Carbide extraction replicas were prepared from the angle cut specimens and the carbides extracted from the soft region were examined using the scanning transmission electron microscope (STEM) at magnifications up to 50,000X.

Figure 93 shows micrographs of the soft region in as welded NKK 9Cr-1Mo in the normalized condition. In Figure 93b, carbides 1, 2 and 3 were analyzed to be of the $M_{23}C_6$ type, whereas carbides labelled 4 is probably of the MC (Nb-V, C) type. Figure 94 shows micrographs of a similar region in a sample that was PWHT at 1350°F (730°C) for 1 hour. All the carbides, labelled 5, 6, 7 and 8, were analyzed to be the $M_{23}C_6$ type. It appears

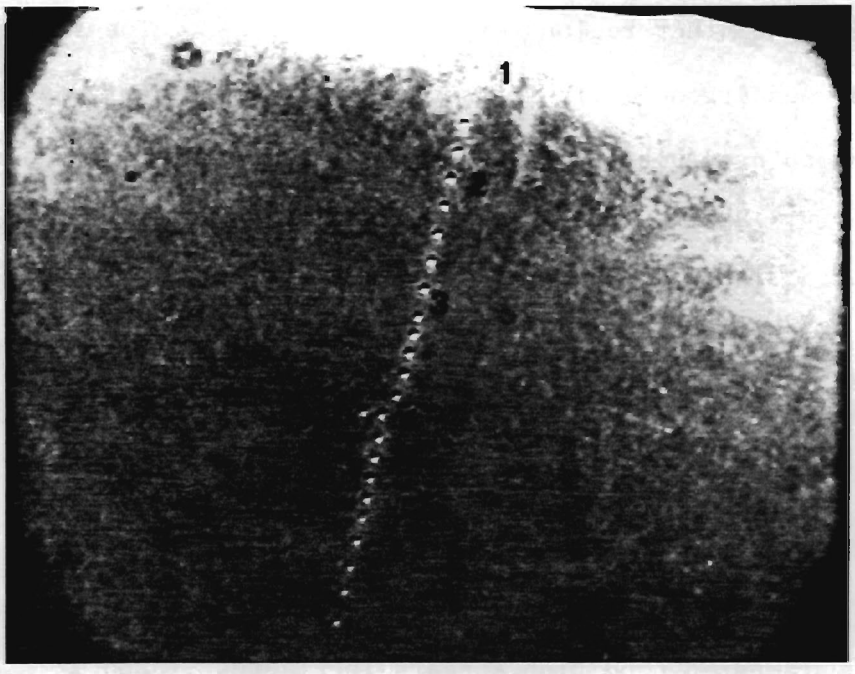

(a) SEM Micrograph of 9Cr-1Mo-V-Nb autogenous weld, five passes, PWHT 1350°F(730°)-10 hours, 12X.

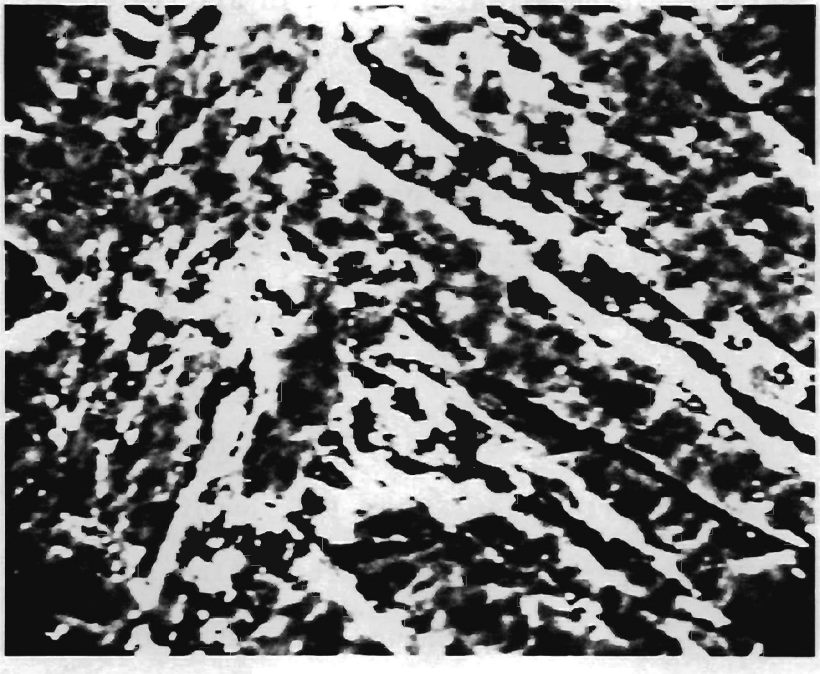

(b) Location 1, Weld Metal, 5000X.

Figure 90. PWHT SEM micrographs of normalized and tempered 9Cr-1Mo-V-Nb NKK steel weldment at various locations along the hardness profile marked in (a).

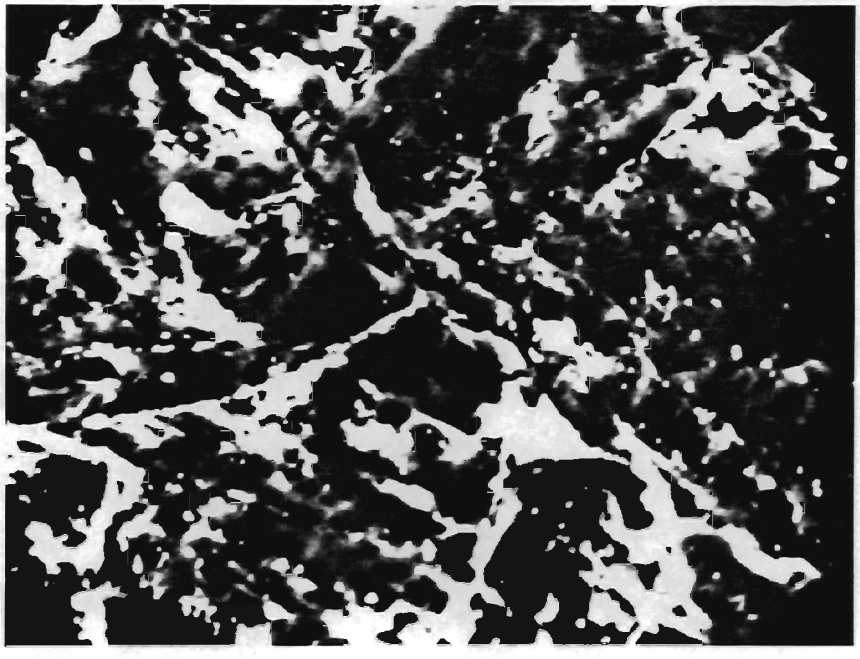

(c) Location 2, Coarse grained region, 5000X.

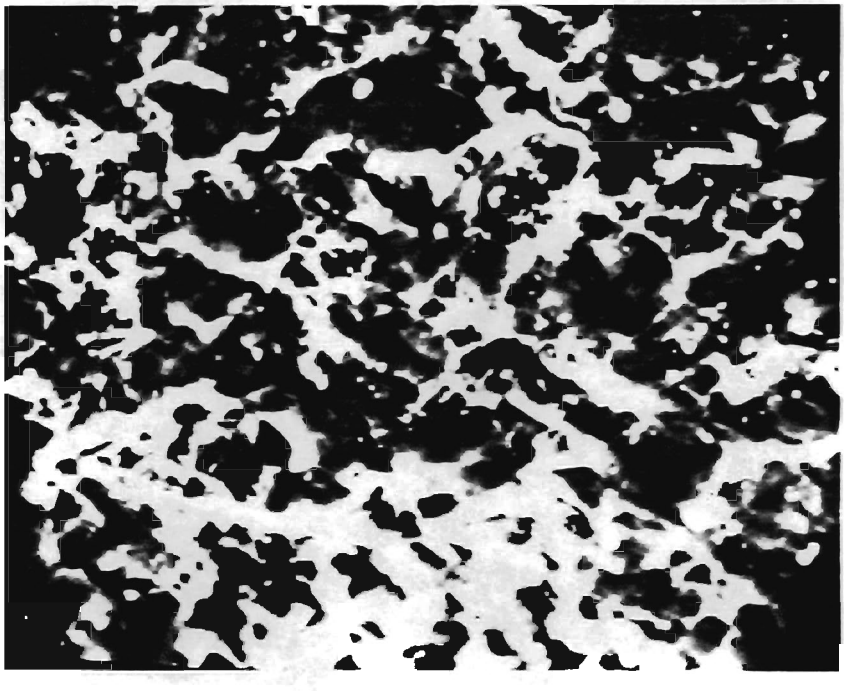

(d) Location 3, Refine grained region, 5000X.

Figure 90. -Continued

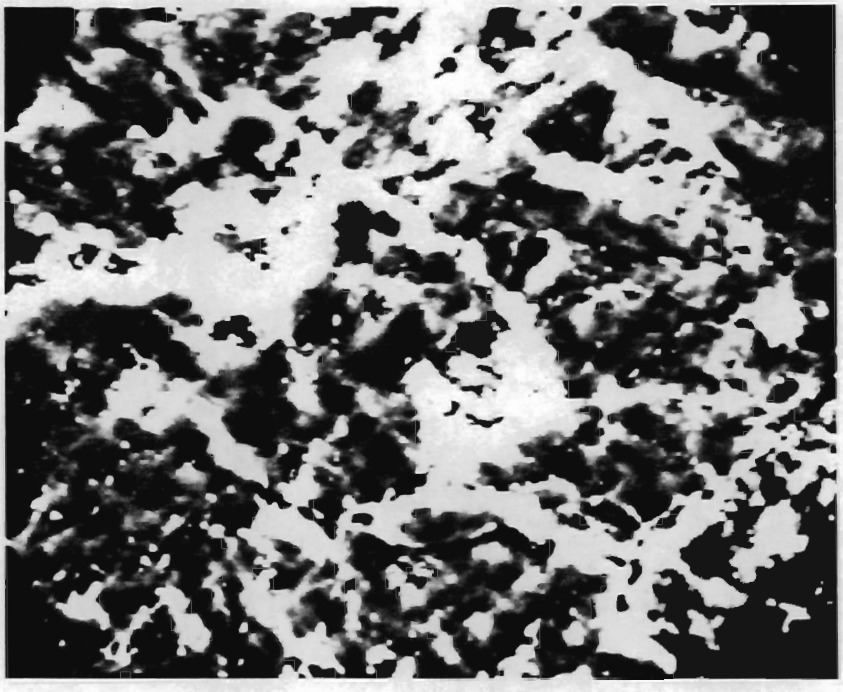

(e) Location 4, Base Metal near HAZ, 5000X.

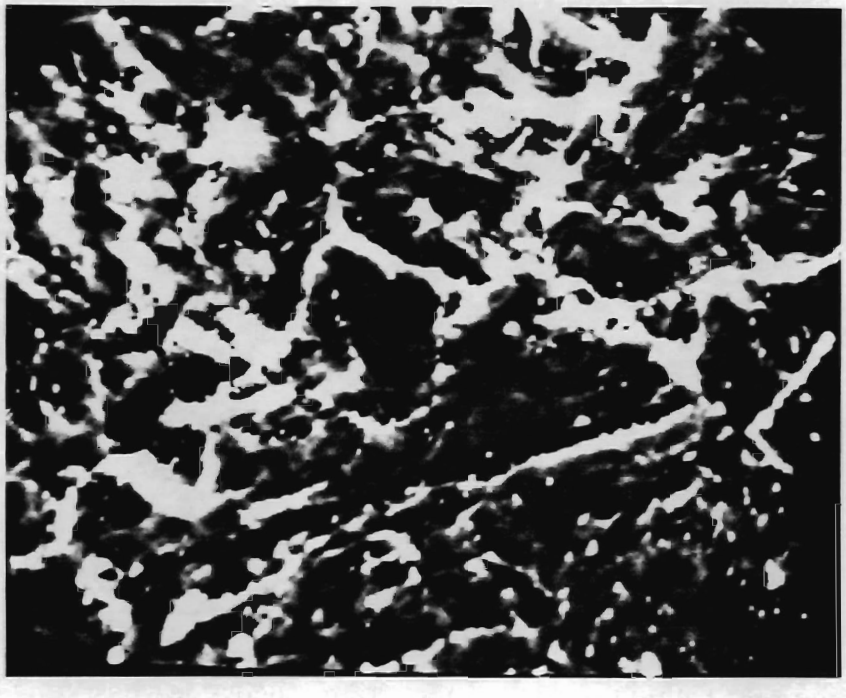

(f) Location 5, Base Metal, 5000X.

Figure 90. - Continued

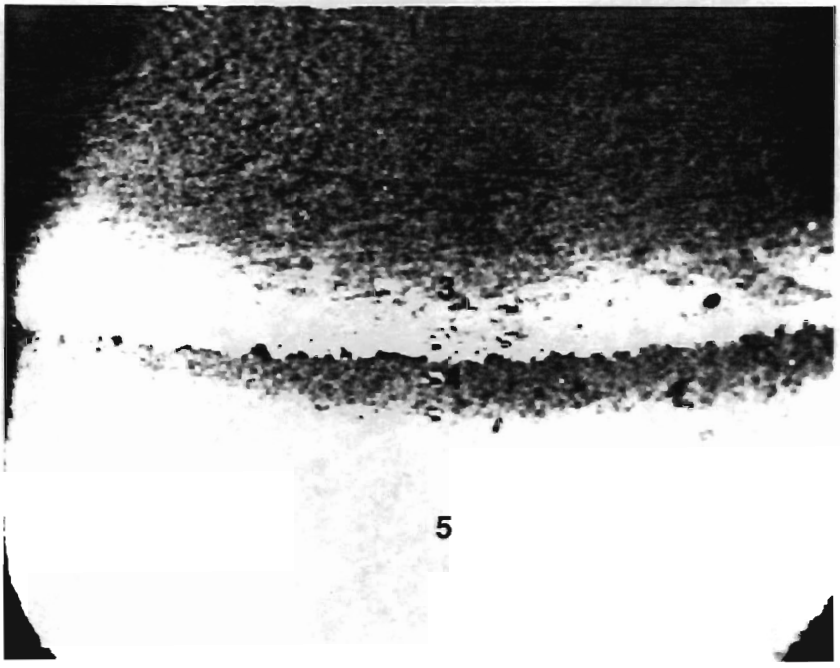

(a) SEM micrograph of 9Cr-1Mo-V-Nb autogenous weld, five passes, as-welded, 18X.

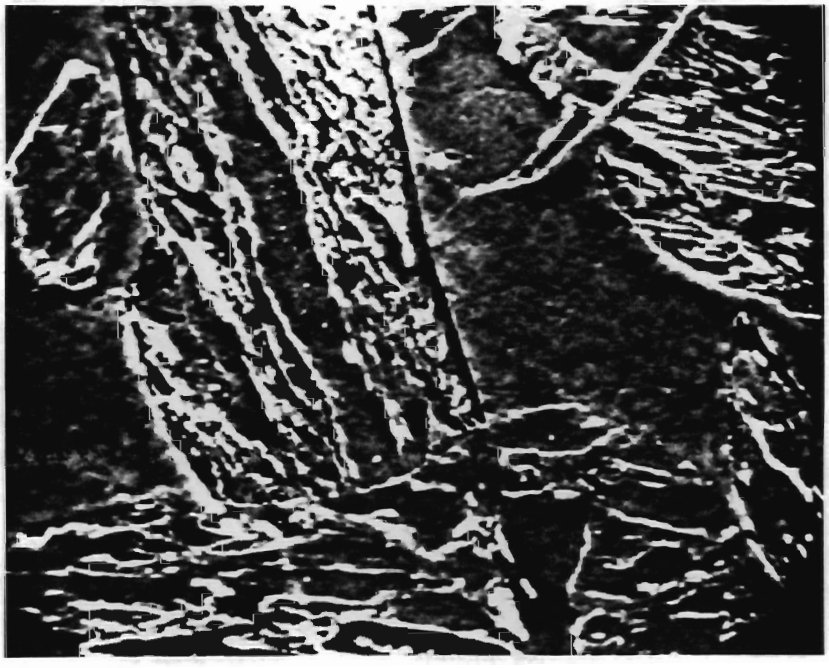

(b) Location 1, Weld Metal, 5000X.

Figure 91. As-welded SEM micrographs of normalized 9Cr-1Mo-V-Nb NKK steel weldment at various locations along the hardness marked in (a).

(c) Location 2, Coarse grained region, 5000X.

(d) Location 3, Refine grained region, 5000X.

Figure 91. -Continued

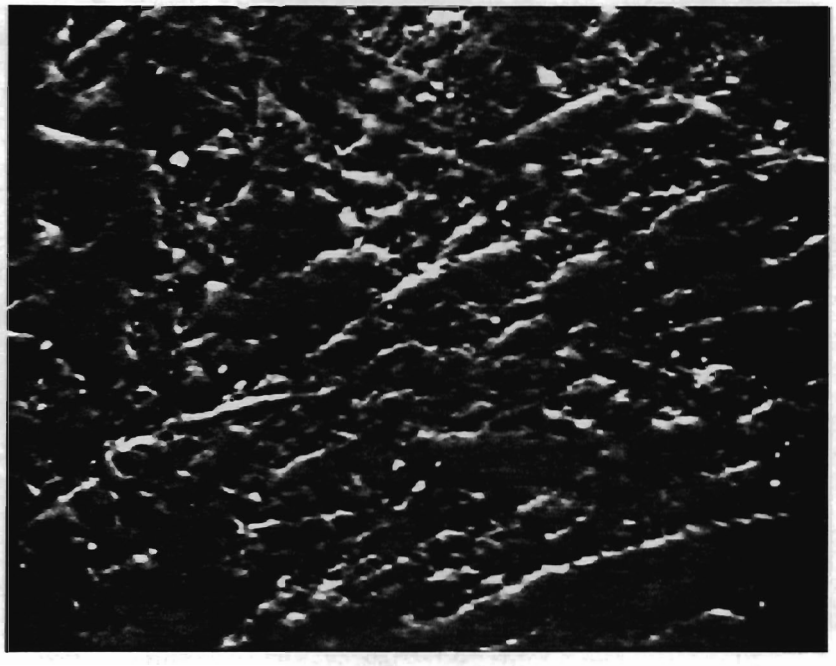

(e) Location 4, Base Metal near HAZ, 5000X.

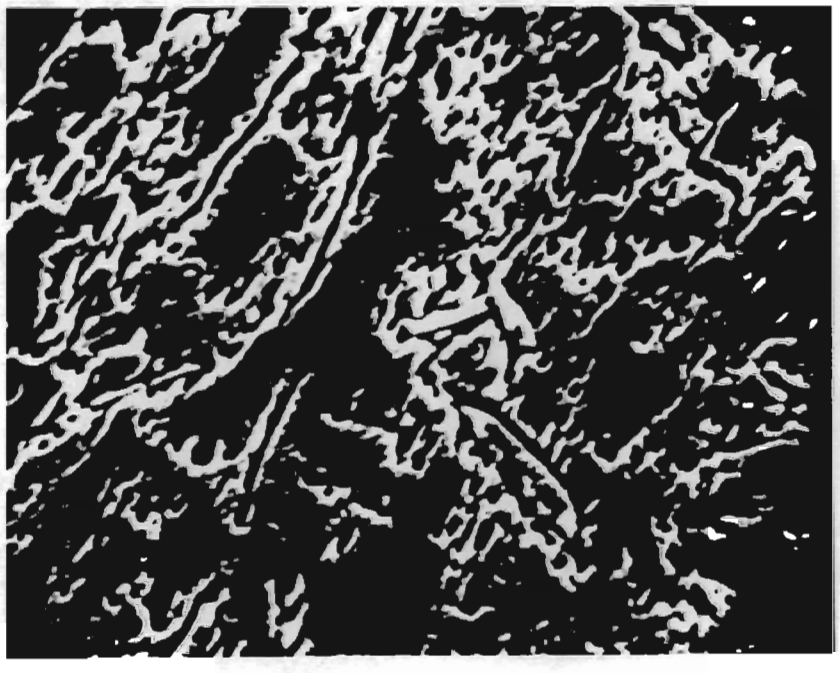

(f) Location 5, Base Metal, 5000X.

Figure 91. -Continued

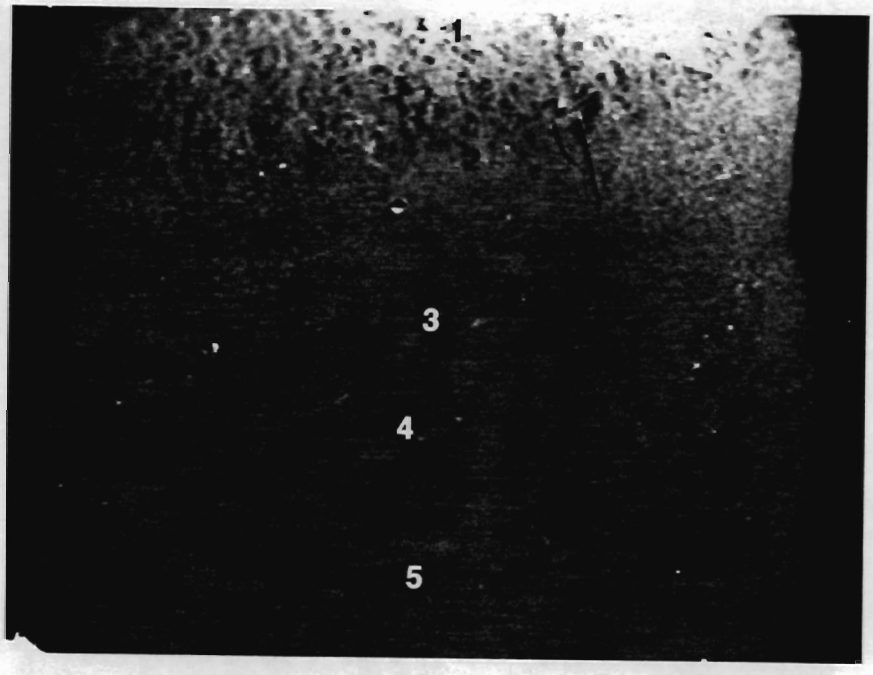

(a) SEM micrograph of 9Cr-1Mo-V-Nb autogenous weld, five passes, PWHT 1350°F(730°C)-10 hours, normalized condition, 20X.

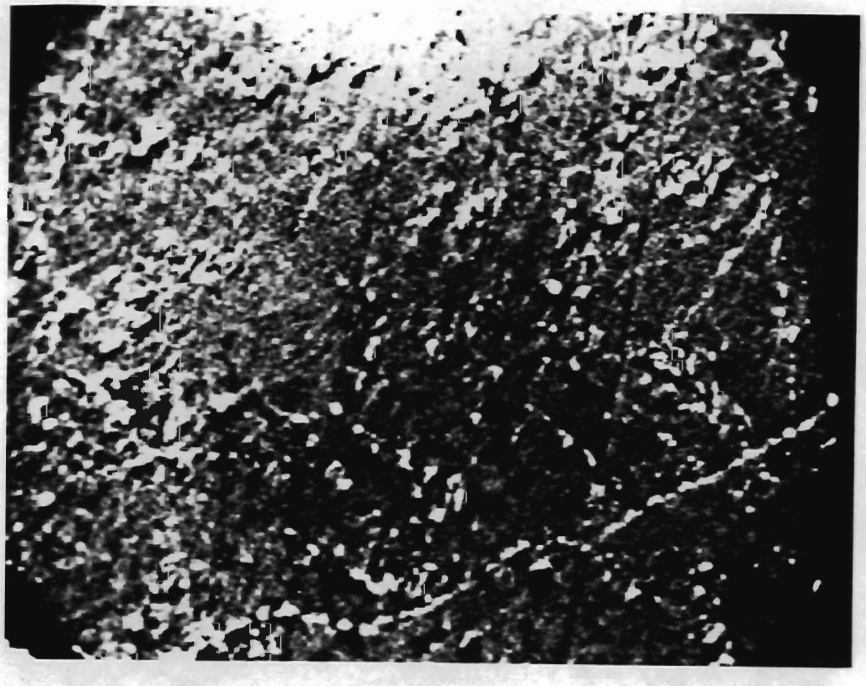

(b) Location 1, Weld Metal, 5000X.

Figure 92. PWHT SEM micrographs of normalized 9Cr-1Mo-V-Nb NKK steel weldment at various locations along the hardness profile marked in (a).

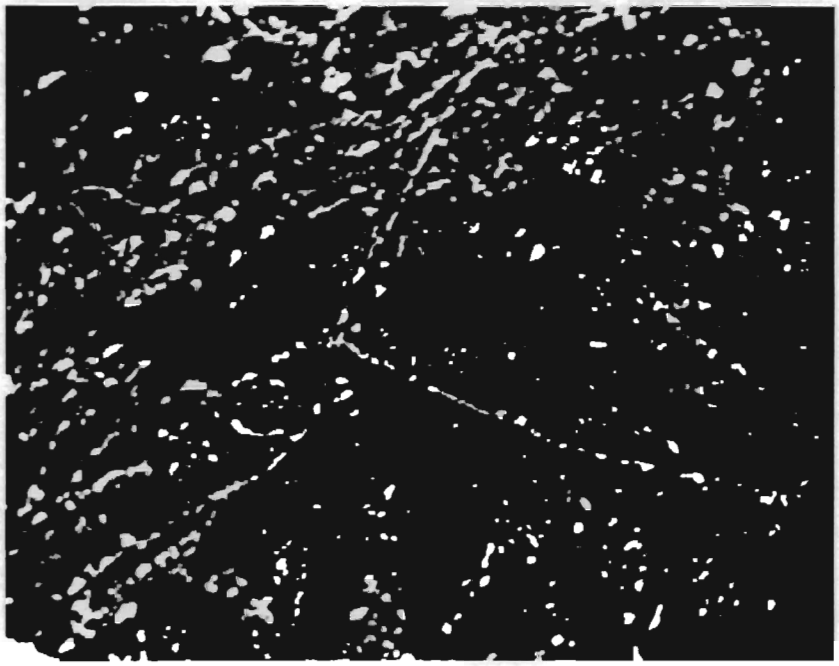

(c) Location 2, Coarse grained region, 5000X.

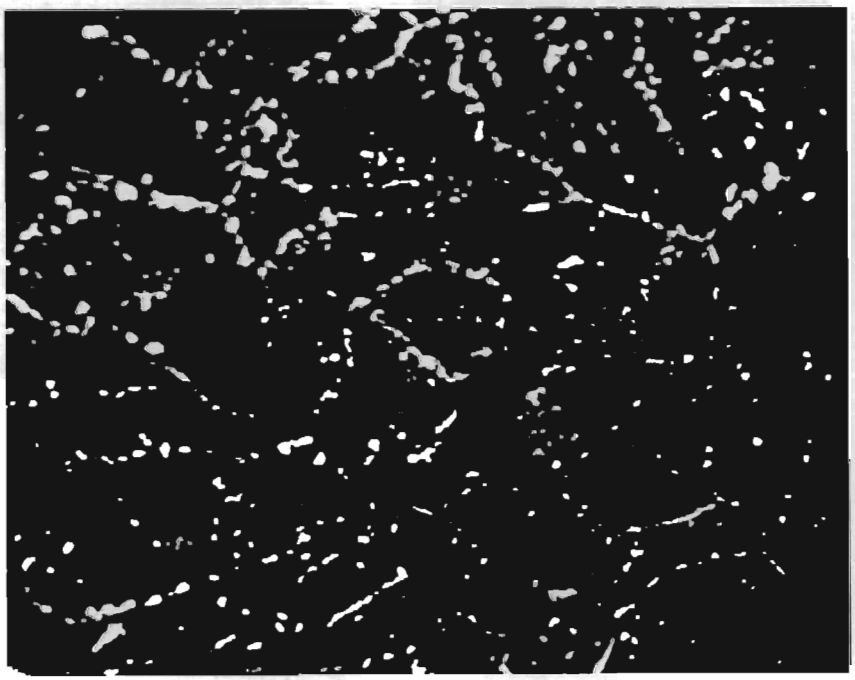

(d) Location 3, Refine grained region, 5000X.

Figure 92. -Continued

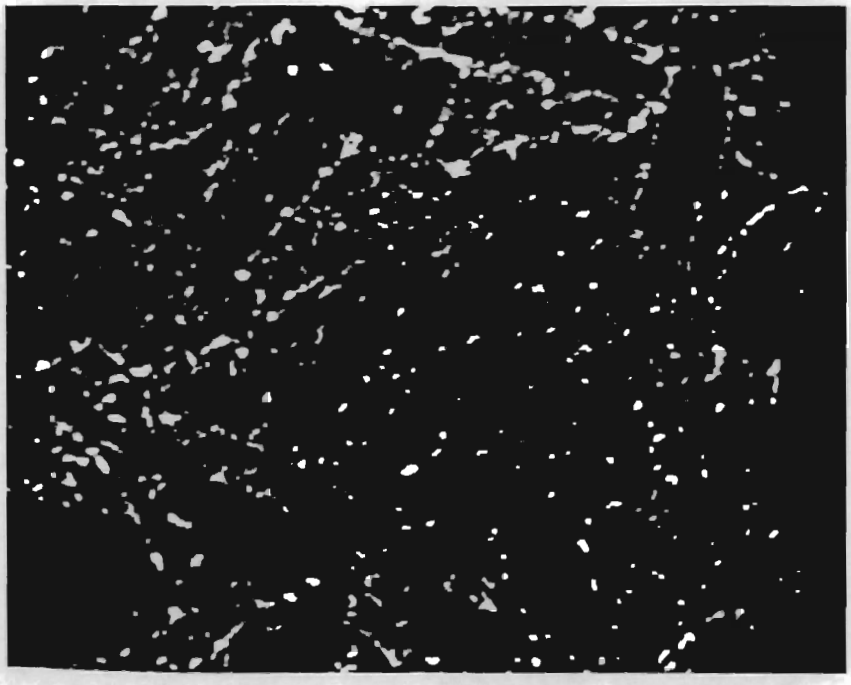

(e) Location 4, Base Metal near HAZ, 5000X.

(f) Location 5, Base Metal, 5000X.

Figure 92. -Continued

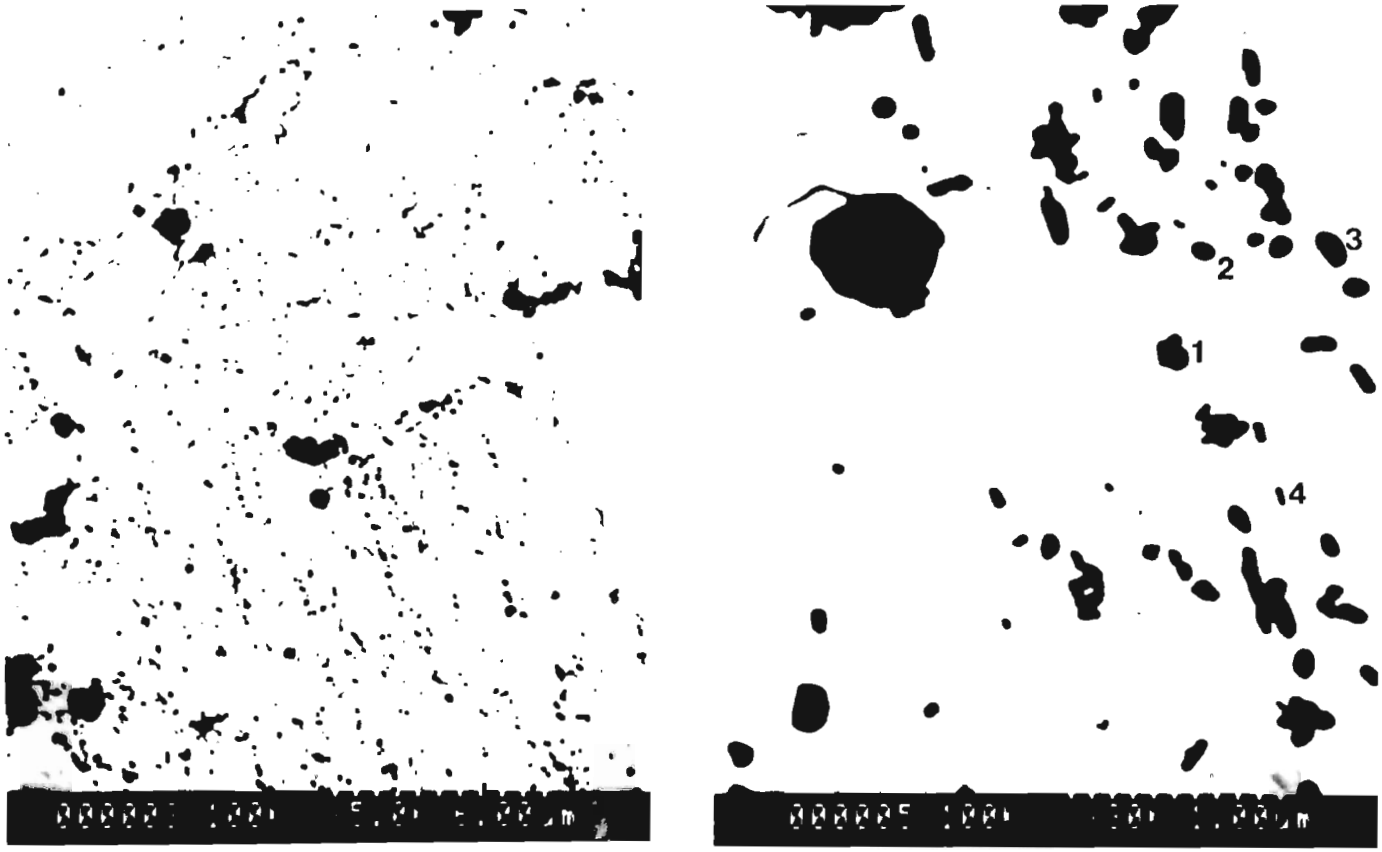

Figure 93. STEM micrographs of base metal near HAZ in NKK 9CR-1Mo-V-Nb weldment, normalized, as-welded, angle cut section. (a) 5000X, (b) 30,000X.

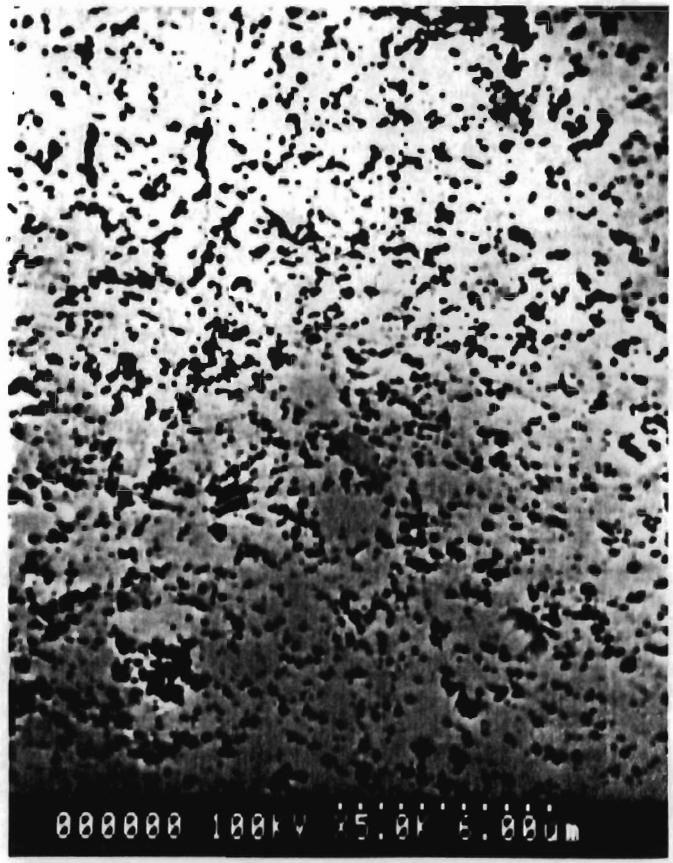

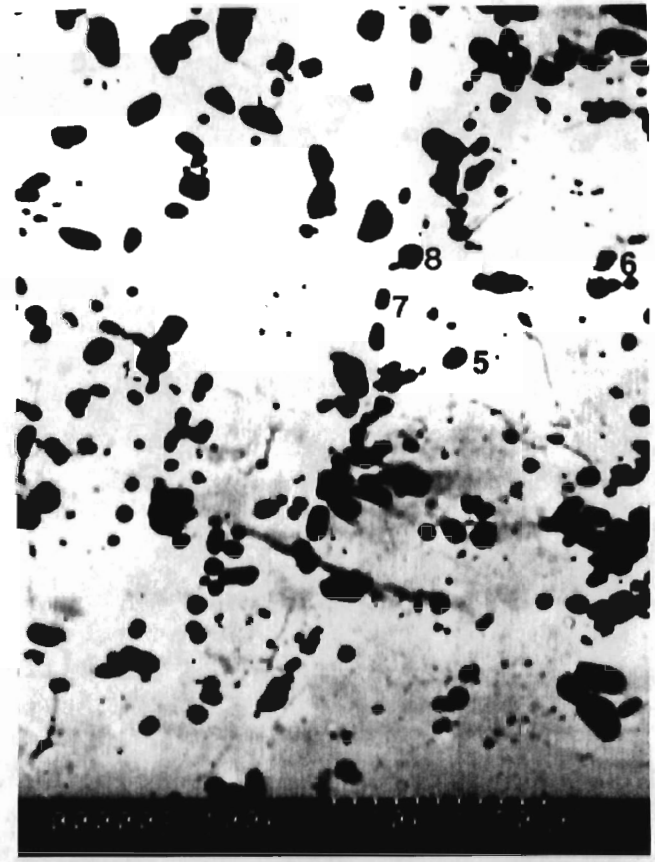

Figure 94. STEM micrographs of base metal near HAZ in NKK 9Cr-1Mo-V-Nb weldment, normalized, PWHT 1350°F(730°C)-1 hour, angle cut section. (a) 5000X, (b) 20,000X.

that PWHT for 1 hour causes some coarsening as well as an increase in precipitation. Further, the type of precipitate appears to change from the coherent MC type to the incoherent $M_{23}C_6$ type, thus resulting in softening.

Figure 95 shows STEM micrographs from the extraction replicas of soft regions in PWHT angle cut specimens of the NKK 9Cr welded in the normalized and tempered condition. Precipitates labelled 9 - 12, were identified to be of the $M_{23}C_6$ type, as in the case of the normalized plate.

STEM examinations therefore reveal that the carbides present in the soft region of the NKK 9Cr-1Mo-V-Nb steel in the as welded condition consists of MC and $M_{23}C_6$ types and in the PWHT condition consist of the $M_{23}C_6$ type.

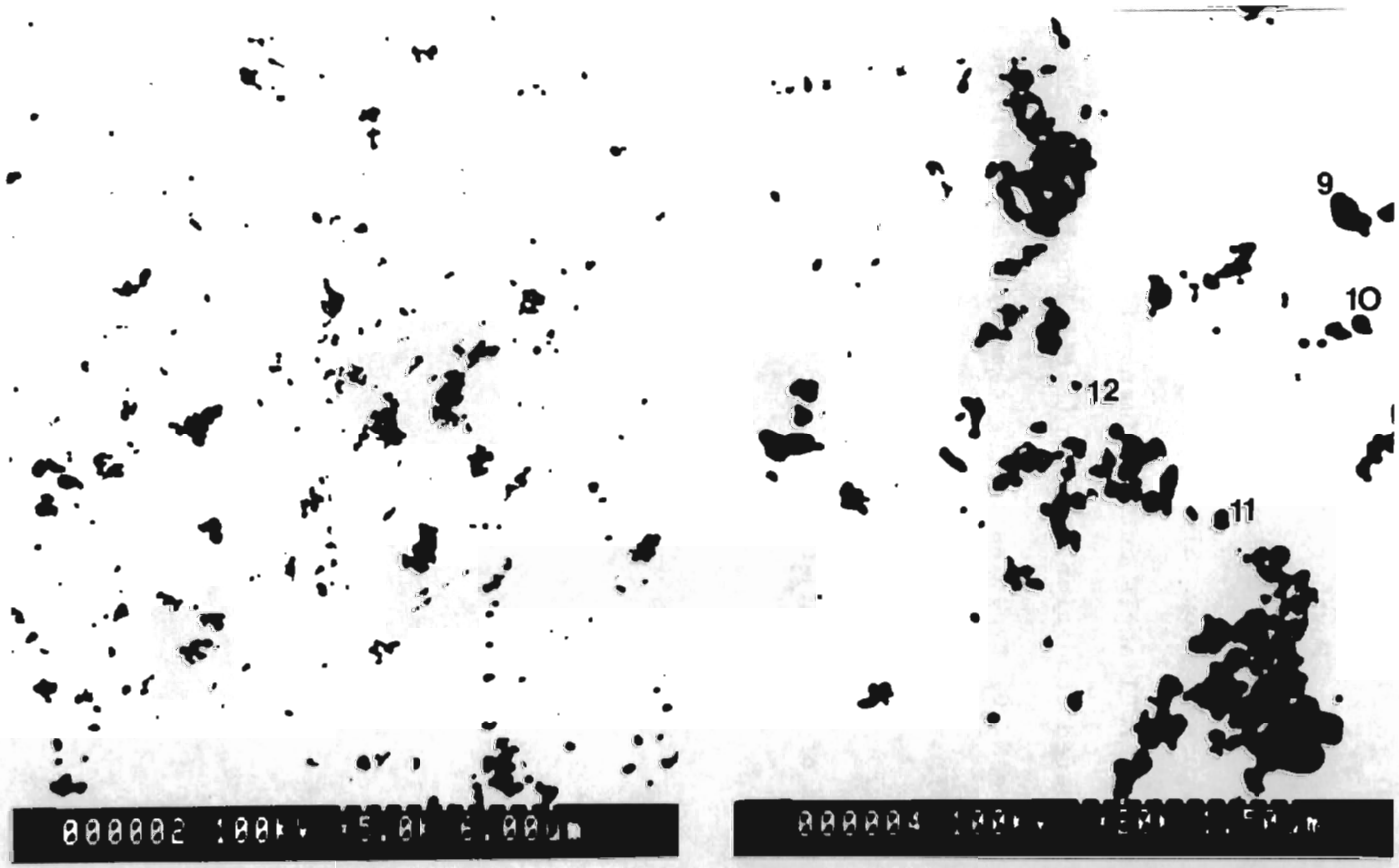

Figure 95. STEM micrographs of base metal near HAZ in NKK 9Cr-1Mo-V-Nb weldment, normalized and tempered, PWHT 1350°F(730°C)-1 hour, angle cut section. (a) 5000X, (b) 20,000X.

CONCLUSIONS

The purpose of this study was to determine the transformation characteristics, susceptibility to post weld heat treatment cracking hydrogen assisted cracking sensitivity and soft zone characteristics of alloys representative of the new generation of modified 9Cr-1Mo, 3Cr-Mo and 2 1/4Cr-1Mo alloys. The conclusions derived from this study may be summarized as follows:

I. Transformation Characteristics.

A. Transformation characteristics of the 9Cr-1Mo-V-Nb commercial commercial heats.

1. The rapid heating rates associated with the welding thermal cycle resulted in the A_{C1} and A_{C3} temperatures being higher than those reported in the literature for a similar composition material by 94 to 124F^{o} (50 to 65C^{o}) and 89 to 109F^{o} (35 to 45C^{o}) respectively.
2. The M_s temperatures range from 710 to 755°F (375 to 400°F) and are in agreement with those obtained under CCT conditions.
3. The minor variations in chemical composition of the three commercial heats had no observable effect on the M_s or M_f temperatures.
4. The M_s and M_f temperatures were independent of cooling rate over the range of simulated weld thermal cycles employed.
5. The primary microstructural constituents were martensite and autotempered martensite.

6. The Timken 9Cr-1Mo-V-Nb material, with a chromium equivalent of 13.4, contained delta ferrite in the simulated coarse grained HAZ as anticipated.

B. Transformation characteristics of the modified 3Cr-Mo and 2 1/4Cr-1Mo alloys.

1. The rapid heating rates associated with the welding thermal cycle resulted in the A_{C1} and A_{C3} temperatures being higher than those reported in the literature for AMAX (Climax) 3Cr-1 1/2Mo-0.1V, Berkeley 3Cr-1 1/2Mo-1/2Ni, JSW 3Cr-1Mo-V-Ti-B, JSW 2 1/4Cr-1Mo-V-Ti-B by 22 to 45F^{o} (12 to 25C^{o}) and 18 to 54F^{o} (10 to 28C^{o}) respectively.
2. No discernible separate M_f or B_S temperature could be detected for any of the materials.
3. The M_s temperatures obtained under simulated welding conditions were approximately 45F^{o} (25C^{o}) lower than those determined under standard CCT conditions.
4. The JSW 2 1/4Cr-1Mo-V-Ti-B material exhibited the highest on-cooling transformation temperatures of the modified alloys due to the lower carbon content (0.12%) and overall lower alloying element content.
5. The Berkeley 3Cr-1 1/2Mo-1/2Ni material exhibited the lowest transformation temperatures of the modified materials due to the higher carbon content (0.16%) and nickel content (0.51%).
6. The microstructures obtained under simulated welding conditions depend on the energy input (cooling rate). With low energy inputs (fast cooling rates), the microstructures consisted of

martensite and autotempered martensite. With intermediate energy inputs, the microstructures consisted of autotempered martensite and lower bainite. With the highest energy input (slowest cooling rate) employed, 150KJ/in (5.9 KJ/mm), the microstructure consisted of lower bainite and granular bainite.

II. Hydrogen assisted cracking susceptibility.

A. Hydrogen assisted cracking susceptibility in 3Cr materials.

1. At relatively low levels of diffusible hydrogen (3.71 ml/100g) HAC can be avoided using a preheat temperature of 275°F (135°C).

2. Susceptibility to HAC is extremely sensitive to the diffusible hydrogen content of welds deposited. A preheat of 450°F (232°C) is required to prevent cracking when the diffusible hydrogen level is increased to 5.07 ml/100g.

3. There is no decernable difference in behavior between the modified and unmodified 3Cr steels used for this study using Y-groove technique.

B. Hydrogen assisted cracking susceptibility in 2 1/4Cr-1Mo materials.

1. At relatively low levels of diffusible hydrogen (2.38 ml/100g) a preheat of 150°F (65°C) is required to avoid HAC.

2. At higher levels of diffusible hydrogen (8.04 ml/100g) the preheat temperature required to avoid HAC is increased to 375°F (191°C).

3. There is no difference in HAC susceptibility between modified and unmodified 2 1/4Cr alloys.

III. Postweld heat treatment cracking susceptibility.

A. Gleeble simulation evaluation of the 9Cr-1Mo-V-Nb commercial heats.

1. The 9Cr-1Mo-V-Nb alloys exhibit lower rupture ductilities (RA 15 to 56%) than unmodified 9Cr-1Mo (70% minimum RA). The lower rupture ductility of the modified materials is most likely the result of precipitation of fine V/Nb carbo-nitrides, nucleation of $M_{23}C_6$ on the V/Nb carbo-nitrides in a fine dispersed form, and a reduction in the the rate of growth of $M_{23}C_6$ due to a lowering of chromium mobility by vanadium.

2. The primary mode of fracture was microvoid coalescence.

3. The higher phosphorus content of the Sumitomo alloy (0.014%) may be the primary factor in the lower relative rupture ductility (RA 15 to 31%) of this material.

4. Macroscopic and microscopic ductility of the 9Cr-1Mo-V-Nb alloys is sufficient to preclude PWHT cracking as a problem in fabrication.

B. Gleeble simulation evaluation of the modified 3Cr-Mo and 2 1/4Cr-1Mo alloys.

1. The Berkeley 3Cr-1 1/2Mo-1/2Ni alloy with no vanadium addition exhibited significantly higher rupture ductility at both PWHT temperatures than the vanadium modified alloys; AMAX (Climax) 3Cr-1 1/2Mo-0.1V, JSW 3Cr-1Mo-V-Ti-B, and JSW 2 1/4Cr-1Mo-V-Ti-B.

2. By the Vinckier and Pense criteria[73,98] the Berkeley 3Cr-1 1/2Mo-1/2Ni alloy would be considered "not" susceptible to cracking when PWHT at 1250°F (680°C) and "slightly"

susceptible at 1150°F (620°C), the JSW 3Cr-1Mo-V-Ti-B and JSW 2 1/4Cr-1Mo-V-Ti-B alloys would be considered "highly" susceptible to cracking at 1250°F (680°C) and "extremely" susceptible at 1150°F, and the AMAX (Climax) 3Cr-1 1/2Mo-0.1V alloy would be considered "extremely" susceptible to cracking at both PWHT temperatures.

3. Rupture ductility was lower for all materials PWHT at 1150°F (620°C) than when PWHT at 1250°F (680°C). At the lower PWHT temperature longer duration of coherency and slower growth of Mo_2C or $(CrMo)_2CN$ in the matrix would result in increased susceptibility to cracking.

4. Rupture ductility for the base material subjected to simulated PWHT was in excess of 70% RA and for the simulated fine grained HAZ was in excess of 54% and thus shows that the grain coarsening thermal cycle is the precursor to metallurgical events which result in embrittlement.

5. The primary fracture mode for the Berkeley 3Cr-1 1/2Mo-1/2Ni alloy was IGMVC, for the JSW 3Cr-1Mo-V-Ti-B was mixed IGMVC and LDIGF with microvoids initiating on grain boundary particles, and for the AMAX (Climax) 3Cr-1 1/2Mo-0.1V and JSW 2 1/4Cr-1Mo-V-Ti-B was LDIGF.

6. The scanning electron microscopy examination of samples PWHT at 1250°F (680°C) for 70 to 100 minutes revealed almost complete break down of the lath type morphology and extensive carbide formation at the grain boundaries. The grain boundary carbides

in the Berkeley 3Cr-1 1/2Mo-1/2Ni material were coarser than the grain boundary carbides in the other modified materials.

7. The scanning transmission electron microscopy of carbide extraction replicas showed that the precipitation of grain boundary carbides was retarded in the vanadium modified materials in comparison to the Berkeley 3Cr-1 1/2Mo-1/2Ni alloy. Grain boundary carbides in the Berkeley alloy were $M_{23}C_6$ and M_6C, in the AMAX (Climax) 3Cr-1 1/2Mo-0.1V were M_7C_3, $M_{23}C_6$, and M_6C and in the JSW 3Cr-1Mo-V-Ti-B and JSW 2 1/4Cr-1Mo-V-Ti-B were $M_{23}C_6$ and M_7C_3. The predominant grain boundary carbide in the JSW 3Cr was chromium rich M_7C_3 and in the JSW 2 1/4Cr was molybdenum rich $M_{23}C_6$. Precipitation of the grain boundary carbides was accompanied with the formation of denuded zones in the AMAX (Climax), JSW 3Cr and JSW 2 1/4Cr alloys being 0.3 μm , 0.1 μm and less than 0.1 μm in width respectively.

8. The scanning transmission electron microscopy of carbide extraction replicas identified the matrix carbides in the Berkeley 3Cr-1 1/2Mo-1/2Ni and AMAX (Climax) 3Cr-1 1/2Mo-0.1V alloys as $(CrMo)_2CN$ and in the JSW 2 1/4Cr-1Mo-V-Ti-B and JSW 3Cr-1Mo-V-Ti-B alloys as Mo_2C containing molybdenum, chromium and vanadium.

9. The retarded evolution of the grain boundary carbides is probably accompanied by a concomitant slow growth of Mo_2C or $(CrMo)_2CN$ in the grain matrix. Slower growth of Mo_2C or $(CrMo)_2CN$ in the matrix will be associated with longer times of

coherency and matrix strengthening resulting in greater susceptibility to PWHT cracking. The transmission microscopy examination showed a greater volume fraction of matrix precipitates in the vanadium modified alloys and the scanning electron microscopy examination showed the carbides to be coarser in the Berkeley alloy thus supporting the hypothesis of slower development of the matrix carbides in the vanadium modified alloys.

10. The formation of chromium rich $M_{23}C_6$ as the predominant grain boundary carbide may be the result of the higher chromium to molybdenum ratio of the JSW 3Cr-1Mo-V-Ti-B alloy in comparison to the other vanadium modified alloys. Due to the preferential formation of chromium rich M_7C_3, more molybdenum may remain in solution promoting the growth and loss of coherency of Mo_2C in the matrix. This may be the cause of the increasing ductility with time to fracture observed in the 1250°F (680°C) PWHT results.

11. The low rupture ductility of the AMAX (Climax) 3Cr-1 1/2Mo-0.1V material may be the result of embrittlement due to higher phosphorus content (0.012%) compared to the other modified materials (0.006 to 0.007%) combined with precipitation strengthening. Further, the relatively high silicon content (0.26%) may enhance the formation of Mo_2C, lowering molybdenum in solution and promoting phosphorus segregation.

12. The presence of aluminum and aluminum bearing particles was found to be associated with regions of LDIGF in the Berkeley

material and limited microductility in the JSW 3Cr material. Thus, aluminum may play a minor role in increasing cracking susceptibility.

13. Superposition of a grain refining thermal cycle on a grain coarsening thermal cycle improves rupture ductility of the vanadium modified materials from less than 5% to more than 12% and therefore suggests that welding techniques which result in refinement of the coarse grained HAZ may prevent PWHT cracking in susceptible materials.

14. The state-of-the-art commercial heats (M10-M50) of modified 2 1/4Cr-1Mo-V-Ti-B appear superior to those used in studying the base program.

15. Calcium treatment during the production process of 2 1/4Cr-1Mo class of materials improves PWHT cracking resistance. This may be due to the modification of inclusion morphology and distribution.

16. Effect of minor addition of Cu to 2 1/4Cr-1Mo class of materials may be beneficial in PWHT cracking resistance.

C. C-ring evaluation of the modified 3Cr-Mo and 2 1/4Cr-1Mo alloys.

1. The Berkeley 3Cr-1 1/2Mo-1/2Ni and unmodified Lukens 2 1/4Cr-1Mo-0.10C materials did not crack in the C-ring test while the AMAX (Climax) 3Cr-1 1/2Mo-0.1V, JSW 3Cr-1Mo-V-Ti-B, and JSW 2 1/4Cr-1Mo-V-Ti-B cracked at both 1250°F (680°C) and 1150°F (620°C) and at all stress levels employed. Thus, the C-ring test confirms the general ranking of materials as either

susceptible or not susceptible to cracking determined from Gleeble simulation.

2. The depth of section cracked decreased in the vanadium modified alloys at the higher PWHT temperature, 1250°F (680°C), indicating decreasing susceptibility with increasing PWHT temperature. This agrees with the results for the two PWHT temperatures obtained in Gleeble simulation testing.
3. An unnotched C-ring of the AMAX (Climax) 3Cr-1 1/2Mo-0.1V material did not crack when PWHT at 1150°F (620°C) and stressed to 100ksi (690MPa) indicating the necessity of stress concentrators in initiating PWHT cracking.
4. The depth of section cracked for the vanadium modified alloys decreased as the stress was decreased.
5. Ranking of the vanadium modified alloys was determined to be JSW 3Cr-1Mo-V-Ti-B (least susceptible), AMAX (Climax) 3Cr-1 1/2Mo-0.1V, and JSW 2 1/4Cr-1Mo-V-Ti-B (most susceptible).
6. The greater susceptibility of the JSW 2 1/4Cr-1Mo-V-Ti-B alloy in comparison to the JSW 3Cr-1Mo-V-Ti-B alloy may be the result of the lower chromium to molybdenum ratio.
7. The C-ring test results for the AMAX (Climax) 3Cr-1 1/2Mo-0.1V alloy indicates that effect of embrittlement due to phosphorus segregation, which occurs simultaneously with decreasing stress due to stress relief, may be attenuated in comparison to the Gleeble simulation test performed with constant load.

8. Fracture morphology for the vanadium modified alloys was intergranular along the prior austenite grain boundaries with the fracture surface showing characteristic LDIGF.
9. C-ring tests conducted on the M10-M50 state-of-the-art modified 2 1/4Cr-1Mo alloy show superior resistance for heat M30. The Ca in this heat modifies the inclusion morphology and thus the resistance to PWHT cracking.
10. The C-ring test incorporates all the factors for an ideal test to evaluate PWHT cracking and appears to be a simple, valid test for determining susceptibility to cracking based on the substantial agreement with results obtained from Gleeble simulation.

IV. Soft zone evaluation

1. The soft region is immediately outside observable HAZ (below Ac_1) of 9Cr-1Mo-V-Nb steel weldments.
2. In the normalized and tempered 9Cr-1Mo-V-Nb steel weldment, the soft region is 25-30 DPH lower than the base metal.
3. In the normalized condition, the hardness of the soft zone is 170-200 DPH below that of the base metal in both single pass and five pass welds.
4. The microstructures at the point of lowest hardness adjacent to the boundary between the transformation zone and the tempered zone shows evidence of tempering characterized by precipitation of carbides along the grain and subgrain boundaries.

5. The carbides present in the soft zone of the weldment were identified as $M_{23}C_6$ and MC types in the as welded condition and $M_{23}C_6$ type in the PWHT condition.

LIST OF REFERENCES

1 Patriarca, P., Hoffman, E. and Cunningham, G., "Ferritic Steels as Alternate Structural Materials for High Temperature Applications," P. Patriarca (ed.), Modified 9Cr-1Mo Steel Techmical Program Data Package for Use in Design Analysis, ORNL Technology Transfer Meeting, April 7, 1982, Oak Ridge National Laboratory, Oak Ridge, TN, 1982, pp. 11 - 17.

2 Sikka, V., "National Program Plan for Commercialization of Modified 9Cr-1Mo Alloy," Oak Ridge National Laboratory, Oak Ridge, TN, 1980.

3 Swindeman, R.W., Thomas, R.G., Nanstad, R. and Long, C.J., "Assessment of the Need for an Advanced Chromium-Molybdenum Steel for Construction of Third Generation Gasifier Pressure Vessels," Oak Ridge National Laboratory, Oak Ridge, TN, 1980.

4 Ishiguro, T., Ohnishi, K., Murakami, Y., Mima, S. and Watanabe, J., "Development of a 3Cr-1Mo-1/4V-Ti-B Pressure Vessel Steel for the Enhanced Design Stress," R.A. Swift (ed.), Research on Cr-Mo Steels, American Society of Mechanical Engineers, New York, 1984, pp. 43 - 53.

5 Tagawa, H. and Tsuyama, S., "Modified 3Cr-1Mo Steel with Improved Toughness and Elevated Temperature Strength," Compilation of Recent Technical Information for the Program - Materials for Service with Hydrogen at High Temperatures and Pressures, Metals Property Council, New York, 1983, pp. 15 - 26.

6 Klueh, R.L. and Nasreldin, A.M., "Microstructure and Mechanical Properties of a 3Cr-1.5Mo Steel," Oak Ridge National Laboratory, Oak Ridge, TN, 1985.

7 Swindeman, R.W., Nasreldin, A.M., Klueh, R.L. and King, J.F., "Metallographic Examination of Response of 3Cr-1.5Mo Steel to Heat Treatment," ORNL/TM-9691, Oak Ridge National Laboratory, Oak Ridge, TN, 1985.

8 Wada, T. and Cox, T.B., "3Cr-1.5Mo Steel for Pressure Vessels in Hydrogen Service," Climax Molybodenum Co., Ann Arbor, MI, 1982.

9 Wada, T. and Cox, T.B., "A New 3Cr-1.5Mo Steel For Pressure Vessel Applications," R.A. Swift (ed.), Research on Cr-Mo Steels, American Society of Mechanical Engineers, New York, 1984, pp. 77 - 94.

10 Ritchie, R.O., Parker, E.R., Spencer, P.N. and Todd, J.A., "Topical Report: A New Series of Advanced 3Cr-Mo-Ni Steels For Thick Section Pressure Vessels In High Temperature and Pressure Hydrogen Service," UCB/RP/84/D1020, Oak Ridge National Laboratory, Oak Ridge, TN., 1984.

11 Mima, S., "Technical Data Sheet of 3Cr-1Mo-1/4V-Ti-B Steel for Elevated Temperature Applications," The Japan Steel Works, Muroran, Japan, 1983.

12 "Modified 2 1/4Cr-1Mo and 3Cr-1Mo Steels - Mechanical Properties, Hydrogen Resistance and Weldability," Nippon Kokan K.K., Kawasaki, Japan, 1985.

13 "Development of Advanced 2 1/4Cr-1Mo and 3Cr-1Mo Steels," Kawasaki Steel Corporation, Kawasaki, Japan, 1985.

14 Yukitoshi, T., Nishida, K., Oda, T. and Daikoku, T., "Low-Alloy High-Strength Steel for Boiler Tubes (Low C-9Cr-2Mo)," Transactions of the American Society of Mechanical Engineers, 98(1), 1976, pp. 173 - 178.

15 Yukitoshi, T., Yoshikawa, K., Tokimasa, K., Shida, Y. and Imaba, Y., "Application of 9Cr-2Mo Steel (HCM9M) for Fast Breeder Reactor Steam Generators," The Sumitomo Search, 23, 1980, pp. 45 - 58.

16 Devletian, J.H. and Wood, W.E., "Principles of Joining Metallurgy," E.F. Nippes (ed.), Welding, Brazing, and Soldering - Metals Handbook Ninth Edition, American Society for Metals, Metals Park, OH, 1984, pp. 21 - 49.

17 Linnert, G.E., Welding Metallurgy, American Welding Society, Miami, FL, 1983.

18 Ito, Y. and Nakanishi, M., "Study of Stress Relief Cracking in Welded Low Alloy Steels," The Sumitomo Search, 7, 1972, pp. 27 - 36.

19 Eyre, B.L., Edwards, B.C. and Titchmarsh, J.M., "Physical Metallurgy of Reversible Temper Embrittlement," Proc. of Conf. Advances in the Physical Metallurgy and Applications of Steels, University of Liverpool, 21-24 September, 1981, Metals Society, London, 1981, pp. 246 - 258.

20 Viswanathan, R. and Joshi, A., "Effect of Microstructure on the Temper Embrittlement of Cr-Mo-V Steels," Metallurgical Transactions A, 6A, 1975, pp. 2289 - 2295.

21 Easterling, K., Introduction to the Physical Metallurgy of Welding, Butterworths, Boston, 1983.

22 Udin, H., Funk, E.R. and Wulf, J., Welding for Engineers, John Wiley and Sons, New York, 1954.

23 Torok, T.E. and Stout, R.D., "Relation of dilatometric Characteristics of Steels to Delayed Cracking in Welds," Welding Journal, 44(12), 1965, pp. 592s - 544s.

24 Nippes, E.F., "The Weld Heat Affected Zone," Welding Journal, 38(1), 1955, pp. 1s - 18s.

25 Richey, M.W., The Weldability of Cr-Mo Steels for Fossil Energy Applications, M.S. Thesis University of Tennessee, Knoxville, TN, 1984.

26 Habraken, C.J. and Economopoulos, M., "Bainitic Microstructures in Low-Carbon Alloy Steels and Their Mechanical Properties," Transformation and Hardenability in Steels, Climax Molybdenum Company, Ann Arbor, 1967, pp. 69 - 108.

27 Biss, V. and Cryderman, R.L., "Martensite and Retained Austenite in Hot Rolled Low Carbon Bainitic Steels," Metallurgical Transactions, 2(8), 1971, pp. 2267 - 2276.

28 Thomas, G., Sarikaga, M., Smith, G.D.W. and Barnard, S.J., "Microstructure, Retained Austenite, and Mechanical Properties of Experimental 0.3%C Steels," Proc. of Conf. Advances in the Physical Metallurgy and Applications of Steel, University of Liverpool, 21-24 September, 1981, Metals Society, London, 1981, pp. 259 - 265.

29 Baker, R.G. and Nutting, J., "The Tempering of 2 1/4%Cr-1%Mo Steel After Quenching and Tempering," Journal of the Iron and Steel Institute, 192, 1959, pp. 257 - 267.

30 Stone, P.G. and Murray, J.D., "Creep Ductility of Cr-Mo-V Steels," Journal of the Iron and Steel Institute, 203, 1965, pp. 1094 - 1107.

31 Woodhead, J.H. and Quarrell, A.G., "The Role of Carbides in Low-Alloy Creep-Resisting Steels," Climax Molybdenum Co. Ltd., London, 1965.

32 Vitek, J.M. and Klueh, R.H., "Precipitation Reactions During the Heat Treatment of Ferritic Steels," Metallurgical Transactions A, 14A(6), 1983, pp. 1047 - 1055.

33 Sikka, V., Personal Communication, 2/14/1985.

34 Seal, A.K. and Honeycombe, R.W.K., "Carbide Precipitation in Several Steels Containing Chromium and Vanadium," Journal of The Iron and Steel Institute, January, 1958, pp. 9 - 15.

35 "Welding Metallurgy," Welding Handbook, 7th Edition, Vol.1, Chap. 4, American Welding Society, 1982.

36 Luther, G.G., Jackson, C.E., and Hartbower, C.E., "A Review of Wedability Test of Carbon and Low Alloy Steels," Welding Journal, 20(10), 1949, pp. 376s - 396s.

37 Coe, F.R., The Avoidance of Hydrogen Cracking in Welding, The Welding Institute, 1973.

38 Beachem, C.D., "A New Model for Hydrogen-Assisted Cracking(Hydrogen "Embrittlement")," Met. Trans., 3(2), 1972, pp 437 - 451.

39 Coe, F.R., Welding Steels Without Hydrogen Cracking, The Welding Institute, 1973.

40 McGannon, H.E., The Making, Shaping and Treating of Steel, 9th Edition, Chapter 19, United States Steel Corporation, 1971.

41 Lancaster, J.F., Metallurgy of Welding, Chapter 7, Allen and Unwin, 1980.

42 Berstein, I.M., "The Role of Hydrogen in the Embrittlement of Iron and Steel," Mat. Sc. and Engineering, Vol. 6, 1970, pp. 1 - 19.

43 Zapffe, C. and Sims, C., "Hydrogen Embrittlement, Internal Stress and Defects in Steel," AIME Trans., Vol. 145, 1941, pp. 225 - 237.

44 Petch, N.O. and Sables, P., "Delayed Fracture of Metals Under Static Load," Nature, Vol. 169, 1952, pp. 842 - 843.

45 Linnert, G.E., Welding Metallurgy, Vol. 2, American Welding Society, 1967.

46 Troiano, A.R., "The Role of Hydrogen and Other Interstitials in the Mechanical Behavior of Metals," Trans. ASM., Vol. 52, 1960, pp. 54 - 80.

47 Apblett, W.R., Dunphy, R.P. and Pellini, W.S., "Transformation of Cr-Mo Steels During Welding," Welding Journal, 33(1), 1954, pp. 57s - 64s.

48 Hart, P.H.M. and Watkins, E., "Weld Metal Implant Test Ranks Cr-Mo Hydrogen Cracking Resistances," Welding Journal, 56(9), 1975, pp. 288s - 295s.

49 Smith, E., Blanchard, B.E. and Apps, R.L., "The Weld HAZ in 2 1/4Cr-1Mo Steels," Proc. of Conf. on Welding Creep-Resistant Steels, The Welding Institute, Cambridge, England, 1970, pp. 79 - 89.

50 Linnert, G.E., "Welding Characteristics of Stainless Steels," Source Book on Stainless Steels, American Society for Metals, 1976.

51 "Welding High Temperature Steels: The Heat Affected Zone," Engineering, Vol. 207, No. 5359, 1969, pp. 73.

52 Colombe, G., Dibiez, S., Donati, J.R., Petreguin, P. and Zacharie, G., "Metallurgical Aspects of the Weldability of Cr-Mo Stabilized Ferritic Steels," Proc. Int. Conf. on Ferritic Steels for Fast Reactor Steam Generators, British Nuclear Energy Society, London, England, 1978, pp. 447 - 458.

53 Granjon, H., "The Implant Method for Studying the Weldability of High Strength Steels," Metal Construction and British Welding Journal, 1(11), 1969, pp. 447 - 458.

54 Terai, K., Shimizu, S., Nakai, Y., Murakami, T., Ota, S. and Fujiwara, M., "Weldability and Joint Properties of Advanced Carbon Stabilized 2.25Cr-1Mo for LMFBR," Proc. Int. Conf. on Ferritic Steels for Fast Reactor Steam Generators, British Nuclear Energy Society, London, England, 1978, pp. 442 - 446.

55 Murray, J.D., "Stress-Relief Cracking in Carbon and Low Alloy Steels," British Welding Journal, 14(8), 1967, pp. 447 - 456.

56 Tamaki, K. and Suzuki, J., "Effect of Chromium and Molybdenum on Reheat Cracking Sensitivity of Steels (Study of Reheat Cracking of Cr-Mo Steels, Report 2)," Transactions of the Japan Welding Society, 14(2), 1983, pp. 39 - 43.

57 Erwin, W.E. and Kerr, J.G., "WRC Bulletin 275 - The Use of Quenched and Tempered 2 1/4Cr-1Mo Steel for Thick Wall Reactor Vessels in Petroleum Refining Processes: An Interpretive Review of 25 Years of Research and Application," Welding Research Council, 1982.

58 McPherson, R., "Compositional Effects on Reheat Cracking of Low Alloy Ferritic Steels," Metals Forum, 2(3), 1980, pp. 175 - 186.

59 Vinckier, A., "Use of Weld Simulation Tests to Study Susceptibility to Reheat Cracking," Proc. of Conf. Welding Research Related to Power Plant, University of Southampton, 17 - 21 September, 1972, Central Electric Generating Boar, London, 1972, pp. 336 - 355.

60 Meitzner, C.F., "WRC Bulletin 211 - Stress Relief Cracking in Steel Weldments," Welding Research Council, 1975.

61 Vinckier, A.G. and Pense, A.W., "WRC Bulletin 197 - Review of Underclad Cracking in Pressure-Vessel Components," Welding Research Council, 1974, pp. 1 - 35.

62 Swift, R.A. and Rogers, H.C., "A Critical Review of Weld Metal Embrittlement," Welding Journal, 60(7), 1971, pp. 357s - 363s.

63 Nichols, R.W., "Reheat Cracking in Welded Structures," Welding in the World, 7(4), 1969, pp. 36 - 44.

64 Swift, R.A., "The Mechanism of Stress Relief Cracking in 2 1/4Cr-1Mo Steel," Welding Journal, 50(5), 1971, pp. 195s - 200s.

65 Swift, R.A. and Rogers, H.C., "Embrittlement of 2 1/4Cr-1Mo Steel Weld Metal by Postweld Heat Treatment," Welding Journal, 52(4), 1973, pp. 145s - 153s.

66 Swift, R.A., "Creep-Rupture Tests on 2 1/4Cr-1Mo Simulated Heat Affected Zone," Lukens Steel Company Research Report RDR 69-11 Lukens Steel Company, Coatesville, Pa, 1969.

67 Orr, J., Beckitt, F.R. and Fawkes, G.D., "Paper 16: The Physical Metallurgy of Chromium-Molybdenum Steels for Fast Reactor Boilers," Proceedings of the International Conference on Ferritic Steels for Fast Reactor Steam Generators, British Nuclear Energy Society, London, 1978, pp. 91 - 109.

68 Bentley, K.P., "Precipitation During Stress Relief of Welds in Cr-Mo-V Steels," British Welding Journal, 11(10), 1964, pp. 507 - 515.

69 Mullery, F. and Cadman, R., "Cracking of Welded Joints in Ferritic Heat Resisting Steels," British Welding Journal, 9(4), 1962, pp. 212 - 220.

70 Vinckier, A. and Dhooge, A., "Reheat Cracking in Welded Structures During Stress Relief Heat Treatments," Journal of Heat Treating, 1(1), 1979, pp. 72 - 80.

71 Meitzner, C.F. and Pense, A.W., "Stress Relief Cracking in Low-Alloy Steel Weldments," Welding Journal, 48(10), 1969, pp. 431s - 440s.

72 Edwards, R.H., Barbaro, F.J. and Gunn, K.W., "Stress Relief Cracking in Cr-Mo-V Steels," Metals Forum, 5(2), 1982, pp. 119 - 129.

73 Dhooge, A., Dolby, R.E., Sebile, J., Steinmetz, R. and Vinckier, A.G., "A Review of Work Related to Reheat Cracking in Nuclear Reactor Pressure Vessel Steels," International Journal of Pressure Vessels and Piping, 6, 1978.

74 Presser, R.I. and McPherson, R., "The Role of Trace Elements in Reheat Cracking," Proc. of Conf. Residual Stresses in Welded Construction and Their Effects, London, 15-17 November, 1977, Welding Institute, Cambridge, 1978, pp. 387 - 398.

75 Vinckier, A. and Dhooge, A., "Paper 36: Reheat Cracking in Welded Structures During Stress Relief Heat Treatments," Proc. of Conf. Residual Stresses in Welded Construction and Their Effects, London, 15-17 November, 1977, The Welding Institute, Cambridge, 1978, pp. 375 - 385.

76 Hippsley, C.A., King, J.E. and Knott, J.F., "Toughness Variations and Intergranular Fracture During the Tempering of Simulated HAZ Structures in a Mn-Mo-Ni Stel," Proc. of Conf. Advances in the Physical Metallurgy and Applications of Steel, University of Liverpool, 21-24 September 1981, Metals Society, London, 1981, pp. 147 - 155.

77 Hippsley, C.A., Knott, J.F. and Edwards, B.C., "A Study of Stress-Relief Cracking in 2 1/4Cr-1Mo Steel - II. The Effects of Multicomponent Segregation," Acta Metallurgica, 30, 1982, pp. 641 - 652.

78 Troiano, A.R., "The Role of Hydrogen and Other Interstitials in the Mechanical Behavior of Metals," Transactions of the American Society for Metals, 52, 1960, pp. 54 - 80.

79 Debiez, S. and Granjon, H., "Work Carried Out by the Institut de Soudure on Reheat Cracking," Proc. of Conf. Resiudual Stresses in Welded Construction and Their Effects, London, 15-17 November, 1977, Welding Institute, Cambridge, 1978, pp. 231 - 239.

80 Nakamura, H., Naiki, T. and Okabayashi, H., "Fracture in the Process of Stress-Relaxation Under Constant Strain," Proceedings of the First International Conference on Fracture, Sendai, Japan, September, 1965, Japan Welding Society, 1965, pp. 863 - 878.

81 Pense, A.W., Galda, E.J. and Powell, G.T., "Stress Relief Cracking in Pressure Vessel Steels," Welding Journal, 50(8), 1971, pp. 374s - 378s.

82 McMahon, C.J., Jr., Dobbs, R.J. and Gentner, D.H., "Stress-Relief Cracking in MnMoNi and MnMoNiCr Pressure Vessel Steels," Materials Science and Engineering, 37, 1979, pp. 179 - 186.

83 Wada, T., Grobner, P.J. and Vineberg, E.J., "Duplex Structure 12Cr-2Mo Steels With Improved Weldability," Proc. of Conf. Production, Fabrication, Properties, and Applications of Ferritic Steels for High Temperature Applications, American Society for Metals, Warren, Pa, 1981.

84 Hippsley, C.A., Knott, J.F. and Edwards, B.C., "A Study of Stress-Relief Cracking in 2 1/4Cr-1Mo Steel - The Effects of P Segregation," Acta Metallurgica, 28, 1980, pp. 869 - 885.

85 Miller, R.C. and Batte, R.D., "Reheat Cracking in 1/2CrMoV/2 1/4CrMo Welded Joints," Metal Construction, 7(11), 1975, pp. 550 - 558.

86 Muraki, T., Jahaco, J. and Watanabe, J., "Reheat Cracking of 2 1/4Cr-Mo Pressure Vessel Steel," Research Report, Japan Steel Works, Muroran Plant Research Laboratory, PV76-78, 1975, pp. 1 - 17.

87 Imanaka, T., Sato, S., Shimomura, J. and Aso, K., "Improvements in the Susceptibility to Hydrogen Attack and Stress-Relief Cracking of 2 1/4Cr-1Mo Steels," Kawasaki Steel Corporation, Mizushima, Japan, 1985.

88 Boniszewski, T., "Reheat Cracking in 2 1/4Cr-1Mo Submerged Arc Weld Metal," Metal Construction, 14(9), 1982, pp. 495 - 496.

89 Tamaki, K. and Suzuki, J., "Reheat Cracking Test on High Strength Steels by a Modified Implant Test," Transactions of The Japan Welding Society, 14(2), 1983, pp. 33 - 38.

90 Tamaki, K., Suzuki, J., Nakaseko, Y. and Tajiri, M., "Effect of Carbides on Reheat Cracking Sensitivity (Study of Reheat Cracking of Cr-Mo Steels, Report 3)," Transactions of The Japan Welding Society, 15(1), 1984, pp. 8 - 16.

91 Tamaki, K. and Suzuki, T., "Assessment of Reheat Cracking Sensitivity of Steels from their Chemical Compositions," Proc. of Conf. 1985 American Ssociety for Metals' International Welding Congress/JDC University Research, Toronto, Canada, 14-17 October 1985.

92 "Discussion Session 4, Part 1 - Heat Treatment Cracking Paper 11 (Reheat Cracking in Cr-Mo-V steel Weldments)," Metal Construction and British Welding Journal, 1(2), 1969, pp. 125 - 128.

93 Chu, C., Yue-Chang, Z., Shou-Shan, Y., Lu-Hai, W., Miao-Tao, L. and Xi-Zhen, L., "Study of Reheat Cracking Mechanism in 15CrMoV Steel," The Fourth International Symposium of the Japan Welding Society, November, 1982, Japan Welding Society, Osaka, Japan, pp. 461 - 466.

94 "Improvement in High Temperature Properties of Heavy Section 2 1/4Cr - 1Mo Steel," Kawasaki Steel Corporation, 1982.

95 Meyers, J., "Influence of Alloy and Impurity Content on Stress-Relief Cracking in Cr-Mo-V Steels," Metals Technology, 5(pt.2), 1978, pp. 391 - 396.

96 Jones, K.E., "Paper 5: Stress-Relief Cracking of Welded Pipe/Casting Joints in Cr-Mo-V Steel," Proc. of Conf. Welding of Creep Resisting Steels, The Welding Institute, Cambridge, England, 1970, pp. 66 - 78.

97 Stone, P.G. and Murray, J.D., "Creep Ductility of Cr-Mo-V Steels," Journal of the Iron and Steel Institute, 203, 1965, pp. 1094 - 1107.

98 Vinckier, A., (chrmn.), "Testing Techniques to Study the Susceptibility to Reheat Cracking of Carbon-Manbganese and Low Alloy Steels," Welding in the World, 12, 1974, pp. 1 - 22.

99 Yu, J. and McMahon, C.J., Jr., "The Effects of Composition and Carbide Precipitation on Temper Embrittlement of 2.25Cr-1Mo Steel: Part II - Effects of Mn & Si," Metallurgical Transactions A, 11A(2), 1980, pp. 291 - 300.

100 Ratliff, J.L. and Brown, R.M., "The Deleterious Effect of Small Quantities of Aluminium on the Stress Rupture Propperties of a Cr-Mo-V Steel," Transactions of the American Society for Metals, 60, 1967, pp. 176 - 186.

101 Meyers, J., "Effects of Deoxidants and Impurities on Simulated Stress Relief Cracking of 1/2Cr 1/2Mo 1/4V Steel," Proc. of Conf. Welding Research Related to Power Plant, University of Southampton, 17-21 September, 1972., Central Electric Generating Board, London, 1972, pp. 356 - 368.

102 Harris, P. and Jones, K.E., "The Effect of Composition and Deoxidation Practice on the Reheat Cracking Tendencies of 1/2Cr 1/2Mo 1/4V Steel," Proc. of Conf. Welding Research Related to Power Plant, University of Southampton, 17-21 Sept. 1972, Central Electric Generating Board, London, 1972, pp. 369 - 380.

103 Spaeder, G.J. and Ploder, G., "Technical Report: Stress Rupture Properties of the Simulated Heat-Affected Zone of USS "T-1" Steel," Applied Research Laboratory, US Steel, Monroeville, Pa., 1963.

104 Wyatt, L.M., (chrmn.) and Edmondson, B., (rapporteur), "Rapporteur's Remarks and Discussion (Discussion of Papers 24-31)," Proc. of Conf. Welding Research Related to Power Plant, University of Southampton, 17-21 Sept. 1972, Central Electric Generating Board, London, 1972, pp. 435 - 448.

105 Presser, R.I. and McPherson, R., "Boron Segregation and Elevated Temperature Embittlement of Ferritic Steel," Scripta Metallurgica, 11(9), 1977, pp. 745 - 749.

106 Hunter, A.N.R., "Reheat Cracking in 2 1/4Cr-1Mo Submerged Arc Weld Metal - Part 1 Materials, Welding and Testing," Metal Construction, 14(4), 1982, pp. 198 - 201.

107 Hunter, A.N.R., "Reheat cracking in 2 1/4Cr-1Mo Submerged Arc Weld Metal - Part 2 Results and Discussion," Metal Construction, 14(5), 1982, pp. 266 - 270.

108 Wittig, J.E., Sinclair, R. and Viswanathan, R., "Precipitation of Phosphorous and Tin in Temper Embrittled Low Alloy Steel," Scripta Metallurgica, 19(1), 1985, pp. 111 - 117.

109 Kikuchi, T. and Nakao, Y., "Effects of Impurity Elements on the Reheat Cracking in Weld Zones of Steels," The Fourth International Symposium of The Japan Welding Society, November, 1982, Japan Welding Society, Osaka, Japan, pp. 455 - 460.

110 Horn, H. and Kunze, H.D., "Reheat Cracking Studies by Weld Simulation and Scanning Auger Investigation," The Fourth International Symposium of the Japan Welding Society, November 1982, Japan Welding Society, Osaka, Japan, pp. 449 - 454.

111 Yu, J. and McMahon, C.J., Jr, "The Effects of Composition and Carbide Precipitation on Temper Embrittlement of 2.25Cr-1Mo Steel: Part 1. Effects of P and Sn," Metallurgical Transactions A, 11A, 1980, pp. 277 - 289.

112 Hippsley, C.A., "Precipitation Sequences in Heat Affected Zone of 2.25Cr-1Mo Steel During Stress-Relief Heat Treatment," Metal Science, 15(4), 1981, pp. 137 - 147.

113 Muhammad, A.B., Szkopiak, Z.C. and Waldron, M.B., "Effect of Types of Carbides on Temper Embrittlement in Commercial 2.25Cr-1Mo Steel," Proc. of Conf. Advances in the Physical Metallurgy and Applications of Steel, University of Liverpool, 21-24 September, 1981, Metals Society, London, 1981, pp. 340 - 348.

114 You, C.P., Hippsley, C.A. and Knott, J.F., "Stress Relief Cracking Phenomena in High Strength Structural Steel," Metal Science, 18(8), 1984, pp. 387 - 394.

115 Dolby, R.E., "Advances in the Welding Metallurgy of Steel," Proc. of Conf. Advances in the Physical Metallurgy and Applications of Steels, University of Liverpool, 21-24 September, 1981, Metals Society, London, 1981, pp. 111 - 125.

116 Colombe, G., Debiez, S., Donati, J.R., Petrequin, P. and Zacharie, G., "Paper 75: Metallurgical Aspects of the Weldability of Cr-Mo Ferritic Steels," Proceedings of the International Conference on Ferritic Steels for Fast Reactor Steam Generators, British Nuclear Energy Society, London, England, 1978, pp. 447 - 458.

117 Meyers, J. and Price, A.T., "Stress-Relief Cracking Studies of 0.5Cr-Mo-V and 2Cr-Mo Steels Using HAZ Simulation," Metals Technology, 4(8), 1977, pp. 406 - 410.

118 Stout, R.D., "WRC Bulletin 302 - Post Weld Heat Treatment of Pressure Vessel Steels," Welding Research Council, 1985, pp. 1 - 14.

119 Price, A.T. and Siverns, M.J., "Stress Relief Cracking In Low Alloy Ferritic Steels," Metal Construction and British Welding Journal, 2(6), 1970, pp. 239 - 245.

120 Glossop, B.A., Eaton, N.F. and Boniszewski, T., "Reheat Cracking in Cr-Mo-V Steel Weldments," Metal Construction and British Welding Journal, 16(2), 1969, pp. 68 - 73.

121 Hippsley, C.A., "The Influence of Heating Rate on Reheat-Cracking in a Commercial 2 1/4Cr-1Mo Steel," Report #AERE-R-10840 (DE 83911013), UKAEA Atomic Energy Research Establishment, Metallurgy Division, United Kingdom, Harwell, Oxfordshire, 1983.

122 Progrebnoi, N., Tananko, I. and Zozulya, V., "The Effect of Heat Treatment on the Properties of the Softened Zone in Steel 15Kh11MF," Welding Production, 1979, pp. 27 - 30.

123 Challenger, K., Brucker, R., Elger, W. and Sovek, M., "Microstructure-Thermal History Correlations for HY-130 Thick Section Weldments," Welding Journal, 63(8), 1984, pp. 254s - 262s.

124 King, J., "Weldability," Advanced Alloy Technology Program - Welding Development, ORNL/MSP/1.7-81/3, June 1982.

125 Biss, V., "Metallographic Investigation of Soft Regions Near Heat Affected Zones of Modified 9Cr-1Mo Steel Weldments," Climax Molybdenum Company Report J-4747 to ORNL, March 1982.

126 Reed-Hill, R., Physical Metallurgy Principles, Chapter 11, Brooks/Cole Engineering Division, 1973.

127 Christian, J., The Theory of Transformation in Metals and Alloys, Pergammon Press, 1965, pp. 691 - 696.

128 Ishiguro, T., Murakami, Y., Ohnishi, K. and Watanabe, J., "Interim Reports of the R&D Program for Coal Liquefaction Reactor Materials," Compilation of Recent Tech. Information for the Program Materials for Service with Hydrogen at High Temperatures and Pressures, Metals Property Council, New York, 1983, pp. 1 - 29.

129 George, T., Parker, E.R. and Ritichie, R.O., "Susceptibility to Hydrogen Attack of a Thick Section 3Cr-1Mo-1Ni Pressure Vessel Steel - Role of Cooling Rate," Materials Science and Technology, 1, 1985, pp. 198 - 208.

130 Kar, R.J. and Todd, J.A., "Alloy Modification of Thick-Section 2 1/4Cr-1Mo Steel," G.S. Sangdahl and M. Semchyshen (eds.), ASTM STP 755 The Symposium on Applications of 2 1/4Cr-1Mo Steel for Thick-Wall Pressure Vessels, Metals Property Council - American Society for Testing and Materials, Denver, 1980, pp. 228 - 252.

131 Ishiguro, T., Murakami, Y., Ohnishi, K. and Watatnabe, J., "A 2 1/4Cr-1Mo Pressure Vessel Steel with Improved Creep Rupture Strength," G.S. Sangdahl and M. Semchyshen (eds.), ASTM STP 755 The Symposium on Applications of 2 1/4Cr-1Mo Steel for Thick-Wall Pressure Vessels, Metals Property Council - American Society for Testing and Materials, Denver, 1980, pp. 129 - 147.

132 Bodine, G.C., Jr., Chakravarti, B., Owens, C.M., Roberts, B.W., Vandergriff, D.M. and Ward, C.T., "A Program for the Development of Advanced Ferritic Alloys for LMFBR Structural Applications," Topical Report. ORNL/SUB-4291/1, 1977.

133 Savage, W.F., "Apparatus for Studying the Effects of Rapid Thermal Cycles and High Strain Rates on the Elevated Temperature Behavior of Materials," Journal of Applied Polymer Science, 6(21), 1962, pp. 303 - 315.

134 "Standard Recommended Practice for Making and Using C-Ring Stress-Corrosion Test Specimens - Designation G38-73 (Reapproved 1979)," R.P. Lukens, J.L. Cornillot, R.A. Priemon, and D.F. Savini (eds.), 1982 Annual Book of ASTM Standards, Metals - Physical, Mechanical, Corrosion Testing, American Society for Testing and Materials, Philadelphia, PA, 1982, pp. 1003 - 1011.

135 Peterson, R.E., Stress Concentation Factors, John Wiley & Sons, New York, 1974.

136 Schrader, A. and Rose, A., De Ferri Metallographia (Metallograpic Atlas of Iron, Steels, and Cast Irons) - Structure of Steels, W. B. Saunders Company, Philadelphia, PA, 1966.

137 Brown, R.M., Rege, R.A. and Spaeder, C.E., "The Properties of Normalized and Tempered and Quenched and Tempered 6 1/4 inch Thick Plates of 2 1/4Cr-1Mo Steel," Symposium of Heat Treated Steels for Elevated Temperature Service, American Society of Mechanical Engineers, New York, 1966, pp. 27 - 44.

138 Smith, E., Blanchard, B.E. and Apps, R.L., "The Weld HAZ in 2 1/4%Cr-1%Mo Steels," Proc. of Conf. Welding Creep-Resistant Steels, The Welding Institute, Cambridge, 1970, pp. 79 - 89.

139 Boniszewski, T., Watkinson, F., Baker, R.G. and Tremlett, H.F., "Hydrogen Embrittlement and Heat-Affected Zone Cracking in Low-Carbon Alloy Syeels with Acicular Microstructures," British Welding Journal, 34, 1965, pp. 14 - 36.

140 Todd, J.A., Lundin, C.D. and Henning, J.A., "Microstructural Characterization of Weld Heat Affected Zones in Modified Cr-Mo Steels," (unpublished paper), (1986).

141 Tamaki, K. and Suzuki, J., "Effect of Phosphorous on Reheat Cracking of Cr-Mo Steels," Research Reports of the Faculty of Engineering, Mie University, 9, 1984.

142 Dickinson, D.W. and Liu, J.H., "A New Test Method to Study Reheat Cracking in Low Alloy Steel," unpublished paper presented at the 67th Annual American Welding Society Convention, April 13-18,1986.

APPENDIX - 1
Distribution List

1. ALLISON GAS TURBINE OPERATIONS, Mail Stop W-5, P.O. Box 420, Indianapolis, Indiana 46206

   P. Khandelwal

2. ARGONNE NATIONAL LABORATORY, 9700 S. Cass Avenue, Argonne, Illinois 60439

   W. A. Ellingson

3. AMERICAN WELDING SOCIETY, 550 LeJeune Road, Miami, Florida 33126

   H. G. Ziegenfuss

4. BABCOCK AND WILCOX, Fossil Power Generation Division, 20 South Van Buren Avenue, Barberton, Ohio 44203

   M. Gold

5. BATELLE COLUMBUS LABORATORIES, 505 King Avenue, Columbus, Ohio 43201

   I. G. Wright

6. BETHLEHEM STEEL CORPORATION, Bethlehem, Pennsylvania 18016

   B. L. Bramfitt

7. CBI INDUSTRIES, 800 Jorie Blvd., Oak Brook, Illinois 60521

   W. R. Mikesell

8. CANADA CENTER FOR MINERAL AND ENERGY TECHNOLOGY, 555 Booth Street, Ottawa, Ontario, Canada K1A 0G1

   Mahee Sahoo

9. CHEVRON CORPORATION, P. O. Box 4012, Richmond, California 94804

   A. G. Imgram

10. CLIMAX MOLYBDENUM COMPANY OF MICHIGAN, P. O. Box 1568, Ann Arbor, Michigan 48106

    T. B. Cox

11. COLORADO SCHOOL OF MINES, Department of Metallurgical Engineering, Golden, Colorado 80401

    G. R. Edwards

12. CORNELL UNIVERSITY, Materials Sciences and Engineering Department, Bard Hall, Ithaca, New York 14853

    Che-Yu Li

13. DOW CORNING CORPORATION, 3901 S. Saginaw Road, Midland, Michigan 48640

    H. W. Foglesong

14. EG&G IDAHO, INC., Idaho National Engineering Laboratory, P.O. Box 1625, Idaho Falls, Idaho 83415

    A. D. Donaldson

15-16. ELECTRIC POWER RESEARCH INSTITUTE, 3412 Hillview Avenue, P. O. Box 10412, Palo Alto, California 94303

    W. T. Bakker
    J. T. Stringer

17. FOSTER WHEELER DEVELOPMENT CORPORATION, Materials Technology Department, John Blizard Research Center, 12 Peach Tree Hill Road, Livingston, New Jersey 07039

    J. L. Blough

18. GAS RESEARCH INSTITUTE, 8600 West Bryn Mawr Avenue, Chicago, Illinois 60631

    H. S. Meyer

19. GIBBS & HILL ENGINEERING-DRAVO, 11 Penn Plaza, New York, New York 10001

    T. A. Flynn

20. KENTUCKY CENTER FOR ENERGY RESEARCH, Iron Works Pike, P.O. Box 13015, Lexington, Kentucky 40512

    V. K. Sethi

21. KENNAMETAL, INC., Philip McKenna Laboratory, 1011 Old Salem Road, P. O. Box 639, Greensburg, Pennsylvania 15601

    B. North

22. LUKENS STEEL COMPANY, R&D Center, Coatesville, Pennsylvania 19320

    J. A. Gulya

23. THE MATERIALS PROPERTIES COUNCIL, INC., United Engineering Center, 345 E. Forty-Seventh Street, New York, New York 10017

    M. Prager

24. MOBIL RESEARCH AND DEVELOPMENT CORPORATION, P. O. Box 1026, Princeton, New Jersey 08540

    R. C. Searles

25. NASA-LEWIS RESEARCH CENTER, Lewis Library, MS 60-3, 21000 Brookpark Road, Cleveland, Ohio 44135

    K. Grasse

26. NATIONAL BUREAU OF STANDARDS, Materials Building, Gaithersburg, Maryland, 20899

    S. J. Dapkunas

27. NATIONAL MATERIALS ADVISORY BOARD, National Research Council, 2101 Constitution Avenue, Washington, D.C. 20418

    K. M. Zwilsky

28-39. OAK RIDGE NATIONAL LABORATORY, P.O. Box X, Oak Ridge, Tennessee 37831

    R. A. Bradley
    P. T. Carlson
    W. N. Drewery, Jr. (8)
    R. R. Judkins
    R. W. Swindeman

40. OFFICE OF NAVAL RESEARCH, Code 431, 800 N. Quincy Street, Arlington, Virginia 22217

    S. G. Fishman

41. SHELL DEVELOPMENT COMPANY, P.O. Box 1380, Houston, Texas 77001

    L. W. R. Dicks

42. THE TORRINGTON COMPANY, Research Department, 59 Field Street, Corrington, Connecticut 06790

    W. J. Chmura

43. UNITED TECHNOLOGIES RESEARCH CENTER, East Hartford, Connecticut 06108

K. M. Prewo

44. UNIVERSITY OF CALIFORNIA AT BERKELEY, Department of Materials Science and Mineral Engineering, Berkeley, California 94720

E. R. Parker

45. UNIVERSITY OF ILLINOIS, Department of Mechanical and Industrial Engineering, 1206 West Green Street, Urbana, Illinois 61801

D. L. Marriott

46. UNIVERSITY OF SOUTHERN CALIFORNIA, Department of Materials Science, Los Angeles, California 90089

J. A. Todd

47. UNIVERSITY OF TENNESSEE, Department of Materials Science and Engineering, Knoxville, Tennessee 37916

C. D. Lundin

48. UNIVERSITY OF WASHINGTON, Department of Materials Science and Engineering, Roberts Hall, FB-10, Seattle, Washington 98195

J. Mueller

49. DEPARTMENT OF THE ARMY, Army Materials and Mechanics Research Center, Watertown, Massachusetts 02172

D. R. Messier

50-52. DOE, MORGANTOWN ENERGY TECHNOLOGY CENTER, P.O. Box 880, Morgantown, West Virginia 26505

D. Dubis
M. Ghate
J. S. Wilson

53. DOE, OFFICE OF FOSSIL ENERGY, Washington, D.C. 20545

J. P. Carr
K. N. Frye
F. M. Glaser

54. DOE, OFFICE OF BASIC ENERGY SCIENCES, Materials Sciences Division, Washington, D. C. 20545

F. V. Nolfi, Jr.

55. DOE, ENERGY CONVERSION & UTILIZATION TECHNOLOGIES DIVISION, Route Symbol CE-142, Forrestal Building, Washington, D.C. 20585

    J. J. Eberhardt

56. DOE, OFFICE OF VEHICLE AND ENGINE R&D, Route Symbol CE-131, Forrestal Building, Washington, D. C. 20585

    R. B. Schulz

57. DOE, OAK RIDGE OPERATIONS OFFICE, P.O. Box E, Oak Ridge, Tennessee 37831

    E. E. Hoffman

58. DOE, PITTSBURGH ENERGY TECHNOLOGY CENTER, P.O. Box 10940, Pittsburgh, Pennsylvania 15236

    S. W. Chun